Energy and Paper Recycling: An Investigation of Repulping

by

Frank Saville

BASc. Mechanical Engineering, The University of British Columbia, 2009.

A THESIS SUBMITTED IN PARTIAL FULFILLMENT

OF THE REQUIREMENTS FOR THE DEGREE OF

Doctor of Philosophy

in

THE FACULTY OF GRADUATE AND POSTDOCTORAL STUDIES

(Chemical and Biological Engineering)

The University of British Columbia

(Vancouver)

May 2016

Abstract

Fibers from waste paper are recovered through repulping. Repulping is accomplished using machines called repulpers. Repulpers are large machines which use a high-speed rotor mounted in a vat to disintegrate waste paper for the recovery of fibers. Repulpers consume a significant amount of energy to recover fibers from waste paper. For the work in this thesis, a $0.25m^3$ laboratory repulper was built for the purpose of determining which variables affect the specific energy (energy/mass) required for repulping. Scale replicas of 3 commercial repulper rotors were constructed to test the effect of rotor geometry on repulping specific energy. It was found that the flake content as a function of specific energy follows the form $dF/dE = -\lambda F$ where F is flake content, E is specific energy, and λ is a rate constant. The rate constant λ varies with pulp type, temperature, consistency, repulper volume, and rotor design. It was found that a given material at a given temperature and consistency requires a unique quantity of energy to be repulped independent of the rate of energy addition. An analytical model for repulping linking pulp material properties, consistency, temperature, and rotor and vat geometry is provided which allows for the accurate prediction of the time and energy required for repulping in both the $0.25m^3$ laboratory scale repulper and a $15m^3$ industrial repulper. The model assumes that all work to deflake is done by the repulper rotor in the rotor swept volume by turbulence and that no deflaking occurs in the rest of the vat. CFD simulations of the flow field produced by each rotor and high-speed film of each rotor indicate that the rotors tested in this thesis all produce strong trailing vortices akin to those produced by common mixing impellers like the Rushton turbine. Uniform mixing is important for efficient repulping. Solid body motion of the suspension in the repulper makes for poor repulping energy efficiency. Repulping time and energy savings can be accomplished by increasing the suspension consistency and the rotor swept-volume/vat volume ratio by either increasing rotor size or reducing vat volume all while ensuring complete mixing and circulation in the vat.

Preface

This thesis is an unpublished original work by Frank Saville hereafter referred to as the “author”. This research program was proposed by Dr. James Olson and Dr. Mark Martinez. All of the research and experiments presented in this work was accomplished by the author. Furthermore, the design of the major equipment used to accomplish this research was also done by the author.

Journal Submittals

Saville, F., Martinez, M., Olson, J.A., (2013). Variables affecting specific energy requirements for repulping (Early Version). In *TAPPI Papercon 2013 Conference Proceedings – Peer Reviewed*. Atlanta GA: TAPPI Press.

Saville, F., Martinez, M., Olson, J.A., (2015). Variables affecting specific energy requirements for repulping. *Canadian Journal of Chemical Engineering*, 93(3), 486-493.

Saville, F., Martinez, M., Olson, J.A. (2016). Energy and paper recycling: Modeling the time and energy requirements for low consistency batch repulping. *Canadian Journal of Chemical Engineering*. 94(3), 446-453.

Table of Contents

List of Tables

List of Figures

Nomenclature

Roman Nomenclature

B – number of rotor vanes when used in Equation 1.6.

B – distribution function when used in Equations 1.18 and 1.20.

c_B – Bond work constant having SI units of [J/kg].

c_R – Rittinger work constant having SI units of [J/kg].

c_K – Kick work constant having SI units of [J/kg].

C_m- mass based consistency.

C_R- cumulative rotor to fiber contact as defined by Bennington et al. (1998a).

C_V- volume based consistency.

D – diameter.

E – Energy per unit mass having SI units of [J/kg].

E_F – energy applied to flakes from a repulper rotor.

F – TAPPI Flake Content.

F_R – rotor to flake impact force from the model of Bennington et al. (1998a).

F_V – viscous force on a flake as defined by Holik (1988).

G – rotor vane frontal area.

H_R – rotor height.

k – rate constant having SI units of [1/s].

k' – rate constant based on cumulative rotor to flake contact as defined by Bennington et al. (1998a) and having SI units of [1/m^2].

k'_0 – a fitting constant for the impact based repulping model of Bennington et al. (1998a).

K– a fitting constant for the impact based repulping model of Bennington et al. (1998a).

L – length.

m – mass.

m_F – dry mass of flakes in suspension.

m_p- dry mass of pulp in suspension.

m_w – mass of water in a pulp suspension.

n – Kolmogorov length scale when used in Equation 1.23.

$n(\gamma)$ – dynamic viscosity.

N – rotor/impeller rotational speed having units of revolutions per second.

N_P – dimensionless impeller/rotor power number.

N_{total} – the total number of rotor revolutions during a repulping operation.

P – power.

P_k – turbulence energy for 2-equation turbulence models.

PR – repulping production rate.

P_V – power dissipated per unit volume.

Q – volumetric flow rate.

Re – Reynolds number.

S – cumulative area swept out by a repulper rotor when used in Equations 1.5 and 1.6.

S – comminution rate constant having SI units of [1/s] when used in Equations 1.18 and 1.19.

S^E – comminution rate constant having SI units of [kg/J].

t – time.

T – temperature or vat/tank diameter. The context is given in the text of the document.

t_k – Kolmogorov time scale.

T_M – pulp wet-tensile strength.

V_{Swept} – rotor/impeller swept volume.

V_{Vat} – vat volume.

v_{tip} – rotor/impeller tip speed.

W – width.

W_B – specific work.

W_K – specific work.

W_R – specific work.

x – in comminution, the product class particle size.

X – in comminution, the feed class particle size.

Greek Nomenclature

α – shear factor as defined by Vilaseca et al. (2011).

ϑ- fitting factor as defined by Vilaseca et al. (2011).

ε – dissipation per unit mass.

ε_F – dissipation per unit volume required for pulp suspension fluidization.

ε_V – dissipation per unit volume.

γ – in Equations 3.2 and 3.3 gamma represents the repulper rotor power split between deflaking and direct dissipation by turbulence.

γ – shear rate when not used in Equations 3.2 and 3.3.

θ_m – mixing time.

λ – rate constant having SI units of [kg/J].

ρ – density.

σ – wet material toughness/tensile energy absorption.

τ – shear stress in Equations 1.10 and 1.31 only.

τ_R – time spent by flakes near a repulper rotor being repulped.

τ_{Swept} – a variation of τ_R and the time spent by flakes within the swept volume of a repulper rotor being repulped.

τ_{Vat} – time spent by flakes circulating around a repulper vat away from the repulper rotor not being repulped.

μ – dynamic viscosity.

μ_{H_2O} - dynamic viscosity of water.

ν – kinematic viscosity.

Acknowledgments

First off, I'd like to thank my supervisors Dr. James Olson and Dr. Mark Martinez for all of their support and especially for all of their patience. I'd also like to thank George Soong for all of his help over the years in the laboratory.

My mom and dad have been hugely supportive of me and I will forever be grateful to them for this. I don't know if I could ever repay them for all the support they have given me but I will surely try. Thank you mom and dad.

I'd like to thank my sister Chrissy for the super precise lab work she did for me – the lab analysis for the results presented in Chapter 2 of this thesis are 90% Chrissy. I'd also like to thank Chrissy for being such a great sister.

I'd like to thank my friends Riley and Roy. Riley, thank you for finding me the stainless steel tank out of which I built the machine that this thesis study revolves around. Roy, thank you for building and overclocking my computers so expertly.

And finally, I'd like to thank my crazy cattle-dog/sled-dog cross Linkin for being at my side for every keyboard stroke that makes up this thesis, all 285,993 of them.

Chapter 1: Introduction

Paper recycling saves substantial space in landfills, reduces the need for tree harvesting, and saves considerable water and energy over the production of virgin fibers. Recycled paper is also a valuable source of fibers for papermaking.

Paper is made up of a mat of interwoven cellulose fibers. In order to produce new paper/pulp products from waste paper, the fibers within waste paper must be separated from one another - only then can these fibers be used to produce new paper/pulp products.

Fibers from waste paper are recovered through repulping. Repulping literally means to "re-pulp", as in to turn waste paper back into pulp to be used to make new paper products. As paper consists of a mat of interlaced wood fibers, repulping involves mechanically (often with the aid of chemicals) breaking down this mat to separate the individual fibers to make a new pulp suspension of recovered fibers.

Repulping is accomplished in machines called "repulpers". Repulpers come in two basic forms; the drum-type and the type having a high-speed rotor mounted in a large vat, also known as a hydrapulper. The work presented in this thesis focuses on the latter type as the gentle action of the drum-type repulper is only suitable for the repulping of weak paper grades. The repulper type employing a high-speed rotor in a vat is used to repulp all grades of waste paper.

Hydrapulpers operate, albeit superficially, like the common kitchen blender. Waste paper is fed to the repulper vat and it is broken down by the high-speed repulper rotor. The rotor also functions to uniformly mix the newly formed pulp suspension within the repulper vat.

Although recycling paper saves substantial energy and other resources over the production of new fibers, repulpers themselves consume a significant amount of energy. Repulpers having an installed power greater than 500kW are common and repulpers often operate 24 hours per day. According to repulper manufacturers, a 500kW repulper can typically repulp 300 tons per day, meaning the breakdown of waste paper requires about 40kW-h/Ton. In the United States alone, 69 million tons of paper and paperboard are recycled every year (United States EPA 2015). The approximate energy required to repulp 69 million tons of paper is then 2800GW-h. In 2014, the average cost of electricity for industrial users of electricity in the United States was $0.0701/kW-h (U.S. Energy Information Administration 2015). Thus, the approximate electrical cost to repulp 69 million tons of waste paper in the United States is $200 million dollars in the year 2014.

Despite this massive energy use in repulping, not much is actually known about how waste paper is broken up in a repulper. No theory is available that presents a repulping mechanism to link together repulper design, the mechanical properties of the feed waste paper, and other operating factors known to impact repulper operation. The evolution of repulper design since the first hydrapulper was put into service in 1939 has been more a result of trial and error rather than of conclusive theory (*Pulping of Secondary Fiber* 1990).

The lack of a theory to explain repulping combined with the substantial energy used by repulpers is the impetus behind this thesis study.

In order to study repulping, one requires a repulper. To this end, a laboratory scale repulper was designed and built specifically for this study. Replicas of three modern repulper rotors currently being used in mills around the world were created for testing in the laboratory repulper.

The laboratory repulper is used in this study to determine which variables affect the time and energy requirements in repulping. Based on this testing, and culling knowledge from other fields having relevance to repulping (such as stirred mixing and general comminution), a theory-based model that accurately predicts the time and energy requirements for repulping is presented in this thesis. This model is shown to not only accurately predict the time and energy requirements for repulping in the laboratory repulper built for this study, but also in a full-size industrial repulper operating in a running mill. The model enables the scaling of repulping performance between different size repulpers having different operating conditions.

The three replica test rotors are not only compared performance-wise in the laboratory repulper, but also using computational fluid dynamics (CFD). Specific rotor design features are identified as those being responsible for the repulping of waste paper.

Finally, all three test rotors are observed actually breaking up paper in the laboratory repulper using high-speed film.

The work presented in this thesis supports the development of more efficient repulper operation and better repulper design. This work is the first known to the author to provide a theory based model explaining how waste paper is broken up in a repulper.

1.1 Repulping

Repulpers are found in two major permutations, those having bottom, or side, mounted rotors in a large vat, known as hydrapulpers, and horizontal drum type repulpers. Repulper design is in part dictated by the pulp suspension consistency range at which a repulper is meant to operate. Consistency is a measure of the concentration of pulp in suspension. The mass based consistency, C_m, is defined as:

$$C_m = \frac{m_p}{m_p + m_w} \tag{1.1}$$

where m_p is the dry mass of pulp in suspension and m_w is the mass of water suspending the pulp. The rheology of pulp suspensions is complex and varies greatly with changing consistency. Qualitatively, pulp suspensions "thicken" as consistency is increased and the repulper design must account for this. The rheology of pulp suspensions is reviewed later on. Repulpers having a rotor-in-vat configuration are classified as either low consistency (LC) or high consistency (HC) types with the main differentiating feature between the two types being the design of the rotor.

LC repulpers, as the name implies, process low-consistency pulp suspensions in the range of $3 \leq C_m \leq 8\%$. LC repulper rotors are high-speed and low-profile and bear a strong resemblance to both centrifugal pump impellers and impellers used in turbulent stirred mixing such as the Rushton turbine. LC repulper rotors operate at tip-speeds of 15 - 20m/s (Holik 2006).

High-consistency (HC) repulpers are used for repulping in the range of $8 \leq C_m \leq 18\%$. HC repulpers employ a tall, helical rotor. The height of an HC rotor is typically equal to its diameter. HC rotors are larger in diameter for a given vat size than LC rotors. HC rotors have a rotor diameter-to-vat diameter ratio (D/T) of 0.4 compared to 0.3 for LC repulpers. HC repulper rotors operate at slower tip speeds than LC repulpers, typically 11 - 14m/s (Bahr 1990).

Drum repulpers follow a very different concept than either LC or HC repulpers. A drum repulper consists of a horizontal drum having internal baffles. Feed material to be repulped is fed into one end of the drum at high-consistency (approximately 20%) where it is repulped by being gently tossed by the internal baffles of the slowly rotating drum (17 rpm). The repulped material is then extracted at the extraction end of the drum. The operation of drum repulpers is analogous to that of the horizontal ball mills commonly used for the comminution of minerals. LC and HC repulpers can repulp high wet-strength pulps. Drum repulpers, due to their gentle action and slow rotation, are suitable for repulping low wet-strength pulps only (Bahr 1990; Fricker et al. 2007). This thesis concerns repulping using hydrapulper type machines. Drum repulpers are only mentioned here for the sake of thoroughness.

The vat interior of an LC repulper is shown in Figure 1.1. Notice that the rotor sits on top of a perforated extraction plate. Fibers are extracted from the repulper through the extraction plate.

Figure 1.1: Looking inside a 15m^3 LC repulper having a 900mm diameter rotor. Notice the extraction plate below the rotor (photo taken by the author Sept. 2011).

The exact mechanism by which waste paper is disintegrated in a repulper has not been reported in the literature. It is generally thought though that repulping occurs because of (Holik 1988; Paraskevas 1983):

- Flakes are broken down by being sheared between the rotor and extraction plate.
- Flakes are broken down by direct impact with the rotor.
- Flakes are worn down by fiber-to-flake/flake-to-flake rubbing.
- Flakes are broken down by turbulence.

The evolution of repulper design reflects attempts to maximize one or more of the above possible repulping mechanisms. LC rotor designs are usually described by individual design elements intended for either pumping, turbulence generation, rotor-to-flake impact, or attrition – attrition being industry jargon for the shearing of flakes between the rotor and extraction plate (*Pulping of Secondary Fiber* 1990). The first repulpers (called hydrapulpers) entered service in 1939 (*Pulping of Secondary Fiber* 1990). An original hydrapulper style rotor is shown in Figure 1.2. This rotor used six back-swept vanes intended to pump/circulate the pulp suspension throughout the repulper vat along with an outer ring of turbulence generators. This rotor was designed to deflake the suspension via turbulence. In early hydrapulpers, the extraction plate consisted of a perforated ring around the rotor perimeter. One extra-large turbulence generator on the rotor was designed to keep the ring shaped extraction plate clear.

The 1960's saw repulper designers attempt to improve rotor function by incorporating forward canted vanes intended to wedge flakes between the rotor and extraction plate which was now underneath the rotor. The underside of the rotor vanes now incorporated airfoil sections designed to back-flush the extraction plate in a manner analogous to the rotor foils in a pulp pressure screen. An example of this style of rotor is the Vokes rotor (Vokes 1963). This rotor incorporates pumping vanes atop every other vane. There are many Vokes rotor derivatives with two versions of one of these derivatives shown in Figure 1.2.

Modern rotors include the Voith HM, Voith Plate Rotor, Kadant Vortech, and many others. Some modern LC repulper rotors are shown in Figure 1.2. The manufacturers of these rotors all claim improved repulping performance and superior energy efficiency (Egan et al. 2004; Aue and Fineran 2006). The claims made by rotor designers and manufacturers remain untested in peer-reviewed literature.

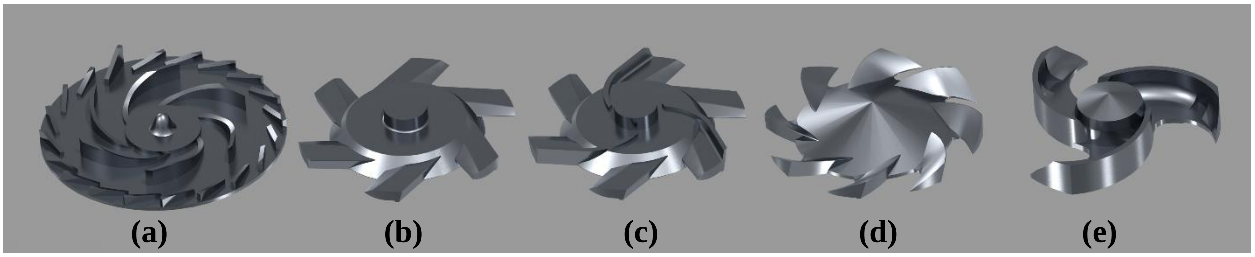

Figure 1.2: Examples of LC repulper rotors. (a) An original hydrapulper style rotor. (b) A 1960's style rotor having forward canted vane faces. (c) A 1960's style rotor with added flutes. (d) A modern rotor style. (e) Another modern rotor style.

HC repulpers were developed based on the knowledge that repulping energy efficiency and throughput are increase as consistency is increased. This phenomenon is often attributed to more fiber-to-flake/flake-to-flake rubbing as consistency increases (Holik 1988; Paraskevas 1983). HC repulper rotors are variations on the helical designs used in stirred mixers for processing highly viscous fluids. The helical design used for HC repulper rotors maintains suspension motion when repulping high-consistency, high-apparent viscosity, pulp suspensions.

The original hydrapulper used a cylindrical vat with a centrally mounted rotor. It employed baffles to stop solid body motion of the suspension in the repulper. Proper mixing is cited as being important for efficient repulping but maintaining fluid motion in pulp suspensions in repulpers can be difficult (Holik 1988; Paraskevas 1983). Pulp suspensions behave as non-Newtonian fluids and display both shear-thinning and yield-stress behavior. Some efforts toward improving the mixing and vat turnover in a repulper come in the form of the D-shaped vat and the offset rotor. The D-shape is claimed to effectively baffle the vat with the additional claim made that the D-shape creates an off-center vortex which improves the draw-down of buoyant pulp bales to the repulper rotor (*Pulping of Secondary Fiber* 1990). Repulpers can also be found having an eccentrically mounted rotor. With this design, claims of improved energy efficiency and throughput are made due to the claimed greater mixing efficiency offered by the eccentrically placed rotor (Muller 2010). These claims of improved performance for both of these design variations have not been verified in peer-reviewed literature.

The completeness of a repulping operation can be quantified by the TAPPI Flake Content measurement. Paper, being effectively 2-dimensional, appears as ragged-edged flakes when partially broken down in a repulper, hence the term "flake content". The TAPPI Flake Content (F) is defined as (*TAPPI T-270 pm-88 Standard* 1988):

$$F = \frac{m_F}{m_p} \tag{1.2}$$

where m_F is the dry mass of flakes in suspension and m_p is the dry mass of all pulp in suspension including both flakes and fibers. The percentage of flakes at any time during a repulping operation can be estimated from samples of the suspension in a repulper using the TAPPI Flake Content definition (a description of how Flake Content is measured is given in Appendix A3). Samples can be correlated with both the time and energy during a repulping operation to obtain the time and energy requirements for a given repulping operation.

First reported by Bennington et al. (1998a), the flake content versus repulping time follows first order kinetics:

$$\frac{dF}{dt} = -kF \tag{1.3}$$

where F is the TAPPI Flake Content, t is time, and k is a rate constant having SI units of [1/s]. The time and energy required for repulping have been shown to depend on both repulper design and on a number of operating factors.

Holik (1988) performed repulping trials using label paper, two grades of laminating paper, and punched card and found that the specific energy required for repulping to a given flake content level is linearly proportional to the pulp wet breaking strength as found from wet tensile testing performed for each grade. Bennington et al. (1998a) showed a similar finding in that the rate constant k in Equation 1.3 is linearly proportional to the wet tensile strength of the material being pulped. The materials tested by Bennington et al. (1998a) included old magazine (OMG), #2/3 Pub, and old newspaper (ONP) with ONP being tested in tap water and at a pH=10. Increasing the pH of the ONP suspension resulted in reduced wet tensile strength and reduced repulping time for ONP. Brouillette et al. (2003) treated several different grades of pulp (ONP, Lightweight Coated and Supercalendared A) and also found a linear dependence for the rate constant k on material wet tensile strength.

Many pulp/paper grades are of the wet-strength variety. A pulp/paper sheet is made up of a mat of interlaced fibers. The mechanical strength of a sheet is due to a combination of friction and chemical bonding between networked fibers with the most significant bond type being hydrogen bonds. Water destroys hydrogen bonds so many paper/pulp grades, in order to have some level of wet-strength, incorporate organic resins (Neimo 1999). Common paper towel used for cleaning up kitchen spills is a good example of a wet-strength grade.

The addition of resins can result in high wet-strength for some grades and can make these grades difficult to repulp. Chemical and enzyme treatments can make repulping easier but care must be taken so as to not adversely affect the properties of the fibers being recovered (Bhardwaj and Rajan 2004; Espy 1992; Espy and Geist 1993; Fischer 1997; Wang et al. 2004).

Temperature has been shown to have a profound effect on the time and energy required for repulping (Bhardwaj and Rajan 2004; Cho et al. 2009; Savolainen et al. 1991). Raising the suspension temperature by 20^0C can cut the time and energy requirements for repulping in half depending on other process variables (Savolainen et al. 1991). The rate constant k from Equation 1.3 has been shown to increase linearly with increasing temperature (Cho et al. 2009).

To summarize the preceding, the wet strength of different pulp types varies. Pulp types showing higher tensile strength take more time and energy to repulp. Increasing the suspension temperature and/or adding chemicals or enzymes reduces the wet strength of pulp making for easier repulping.

Repulping operating factors that are independent of the feed material properties are suspension consistency and rotor power. The rate constant k in Equation 1.3 has been shown to increase linearly with increasing rotor power both by Amaral et al. (2000) and Vilaseca et al. (2011). It is not known if/how altering rotor power affects the total amount of energy required to complete a repulping operation.

Both the time and energy required for repulping are reduced as suspension consistency increases (Amaral et al. 2000; Bennington et al. 1998a; Cho et al. 2009; Holik 1988; Paraskevas 1983; Savolainen et al. 1991; Vilaseca et al. 2011). Cho et al. (2009) showed that the rate constant k in Equation 1.3 increases linearly with increasing consistency, tested over a range 4 – 18% consistency. Data from Vilaseca et al. (2011) shows the same linear dependence for k tested over a range of 6 – 18% consistency.

The influence of rotor and vat design on repulper performance is largely untested in peer reviewed literature. Design features contributing to improved repulper performance are often extolled in manufacturer white papers where these features are often claimed to reduce energy consumption by up to 30% (Aue and Fineran 2006).

The only published peer-reviewed tests concerning any aspects of repulping geometry are those of Bennington et al. (1998b) and Savolainen et al. (1991). Bennington et al. (1998b) and Savolainen et al. (1991) measured repulping performance in time and energy respectively for varying rotor-to-vat diameter ratios (D/T). In both measures, repulping performance improved markedly for larger D/T ratios. Savolainen et al. (1991) also compared the repulping performance of two different LC rotors having different designs and found an efficiency difference between them. They did not offer a reason why this was so.

Bennington et al. (1998b) also tested the repulping efficiency of a high-shear mixer normally used to study the fluidization of pulp (see Bennington and Kerekes (1996) for a thorough description of this machine). This high-shear mixer/fluidizer is configured as a Couette device with vanes on both the inner and outer cylinders. Bennington et al. (1998b) found that the high-shear mixer/fluidizer made for a far more efficient repulper than the laboratory HC repulper used for the rotor diameter comparison in the same article. They attributed the superior efficiency of the high-shear mixer to the fully turbulent flow within the mixer during repulping versus the mostly laminar flow conditions within the laboratory HC repulper. They suggested that the turbulence was the dominant repulping mechanism in the high-shear mixer/fluidizer.

Investigations in peer-reviewed literature of the mechanism(s) by which repulping is accomplished begin with Paraskevas (1983). Even here though, only a qualitative description of possible repulping mechanisms are given. Paraskevas (1983) contends that repulping is accomplished by a combination of turbulence, attrition between the rotor and the extraction plate, and fiber-to-flake rubbing. He asserts that the fiber to flake rubbing is the dominant deflaking mechanism for two reasons: 1) Energy efficiency improves as consistency is increased which he attributes to more fiber-to-flake rubbing; 2) Fiber-to-flake rubbing acts throughout the entire tank whereas highly turbulent flow and attrition between the rotor and extraction plate is only localized to the vicinity of the rotor. Paraskevas (1983) also identifies the presence of cavitation on the trailing edge of repulper rotor vanes as being common.

Holik (1988) examined possible repulping mechanisms in terms of the magnitude of the force each mechanism could apply to flakes and by the frequency of occurrence for each mechanism. He also judges the effectiveness of each mechanism by the minimum attainable flake size for each mechanism. Holik

(1988) names three mechanisms: 1) “Clinging” – Holik’s term for the shearing of flakes between the rotor and extraction plate. The possible force applied to a flake by clinging is very high, in the kilo-Newton range, as the repulper rotor drive torque is in the kN-m range. All flakes subject to clinging will rupture. However, the frequency of occurrence of clinging is low as it only happens between the rotor and extraction plate. Furthermore, the minimum attainable flake size as a result of clinging is dictated by the clearance between the rotor and extraction plate which is usually approximately 5 – 10mm; 2) “Viscosity” – Flakes are sheared by velocity gradients in the flow. The force on a flake (F_V) is then:

$$F_V = L\, W\, \eta(\gamma) \tag{1.4}$$

where L and W are the length and width of a flake respectively and $\eta(\gamma)$ is the apparent viscosity of the pulp suspension. Holik (1988) estimates the force applied to flakes by viscosity to be ~ 1 Newton although he does not explain how the shear-rate and apparent viscosity were determined in order to make this estimate. Holik (1988) suggests that the frequency of occurrence for this “viscosity” mechanism is high as velocity gradients exist throughout the repulper vat. The steepest gradients are suggested to occur at the rotor; 3) “Acceleration” – Flakes are ruptured due to the accelerative forces provided by fluid convection or directly by the rotor. Holik (1988) estimates the possible force from “acceleration” to be approximately 10N. Again, Holik (1988) does not give details on how this estimate was made. The frequency for this mechanism is high as convection is present everywhere in the repulper vat with the greatest “acceleration” forces occurring at, or near, the rotor.

Holik (1988) states that any combination of “clinging”, “viscosity”, and “acceleration” are possible and that repulping occurs when the wet tensile strength of the material being repulped is overcome by these forces. Holik (1988) does show that the energy required for repulping is proportional to the wet breaking length of the feed material. However, a theoretical link between the wet breaking length and the forces involved in repulping is not provided.

Bennington et al. (1998a) formulated a repulping model based on cumulative contact between the rotor and the pulp in suspension. This cumulative contact, designated C_R, is defined by Bennington et al. (1998a) as:

$$C_R = SC_V \tag{1.5}$$

where C_V is the volume based concentration of pulp in suspension and S is the cumulative area swept out by the repulper rotor during a repulping operation and is defined taking into account the rotor geometry where:

$$S = BGN_{total} \tag{1.6}$$

where B is the number of rotor vanes, G is the vane frontal area, and N_{total} is the total number of rotor revolutions made during repulping. Bennington et al. (1998a) replaced the rate constant k in Equation 1.3 so that:

$$\frac{dF}{dC_R} = k'F \tag{1.7}$$

where k' is a new rate constant based on cumulative rotor-to-pulp contact and has SI units of $[1/m^2]$. Bennington et al. (1998a) found that the completeness of a given repulping operation is dependent on cumulative rotor-to-pulp contact and on the pulp type. Bennington et al. (1998a) showed that k' is proportional to the test material wet tensile strength.

Bennington et al. (1998a) proposed a model based on the cumulative contact finding above and the assumption that deflaking is solely a result of rotor-to-flake impact. The criteria for flake rupture used by this model is:

$$k' = k_0' \, exp\left(-\frac{T_M}{KF_R}\right) \tag{1.8}$$

where T_M is the pulp wet tensile strength, k_0' and K are fitting parameters, and F_R is the force applied to the flakes from impact with the repulper rotor based on the rotor dimensionless power number (N_P) and the rotor geometry:

$$F_R = \frac{N_P}{\pi DNBH} \tag{1.9}$$

where D is the rotor diameter, and H is the contact height between the rotor and the pulp suspension - in an HC repulper, the rotor is very tall and may protrude from the suspension free surface. The criteria for flake rupture posed by this model is that rupture occurs when the impact force from the rotor overcomes the wet tensile strength of the flakes. This model was applied to compare three different diameter HC rotors in a laboratory HC repulper in Bennington et al. (1998b). The rotor tip speed for the comparisons was 9 m/s and the consistency was 6% for all three rotors. This is much slower than is typical for HC repulpers where rotor tip speeds are 11 – 14m/s (Bahr 1990). Bennington et al. (1998b) noted that the flow appeared to be laminar in the laboratory HC repulper at the 9 m/s test speed. The model fit to the data gathered for all three test rotors fit with a correlation of R^2=0.64. In the same study, the repulping performance of a high-shear mixer was tested. The k' measured for the high-shear mixer was 7.5 times larger than that for the three HC rotors for the same material and consistency. The premise of the model is such that k' should be the same for a given material. Benninton et al. (1998b) attributed the better performance of the high-shear mixer to the fully turbulent flow conditions within the mixer and that high-intensity turbulence was responsible for repulping in this device, a phenomenon not accounted for in the impact based model.

Another approach taken to model the kinetics in repulping is to relate the repulping rate, k in Equation 1.3, to the rotor power dissipated per unit volume in the repulper. This approach, first proposed by Amaral et al. (2000) has been expanded upon by Fabry et al. (2001), Roux et al. (2001), and Vilaseca et al. (2011). The original postulate by Amaral et al. (2000) was to assume that all repulping is accomplished by flake-to-flake/fiber-to-flake friction. The intensity of this friction is in turn dependent upon the rotor power dissipated by the pulp suspension in the repulper. The power per unit volume (P_V) dissipated in the suspension by fiber-to-fiber/flake friction is modeled by Rayleigh's Dissipation Function in the form of:

$$P_V = \frac{\tilde{\tau}^2}{\mu} \tag{1.10}$$

where $\tilde{\tau}$ is the average shear-stress in the pulp suspension and μ is the suspension viscosity. This in turn leads to:

$$k = \alpha\left(\mu_{H_2O}\, P_V\right)^{0.5} exp(\vartheta\, C) \tag{1.11}$$

where C is the mass fraction of pulp in suspension, ϑ is a dimensionless fitting factor, and α is defined by the authors to be the "shear factor" and has SI units of [Pa s] (Vilaseca et al. 2011). The shear factor represents a given material's resistance to being repulped. It is interesting to note that by this model:

$$k \propto P_V^{0.5} \tag{1.12}$$

although it is explicitly stated by, Vilaseca et al. (2011) that:

$$k \propto P_V \tag{1.13}$$

The data in Vilaseca et al. (2011) also supports the form of Equation 1.13.

At this point, the influence of rotor and vat design on repulping, and the mechanism(s) by which repulping is accomplished are unknown.

To recap the preceding, the repulping process is known to be influenced by:

1. Pulp Type – the stronger the pulp, the more time and energy required for repulping (Bennington et al. 1998a; Brouillette et al. 2003; Holik 1988).

2. Chemical/Enzyme Addition – the addition of chemicals or enzymes reduces the strength of the material being repulped thereby reducing the time and energy required for repulping (Bennington et al. 1998a; Bhardwaj and Rajan 2004; Brouillette et al. 2003; Espy 1992; Espy and Geist 1993; Fischer 1997; Wang et al. 2004).

3. Temperature – increasing the pulp suspension temperature reduces the time and energy required for repulping (Bhardwaj and Rajan 2004; Cho et al. 2009; Savolainen et al. 1991). The rate constant k from Equation (1.3) has been shown to increase linearly with increasing pulp temperature (Cho et al. 2009).

4. Rotor Power – Repulping time is reduced as rotor power is increased. The rate constant k in Equation (1.3) is linearly proportional to rotor power (Amaral et al. 2000; Vilaseca et al. 2011).

5. Consistency – Increasing suspension consistency reduces both the time and energy required for repulping (Bennington 1998a; Cho et al. 2009; Holik 1988; Paraskevas 1983; Savolainen et al. 1991; Vilaseca et al. 2011). The rate constant k from Equation (1.3) has been shown to increase linearly with increasing pulp consistency (Cho et al. 2009; Vilaseca et al. 2011).

6. Increasing Rotor Size – Increasing the rotor diameter for a fixed vat diameter reduces both the time and energy required for repulping (Bennington et al. 1998b; Savolainen et al. 1991).

7. Rotor Design – Savolainen et al. (1991) measured the performance of two different LC repulper rotor designs and found one was more energy efficient than the other.

8. Turbulence – Repulping is more efficient in fully turbulent flow (Bennington et al. 1998b).

At this point, there is no theory tying together points 1-8 above. The previous research also raises a number of questions.

Unfortunately, peer-reviewed literature concerning repulping is somewhat sparse. However, repulping incorporates aspects of other, well studied fields. The goal of repulping is to disintegrate waste paper for fiber recovery. This makes repulping a comminution process. Is the energy use in a repulper in any way similar to the energy use in other comminution processes?

A repulper, in a mechanical sense, is a strengthened version of a stirred mixer. Flow fields, turbulence, impeller performance etc. are all very well studied in the field of stirred mixing.

Repulper rotors operate at tip speeds akin to that of centrifugal pump impellers – machines classified as turbomachines. At the same time, the flow at the pulp suspension free surface in a repulper may be creeping, or even stagnant due to the yields stress behavior of pulp. The complex, highly shear-rate dependent rheology of pulp suspensions must be considered.

The following sections entail a review of work in these other fields with the hope that clues toward a better understanding of repulping are revealed.

1.2 General Comminution

Repulping is a comminution process in which waste paper is broken down for fiber recovery. The nature of energy use as dependent upon rotor power is unknown in repulping. Furthermore, no theoretical link between material properties and the time and energy in repulping has been found. Following, studies focusing on energy use in comminution in general, and studies linking material properties to energy use in comminution are reviewed. It is hoped that the review of these studies will help toward the formation of a hypothesis to explain the energy use in repulping, and in particular, the dependence of this energy use on material properties.

Typically, in any comminution process, a certain particle size distribution (PSD) is sought. The design and operation of comminution equipment is optimized to reduce feed material to a desired PSD with a minimum energy input, albeit within the current limitations of our understanding of comminution.

It is generally accepted that the forces seen in comminution processes consists of one, all, or any combination of the following:

- Compression forces
- Friction/Shear forces - attrition
- Inter-particle contact forces
- Impact forces

The energy input to a given comminution process to obtain a desired PSD has been postulated to depend upon the break-down of particles according to the three “Laws of Comminution.” The “First Law of Comminution” was proposed by von Rittinger (1867) and states that the energy required for the size reduction of particles is directly proportional to the newly evolved particle surface area created during a comminution process as per Equation 1.14:

$$W_R = c_R\left(\frac{1}{x} - \frac{1}{X}\right) \tag{1.14}$$

where W_R is the specific work (having SI units of [J/kg]) required to reduce the feed particle size class X to size class x. The parameter c_R is determined empirically for a given process.

The “Second Law of Comminution” was proposed by Kick (1885) and postulates that the energy required in a comminution process is proportional to the volume reduction of particles during comminution according to Equation 1.15:

$$W_K = c_K \, ln\left(\frac{X}{x}\right) \tag{1.15}$$

where W_K is the specific work (having SI units of [J/kg]) required to reduce the feed particle size class X to size class x. The parameter c_K is determined empirically for a given process.

The “Third Law of Comminution” was proposed by Bond (1952) and posits the idea that the energy required in a comminution process is proportional to the new particle crack length developed during comminution according to Equation 1.16:

$$W_B = c_B\left(\frac{1}{\sqrt{x}} - \frac{1}{\sqrt{X}}\right) \tag{1.16}$$

where W_B is the specific work (having SI units of [J/kg]) required to reduce the feed particle size class X to size class x. The parameter c_B is determined empirically for a given process.

Note that although the above are known as the three “Laws of Comminution”, they are all more accurately described as approximations and empirical findings. Nonetheless, these “Laws” have proven to be useful and enduring for scaling and performance prediction in comminution processes. Bond (1952, 1960, 1961) showed that the parameters c_B and W_B from Equation 1.16 remained constant between pilot scale batch ball mill experiments and large industrial batch ball mill experiments so long as the number of balls, ball fill ratio and process material were identical between the pilot mill and industrial mill. Bond's findings form the basis for the scaling of comminution processes and the parameters c_B and W_B from Equation 1.16 are considered to be material properties. As long as the design and operational parameters remain constant between mills of different sizes, the specific work required to reduce a feed material to a desired PSD is identical in both mills. Equations 1.14 and 1.15 are applied to scale comminution processes in a manor analogous to that for Equation 1.16.

Walker (1937) proposed that the energy required for size reduction in comminution follows the general form outlined by Equation 1.17:

$$\frac{dX}{dE} = -cX^n \tag{1.17}$$

where X is particle size, E is energy per unit mass, c is a rate constant, and n is the "order" of the process. Hukki (1962) showed that when Equation 1.17 was solved with the exponent n set to 2, 1, and 3/2, the equations of Von Rittinger, Kick, and Bond (Equations 1.14, 1.15, and 1.16) are obtained respectively. Hukki (1962) explored the variation of the exponent n in Equation 1.17 and suggested that the theories of Von Rittinger, Kick, and Bond are each applicable within a specific size window. Von Rittinger's equation (Equation 1.14) is applicable to fine grinding, Kick's equation (Equation 1.15) is applicable to the crushing of large particles, and Bond's equation (Equation 1.16) is applicable to most milling processes.

The "Laws of Comminution" represent a high level approach where the particle breakage and transport kinetics and the particle size classification are lumped into the empirically determined parameters c_R, c_k and c_B in Equations 1.14, 1.15, and 1.16 respectively. Nonetheless, these laws find enduring use in industry, specifically the Bond Law. The parametersc_R, c_K, and c_B from Equations 1.14, 1.15, and 1.16 have been cataloged for many processes and equipment types (e.g. Smith and Lee 1968).

A more detailed comminution model which takes into account the sub-processes of particle breakage, particle transport, and particle size classification was proposed by Reid (1965) as a population balance model in the form of Equation 1.18:

$$\frac{dm_i}{dt} = -S_i m_i + \sum_{j=1}^{i-1} S_j B_{ij} m_j \tag{1.18}$$

where m_i represents the mass of particles in the ith size class, S_i represents a breakage rate function, B_{ij} is a breakage distribution function and corresponds to the amount of material broken in size class j which is distributed to size class i, and t is time. The first term on the right hand side of Equation 1.18 represents the breakage rate in size class i while the second term represents the size class distribution of broken particles.

Herbst and Fuerstenau (1973, 1980) scaled milling performance based on the contention that the breakage rate function is proportional to mill specific power in the form of Equation 1.19:

$$S_i = S_i^E \frac{P}{m} \tag{1.19}$$

where S_i^E is a rate constant with SI units of [kg/J], P is the power input to the mill, and m is the total mass of material being milled. The implication of Equation 1.19 is that the breakage function is proportional to the mill specific power only and that specific energy input is the principle factor for mill scale-up. Herbst and Fuerstenau (1973, 1980) found that Equation 1.19 accurately fit the breakage rate data from actual milling experiments. Herbst and Fuerstenau (1973, 1980) then combined Equations 1.18 and 1.19 to obtain Equation 1.20 for a mill drawing constant power such that Pt/m is equal to the mill specific energy E:

$$\frac{dm_i}{dE} = -S_i^E m_i + \sum_{j=1}^{i-1} S_j^E B_{ij} m_j \tag{1.20}$$

Equation 1.20 predicts that for a given material and initial PSD, the final desired PSD can be obtained identically in different sized mills at different speeds given that the specific energy input to each mill is identical. Herbst and Fuerstenau (1980) then used breakage and selection parameters measured in a 25.4 x 29.2 cm ball mill along with Equation 1.20 to predict the PSD obtained using 76.2 x 40.6 cm ball mill for a 10-mesh limestone feed. The accuracy of this prediction proved excellent when compared with actual milling experiments and confirms the use of specific energy as the principle factor in mill scaling. Herbst and Fuerstenau (1980) show that the final products in a comminution process depend on the total specific energy input to the process and on the properties of the material being broken down. For comminution processes, this material property has long been recognized to depend on a given material's toughness, specifically fracture toughness (Austin 1984; Bearman et al. 1991; Napier-Munn et al. 1999; Schoenert, 1972; Fuerstenau and Abouzeid 2002).

In a comminution process, solids are fractured into smaller pieces. In order to fracture a solid, some bonds holding the solid together must be broken. Energy is required to break these bonds. For a reversible fracture, the energy required to break these bonds is equal to the energy contained in the newly evolved surfaces after fracture. This new energy is termed "surface energy". Surface energy is related to fracture toughness, commonly denoted by G_C. Fracture toughness represents the energy required to evolve new crack surface area and is a material property having SI units of [J/m^3]. For brittle materials, the surface energy formed as a result of cracking is proportional to the material fracture toughness. For ductile materials, the energy from plastic deformation at the crack tip must also be considered (Ashby and Jones 2003).

The comminution studies reviewed above concern brittle minerals. Pulp/paper, especially wet pulp/paper, is a very different compared to these brittle minerals.

A paper sheet is made up of a network of interlaced cellulose fibers. A paper sheet derives its mechanical strength from frictional forces between the interlaced/interlocked fibers and through chemical bonding with hydrogen bonds being the dominant bond type (Neimo 1999).

The mechanical properties of paper are affected by both temperature and moisture. Temperature affects both the strength and length of bonds (Dougherty 1998). To this end, Andersson and Berkyto (1951) found that the tensile strength of dry newspaper decreases in a linearly proportional manner to increasing temperature over a range spanning from -50 to 150^0C. Similar findings have been made for wet paper. Back and Andersson (1992) reported a tensile strength loss of 1% per degree Celsius for wet paper. This finding is echoed by that of Kouko et al. (2014). Interestingly, both researchers found that with wet paper, increased temperature reduced ultimate tensile strength and Young's Modulus but not the maximum strain. For all tensile test samples at all test temperatures, the strain at rupture was found to be constant. Dry paper does not show this behavior. Instead, the Young's Modulus of dry paper remains constant and the maximum strain value is reduced as temperature increases – the dry material follows the same stress-strain path but ruptures at lower strain values with increasing temperature (Borodulina et al. 2012; Seth and Page 1983). Kouko et al. (2014) presents the argument that the difference in behavior between the wet and dry test cases is due to a difference in failure mode. Kouko et al. (2014) argues that the stiffness of bonds is not affected by temperature but the strength is, hence the reduced strain at failure for dry materials. For the wet case, Kouko et al. (2014) suggests that the fibers themselves are softened by water leading to a loss in stiffness but not maximum strain.

The implication for the wet testing case is that because maximum strain is independent of temperature and the ultimate tensile strength is linearly proportional to temperature, the energy required to rupture a material, the area under the stress – strain curve, or toughness, is also linearly dependent on temperature.

1.2.1 Section Summary

Recall that the completeness of a repulping operation is defined by the flake content of the suspension within the repulper at any given time. All flakes, regardless of size are lumped into a single size class. Equation 1.3 is shown again for reference:

$$\frac{dF}{dt} = -kF \tag{1.3}$$

Equation 1.3 represents the breakage rate of flakes as a single size class. Recall also that the measure of flake content is a ratio of the dry mass of flakes to the dry mass of all pulp in suspension. In a batch repulping operation, the mass of pulp in suspension is constant. Equation 1.3 can then be rewritten as Equation 1.3* for a batch repulping operation:

$$\frac{dm_F}{dt} = -km_F \tag{1.3*}$$

This is the same form as Equation 1.18 if only the breakage rate of the initial size class is considered as is done in repulping. As repulper rotors operate at a constant speed, it is a reasonable assumption that they operate at a constant shaft power. Given constant shaft power Equation 1.3* becomes:

$$\frac{dm_F}{dE} = -\lambda m_F \tag{1.3**}$$

where λ is a rate constant and is equivalent then to S_i^E in Equations 1.19 and 1.20. In terms of breakage rate kinetics, repulping appears to mirror the form seen in comminution in general. The completeness of repulping then should be independent of rotor power and depend only on total energy input to a repulping process as is the case with other forms of comminution. The form of Equation 1.3** is supported by the finding by Bennington et al. (1998a) that the completeness of a repulping operation depends on the total number of rotor revolutions.

The energy use in comminution is related to measures of material toughness. Measures of material toughness represent the energy a material can absorb before failure. For the ball milling of brittle minerals, the applicable measure of toughness is fracture toughness (Austin 1984; Bearman et al. 1991; Fuerstenau and Abouzeid 2002; Napier-Munn et al. 1999; Schoenert 1972). Fracture toughness quantifies the energy for crack propagation in a high strain-rate event and thus is applicable to the ball milling of brittle minerals.

It is proposed based on the equivalency of Equations 1.18 and 1.3* and Equations 1.20 and 1.3** that the energy use in repulping is related to a measure of material toughness. A relation to fracture toughness indicates rotor-to-flake impact as a mechanism and a relation to toughness (stress-strain area) indicates another mechanism.

1.3 Stirred Mixing

Repulpers are essentially high-intensity stirred mixers. The goal of the repulping process is to create a homogeneous suspension of fibers in water from the disintegration of waste paper. The repulper rotor is responsible for the transport, and mixing of material in the repulper vat as well as for the disintegration of waste paper. As noted earlier, repulper rotors come in two basic forms, low profile rotors that operate at high speeds in low consistency pulp suspensions and tall, helical rotors for repulping high apparent viscosity pulp suspensions. As with mixers, repulpers also use baffles, and/or offset rotors and non-round vats (D-shaped) to combat solid body rotation.

Unfortunately, the true effectiveness of all of the design permutations found among repulper vats and rotors remains the domain of repulper manufacturers. At this time, the only available data addressing rotor and vat design is found in the form of industry-sponsored white papers. This is in considerable contrast to the subject of stirred mixing where a tremendous number of peer-reviewed studies have been published. Mixing/mixing impellers have been studied for a huge number of different processes, impeller types, baffle arrangements, laminar, turbulent, and transitional flow, Newtonian and non-Newtonian fluids, and for liquid-solid suspensions. The flow field within stirred mixers for various impeller types is well studied. It has been measured using laser-Doppler velocimetry (LDV), particle image velocimetry (PIV) etc. and simulated computationally.

Topics in stirred mixing reviewed here as being relevant to repulping include:

- The spatial distribution of the dissipation of rotor/impeller power by turbulence.
- The influence of mixing impeller design on the flow field within a mixer.
- Baffle/Vat design used to maintain complete mixing and vat turnover with difficult non-Newtonian fluids.

Stirred mixing processes can be segregated into two basic categories; processes that are laminar, and those that are turbulent. Stirred mixing equipment is markedly different between these two categories with relatively minor design variations within each category to account for various processes.

Laminar mixing operations are usually the result of very high fluid viscosity rather than low impeller speed (Hemrajani and Tatterson 2004). Laminar impellers are either of the anchor type, or helical type and run very close clearance to the mixing vat wall. This close clearance is needed in order to maintain bulk motion in the mixing vat as very high viscosity fluids quickly damp out momentum given to the fluid by the impeller. HC repulpers use a helical type impeller but do not run close clearance to the repulper vat wall. As noted earlier, high-consistency pulp suspensions show high apparent viscosity and the helical screw type impeller design is able to pump high viscosity fluids in a manner equivalent to a positive displacement screw pump.

In a laminar mixing operation, for instance the blending of two liquids, the impeller works to create a finely stratified mixture of fluids with diffusion completing the mixing process across the stratified layers. The stratification is achieved as the impeller continually "folds" the fluid over on itself (Dong et al. 1994; Hobbs et al. 1997; Hobbs and Muzzio 1998; Lamberto et al. 1996).

Impellers designed for turbulent mixing applications typically have blunt vanes arranged radially around a center hub. These impellers operate in lower viscosity fluids and thus are able to maintain bulk motion in the mixing vat without running close clearance to the vat walls ($D = T/3$ is common where T is the diameter of the mixing tank).

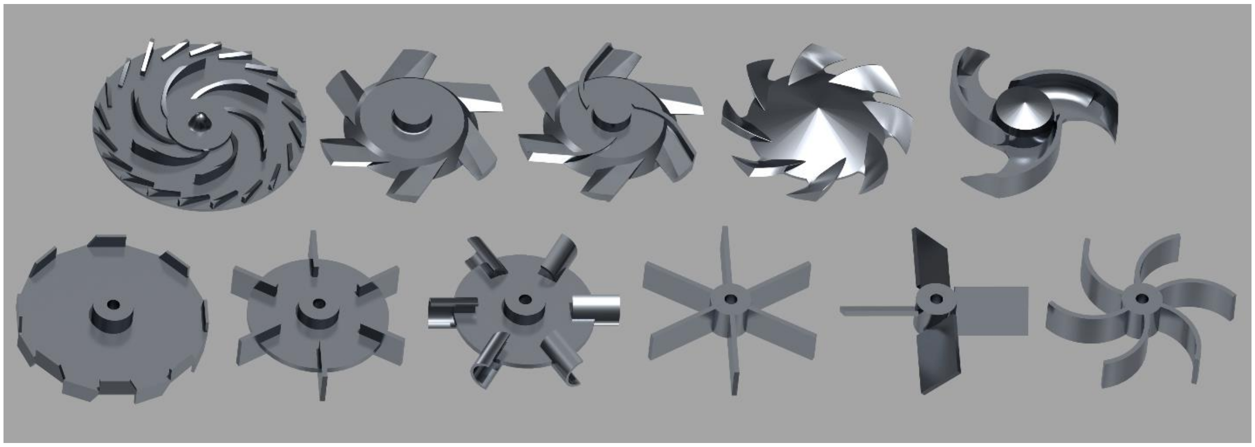

Figure 1.3: LC repulper rotors (top row) shown with common mixing impellers (bottom row) used for turbulent stirred mixing. The mixing impellers from left to right are: a sawtooth impeller, a Rushton turbine, a Scaba 6SRGT, a paddle impeller, a pitched-blade turbine, and a backswept-open impeller. All repulper rotors and mixing impellers can be considered to rotate counterclockwise from the vantage shown in the figure. Notice how similar the mixing impellers and repulper rotors are to one another.

Common repulper rotors are shown compared with common mixing impellers, in Figure 1.3. Notice how similar the repulper rotors and mixing impellers are with the only major obvious difference being that the repulper rotors are built for strength and have forgone some bluntness in this pursuit. In a turbulent blending operation of two miscible liquids for example, the blunt mixing impeller vanes produce turbulent eddies. These eddies blend the two fluids with molecular diffusion completing the mixing on scales smaller than the smallest turbulent scales. The fact that repulper rotors also employ blunt vanes suggests that turbulence is also important in repulping.

1.3.1 Spatial Dissipation of Impeller Power by Turbulence

The blunt impellers used for turbulent stirred mixing are shaped as such to produce turbulence to improve mixing rates. At the smallest scales of the mixing process – the Kolmogorov Scales, the rate of mixing depends on both the mixing action of turbulent eddies and molecular diffusion. Turbulent eddies bring the substances to be mixed together with molecular diffusion completing the mixing on scales smaller than the smallest turbulent eddies.

The turbulent flow produced by a mixing impeller has been investigated within the framework of what is known about turbulence as the mechanism(s) governing turbulent flows are complex to the point that no general theory to describe turbulence is known. Turbulent flows are identified as being highly chaotic, inertia/convection dominated flows. Turbulent flows are characterized by a high degree of mixing due to convection in the form of turbulent eddies.

Turbulent flow can be described as being made up of a hierarchal system of eddies where large scale, energy containing eddies decay to form smaller and smaller eddies in a cascading fashion (Richardson 1922; Kolmogorov 1941). At all but the very smallest flow scales, forces in the flow due to inertia dominate over those that arise from molecular viscosity. The energy in a turbulent flow is dissipated only at the very smallest scales of the flow where viscosity once again takes effect. For this reason, the flow Reynolds number, being a comparison between the inertia of a flow to flow viscosity, can be correlated with the onset of turbulent flow, albeit only empirically at this time. The Reynolds Number for a mixing impeller is defined as:

$$Re = \frac{\rho N D^2}{\mu} \tag{1.21}$$

where ρ is the process fluid density, N is the rotor speed in revolutions per second, D is the impeller diameter, and μ is the process fluid viscosity.

Turbulent operation of an impeller can be determined through a comparison of the impeller power number (N_P) with the impeller Reynolds number. The impeller power number is defined as:

$$N_P = \frac{P}{\rho N^3 D^5} \tag{1.22}$$

where P is the impeller shaft power. The impeller Power Number acts as a “drag coefficient” for the impeller and contains terms for dynamic pressure (ρN^2) and geometry (impeller diameter-D). Plotting N_P versus Re for an impeller results in a curve like that shown in Figure 1.4.

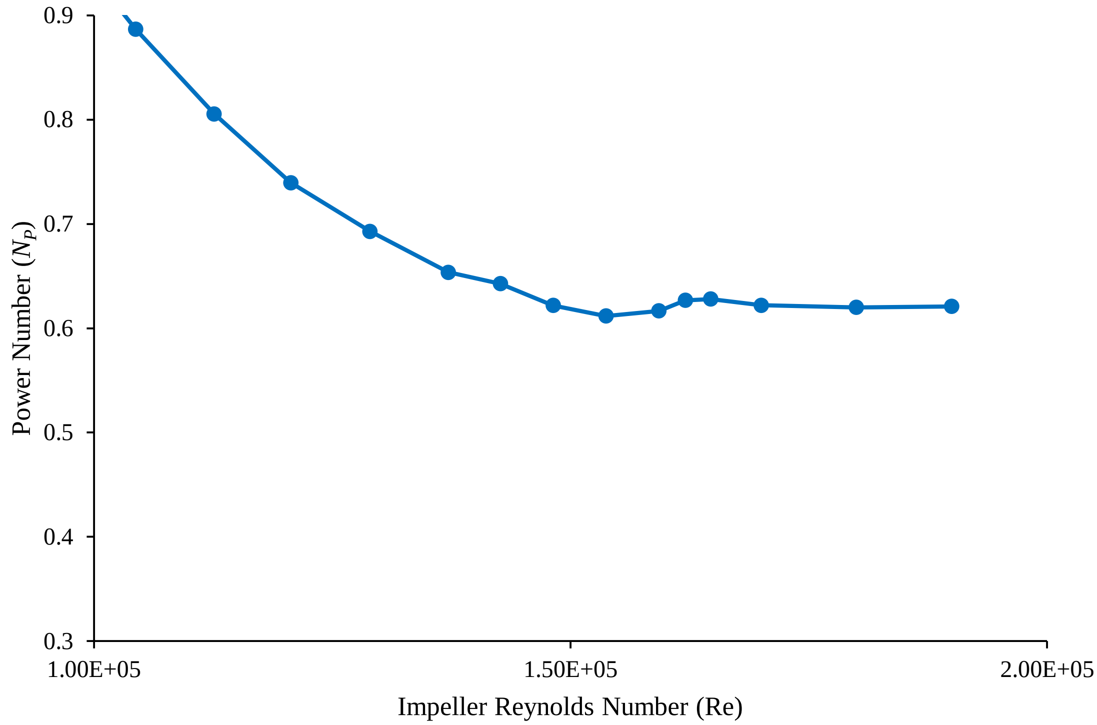

Figure 1.4: Plot showing Reynolds independence for a high-speed impeller. This data was measured by the author in a small laboratory mixer having a paddle impeller.

In the laminar and transitional flow regions, N_P varies with Re by:

$$N_P \propto \frac{1}{Re} \tag{1.23}$$

The impeller power number is a comparison between the total impeller power from both viscous and pressure drag and a dynamic pressure x geometry/flow inertia quantity (the denominator in Equation 1.22). Thus, the point at which the impeller power number becomes invariant with increasing impeller Reynolds number signifies the point where forces in the flow due to flow inertia dominate over forces due to fluid viscosity. The effect of viscosity after this point is negligible at all but the smallest scales of the flow. The flow regime correlating to the independence of impeller Power number with increasing Reynolds number is said to be fully turbulent.

The very smallest scales in a turbulent flow, the Kolmogorov Scales (n) are defined by:

$$n = \left(\frac{v^3}{\varepsilon}\right)^{\frac{1}{4}} \tag{1.23}$$

where v is kinematic viscosity and ε is the power dissipation per unit mass (Kolmogorov 1941). The rate of mixing is enhanced with increasing dissipation as the turbulent eddy length scale is reduced.

The rate of dissipation of impeller shaft power by turbulence varies spatially in a stirred mixer. The distribution of energy dissipation is extremely important in mixing. The point of highest dissipation is almost always the optimum feed point for chemicals undergoing fast reactions; the size distribution of bubbles or drops in multiphase systems is also greatly determined by the spatial variation of ε (Assirelli et al. 2002; Assirelli et al. 2005; Baldi and Yianneskis 2004; Wu and Patterson 1989; Yang et al. 2013; Zhou and Kresta 1998). For these reasons, the magnitude and spatial distribution of ε has been widely studied for stirred mixers.

A number of researchers have measured the spatial variation of turbulent dissipation in mixers for a number of impeller types using optical techniques such as laser-Doppler anemometry (LDA) and particle image velocimetry (PIV). A number of researches have also estimated the spatial dissipation using computational fluid dynamics (CFD).

Estimation of the spatial dissipation by turbulence has historically proven difficult. The dissipation in turbulent flows occurs at the very smallest scales of the flow, the Kolmogorov Scales. For all but very low Reynolds number flows, neither velocimetry nor simulation can resolve the smallest flow scales. Therefore models which enable estimates of the turbulent dissipation to be made from coarse velocity fields must be created. However, at present the complexity of turbulent fluid motion has prevented the formation of a general theory with which to explain it. As such, models for turbulence must invariably be implemented with simplifying assumptions.

In terms of the measurement of the dissipation in a stirred mixer using optical velocimetry methods, Kresta and Wood (1993) give a detailed overview of common methods used for the estimation of turbulent dissipation from coarse velocity fields. To give at least one example here, a common method used for estimating dissipation rates from the coarse velocity fields obtained from optical velocimetry methods uses the dimensional argument:

$$\varepsilon = A\frac{u'^3}{L} \tag{1.24}$$

where u' is a measured velocity fluctuation, L is the integral scale for the flow, and A is a proportionality constant which is known to be approximately equal to 1 for isotropic turbulence (Batchelor 1970; Cutter 1966; Kresta and Wood 1993; Wu and Patterson 1989). The validity of this scaling argument is that the rate of dissipation is determined by the large, energy containing scales - the integral scales or "L" in Equation 1.24 of the flow rather than microscales where dissipation actually occurs. The viscous scales can rapidly dissipate any amount of energy sent down the turbulent energy cascade from the integral scales as the viscous scales operate on a very small time scale t_k (Brodkey 1975; Hinze 1987; Kolmogorov 1941; Kresta and Wood 1993; Laufhutte and Mersmann 1985):

$$t_k = \left(\frac{\nu}{\varepsilon}\right)^{\frac{1}{2}} \tag{1.25}$$

Because of the different methods for the estimation of dissipation rates from coarse velocity fields, and depending on the velocimetry technique, estimates of the rate of dissipation differ among researchers. It has been reported that dissipation rates near mixing impellers are 20-140 times that of the average dissipation rate in the vat for various mixing impellers (Calabrese and Stoots 1989; Cutter 1966; Wu and Patterson 1989; Zhou and Kresta 1996).

Advances in computing power and turbulence modeling techniques have made CFD simulations an attractive alternative by which to estimate the flow field and dissipation in stirred mixers. CFD also allows for the freedom to study various impeller and vat geometries and mixing processes including blending, chemical reactions, and flocculation (Joshi et al. 2011). However, CFD has limitations imposed by available computing power and by our lack of complete understanding of turbulence.

The estimated dissipation rates in stirred mixers varies greatly depending on the chosen CFD modeling technique. For stirred mixers at high Reynolds numbers, either the Reynolds Averaged Navier-Stokes (RANS) or Large Eddy Simulation (LES) methods are applicable at this time.

With RANS, time averaged quantities are resolved and turbulence is modeled for all scales of the flow. To this end, a number of turbulence models have been proposed. A description of RANS and the basic principles of turbulence modeling is given in White (2003) among many other sources. However, the accuracy of RANS simulations is hindered by our incomplete understanding of turbulence which limits our ability to create completely accurate turbulence models for the closure of the RANS equations.

There are many turbulent stirred mixer simulations reported in peer reviewed literature employing the RANS technique along with an eddy-viscosity based 2-equation turbulence model. Two equation eddy-viscosity models treat all turbulent scales as being isotropic.

The standard $k - \varepsilon$ model (Launder and Spalding 1974) is possibly the most common model used in engineering applications and many of the stirred mixer simulations reported in peer-reviewed literature use this model. RANS in conjunction with a 2-equation turbulence model has proven to be a good compromise in terms of simulation accuracy versus computing expense for many engineering problems. This approach has been shown to evolve important flow features in stirred mixers including the important impeller trailing/tip vortices (these important vortices are expanded upon shortly) for various impeller types including the Rushton turbine and pitched-blade turbine (Joshi et al. 2011).

The 2-equation turbulence models have proven to underestimate the turbulence dissipation rate in stirred mixers. Authors historically report that the $k - \varepsilon$ model under-predicts the turbulent kinetic energy and dissipation for both Rushton turbines and pitched blade turbines by up to 50% (Fokema and Kresta 1994; Javed et al. 2006; Kresta and Wood 1991; Kumaresan and Joshi 2006; Lee et al. 1996; Ng et al. 1998; Nogueira et al. 2012; Ranade 1997; Ranade 2001; Venneker and van den Akker 1997).

The Reynolds Stress Model (RSM) offers a theoretical improvement over the 2-equation eddy-viscosity models in that all six Reynolds stresses are modeled and the isotropic eddy-viscosity hypothesis of the 2-equation models is abandoned. RSM models better account for phenomena seen in complex flows than do 2-equation models. These phenomena include streamline curvature, swirl, rotation, and rapid changes in strain-rate. The RSM models seem ideally suited for the application of modeling the flow in stirred mixers. However, the drawback of RSM models is the greater number of assumptions required for turbulence closure.

Studies published comparing the performance of RSM models to 2-equation models for the modeling of stirred mixers showed that RSM models out-performed the 2-equation models in this application (Bakker and van den Akker 1994; Murthy and Joshi 2008; Oshinowo et al. 2000).

The LES method differs from the RANS approach in that with LES, the large scales of the flow are directly simulated and the small scales, or sub-grid scales (SGS) are modeled using an isotropic eddy-viscosity approach. This is in contrast to the RANS approach in which ensemble averaged quantities are resolved and all scales of turbulence are modeled.

Common methods for modeling the SGS eddy-viscosity are the WALE (Nicoud and Ducros 1999), Smagorinsky (Smagorinsky 1963), and the Dynamic Smagorinsky-Lilly models (Germano et al. 1991). The LES approach requires extensive computing resources compared to RANS. In wall-bounded flows, the length scales in turbulent boundary layers are very small meaning a very fine mesh is required with LES.

As applied to stirred mixers, a number of studies have shown that the LES approach provides superior accuracy compared to the RANS approach (Derksen and van den Akker 1999; Fan et al. 2007; Hartmann et al. 2004; Jahoda et al. 2007; Joshi et al. 2011; Murthy and Joshi 2008; Soos et al. 2013; Yeoh et al. 2005; Zadghaffi et al. 2010). Velocity field and turbulent kinetic energy predictions have been shown to agree well with experimental values (within a 15% error window for turbulent kinetic energy.)

Values measured for $\varepsilon_{max}/\bar{\varepsilon}$ using optical techniques range from 20 – 140 (Zhou and Kresta 1996). Values reported for $\varepsilon_{max}/\bar{\varepsilon}$ from LES are as high as 400 (Soos et al. 2013). Despite the disagreement among the reported values for $\varepsilon_{max}/\bar{\varepsilon}$, the consensus among researchers is that the dissipation of impeller shaft power by turbulence is very high near the impeller compared to in the rest of the vat.

For the aforementioned reasons, it is considered good practice when scaling micromixing performance between mixers of different sizes and geometries to scale based on constant power per unit mass within the impeller swept volume (Kresta and Brodkey 2004):

$$\varepsilon = \frac{P}{\rho V_{Swept}} \tag{1.26}$$

where V_{Swept} is the impeller swept volume.

Another common scaling method for scaling stirred mixing operations is to replace V_{Swept} in Equation 1.26 with V_{Vat}, the volume of the entire mixing vat. This has been shown to work well when the bulk flow characteristics in a mixer dominate the mixing process but is not accurate when there is high dissipation of impeller power in the vicinity of the impeller (Kresta and Brodkey 2004).

The actual flow field produced by various impeller types is dominated by the presence of trailing/vane-tip vortices caused by the blunt vane shapes used by mixing impellers. The majority of the dissipation of impeller power via turbulence occurs within these trailing/tip vortices and as such it is widely accepted that the majority of mixing in a stirred vessel is accomplished by these vortices (Kresta and Wood 1993).

The location and intensity of the trailing/tip vortices has been intensively studied for common impeller types including the Rushton turbine, pitched blade turbine, propeller and for hydrofoil types. All of these impeller types produce strong trailing/tip vortices despite a range of power number operation from $N_P = 0.30$ for the hydrofoils to $N_P = 5.20$ for a 6-balded Rushton turbine (Rushton and Costich 1950; Weetman and Oldshue 1988; Weetman and Coyle 1989).

The Rushton turbine produces a pair of trailing vortices behind each vane. A pair of counter-rotating vortices is produced due to the presence of the disk separating the top and bottom halves of each vane (Lee and Yianneskis 1998; Nienow and Wilson 1974; Sharp and Adrian 2001; Stoots and Calabrese 1995; Van't Riet and Smith 1975; Yianneskis et al. 1987; Yianneskis and Whitelaw 1993).

Similar findings have been made for other common impeller types including the pitched-blade turbine and hydrofoil type impellers. Both of these impeller types produce strong trailing/vane-tip vortices with a large portion of the impeller shaft power being dissipated in these vortices (Jaworski et al. 2001; Kresta and Wood 1993; Shafer et al.1998; Shafer et al. 2000; Shekhar et al. 2012).

Blending is often used as a metric for comparing the micromixing performance of various impeller types. Cooke et al. (1988), Ruszkowski (1994) and Voncken et al. (1964) all reported that the dimensionless blend time (θ_m) is proportional to the impeller and tank diameters by:

$$\theta_m \propto \left(\frac{D}{T}\right)^{-2} \qquad (1.27)$$

Ruszkowski (1994) reported that blending time is inversely proportional to turbulent diffusion by:

$$\theta_m \propto \left(\frac{\varepsilon}{L^2}\right)^{-\frac{1}{3}} \qquad (1.28)$$

where L is the turbulence integral length scale.

For fully turbulent impeller operation, the dimensionless blend time has been shown to be proportional to the total number of impeller revolutions:

$$\theta_m \propto N\Delta t \qquad (1.29)$$

where Δt is the total mixing time (Hartog 1967; Hoogendoorn and den Hartog 1967; Kramers et al. 1953; Khang and Levenspiel 1976; Prochazka and Landau 1961; Sano and Usui 1987). The dimensionless blend time is independent of Reynolds number and Froude number.

Nienow (1997), suggested that the integral length scale in Equation 1.27 be the vat diameter rather than the more commonly used impeller diameter (e.g. Brodkey 1975; Cutter 1966). His argument for the use of the vat diameter as the relevant turbulence length scale is that the mixing rate is limited by the low dissipation levels away from the impeller in the rest of the vat. He used this argument, and Equations 1.27, 1.28, and 1.29 to derive a model for the turbulent blend/mixing time:

$$\theta_m \propto \left(\frac{1}{\varepsilon}\right)^{\frac{1}{3}} \left(\frac{T}{D}\right)^{\frac{1}{3}} T^{\frac{2}{3}} \tag{1.30}$$

This model makes no distinction for impeller type and in fact, as shown by Nienow (1997), impeller type has no bearing on blend time in the fully turbulent flow regime – only impeller specific power input determines blending time. Two different impellers will produce the same blend time for equal specific power inputs. Adherence to Equation 1.30 has been shown for the Rushton turbine, Prochem Maxflow T, Scaba 6SRGT, and Lightnin A310. This finding is supported by Langheinrichet al. (1998).

This finding shows that all impellers are equally energy efficient and achieve the same blend time at the same power per unit mass (ε). Increasing the relative size of the impeller to that of the tank will result in reduced blend time for a given specific power input.

1.3.2 Vat and Baffle Design

Repulper rotors are mounted very close to the bottom of repulper vats. Repulper rotors typically clear the extraction plate by only 5-10mm (Holik 1988). The effect of rotor/impeller to vat bottom clearance in repulping is not well studied. However, the effect of rotor/impeller to vat bottom clearance on the overall flow pattern in stirred mixers is well studied.

Repulpers can be found with a number of different baffle shapes and baffle arrangements. Repulpers can also be found having eccentrically-mounted rotors and non-cylindrical vat shapes. In stirred mixing, the vat and baffle designs greatly influence impeller and mixing performance. This is also likely the case for repulping.

1.3.2.1 Large Scale Flow Patterns in Stirred Mixers

Mixing impellers are either designed to be axial or radial pumping. Common axial types include the pitched blade turbine, hydrofoil, and marine propeller. Common radial types include the basic paddle type impellers and the aforementioned Rushton turbine. As the name suggests, axial type impellers have pitched vanes and direct flow along the impeller drive-shaft axis. Axial flow impellers can be operated in either down-pumping (toward the vat bottom) or up-pumping (toward the free-surface) modes. With radial flow type impellers, fluid enters the domain of the impeller from the axial direction and is expelled radially from the impeller.

The flow field produced by both axial and radial flow impeller types is greatly affected by the mixing vat shape and baffle arrangement. The majority of published research is for impellers operating within cylindrical vats along with standard baffling (baffles are discussed in detail further on) and so all cited literature studies listed here are for this arrangement unless otherwise stated.

The flow field in a cylindrical mixing vat with standard baffling is greatly affected by the clearance between the impeller and vat bottom – termed “off-bottom clearance”. The flow field in a cylindrical mixing tank having standard baffling is also affected by the impeller diameter to vat/tank diameter ratio- D/T.

Radial flow impellers are signified by their characteristic “double-loop” flow pattern. Axial type impellers are characterized by a “single-loop” flow pattern. Both of these patterns are shown in Figure 1.5.

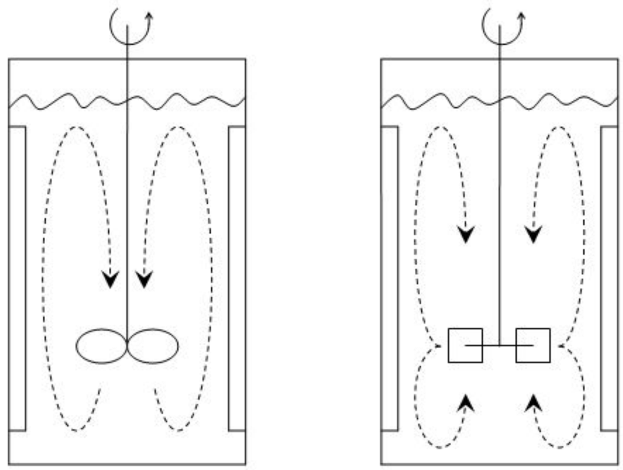

Figure 1.5: Bulk flow patterns in stirred mixers. The "single-loop" pattern is shown at left while the "double-loop" pattern is shown at right.

Off-bottom clearance has a significant effect on these patterns. For radial flow impellers, decreasing the off-bottom clearance past a certain point changes the flow pattern from the characteristic “double-loop” to the “single-loop” pattern seen with axial flow impeller types (Ibrahim and Nienow 1996; Montante et al. 1999). Accompanying the change in flow pattern is a reduction in impeller power number and impeller pumping number.

The “single-loop” flow pattern of an axial flow impeller can become the radial flow “double-loop” pattern by increasing the impeller diameter relative to the tank diameter. Zwietering (1957) found that for a 3-blade marine propeller when $D/T > 0.45$, the flow pattern changes to mimic the “double-loop” pattern characteristic of a radial flow impeller.

1.3.2.2 Baffles

Baffles are necessary in most stirred mixing operations. Mixing vessels are usually cylindrical with centrally mounted impellers. With this arrangement, baffles are required to prevent solid-body rotation of the processes fluid. Interestingly, baffles have a direct impact on impeller power number. With an un-baffled or under-baffled vessel, the condition of Reynolds independence may not achievable (Bates et al. 1966) as illustrated by Figure 1.6.

Adding baffles to a stirred mixer has the effect to increase the impeller power number. Adding a single baffle to an un-baffled mixing vessel generally results in a large gain in impeller power number. Diminishing returns are realized for the addition of more baffles (Myers et al. 2002). The increase in impeller power number from the addition of baffles results as baffles convert solid body motion in the circumferential direction around the mixing vessel to either radial or axial motion, depending on the impeller type.

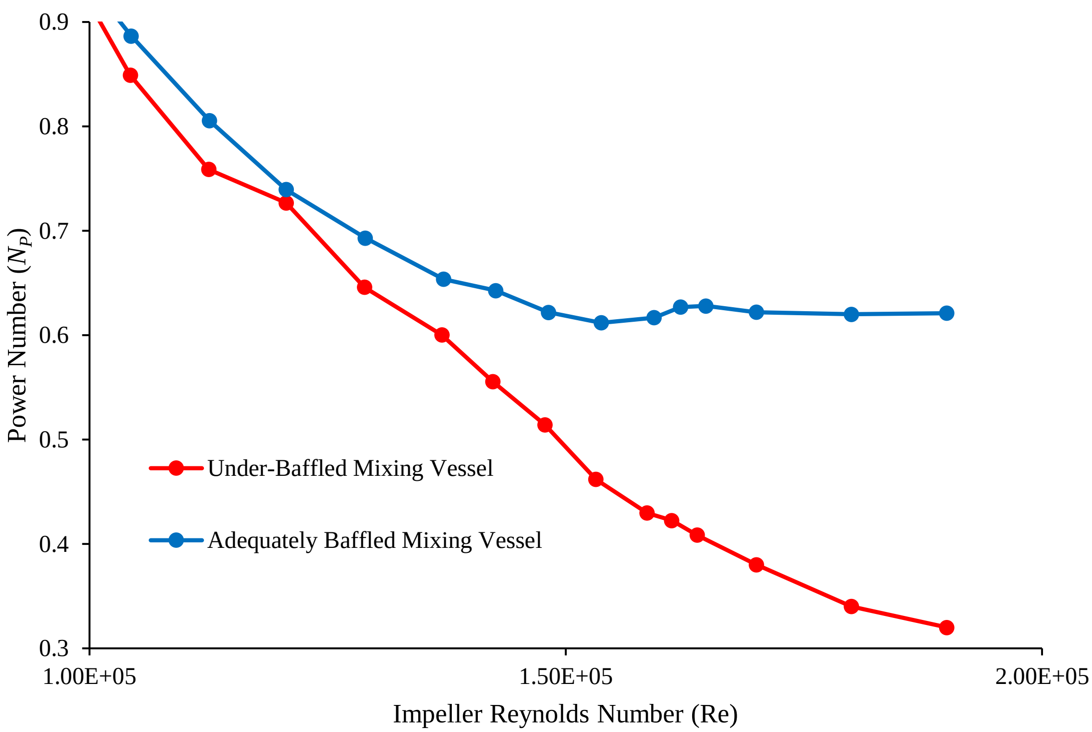

Figure 1.6: Power number versus Reynolds number curves compared for the case of a high-speed impeller operating in an adequately baffled mixing vessel and the case for the same high-speed impeller operating in an under-baffled vessel. The condition of Reynolds independence cannot be achieved without adequate baffling. The solid-body fluid swirl arising from under-baffling results in poor mixing. The data for the above plots was collected by the author in a laboratory scale stirred mixer having a paddle impeller.

Standard baffling consist of 4 baffles arranged in 90° increments around the mixing vessel. These baffles consist of flat plates $^{1}/_{10}$ of the vessel diameter wide having ¼ of a baffle width clearance to the vessel bottom. This arrangement has been shown for a number of stirred mixing processes to maximize impeller Power number with the addition of further baffles being inconsequential (Myers et al. 2002).

Standard baffles are not used in all mixing operations. Square and rectangular vessels provide a baffling effect by virtue of their shape. Side entering impellers also may not require baffles. Stirred mixing of filamentous suspensions requires the substitution of triangular, or semicircular baffles in place of the flat plates used in the standard baffling arrangement. Suspended filaments can hang up on the edges of the flat plates or stagnate to create dead zones behind them (Myers et al. 2002).

There are various mixing operations where the use of baffles is undesirable. In the food and pharmaceutical industries, for instance, baffles are often not used for cleanliness reasons (Assirelli et al. 2008). Baffles can also create regions of stagnation when mixing involves fluids having high apparent viscosity and/or yield-stress behavior (Bates et al. 1966). Two methods are used to combat swirl in un-baffled systems: 1) Off-center/eccentric mounting of the mixing impeller in cylindrical mixing tanks; 2) Non-cylindrical tank shapes.

Eccentric mounting of an impeller in an un-baffled cylindrical tank can yield performance very close to that of an impeller centrally mounted in a fully baffled tank. Kramers et al. (1953) showed that an eccentrically located propeller in an un-baffled cylindrical tank could draw 90% of the power it could draw in a fully baffled cylindrical tank. For turbulent mixing, better mixing efficiency is achieved the farther off-center an impeller is located (Karcz et al. 2005).

Mixing times for turbulent mixing in square tanks have been shown to be very close to that for cylindrical tanks with standard baffling. Kresta et al. (2006) measured mixing times for 4 different impellers (flat-blade turbine, pitched-blade turbine, Lightnin A310, and HE3) in different sized square and fully-baffled cylindrical tanks. The mixing times were found to be very close between the square and fully-baffled cylindrical tanks for all impellers.

Stirred mixing in non-Newtonian fluids is complicated by cavern formation around the mixing impeller as many non-Newtonian fluids, including pulp, show yield-stress behavior. Cavern formation occurs around a mixing impeller when the fluid shear-stress falls below the fluid yield-stress some distance away from the impeller.

Cavern formation in pulp suspensions has been shown by Bhole et al. (2011) to be well predicted by the model proposed by Hui et al. (2009), which is a modified form of the axial force model proposed by Amanullah et al. (1998). This model uses the axial force produced by an impeller to predict cavern size in the shape of a cylinder. Cavern formation in pulp suspensions has also been shown to be well predicted through the use of CFD simulations where pulp is modeled as a Bingham Plastic fluid (Bhole et al. 2009; Bhole et al. 2011; Ford et al. 2006).

1.3.3 Section Summary

The dissipation of impeller power by turbulence in a stirred mixer is essentially accomplished within the vicinity of the mixing impeller. For this reason, it is considered good practice to scale stirred mixing operations based on the impeller power dissipated in the impeller swept volume according to Equation 1.26 (Kresta and Brodkey 2004). Repulper rotors employ similarly blunt shapes to those used by mixing impellers. Repulper rotors also operate at high speeds. It is reasonable to assume that the spatial dissipation of repulper rotor power is limited to the immediate vicinity surrounding the repulper rotor as it is with mixing impellers. Therefore, it may be possible to scale performance between repulpers based on Equation 1.26 as well.

The actual flow field produced by various impeller types is dominated by the presence of trailing/vane-tip vortices caused by the blunt vane shapes used by mixing impellers. The majority of the dissipation of impeller power via turbulence occurs within these trailing/tip vortices and as such it is widely accepted that the majority of mixing in a stirred vessel is accomplished by these vortices (Kresta and Wood 1993). Repulper rotors use vanes of similar shapes to those used by mixing impellers. It is likely that repulper rotors also produce powerful trailing vortices and that these vortices may be responsible for repulping.

Repulper rotors run very close clearance to the extraction plate at the bottom of the repulper vat. Typical clearances range from 5-10mm. This suggests that any repulper rotor design will produce a “single-loop” flow field when run so close to the repulper vat bottom.

Baffles convert swirling fluid motion within a mixer to axial and/or radial motion. Baffles have a direct effect on impeller power number. With an under-baffled vessel, the condition of Reynolds independence may not be achievable (Bates et al. 1966). The solid-body swirling motion arising from under-baffling results in poor mixing. Evidence produced by Bennington et al. (1998a) suggests that repulping occurs at the repulper rotor only and not in the rest of the repulper vat. If this is the case, then an under-baffled repulper should be less efficient than a properly baffled repulper. Therefore, the efficiency of a repulper will depend not only on individual rotor design, but on the rotor and vat as a system. The combination of the two will determine the rotor power number and proper vat turnover in a repulper as it does in a stirred mixer.

Repulpers can be found having triangular baffles, non-cylindrical vat shapes, and eccentrically mounted rotors. In this regard, repulpers show the designs seen in mixers which enable the mixing of difficult to mix non-Newtonian fluids like polymer melts.

Pulp suspensions show yield stress. There are no studies specifically dealing with cavern formation in repulping although direct conversation with repulper operators by the author reveals that cavern formation and maintaining vat turnover is a problem with repulping.

1.4 Pulp Rheology

Repulper rotors operate at high speeds. LC repulper rotors, if run in water, would operate at Reynolds numbers of $Re > 10^6$. One the other hand, the flow on the free surface of a repulper is often stagnant due to the high apparent viscosity yield/stress behavior of pulp suspensions. It would appear then, that the range of shear-rates/stresses within a repulper varies considerably. The rheology of pulp suspensions is non-Newtonian and extremely complex. Unfortunately, due to this complexity, the rheology of pulp suspensions is still not totally understood. However, considerable research is available and a selection of it, thought pertinent to repulping is reviewed below in order to gain further insights into the repulping process.

Pulp suspensions are made up of a somewhat heterogeneous mix of wood fibers suspended in water. The addition of wood fibers to water gives rise to a suspension having highly complex rheology. Pulp suspensions can exhibit yield-stress behavior, can be shear-thinning, and can behave as a Newtonian fluid. Pulp suspensions also can be viscoelastic and thixotropic. The behavior of a pulp suspension depends on the concentration of the fibers in suspension, the physical properties of the fibers in suspension, and the flow conditions within the suspension.

Wood fibers are hollow tubes made up of spiral-wound cellulose fibrils. The properties of wood fibers can vary by tree species, by tree growth conditions (climate), by harvesting method (i.e. chemical vs. mechanical pulping), and of course by natural variation among fibers. Typically, wood fibers are 1-3mm in length and 15-30μm in diameter (Derakhshandeh et al. 2011). Wood fibers are not rigid, but elastic, lending pulp suspensions to behave in a viscoelastic manner.

In the most basic sense, the behavior of pulp suspensions can be described by suspension consistency, C_m as defined by Equation 1.1. Pulp suspensions are classified as being low-consistency for $C_m \leq 8\%$, medium consistency for $8 < C_m \leq 20\%$, high-consistency for $20 < C_m \leq 40\%$, and ultra-high-consistency for $C_m > 40\%$ (Kerekes et al. 1985). The consistency measurement finds standard use used in the pulp and paper industry. For those experienced working with pulp suspensions, consistency – although itself a quantitative measurement, gives a qualitative idea of the properties of a pulp suspension. For instance, very low consistency pulp suspensions ($C_m < 1\%$) are "thin", behave as dilute, and flow easily like water. As consistency increases, pulp suspensions "thicken" and can form clumps and even show yield-stress behavior and solidify.

Commercial rheometers typical employ a small gap with smooth walls. Complex fluids having suspended particles and/or are made up of long-chain molecules may be able to form agglomerations which can be problematic for these rheometers. Suspended particles and/or agglomerations of particles or large molecules can jam within the small gaps and slip on the smooth walls of typical rheometers. The fibers within pulp suspensions are large enough to jam within the small gaps employed in standard rheometers (Derakhshandeh et al. 2011). Another problem is that even in the absence of jamming, the narrow gap typical to rheometers aligns fibers parallel to the gap walls thereby giving an unrealistic picture of the pulp rheology (Damani et al. 1993; Swerin et al. 1992). Wood fibers in suspension also can network to form structures called flocs which are on the order of 1cm in diameter (Kerekes et al. 1985). Flocs have a profound impact on the behavior of pulp suspensions and are much too large to form within the small gaps used in commercial rheometers. Flocs can also slip along walls in shear flows. The smooth walls used by viscometers and rheometers facilitates this slip (Derakhshandeh et al. 2011).

Researchers in the past have used modified rheometers to tackle the problems caused by difficult fluids such as pulp suspensions. These rheometers use larger gaps along with either roughened (Damani et al. 1993; Swerin et al. 1992), or vaned walls to combat wall slip (Bennington et al. 1990; Derakhshandeh et al. 2010; Duffy and Titchener 1975; Ein-Mozaffari et al. 2005; Gullichsen and Harkonen 1981; Head 1952; Thalen and Wahren 1964).

Derakhshandeh et al. (2010) used a large-gap rheometer with vaned walls to determine that the viscosity function for pulp suspensions is well described by the Herschel-Bulkley model:

$$\tau = \tau_y + K\dot{\gamma}^n \tag{1.31}$$

where τ is the fluid shear-stress, τ_y is the fluid yield-stress, K is the viscosity consistency, and n is the shear index.

The behavior of pulp suspensions varies by species, pulping method, and concentration. Derakhshandeh et al. (2010) determined the Herschel-Bulkley model (Herschel and Bulkley 1926) constants for four different pulp types - softwood bleached kraft (SBK), hardwood (HW), thermomechanical pulp (TMP), and stone-ground wood (SGW) - for consistencies ranging from 1-5%.

Derakhshandeh et al. (2010) found that both the yield-stress and the viscosity consistency correlated with fiber length. The long fiber SBK showed both the greatest yield-stress and viscosity consistency while the short fiber SGW showed the lowest value for each parameter. For each pulp type, increasing the suspension consistency resulted in an increase in both yield-stress and viscosity consistency. Interestingly, the shear index, n, increased slightly with increasing suspension consistency but was invariant with pulp type. At very high shear-rates correlating with the onset of turbulence, Derakhshandeh et al. (2010) found that the Herschel-Bulkley model no longer applied and that the pulp suspensions behaved as Newtonian fluids.

Despite the efforts of a number of researchers, a consistent characterization of the rheology of pulp suspensions remains elusive. This scenario is demonstrated by attempts at quantifying the yield-stress of pulp suspensions. Typically, no sharp, clear transition from the yield-stress condition to the flowing condition is seen on shear-stress versus shear-rate plots for non-Newtonian fluids. This leads to different ways of defining the yield-stress condition. Common definitions include the Apparent Yield-stress, Maximum Viscosity, and Ultimate Shear Strength definitions.

The apparent yield-stress definition involves extrapolating back to the zero shear-rate point on the shear-stress versus shear-rate plot by drawing a straight line back to the vertical plot axis from the point where complete flow is achieved. This method changes the plot shape to mimic that for a Bingham fluid in order to give a clear indication of the transition from the yield-stress condition to the flowing condition.

The maximum viscosity definition defines yield-stress as the stress at which a fluid’s apparent viscosity is highest.

The ultimate shear strength definition defines yield-stress as the maximum stress in a fluid as observed when shear-stress is increased from zero to initiate flow.

Researchers in the past have used either one of two methods to determine the yield-stress of pulp suspensions – conventional rheometry using a modified large-gap vaned rheometer as described earlier or by measuring the stress required to break up a plug flow of pulp in a pipe.

Reported yield-stress values for SBK pulp suspensions at C_m=3% range from 19.3 to 350 Pa (Bennington et al. 1990; Dalpke and Kerekes 2005; Damani et al. 1993; Derakhshandeh et al. 2010; Ein-Mozaffari et al. 2005; Swerin et al. 1992; Wikstrom and Rasmusen 1998). Large differences in yield-stress are reported even between researchers using the same measurement methods and the same definition of yield-stress which highlights the difficulty in characterizing the rheology of pulp suspensions.

Finished paper is made up of an interwoven matt of fibers (although for the case of dry, finished paper, the matt is predominantly held together by hydrogen bonds). The large aspect ratio possessed by wood fibers accommodates contact with a large number of other fibers while the elastic nature of fibers allows fibers to lock together once intertwined.

The propensity of fibers to interact while in suspension can be described by the fiber crowding number. As an extension of the early work by Mason (1950), Kerekes et al. (1985) defined the crowding number (N) as the number of fibers existing within the volume swept out by the length of a single fiber.

For N=1, fiber-to-fiber contact occurs but the suspension still behaves as dilute (Kerekes et al. 1985; Mason 1950). The point at which N=16 is referred to as the "gel crowding number" (Martinez et al. 2001, 2003). At this point, significant fiber-to-fiber contact occurs but not to the point where structures with mechanical strength are formed. Instead, this significant contact results in the suspension behaving as a continuous gel, hence the name. The point at which fibers interact to form agglomerations with mechanical strength is when N=60 (Soszynski and Kerekes 1988). At this crowding number, fibers can be fully constrained by forming 3-point contacts with one another.

The crowding number can be estimated from the suspension consistency by:

$$N \approx 5C_m \frac{L^2}{w} \tag{1.32}$$

where C_m is the suspension consistency, L is the fiber length, and w is the fiber weight per unit length, also called coarseness (Kerekes and Schell 1992).

The networking of fibers is what gives pulp suspensions yield-stress behavior. Fiber networking also results in the formation of flocs. Flocs are local fiber aggregates on the order of 1cm in diameter that have mechanical strength and are suspended in the pulp suspension along with the individual fibers (Kerekes et al. 1985).

In fully turbulent flow, pulp suspensions can behave as Newtonian fluids (Derakhshandeh et al. 2010; Bennington and Kerekes 1996). In the turbulent flow regime flocs are broken up and fibers are thought to be floated in suspension in an analogous manner to that of solid particles suspended in a fluidized bed. Pulp suspensions in this fluidized state behave as a continuous Newtonian fluids. This allows for a fluidized pulp suspension to be pumped in a centrifugal pump.

Achieving fluidization is important to allow the efficient pumping and mixing of pulp suspensions. The onset of fluidization can be correlated with the specific power dissipation in the suspension. Bennington and Kerekes (1996) give the requirement for fluidization as:

$$\varepsilon_f = 7.7 \times 10^3 C_m^{2.2} \tag{1.33}$$

where ε_f is the power dissipated per unit mass of suspension and again, C_m is the suspension consistency.

There has been some research toward understanding the interaction between fibers and turbulence but only for very dilute suspensions (e.g. Olson and Kerekes 1998; Olson 2001; Olson et al. 2004; Parsheh et al. 2005). The behavior at the fiber level for dense suspensions in a complicated 3-dimensional turbulent flow is not well characterized.

1.4.1 Section Summary

Repulper vat design appears to reflect attempts to deal with the difficult rheology of pulp suspensions, particularly the yield-stress behavior. Rounded and triangular baffles are used in place of flat plate type baffles to inhibit the formation of dead zones resulting from the high apparent viscosity and yield-stress behavior of pulp. Non-circular vats without baffles or eccentrically mounted rotors with baffles are also used to avoid the same problem (*Pulping of Secondary Fiber* 1990).

As mentioned in the lead paragraph of this section, repulper rotors operate at high speeds – speeds likely fast enough to qualify repulper rotors as turbomachines. In water, LC repulper rotors would operate with Reynolds numbers of $Re > 10^6$ and the flow produced by LC repulper rotors could be assured to be highly turbulent based on this alone. However, repulper rotors operate in pulp suspensions and the nature of the flow produced by a repulper rotor cannot be known with such certainty based only on the high-speed operation of LC repulper rotors. Equation 1.33 though can be used to provide a better estimate of the flow conditions in the vicinity of a repulper rotor.

A recommended best scaling practice for turbulent stirred mixing, is to scale mixing performance between mixers by assuming a mixing impeller's power is dissipated within the impeller swept volume as per Equation 1.26. If the same is applied to a repulper rotor, the condition of fluidization can be checked for. Take, for example, a medium sized industrial repulper having a 1.5m diameter rotor and a 500hp motor. LC repulper rotors are low profile so using an estimate of 0.15m for the height of the rotor is not unreasonable. The specific dissipation within the rotor swept volume, taking 300hp to be conservative, is:

$$\varepsilon_V = \frac{P}{V_{Swept}} = \frac{300hp \times 746\,\frac{W}{hp}}{\frac{\pi}{4}(1.5)^2 \cdot 0.15} = 8.4 \times 10^5 \frac{W}{m^3}$$

For a 5% consistency pulp suspension, the power required for fluidization according to Equation 1.33 is:

$$\varepsilon_F = 2.66 \times 10^5 \frac{W}{m^3}$$

Given the above, the flow around an LC repulper rotor is likely fluidized and this suggests that LC repulper rotors are operating with sufficient intensity to produce highly turbulent flow in the pulp suspensions they process, at least in the vicinity of the rotor.

1.5 Summary and Hypothesis

1.5.1 Summary

To recap, the repulping process is known to be influenced by:

1. Pulp Type – the stronger the pulp, the more time and energy required for repulping (Bennington et al. 1998a; Brouillette et al. 2003; Holik 1988). The rate constant k from Equation 1.3 has been shown to vary linearly with pulp wet tensile strength.

2. Chemical/Enzyme Addition – the addition of chemicals or enzymes reduces the strength of the material being repulped thereby reducing the time and energy required for repulping (Bennington et al. 1998a; Bhardwaj and Rajan 2004; Brouillette et al. 2003; Espy 1992; Espy and Geist 1993; Fischer 1997; Wang et al. 2004).

3. Temperature – increasing the pulp suspension temperature reduces the time and energy required for repulping (Bhardwaj and Rajan 2004; Cho et al. 2009; Savolainen 1991). The rate constant k from Equation 1.3 has been shown to increase linearly with increasing pulp temperature (Cho et al. 2009).

4. Rotor Power – Repulping time is reduced as rotor power is increased. The rate constant k in Equation 1.3 varies linearly with rotor power (Amaral et al. 2000; Vilaseca et al. 2011).

5. Consistency – Increasing suspension consistency reduces both the time and energy required for repulping. The rate constant k in Equation 1.3 is linearly proportional to suspension consistency (Cho et al. 2009; Vilaseca et al. 2011).

6. Increasing Rotor Size – Increasing the rotor diameter for a fixed vat diameter reduces both the time and energy required for repulping (Bennington et al. 1998b; Savolainen et al. 1991).

7. Rotor Design – Some rotors are more efficient than others (Savolainen et al. 1991).

8. Turbulence – Repulping is more efficient in fully turbulent flow (Bennington et al. 1998b).

9. Repulping follows 1^{st} order kinetics in time as per Equation 1.3. The repulping kinetics in terms of energy input are unknown.

At this point, there is no theory tying together points 1-9 above.

The actual mechanism by which repulping is accomplished is unknown. Rotor design by rotor manufacturers, in general, reflects attempts to maximize one, or more, of the following mechanisms historically thought to be responsible for repulping as relisted below (Holik 1988; Paraskevas 1983):

- Flakes are broken down by being sheared between the rotor and extraction plate.
- Flakes are broken down by direct impact with the rotor.
- Flakes are worn down by fiber-to-flake/flake-to-flake rubbing.
- Flakes are broken down by turbulence.

As such, rotors are often described by, or separated into, the individual design elements intended to implement, or maximize, each of the above listed possible mechanisms. For example, early rotors had "flowing vanes" resembling the flutes on a centrifugal pump impeller ringed by vanes for the generation of turbulence (*Pulping of Secondary Fiber* 1990). These turbulence generating vanes were not unlike the shark-tooth shaped turbulence generators currently used on aircraft wings and over the rear windows of touring car type racing cars. Another popular design feature seen on many rotors is forward canted vane faces. The forward cant is supposed to function to wedge waste paper between the rotor and extraction plate for shearing. The validity of these, or any other, rotor design features is unproven.

1.5.2 Hypotheses

Based on the preceding literature reviewed, a number of hypotheses to explain repulping can be formed:

- **Hypothesis 1: The final flake content in a repulping operation depends on the total energy input to the repulping operation and is independent of the rate of energy addition (rotor power).**

Bennington et al. (1998a) showed that repulping follows Equation 1.3 now redefined as Equation 1.3a:

$$\frac{dF}{dt} = -kF \tag{1.3a}$$

Given constant rotor power, the repulping kinetics in terms of specific energy can be written as Equation 1.3b (this equation is equivalent to Equation 1.3** from Section 1.2.1):

$$\frac{dF}{dE} = -\lambda F \tag{1.3b}$$

Equations 1.3a and 1.3b include only the breakage rate of the initial size class which includes flakes of all sizes in repulping. For a batch repulping process (recall $F = m_F/m_p$ and m_p is constant in batch repulping), Equations 1.3a and 1.3b are equivalent to Equations 1.18 and 1.20 in terms of breakage rate kinetics. Equations 1.18 and 1.20 have been shown to be accurate for describing other forms of comminution. Equations 1.18 and 1.20 are rewritten below:

$$\frac{dm_i}{dt} = -S_i m_i + \sum_{j=1}^{i-1} S_j B_{ij} m_j \tag{1.18}$$

$$\frac{dm_i}{dE} = -S_i^E m_i + \sum_{j=1}^{i-1} S_j^E B_{ij} m_j \tag{1.20}$$

The breakage rate constant S_i^E is known to be independent of mill speed/power input (Herbst and Fuerstenau 1973, 1980). The total amount of breakage in a comminution process according to Equation 1.20 depends only on the total energy input to the process and on the mechanical properties of the material being broken down in the process. Bennington et al. (1998a) found that the degree of completion of a repulping process depended on cumulative rotor revolutions. This all suggests that the final flake content in a repulping process depends on the total energy input to the repulping process.

Based on the above, it is proposed here that the final flake content in a given repulping operation also depends upon the total energy input to the process and that λ is independent of rotor power.

- **Hypothesis 2: The time and energy required for repulping depend on feed pulp toughness, not tensile strength.**

It is known that the rate constants S_i and S_i^E from Equations 1.18 and 1.20 respectively depend on mill feed material fracture toughness, not tensile strength (Austin 1984; Bearman et al. 1991; Napier-Munn et al. 1999; Schoenert, 1972; Fuerstenau and Abouzeid 2002).

Fracture toughness quantifies the energy required for crack propagation throughout a material and is directly related to the evolution of new surface area and crack growth. Hence, fracture toughness relates well to the energy required in the milling of brittle minerals. The fracture toughness of a material depends on strain-rate and is a good measure to quantify the resistance of a material to high strain-rate failure.

Accordingly, tests for fracture toughness are high strain-rate tests - like the Charpy Impact Test where a test specimen is subjected to an impact by a swinging pendulum thereby making the Charpy test a high strain-rate test.

Materials having ductility can fail in a slow, ductile fashion. Plastic deformation in ductile materials acts to blunt crack tips and inhibit crack propagation. The energy associated with this plastic deformation is significant. The energy required in a slow, ductile type failure is obtained from measurement of the area under a stress-strain curve obtained from material tensile testing. This property is referred to as simply “toughness”.

It is also proposed that the rate constants k and λ will depend on a measure of feed material toughness and not on tensile strength. The repulping rate constants in Equations 1.3a and 1.3b will depend either on fracture toughness or tensile toughness.

- **Hypothesis 3: LC Repulping occurs due to turbulence produced by the blunt vane shapes used by repulper rotors – specifically in the form of vane trailing vortices.**

There are many different repulper rotor designs but one commonality exists among all of them – they all have blunt-shaped rotor vanes. LC repulper rotors resemble the impeller designs used for turbulent mixing such as the Rushton Turbine. The blunt shapes used by mixing impellers create turbulence that is known to be beneficial to mixing.

In turbulent stirred mixing, the dissipation of impeller power by turbulence is accomplished very near the impeller. The dissipation has been measured to be 140 times higher right near a mixing impeller as compared to the average dissipation in the rest of the mixing vessel (Zhou and Kresta 1996). For this reason, scaling between different stirred mixing operations is often accomplished by the assumption that all of the power imparted to a mixing operation by an impeller is dissipated with the impeller's swept volume as per Equation 1.26:

$$\varepsilon = \frac{P}{\rho V_{Swept}} \tag{1.26}$$

The defining flow feature of common mixing impellers like the Rushton turbine is that the blunt shapes of these impellers produce powerful trailing vortices (Lee and Yianneskis 1998; Nienow and Wilson 1974; Sharp and Adrian 2001; Stoots and Calabrese 1995; Van't Riet and Smith 1975; Yianneskis et al. 1987; Yianneskis and Whitelaw 1993).

The intensity of the dissipation of impeller power via turbulence within these trailing/tip vortices is extremely high compared to all other areas within a turbulent stirred mixer. As such it is widely accepted that the majority of mixing in a stirred vessel is accomplished by these vortices (Kresta and Wood 1993).

Figure 1.2 shows that repulper rotors have evolved to be ever blunter over time. Repulper rotors have not evolved to be streamlined or to have sharp edges. If impact was the most important repulping mechanism, the shapes used by repulper rotors would be extremely inefficient.

Repulper rotors show a strong resemblance to the mixing impellers used for turbulent mixing (Figure 1.3). Repulper rotors also operate at high-speeds and, as shown in Section 1.4.1, repulper rotors are likely producing turbulent flow in the pulp suspensions which they process. Bennington et al. (1998b) showed that repulping was more efficient under fully turbulent flow conditions and stated that turbulence is likely the dominant repulping mechanism under such flow conditions. It is proposed here that LC repulper rotors breakup waste paper by producing high-intensity turbulence in the vicinity of the repulper rotor, specifically in the form of powerful trailing vortices analogous to those produced by mixing impellers.

- **Hypothesis 4: The relative time spent by flakes circulating past the repulper rotor versus in the rest of the vat in part determines repulping efficiency.**

The general flow field within a stirred mixer depends on impeller off-bottom clearance. Repulper rotors run very tight off-bottom clearance - as little as 5mm even with very large rotors. Tight off bottom clearance results in a single-loop flow field in stirred mixers for both radial and axial impeller types (Ibrahim and Nienow 1996; Montante et al. 1999). This same single-loop flow field is then expected within repulpers. Therefore, repulping can occur as flakes make cumulative passes through high-intensity turbulence at the rotor as they flow around a single-loop flow field within the repulper.

Both Savolainen et al. (1991) and Bennington et al. (1998b) showed that increasing rotor diameter for a given vat size reduces both the time and energy required for repulping. The same situation is observed with turbulent mixing. Both the time and energy required for blending are reduced when rotor diameter is increased. It has been reported by Voncken (1966), Cooke et al. (1988), and Ruszkowski (1994) that mixing time (θ_m) is described by Equation 1.27 rewritten below:

$$\theta_m \propto \left(\frac{D}{T}\right)^{-2} \tag{1.27}$$

Where D is the mixing impeller diameter and T is the mixing vessel diameter. Nienow (1997) explains this result by stating that the mixing time is determined by the slow mixing "…well away from the agitator [impeller]." He states that a larger diameter impeller provides a more even distribution of energy throughout the mixing vessel thus enhancing mixing. An alternative interpretation is proposed here. First, recall the turbulent mixing mechanism reviewed earlier. Higher local dissipation results in reduced eddy size and thus less time for the diffusion required to complete mixing at scales smaller than the turbulent eddies. Recall also that the greatest dissipation happens at the impeller with the dissipation rate at the impeller measured to be up to 140 times as high as the average over the entire mixing vessel (Zhou and Kresta 1996). Now consider the bulk circulation patterns in a mixing vessel. The flow exiting a mixing impeller either performs a characteristic single, or double-loop flow pattern. It is proposed then that the mixing time is limited by the time spent flowing around the mixing vessel where dissipation is low and therefore mixing is highly diffusion limited. The impeller, and thus the region of high dissipation, only occupies a small volume in a mixing vessel. Therefore, the time spent by fluid flowing through this volume is low compared to the time spent by fluid flowing around the mixing vessel away from the impeller. A larger impeller gives a larger volume of high intensity turbulence and hence a higher residence time for fluid within this volume compared to the residence time for fluid flowing away from the impeller around the vat.

This argument can be extended to repulping. If high intensity turbulence at the rotor is the mechanism responsible for repulping then the time flakes spend circulating around the vat away from the rotor not being repulped will also limit repulping time. It is proposed here that the rate of repulping in time and energy is proportional to the residence time for flakes at the rotor (being repulped) versus the residence time for flakes away from the rotor (not being repulped):

$$k \text{ and } \lambda \propto \frac{\tau_R}{\tau_{Vat}} \tag{1.34}$$

where τ_R and τ_{Vat} are the residence times spent by flakes at the rotor and in the vat respectively, following the expected single-loop flow pattern, respectively.

- **Hypothesis 5: Efficient mixing depends on both the rotor and vat as a system and is critical for efficient repulping.**

Paraskevas (1983) and Holik (1988), along with repulper manufacturers state the importance of uniform mixing in repulping. However, the effect of poor mixing on repulping has not been quantified.

Baffles convert swirling fluid motion into axial and/or radial motion in a mixing vat. A lack of proper baffling results in solid body swirl and poor mixing as a result of inefficient transport of the material to be mixed past the mixing impeller. Severe under-baffling can be identified visually. A more rigorous method to identify under-baffling is that the condition of Reynolds independence is not achievable (see Figure 1.6). Achieving Reynolds independence depends on both the impeller and mixing vat as a system.

As evidence suggests that the breakup of waste paper occurs only at the rotor, poor mixing would result in the inefficient transport of waste paper to the rotor and therefore inefficient repulping.

The hypothesis that efficient mixing is required for efficient repulping is proposed here and that this relies on both the repulper rotor and vat designs.

- **Hypothesis 6: Flake attrition between the extraction plate and rotor is not an important repulping mechanism.**

Repulper manufacturers not only frequently introduce new rotor designs, but also extraction plate designs. Does the extraction plate significantly contribute to repulping? The rotor-to-extraction plate clearance is fixed in repulpers. For a flake to be sheared between the rotor and extraction plate, it would have to be the right size to jam in the gap between the rotor and extraction plate. It is reasonable to expect an ever-changing distribution of flake sizes during repulping as is the case in other comminution processes. Flakes of the exact right size to be sheared may be rare among the population of flakes at any given time during a repulping operation. Furthermore, the right size flake must be in the right position to be sheared in the plate-to-rotor gap. This gap occupies only a very small region of the total repulper volume.

For these above reasons, it is suggested here that shearing between the rotor and extraction plate is not an important repulping mechanism.

- **Hypothesis 7: Repulper rotor design affects the time and energy required for repulping.**

Savolainen et al. (1991) compared the repulping energy efficiency of two different LC repulper rotors in three different repulper vat sizes. This study is the only peer-reviewed study available where rotor performance is compared. The testing in this study showed that one rotor routinely used 20% less energy than the other rotor in all three vat sizes. However, this study provided no details concerning the design and dimensions of each of the rotors compared. Furthermore, the performance comparison between the rotors is presented in this study in table-form where one rotor is given an efficiency value of “1” and the other is given an efficiency relative to this – for example “0.8” meaning the difference in efficiency is 20% between the rotors. The authors pick a final flake content value and use the energy at this value for each rotor to get the relative efficiencies. Deflaking in a repulper follows the form of Equation 1.3 in that deflaking in a repulper approaches a flake content of zero in an asymptotic manner as time and energy increase. This makes the method of picking a final flake content near zero and taking the energy at this value suspect as even very small experimental variations in flake content will make for large variations in repulping time and energy due to the asymptotic approach to a zero flake content value by Equation 1.3. No flake content vs. time or energy data are given for the rotor comparison in the Savolainen et al. (1991) study. Based on the approach used in the Savolainen et al. (1991) study, and the lack of information concerning the test rotors in this study, it is the opinion of the author that whether or not repulper rotor design affects the time and energy required for repulping remains an open question.

1.5.3 Conclusion

All 7 hypotheses will be tested in the following chapters of this thesis. A link between material properties, consistency, and vat and rotor geometry will also be presented. This thesis marks the first presentation of such a link.

All of the studies presented in this thesis center around the use of a laboratory scale low consistency repulper designed and built specifically for this study. This machine has a capacity of $0.25m^3$ and was designed based on the designs of full sized repulpers. Three test rotors were constructed in scale from billet aluminum for the studies in this thesis. Each rotor represents a state of the art offering from a different manufacturer with each being used in mills all over the world. This machine is described in Appendix A.

The results presented in this thesis are ordered as follows:

Chapter 2 – This chapter investigates the variables affecting the specific energy consumption in repulping including operational variables like consistency, temperature, vat volume, and pulp type. This section also presents a performance comparison of 3 different LC repulper rotor designs as a test of Hypothesis 7. The validity of the flake attrition between the rotor and extraction plate as a repulping mechanism is tested for in order to test Hypothesis 6. This chapter also tests the influence of rotor power on repulping efficiency in order to test Hypothesis 1.

Chapter 3 – This chapter presents a theory based model for repulping that links pulp material properties, consistency, temperature and basic rotor and vat dimensions. The model is based on Hypotheses 2, 3 and 4 and a fit of the model to the data presented in Chapter 2 tests these hypotheses. This chapter also presents evidence to confirm that efficient repulping depends on efficient mixing thereby testing Hypothesis 5.

Chapter 4 – This chapter presents a scale-up of repulping performance between the $0.25m^3$ laboratory LC repulper designed and built for this study and a $15m^3$ industrial repulper using the repulping model presented in Chapter 3.

Chapter 5 – This chapter presents CFD simulations of the flow-fields produced by each rotor tested for this thesis work. It is suspected that repulper rotors produce powerful trailing vortices in the same vein as those produced by impellers used for turbulent stirred mixing. It is also suspected that the repulper rotor shaft power input to the suspension within a repulper is dissipated by turbulence very near the repulper rotor as is the case with mixing impellers. The aim of the CFD simulations is to identify the presence of trailing vortices and to gain an estimate of the spatial distribution of rotor power dissipation in order to further test Hypotheses 2, 3 and 4. Another aim of this chapter is also to analyze the test rotors in light of Hypothesis 7.

Chapter 6 – This chapter presents high-speed film of the three rotors tested for this thesis actually repulping. Each rotor is filmed interacting with corrugated cardboard at 11,000 frames per second. The aim of this chapter is also to help analyze the test rotors in light of Hypothesis 7.

Chapter 2: Variables Affecting Specific Energy Requirements for Repulping

The physical mechanism responsible for waste paper disintegration in repulping is unknown. As a starting point, an investigation into the influence of a number of operational variables and rotor designs on the specific energy required for waste paper disintegration in a repulper is conducted here.

It is also the aim here to determine if the completeness of a repulping operation depends only on the total energy input to the process and is independent of the rate of energy addition as is the case with other comminution processes as per Hypothesis 1 of Section 1.5.2:

- **Hypothesis 1: The final flake content in a repulping operation depends on the total energy input to the repulping operation and is independent of the rate of energy addition (rotor power).**

The rate constant λ in Equation 1.3b will be independent of rotor power input to the repulping process if this is the case.

Furthermore, all three test repulper rotors are compared in order to test Hypothesis 7 of Section 1.5.2:

- **Hypothesis 7: Repulper rotor design affects the time and energy required for repulping.**

The effect of the following variables on the specific energy consumption in repulping will be tested:

- Pulp Type
- Pulp Suspension Temperature
- Pulp Suspension Consistency
- Repulper Rotor Speed/Power
- Repulper Rotor Design
- Repulper Rotor to Extraction Plate Clearance
- Repulper Vat Fill Level

2.1 Methods and Materials

A $0.25m^3$ laboratory scale repulper was designed and built by the author for these experiments (see Figure 2.1).

Figure 2.1: The $0.25m^3$ low consistency laboratory repulper designed and built by the author for this thesis work. The specifications of this machine are compared to those of industrial repulpers in Table 2.1. A detailed description of this machine is given in Appendix A.

The laboratory repulper extraction plate has a hole pattern having 3.175mm diameter holes. A 6kW 3-phase AC motor operated by a variable frequency drive powers the laboratory repulper. The laboratory repulper is compared with a typical industrial repulper in Table 2.1. Details concerning the design of this machine can be found in Appendix A.

Table 2.1: A comparison of the basic specifications of the laboratory repulper shown in Figure 2.1 with industrial scale repulpers.

	Laboratory Repulper	$15m^3$ Industrial Repulper	$85m^3$ Industrial Repulper
Installed Power	6kW	130kW	450kW
Vat Volume	$0.25m^3$	$15m^3$	$85m^3$
Rotor Diameter	233.7mm	900mm	1575mm
Rotor Diameter/Vat Diameter	0.31	0.30	0.30
Rotor Tip Speed	Up to 16.5m/s	15-20m/s	15-20m/s
Rotor Power/Vat Volume	7-20 kW/m^3	7.5 kW/m^3	4.4 kW/m^3

Scale replicas of 3 commercially available repulper rotors were constructed from billet aluminum (see Figure 2.2). The rotors chosen for testing each represent their respective manufacturer's state of the art offering at the time of this testing. All three test rotors have a diameter of 233.7mm.

Figure 2.2: The three low consistency repulper rotors used for this study. From left to right; Rotor A, Rotor B, and Rotor C. All three rotors have a diameter of 233.7mm and are made from billet aluminum. The black coloring seen on Rotors A and B is from a hard-anodizing treatment. Rotor C is shown here before being hard-anodized.

A number of materials were repulped in the laboratory repulper. The materials employed include C-flute corrugated cardboard, single-sided C-flute corrugated cardboard, kraft aspen, office printing paper, newsprint, and unbleached paper towel.

Readers are likely familiar with newsprint, paper towel and office printing paper and cardboard. However, the "C-flute" designation for corrugated cardboard and an explanation of what kraft aspen is, is likely merited.

C-flute corrugated cardboard is the most produced cardboard type with 80% of corrugated containers being made of C-flute corrugated cardboard (Da-Wen Sun 2012). It finds use in heavy duty packaging. Cardboard types are shown in Figure 2.3. C-flute corrugated cardboard has an overall thickness of 5mm and 128 flutes per meter. Notice in Figure 2.3 that the center fluting is sandwiched between two sheets.

Single-sided C-flute corrugated cardboard has the fluting attached to a sheet on one side only. This is done to make it more flexible so that it can be used to wrap objects for packaging.

Kraft aspen is a hardwood kraft pulp having short fibers. It is not a finished paper product in the same vein as newsprint or office paper. It is commonly blended with other pulp types as it brings the properties of softness and smoothness to a finished paper product. For example, kraft aspen is a common ingredient in tissue papers.

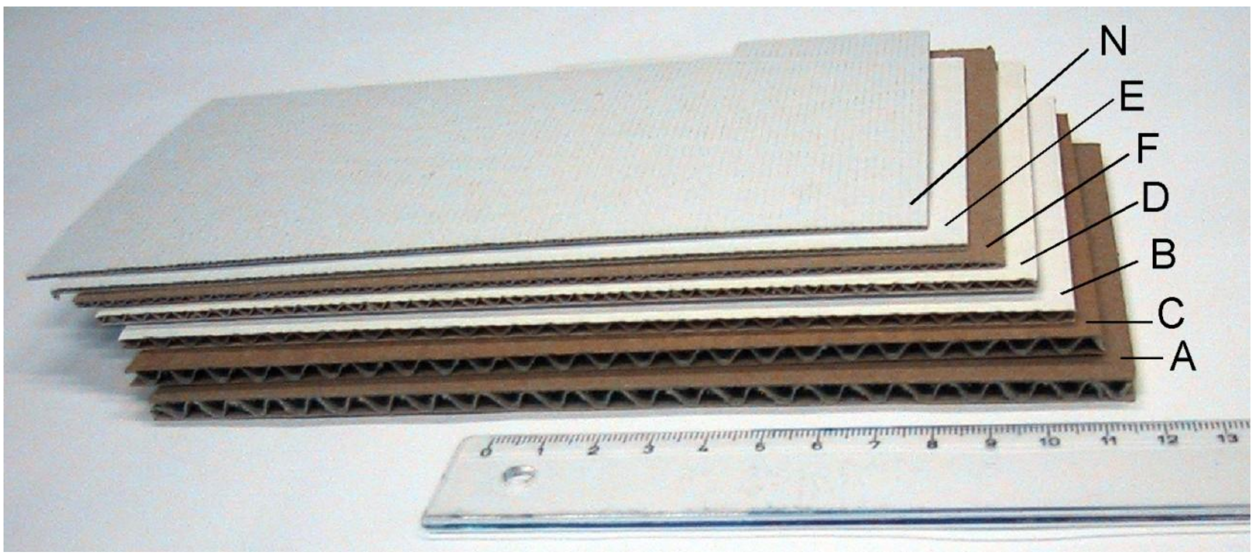

Figure 2.3: Grades of corrugated cardboard. Industry standard lettering is used to define the thickness and frequency of flutes. C-flute corrugated cardboard is used for this study as it is the most common corrugated type. C-flute corrugated cardboard has an overall thickness of 5mm and 128 flutes per meter.

All results shown in the next section are for batch repulper operation. For all test conditions presented here, the pulp suspension in the repulper is completely flowing – i.e. the test parameters were chosen so that the pulp suspension in the laboratory repulper did not solidify anywhere in the repulper vat due to the yield stress property of pulp suspensions.

For all tests, both C-flute corrugated cardboard types, kraft aspen, office printing paper, and newsprint were cut into 50mm x 100mm rectangles before being loaded into the repulper. Paper towel was loaded in 50-sheet discrete stacks.

Samples of the suspension were taken at regular time intervals. The time interval chosen depended on the material being repulped and on the test conditions. C-flute corrugated cardboard repulped very slowly and samples could be taken at 10 minute intervals – the longest interval of any of the materials tested here. Kraft aspen repulped very quickly, especially at elevated suspension temperatures, so sampling occurred at intervals as little as 15 seconds – the shortest interval of the materials tested here.

Samples taken during repulping tests were tested for the level of disintegration, or “flake content”, using the TAPPI T-270 pm-88 standard for flake content measurement. The flake content is the dimensionless ratio of the dry mass of flakes (unbroken pulp/paper) to the total dry mass of pulp in suspension (flakes and fibers). The experimental error for all flake content determinations was determined as a 95% confidence interval based on a T-distribution consisting of 10 flake content tests and was found to be ±2.5%.

The power consumption is logged during each test. The power consumed by each rotor during each test is corrected for motor dynamometer measured efficiency. The repulping energy is calculated through numerical integration of the logged power data. The time and energy required for repulping can then be known through a correlation between repulping time and energy with flake content samples. A sample of data as logged from a repulping test is given in Appendix A.3.

Table 2.2 on the following page shows all of the experiments conducted in this section.

Table 2.2: Test conditions for the results shown in each figure in Section 2.2. The varied quantity for each figure is color-highlighted in the table.

Figure #	Rotor Type	Rotor Tip Speed	Pulp Type	Suspension Consistency	Suspension Temperature	Vat Fill Level	Rotor to Extraction Plate Clearance
Figure 2.4	Rotor A	13m/s	• kraft aspen • office paper • newsprint • paper towel • corrugated cardboard	5%	20^0C	$0.22m^3$	10mm
Figure 2.5	A, B, and C. Results shown are for Rotor A.	13m/s for corrugated cardboard. 12m/s for aspen.	C-flute corrugated cardboard. Kraft Aspen.	5%	• 10^0C • 20^0C. • 40^0C • 55^0C • 60^0C	$0.22m^3$	10mm
Figure 2.6	Rotor A: kraft aspen. Rotor B: C-flute corrugated cardboard.	13m/s	C-flute corrugated cardboard. Kraft Aspen.	**3-6%**	20^0C	$0.22m^3$	10mm
Figure 2.7	Rotor A: kraft aspen. Rotor B: C-flute corrugated cardboard.	12-15m/s	C-flute corrugated cardboard. Kraft Aspen.	5%	20^0C	$0.22m^3$	10mm
Figure 2.8	A, B, and C.	13m/s	C-flute corrugated cardboard.	5%	20^0C	$0.22m^3$	10mm
Figure 2.9	Rotor C	13m/s	C-flute corrugated cardboard.	5%	20^0C	$0.22m^3$	**2mm-14mm**
Figure 2.10	Rotor C	13m/s	C-flute corrugated cardboard.	5%	20^0C	$0.10m^3$ to $0.22m^3$	10mm

2.2 Results

2.2.1 Pulp Type

The specific energy required for disintegration varies significantly with pulp type (Figure 2.4). All results shown in the figure are with Rotor A operating with a 13m/s tip-speed in a 5% consistency pulp suspension at 20°C, and a vat fill level of 220L.

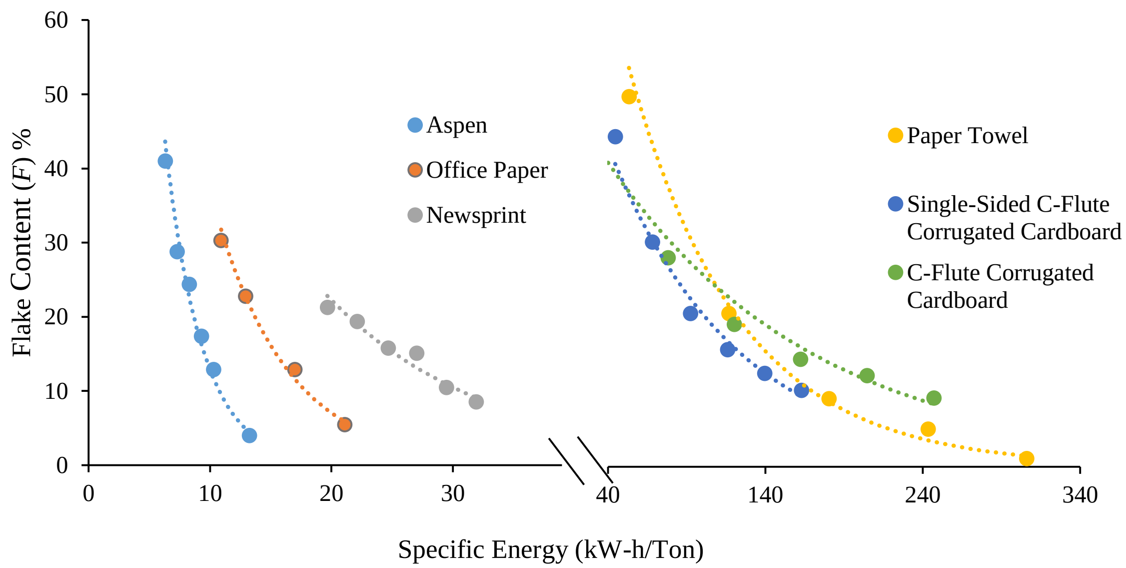

Figure 2.4: Different pulp types require profoundly different amounts of energy to be repulped. Note the split x-axis. The tests shown in the figure are all conducted with Rotor A. Operating conditions are: tip-speed 13m/s, 5% consistency, 20°C, fill volume 0.22m^3.

2.2.2 Temperature

Both C-flute corrugated cardboard and kraft aspen were tested to determine the effect of temperature on repulping specific energy (Figure 2.5). Both tests were conducted at 5% consistency. With C-flute corrugated cardboard, the rotor tip speed was 13m/s. With kraft aspen, the rotor tip speed was chosen to be 11m/s for reasons of practicality. The kraft aspen material is broken down extremely fast at elevated suspension temperatures. At the 11m/s test speed, samples could be taken at 15 second intervals for kraft aspen. Faster rotor speeds would make for unreasonably short sample intervals. C-flute corrugated cardboard could be sampled at 10 minute intervals for all test temperatures. For each test, the initial vat temperature was set to the desired test temperature. For both corrugated cardboard and kraft aspen, the required repulping time and the required repulping specific energy diminish with increasing pulp suspension temperature.

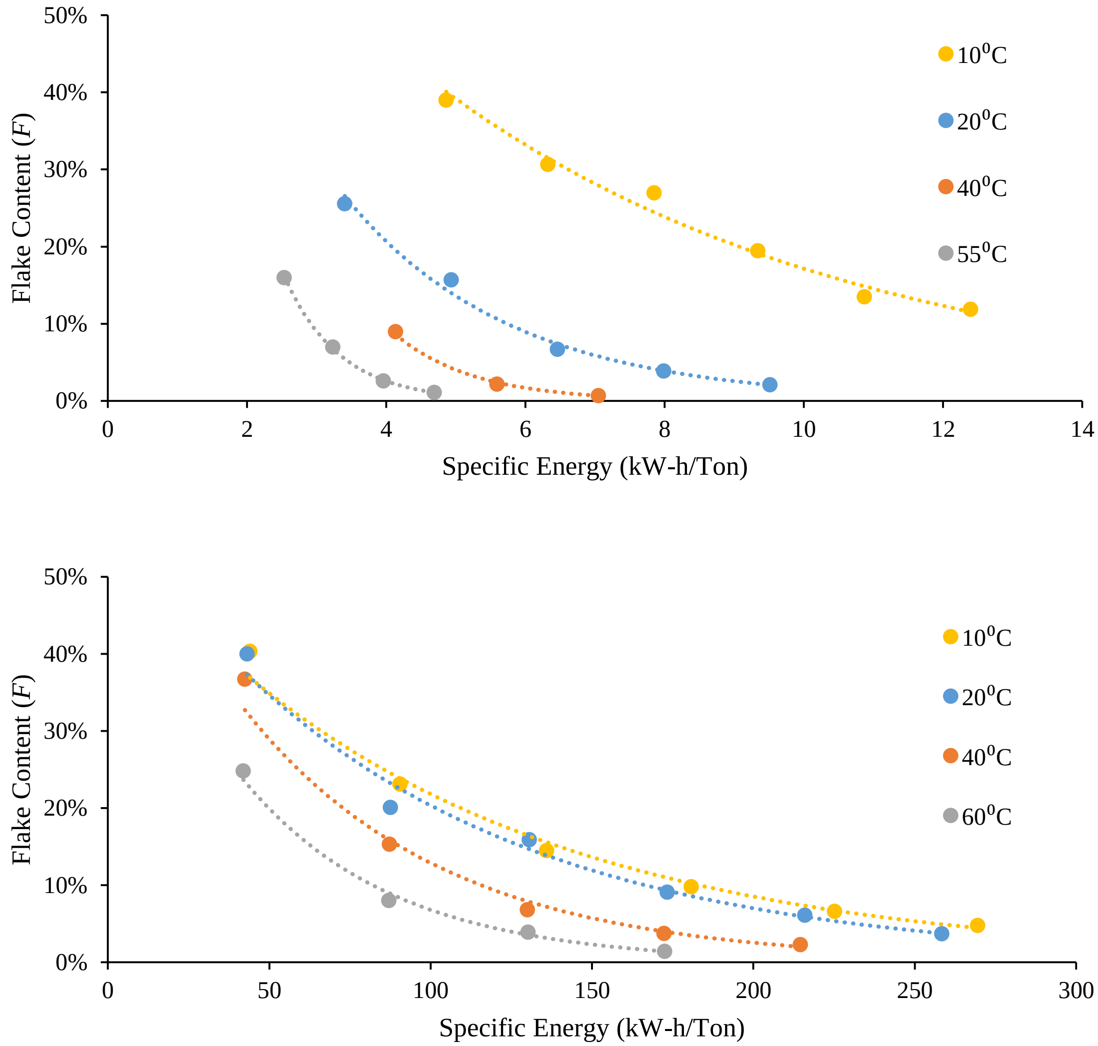

Figure 2.5: Increasing suspension temperature reduces specific energy consumption. Top: kraft aspen with Rotor A operating with a tip speed 11m/s in a 5% suspension consistency and a vat fill 0.22m^3. Bottom: C-flute corrugated cardboard with Rotor B operating with a tip speed 13m/s in a 5% consistency suspension and a vat fill 0.22m^3.

2.2.3 Consistency

Figure 2.6 shows the results for tests conducted using both C-flute corrugated cardboard and kraft aspen to determine how changes in consistency affect the specific energy required for repulping. The tests show that increasing consistency reduces the specific energy required for repulping for both C-flute corrugated cardboard and kraft aspen.

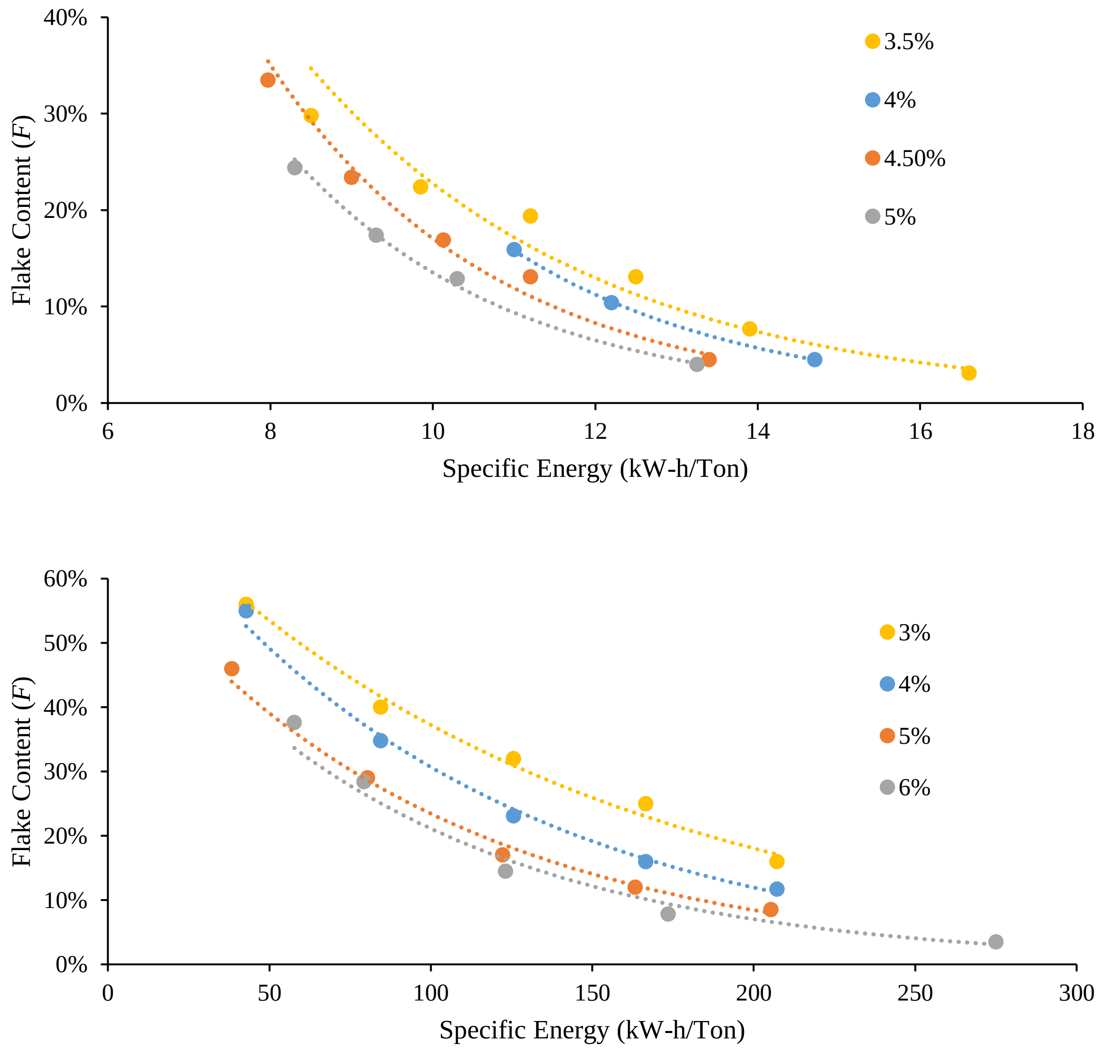

Figure 2.6: Increasing suspension consistency reduces specific energy consumption. Top: kraft aspen with Rotor A; tip speed 13m/s, temperature 20°C, vat fill 0.22m^3. Bottom: C-flute corrugated cardboard with Rotor B; tip speed 13m/s, temperature 20°C, vat fill 0.22m^3.

2.2.4 Rotor Tip Speed

Testing was performed with C-flute corrugated cardboard and with kraft aspen both at 5% consistency. The results for varying rotor tip speed are shown in Figure 2.7.

The required rotor power increases by a factor of 2 when the rotor tip speed is increased from 12m/s to 15m/s for both C-flute corrugated cardboard and kraft aspen pulp suspensions yet the specific energy required for deflaking remains constant for all rotor speeds. Increasing the rotor tip speed decreases the time required for repulping but does not affect the quantity of energy required for repulping. Given the similar behavior between corrugated cardboard and kraft aspen for the tip speed tests conducted, it can be concluded from these tests that the energy required for repulping is a property of the material being repulped; a given material requires a given amount of energy to be repulped and this energy quantity is independent of the rate at which the energy is applied. This confirms the Hypothesis 1 from Section 1.5.2 that the energy use in repulping mirrors that of comminution processes in general.

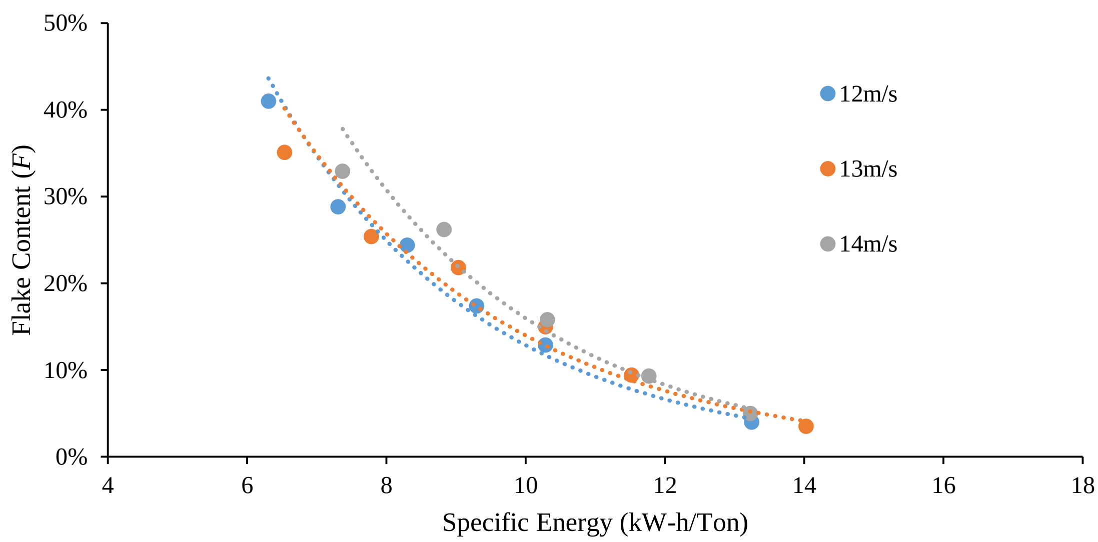

Figure 2.7a: Rotor speed/power has no effect on repulping efficiency. This indicates that the level of paper/pulp disintegration achieved in a repulping process depends on the total energy input to the process. Rotor power influences the speed of a repulping process with faster rotor speeds equaling faster repulping. Above: kraft aspen with Rotor A; 5% consistency, temperature 20°C, vat fill 0.22m^3. This figure is continued on the next page.

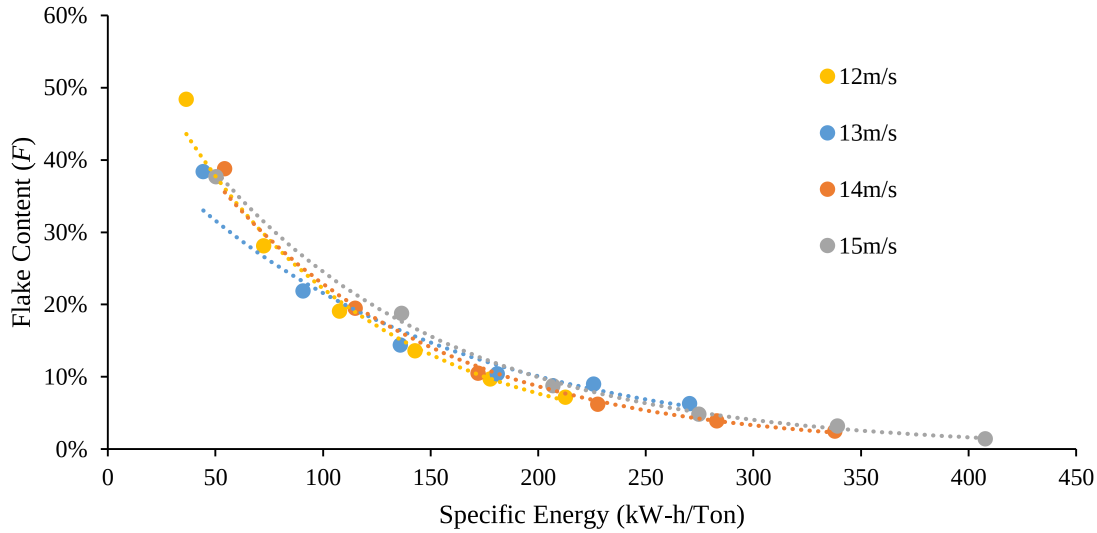

Figure 2.7b: Continued from previous page. Above: C-flute corrugated cardboard with Rotor C; 5% consistency, temperature 20°C, vat fill 0.22m^3.

2.2.5 Rotor Geometry

So far, this study has presented the case that the energy required to repulp a given material is a property of that material. There are many different repulper rotor designs currently in use in industry with some designs marketed as being "energy efficient." Three modern, commercially available "energy efficient" rotors were replicated in scale and compared using the laboratory repulper. Rotor comparison tests were carried out with all three rotors operating with a 13m/s tip speed in a 5% pulp suspension of C-flute corrugated cardboard. Figure 2.8 shows the results of the rotor comparison. Notice from the figure that although Rotor A uses less power than Rotor C, less energy is consumed by Rotor C to accomplish the task of repulping. This indicates that the geometry of Rotor C is more amendable to the task of repulping; it is not simply a matter of applying more or less power to the pulp suspension. A statistically significant difference is seen between rotors A and B in Figure 2.8. This confirms Hypothesis 7: Repulper rotor design affects the time and energy required for repulping.

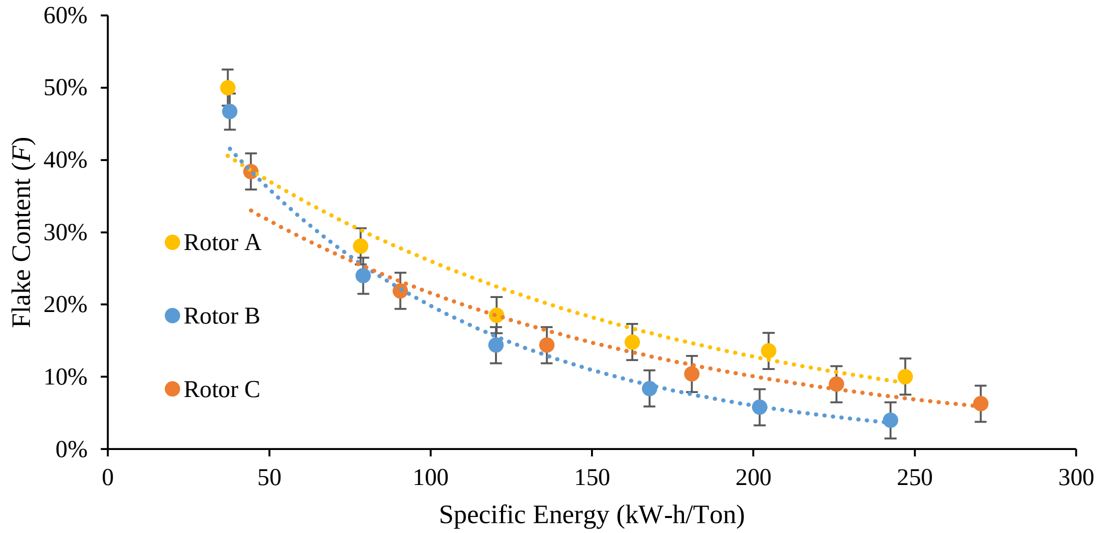

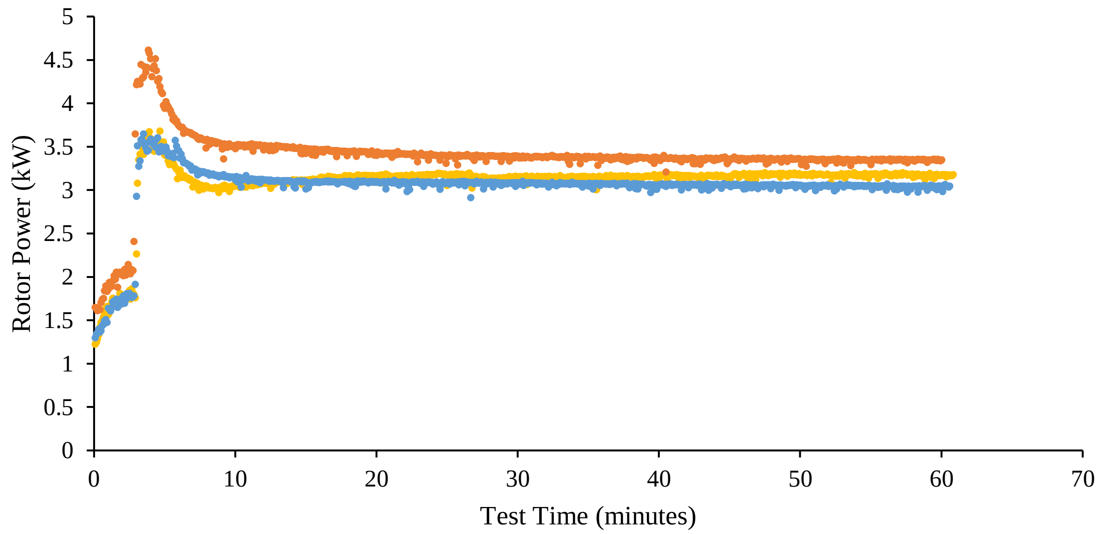

Figure 2.8: A comparison of all three test rotors in a 5% C-flute corrugated cardboard pulp suspension. Test conditions: tip-speed 13m/s, temperature 20°C, vat fill level 0.22m³. Top: Flake content vs. specific energy for each rotor. Bottom: The logged power for each rotor. The single legend applies to both plots. Error bars shown above are calculated as a 95% confidence interval based on a T-distribution of 10 repulping tests.

2.2.6 Rotor to Extraction Plate Clearance

There exists contention that physical shearing of flakes between the rotor and the extraction is an important factor in repulping. The laboratory repulper has a stainless steel extraction plate having a ϕ3.175mm drilled pattern. The clearance between the rotor and the extraction plate was raised via shimming to reduce shearing of the material being repulped. Repulping performance with C-flute corrugated cardboard at three different rotor-to-extraction plate clearances is shown in Figure 2.9. This testing was done with Rotor C which has the forward canted vane feature that supposedly wedges material between the rotor and extraction plate. Changing the rotor to extraction plate clearance did not influence specific energy consumption. This confirms Hypothesis 6 from Section 1.5.2 – flake attrition between the rotor and extraction plate is not a significant repulping mechanism.

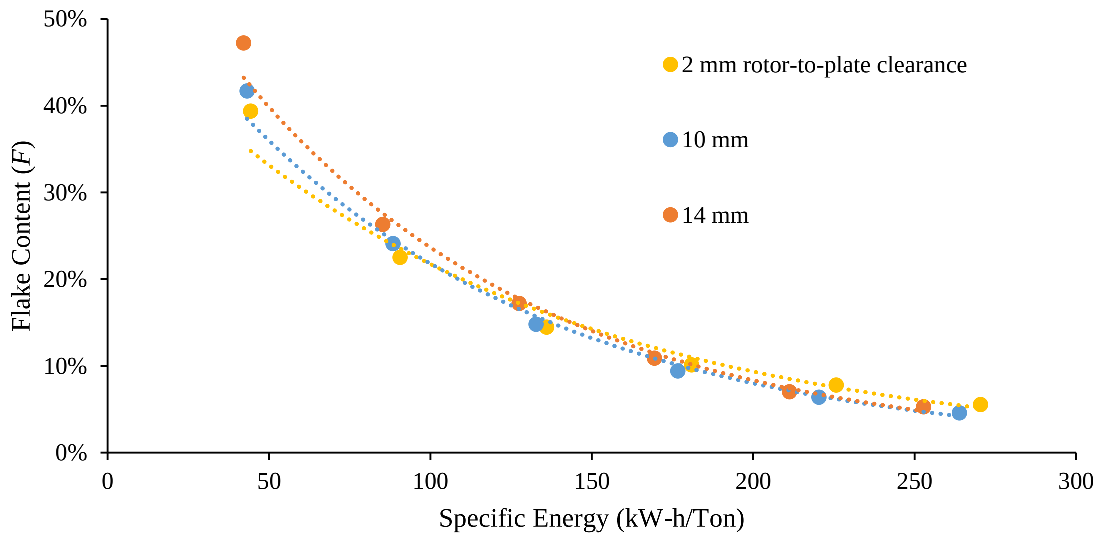

Figure 2.9: Varying rotor-to-extraction plate clearance has no effect on the specific energy consumption in repulping. Rotor C was used for this test as it has forward-canted vane faces – a design feature purported to wedge waste paper between the rotor and extraction plate for shearing. For the tests shown in the figure the material is C-flute corrugated cardboard, the rotor tip-speed is 13m/s, the suspension consistency is 5%, the suspension temperature is 20°C, and the vat fill level is 0.22m^3.

2.2.7 Vat Volume

The effect of varying vat volume is shown in Figure 2.10. All the test results shown in Figure 2.10 are for a pulp suspension of C-flute corrugated cardboard at 5% consistency and for a rotor tip speed of 14m/s. Repulping efficiency improves as vat level is decreased until the level falls low enough that the baffles become ineffective and solid body motion of the suspension starts. This solid body motion is accompanied by a drop in rotor power. Solid body motion correlates with poor mixing. The fact that the efficiency of the repulper falls off upon solid body swirl indicates that uniform mixing is important for efficient repulping.

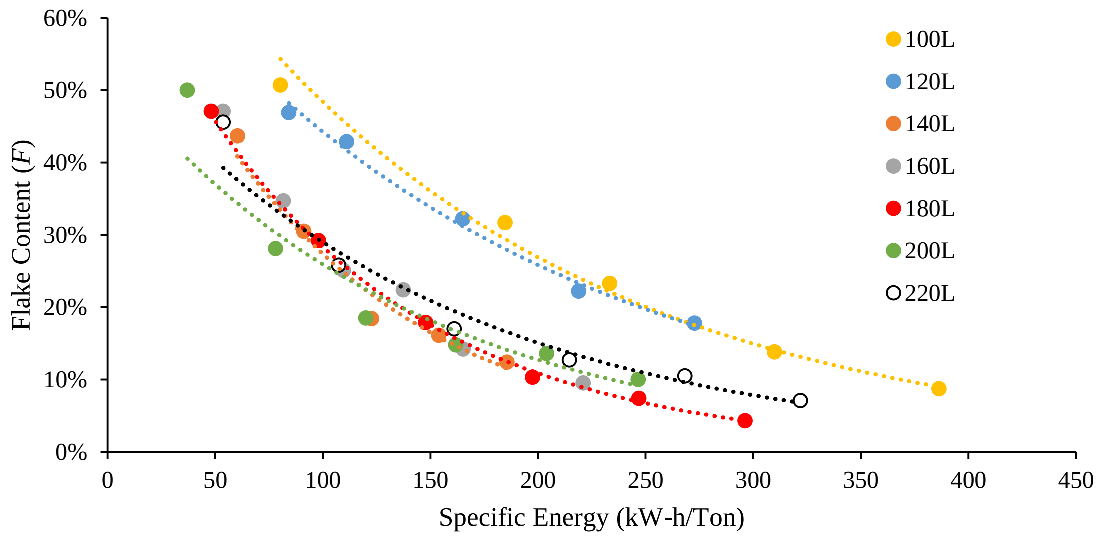

Figure 2.10: A comparison of vat fill levels using Rotor C. For all vat levels the pulp type is C-flute corrugated cardboard, the suspension consistency is 5%, the suspension temperature is 20°C and the rotor tip-speed is 14m/s. The suspension began to swirl in the repulper at volumes of 120L and less. This likely explains the reduction in repulping efficiency seen at lower vat fill volumes as swirl is indicative of poor mixing.

2.2.8 Repulping Kinetics in Energy

The flake content during repulping is seen to decay exponentially as a function of specific energy taking the functional form of Equation 1.3b as predicted by Hypothesis 1:

$$\frac{dF}{dE} = -\lambda F \tag{1.3b}$$

where F is the flake content, E is the repulping energy, and λ is the repulping energy rate constant. It is confirmed that the specific energy required for pulping, and thus the rate constant λ, is material dependent.

The form of Equation 1.3b is confirmed to be the same form as for other comminution processes as per Equation 1.20 in terms of breakage rate kinetics.

The rate constant λ can be found from least-squares curve fitting as is shown in Figure 2.11. For all of the results presented in Figures 2.4-2.10, the fit for λ as per Equation 1.3b fit with a $R^2 > 0.95$.

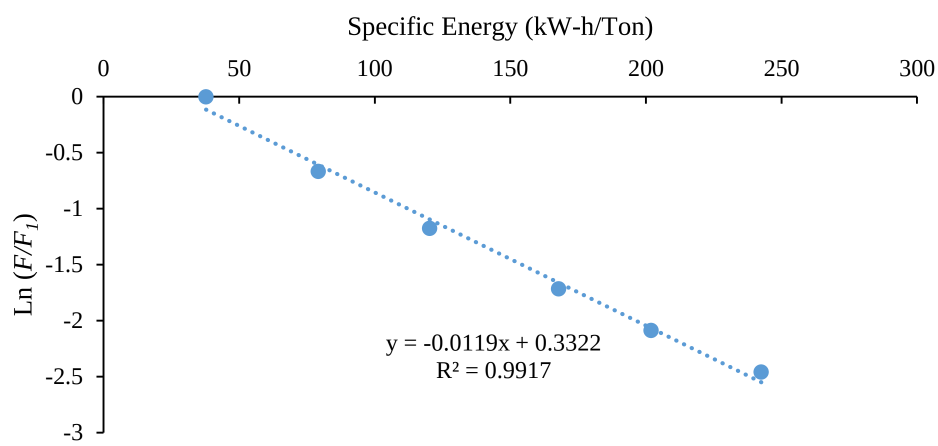

Figure 2.11: The rate constant λ from Equation 1.3b can be found from a least-squares fit. This is shown above where F_1 is the flake content of the first sample. The slope of the fit is the rate constant λ.

2.3 Discussion

Equation (1.3b) can be solved to obtain Equation 2.1.

$$\Delta E = P\Delta t = -\frac{1}{\lambda} ln\left(\frac{F_2}{F_1}\right) \tag{2.1}$$

where ΔE is the repulping specific energy required to change the initial flake content F_1 to the final flake content value F_2, P is the rotor shaft power, and Δt is the specific repulping time with units of time/mass required for the flake content to go from F_1 to the final flake content value F_2. Therefore, the production rate PR in mass/time is proportional to the energy rate constant λ and the repulper rotor power as per Equation 2.2.

$$PR = \frac{1}{\Delta t} \propto \lambda P \tag{2.2}$$

The implication of Equation 2.2 is that an increase in the value of the energy rate constant can be offset by a corresponding decrease in rotor power without affecting the repulping production rate. Or, as λ and P are independent, rotor speed can be increased to improve production rate without increasing specific energy consumption.

Repulper operators can improve the efficiency of their repulping operation by increasing the suspension temperature if possible. Increasing temperature has been shown to reduce both the wet-tensile strength and wet toughness of paper (Back and Andersson 1992; Kouko et al. 2014). This explains the reduction in energy required for repulping as temperature increases.

Repulper operators can also improve the efficiency of their repulping operation by increasing the suspension consistency if possible.

Repulper operators should make sure to maintain a sufficient vat fill level to avoid solid body swirl of the suspension in the repulper as repulping efficiency sharply drops under such a condition. Solid body motion of the suspension in a repulper is not only identifiable from visual observation of the flow within the repulper but is also accompanied by a significant drop in rotor power.

2.4 Chapter Conclusion

To summarize; the rate constant λ in Equation 1.3b is dependent upon the material being repulped, the temperature and the consistency of the pulp suspension, the geometry of the repulper rotor, and the repulper vat volume.

Solid body motion of the suspension in a stirred mixer indicates poor mixing. The efficiency of the laboratory repulper dropped drastically after the onset of solid body motion in the repulper. More evidence to confirm the hypothesis that efficient mixing is required for efficient repulping is presented in the next chapter.

Figure 2.8 shows a performance comparison between the three rotors tested in this thesis work. A statistically significant difference is shown for the energy required to repulp between rotors A and B. The reasons for this difference are investigated in Chapters 5 and 6. This confirms Hypothesis 7 from Section 1.5.2:

- **Hypothesis 7: Repulper rotor design affects the time and energy required for repulping.**

Altering the rotor to extraction plate clearance had no effect on the specific energy required for repulping. If flake attrition between the rotor and extraction plate was a significant repulping mechanism, altering the rotor to extraction plate clearance should have had significant effect on the energy required for repulping. This confirms Hypothesis 6 from Section 1.5.2:

- **Hypothesis 6: Flake attrition between the extraction plate and rotor is not an important repulping mechanism.**

As is the case with other comminution processes, the rate constant λ is independent of process input/rotor power. The final flake content in a repulping process depends the total energy input to a given repulping process and on the material being repulped. This confirms Hypothesis 1 in Section 1.5.2:

- **Hypothesis 1: The final flake content in a repulping operation depends on the total energy input to the repulping operation and is independent of the rate of energy addition (rotor power).**

Chapter 3: Energy and Paper Recycling: Modeling the Time and Energy Requirements for Low Consistency Batch Repulping

The previous chapter concerned identifying variables affecting specific energy requirements for repulping. The tests in Chapter 2 also confirmed that the rate constant λ is independent of rotor power and that the completeness of a repulping operation depends on the total energy input to the operation.

This chapter presents the derivation of a model to predict the time and energy required for repulping. The model includes the operating factors known to affect the time and energy required for repulping as found in previous literature concerning repulping and from the investigation in the previous chapter. The model also takes into account basic rotor and vat dimensions.

The model is based on Hypotheses 2, 3 and 4 from Section 1.5.2:

- **Hypothesis 2: The time and energy required for repulping depend on feed pulp toughness, not tensile strength.**
- **Hypothesis 3: LC Repulping occurs due to turbulence produced by the blunt vane shapes used by repulper rotors – specifically in the form of vane trailing vortices.**
- **Hypothesis 4: The relative time spent by flakes circulating past the repulper rotor versus in the rest of the vat in part determines repulping efficiency.**

3.1 Methods and Materials

The dimensions of each test rotor are given in Table 3.1. The mechanical properties of all of the pulp types tested in the previous chapter need to be known. To this end, wet tensile testing for material properties was performed in adherence to the TAPPI T 456 om-10 standard. Sixty-four wet tensile tests were performed for each material. These test were completed in two sets of thirty-two tests in perpendicular directions. The results shown represent a geometric average of the mean of the tensile tests in each direction. The error shown for all material test data is represents a 95% confidence interval based on a normal distribution.

Table 3.1: Test rotor dimensions. The rotor swept volume measurement is important further on and is defined by Equation 3.1.

	Rotor A	Rotor B	Rotor C
Diameter	233.7mm	233.7mm	233.7mm
Height	39.9mm	28.0mm	25.4mm
Swept Volume	0.00171m^3	0.00112m^3	0.00109m^3
# of Vanes	3	6	8

The plots shown in the previous chapter present specific energy in units of kW-h/Ton as this is in standard use in industry. To make the analysis and modeling easier in this chapter, the rate constant data is presented in this chapter in SI units. To convert from kW-h/Ton to J/kg, multiply the kW-h/Ton value by 3600.

3.2 A Theory Based Model for Repulping

Deflaking in terms of specific energy is known to follow the form of Equations 1.3a and 1.3b:

$$\frac{dF}{dt} = -kF \tag{1.3a}$$

$$\frac{dF}{dE} = -\lambda F \tag{1.3b}$$

where t is time, k is a rate constant with SI units of $[s^{-1}]$, E is specific energy (energy/unit mass), λ is a rate constant with SI units of [kg/J], and again, F is flake content. Given a repulper having a constant rotor speed, and hence constant rotor shaft power, and in batch operation, λ can be obtained from k by using the following relation:

$$dE = \frac{Pdt}{m_P} \tag{1.3c}$$

where P is the rotor shaft power and again, m_P is the total mass of pulp in suspension.

The following operating and design parameters affect the time and energy consumption in repulping:

1) Pulp concentration, or consistency. Increasing consistency reduces specific energy consumption.
2) Pulp suspension temperature. Increasing the suspension temperature reduces specific energy consumption.
3) Pulp type.
4) Geometry in terms of rotor to vat diameter ratio. The more space the rotor occupies in the vat, the less energy is required for repulping.
5) Rotor and vat design. Rotor and vat designs are varied. It is not clear how specific designs affect repulping time and energy consumption other than in terms of rotor/vat diameter ratio.

As of this time, there is no known link between items 1-5. However, based on the findings in Chapter 2, the previous research concerning repulping, and borrowing pertinent knowledge from the field of stirred mixing and from the study of pulp rheology, a theory based model describing repulping can be developed.

Recall the four mechanisms widely thought to be responsible for repulping:

- Flakes are broken down by being sheared between the rotor and extraction plate.
- Flakes are broken down by direct impact with the rotor.
- Flakes are worn down by fiber-to-flake/flake-to-flake rubbing.
- Flakes are broken down by turbulence.

The first item, mechanical shearing between the rotor and extraction plate, was disproven as a repulping mechanism in the previous chapter. This is not surprising as the fixed rotor-to-extraction plate clearance used by repulpers would limit shearing to a single flake size. Based on personal observation of flakes collected during many repulping tests, a population of many flake sizes is contained within each flake sample. Furthermore, the flakes on average appear to get smaller as the repulping process progresses.

The second suspected mechanisms is rotor-to-flake impact. Bennington et al. (1998b) showed that there may be some validity to this being a mechanism as his impact based model for repulping proved adequate for very slow rotor speeds. However, Bennington et al. (1998b) also found that when repulping was attempted in a high-shear mixer, the impact based model proved wholly inadequate and that high intensity turbulence was most likely the dominant repulping mechanism.

The third proposed mechanism is fiber-to-flake/flake-to-flake rubbing. The case often made for this is the fact that repulping efficiency improves with increasing consistency (Holik 1988; Paraskevas 1983). However, Bennington et al. (1998a) showed that repulping occurred as a result of cumulative rotor contact with the pulp in suspension. Based on this, an increase in efficiency comes from increased rotor-to-flake contact per rotor revolution simply from increased pulp concertation. This mechanism would result from motion imparted to the fluid by the rotor. For high rotor speeds, this fluid motion would be turbulent pointing to turbulence as the root mechanism.

Turbulence produced by the rotor is the most likely candidate to be the mechanism responsible for repulping. First, Bennington et al. (1998b) showed that repulping in fully turbulent flow in a high-shear mixer was far more efficient than repulping in a laboratory HC repulper at very slow rotor speeds. Second, LC repulper rotors have always operated at very high tip-speeds – tip speeds in the realm of dedicated turbomachinery such as centrifugal pump impellers. Over the years, repulper manufacturers have attempted to slow down repulper rotors while still maintaining repulper throughput (*Pulping of Secondary Fiber* 1990). It has long been thought that slowing down a repulper rotor improves energy efficiency (although this is not true – see Chapter 2). As a corollary to this, as rotors were slowed down, the shapes used by rotors grew increasingly blunter in order to maintain repulper throughput. This rotor shape evolution is exemplified by Rotor B in this study. The vertical flutes that sit atop every other vane on Rotor B were added to a number of rotors in the 1960's (*Pulping of Secondary Fiber* 1990). Figure 1.2 shows repulper rotor evolution over the years. Repulper rotors have not evolved over time with extra sharp edges, or streamlining of any sort, they have evolved to become ever blunter. This in and of itself is a good argument for turbulence being the repulping mechanism. With all this in mind, a model based on turbulence as the repulping mechanism is derived here.

Repulpers and repulper rotors are very similar to mixers and mixing impellers. Repulper rotors and mixing impellers used for turbulent stirred mixing are similarly blunt. It is common when comparing the performance of different mixing impellers in a fully turbulent flow regime to make the assumption that all of the impeller power is dissipated through turbulence in the impeller swept volume (Kresta and Brodkey 2004). This assumption is valid as a very large proportion of the impeller power is dissipated through turbulence very near the impeller (Lee and Yianneskis 1998; Nienow and Wilson 1974; Sharp and Adrian 2001; Stoots and Calabrese 1995; Van't Riet and Smith 1975; Yianneskis et al. 1987; Yianneskis and Whitelaw 1993). Repulper rotors operate in fully turbulent flow at similar power numbers to mixing impellers so it is also assumed here that the shaft power input to a repulper by a repulper rotor is dissipated by turbulence within the rotor swept volume defined as:

$$V_{Swept} = \frac{1}{4}\pi D_R^2 H_R \tag{3.1}$$

where D_R is the rotor diameter and H_R is the rotor height.

The rheology of pulp suspensions is complex. At low and moderate shear-rates, the behavior of pulp suspensions can be described by the Herschel-Bulkley non-Newtonian model (Derakhshandeh et al.

2010). In fully turbulent flow, pulp suspensions behave as Newtonian fluids (Bennington and Kerekes 1996; Derakhshandeh et al. 2011). It is thought that pulp suspensions "fluidize" in highly turbulent flow in an analogous manner to the way in which particles are floated in turbulent flow in a fluidized bed reactor. This allows a pulp suspension that would otherwise need to be pumped using a positive displacement type pump to be transported using a centrifugal pump. Pulp suspensions have been shown to be able to be pumped in a centrifugal pump up to approximately 15% consistency (Gullichsen and Harkonen 1981). It was determined in Section 1.4.1 that industrial repulper rotors likely "fluidize" the pulp suspensions which they process. This indicates that repulper rotors produce highly turbulent flow in pulp suspensions.

Based on the above, it is proposed that the break-up of waste paper in a low consistency repulper can be modeled as occurring within the rotor swept volume with rotor power being dissipated in part through turbulence in the fluid and in part breaking up waste paper.

Energy is input to the repulper vat in the form of shaft work (P). This shaft work is dissipated in the waste paper/pulp suspension either by repulping (breaking down waste paper) or directly by turbulence in the non-flake portion of the suspension. To this end, the waste paper/pulp to be repulped can be classified as being either flakes (F) or non-flakes ($1 - F$). The ratio of the power split between repulping and direct dissipation by turbulence is given by $\gamma \in [0,1]$ such that the shaft work applied to repulping is:

$$\frac{dE_F}{dt} = \gamma P \tag{3.2}$$

where E_F is the energy to the flakes and t is time.

The shaft work input to the system is split between flakes and non-flakes based on:

- The mass concentration of flakes in suspension (CF). Bennington et al. (1998) showed that repulping occurs from rotor contact with the pulp suspension and that this contact was linearly proportional to the pulp concentration in the suspension.
- The residence time (τ_{Swept}) for flakes within the rotor swept volume (where repulping occurs) versus the residence time (τ_{Vat}) for flakes away from the rotor in the rest of the vat (where repulping does not occur). This is from Hypothesis 4 in Section 1.5.2.

This gives γ as:

$$\gamma = \frac{\tau_{Swept}}{\tau_{Vat}} CF \tag{3.3a}$$

$$\gamma = \frac{\tau_{Swept}/Q}{\tau_{Vat}/Q} CF \tag{3.3b}$$

$$\gamma = \frac{V_{Swept}}{V_{Vat}} CF \tag{3.3c}$$

where C is the mass concentration of all pulp in suspension (both flakes and non-flakes) and Q is the volumetric flow produced by the rotor.

From Hypothesis 2, the energy required for repulping is dependent upon the material toughness by:

$$E_F \sim -\sigma m_P F \tag{3.4}$$

where σ is material toughness having SI units of [J/kg] and the negative sign is present because additional energy input results in a reduction in the mass of flakes in the repulper. Combining Equations 3.2, 3.3c, and 3.4 gives the deflaking rate in time as:

$$\frac{dF}{dt} = -\frac{1}{\sigma} \frac{V_{Swept}}{V_{Vat}} \frac{P}{m_P} CF \tag{3.5}$$

and with specific energy defined as P/m_P:

$$\frac{dF}{dE} = -\frac{1}{\sigma}\frac{V_{Swept}}{V_{Vat}}CF \tag{3.6}$$

where E is energy per unit mass, or specific energy. The rate constants, k and λ, in Equation 1.3 are then:

$$k = \frac{1}{\sigma}\frac{V_{Swept}}{V_{Vat}}\frac{P}{m_P}C \tag{3.7a}$$

$$\lambda = \frac{1}{\sigma}\frac{V_{Swept}}{V_{Vat}}C \tag{3.7b}$$

The forms of Equations 3.7a and 3.7b agree with the findings in previous literature that k is linearly proportional to both the pulp suspension concentration C, and the rotor shaft power (Amaral et al. 2000; Vilaseca et al. 2011). The form of Equation 3.7b agrees with the finding that rotor shaft power does not influence the energy required for repulping and that the completeness of repulping depends upon the total energy input to the process and the material properties of the pulp being repulped.

3.3 Results and Discussion

This section shows both the results of material testing and the accuracy of the model presented by Equation 3.7 for predicting the performance of the laboratory repulper for various operating conditions.

3.3.1 Material Testing Data

The following figures show the measured wet-tensile strength, elongation, and toughness for kraft aspen, office paper, newsprint, paper towel, single-sided C-flute corrugated cardboard, and C-flute corrugated cardboard.

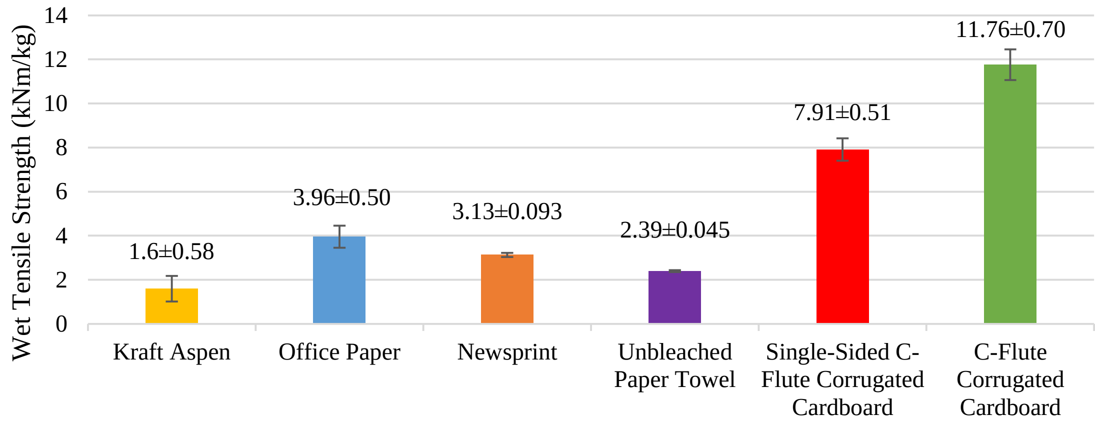

Figure 3.1: Comparison of wet-tensile strength as obtained following the TAPPI T 456 om-10 standard for wet-tensile testing.

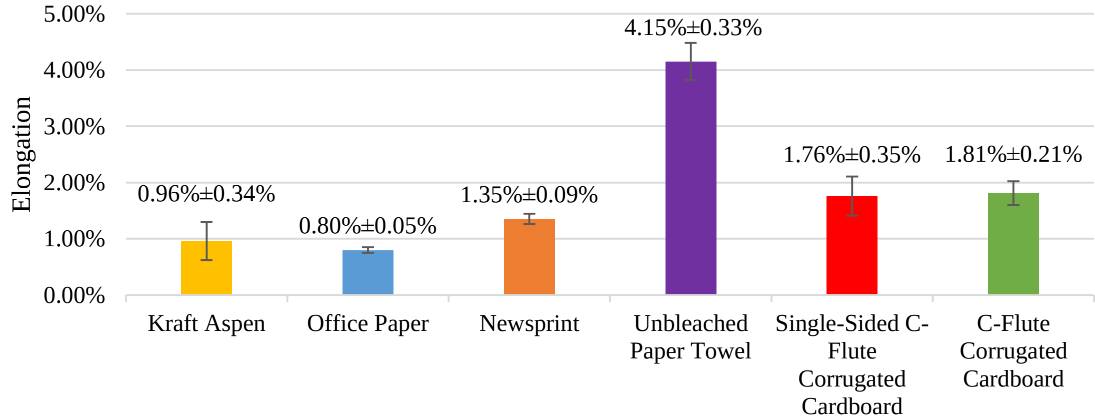

Figure 3.2: Comparison of elongation as obtained following the TAPPI T 456 om-10 standard for wet-tensile testing.

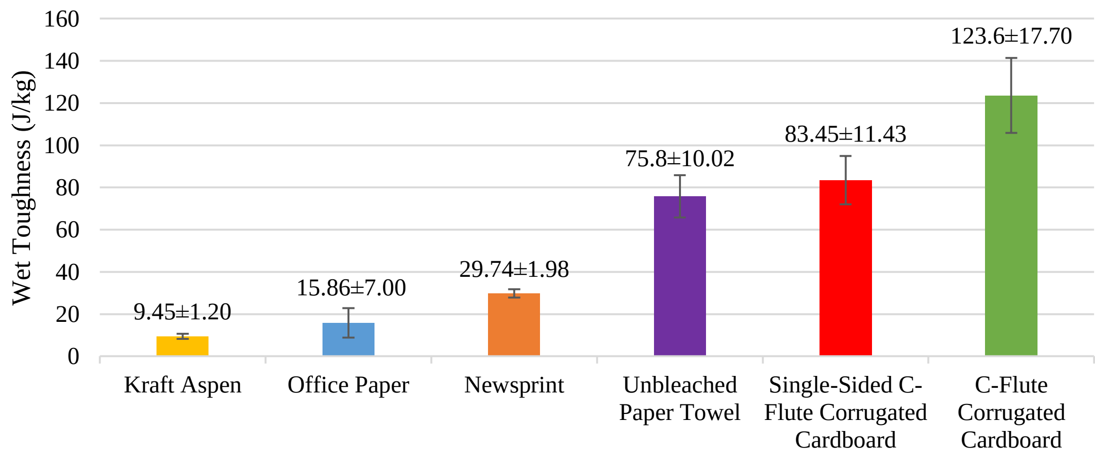

Figure 3.3: Comparison of wet-toughness as obtained following the TAPPI T 456 om-10 standard for wet-tensile testing.

3.3.2 The Rate Constant λ versus Wet-Tensile Strength

Recall that Hypothesis 2 from Section 1.5.2 stated that the rate constant λ should vary with material toughness and not tensile strength. Figures 3.4 shows the variation of λ as measured using the laboratory repulper for each test material with wet-tensile strength. Notice that λ does not correlate with tensile strength. Looking back to Figures 3.1, 3.2 and 3.3 reveals that paper towel shows poorer tensile strength but much greater elongation than the other test materials. The toughness of paper towel is similar to that of single-sided C-flute corrugated cardboard and so is the measured λ for these two materials.

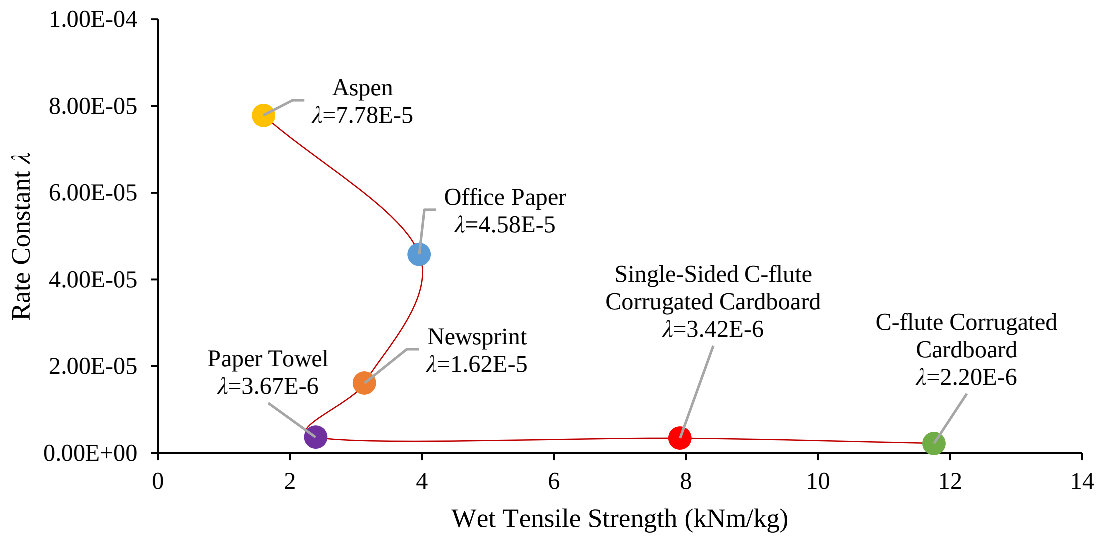

Figure 3.4: Comparison of λ with measured tensile strength. Note that λ does not correlate well with wet tensile strength. Paper towel shows low tensile strength but requires a quantity of energy comparable to single-sided C-flute corrugated cardboard to be repulped. All measurements of λ were measured using Rotor A operating at a 13m/s tip speed in a 5% consistency pulp suspension at 20°C with a vat fill level of 220L. The wet tensile strength for all materials was obtained following the TAPPI T 456 om-10 standard for wet-tensile testing.

3.3.3 Model Fit

The model predictions as per Equation 3.7b are compared with actual measurements taken using the laboratory repulper in this section. The model parameters include material toughness (σ), suspension concertation (C), and rotor swept volume/vat volume (V_{Swept}/V_{Vat}). Therefore, the model predictions for the variation of each of these parameters is compared with measurements taken using the laboratory repulper.

Figure 3.5 shows the predicted λ using Equation 3.7b versus the measured λ for different pulp types. The varied parameter here is material toughness (σ). Figure 3.5 shows that the model not only accurately predicts λ for all of the pulp types, but also confirms Hypothesis 2 which states that λ should depend on a measure of material toughness.

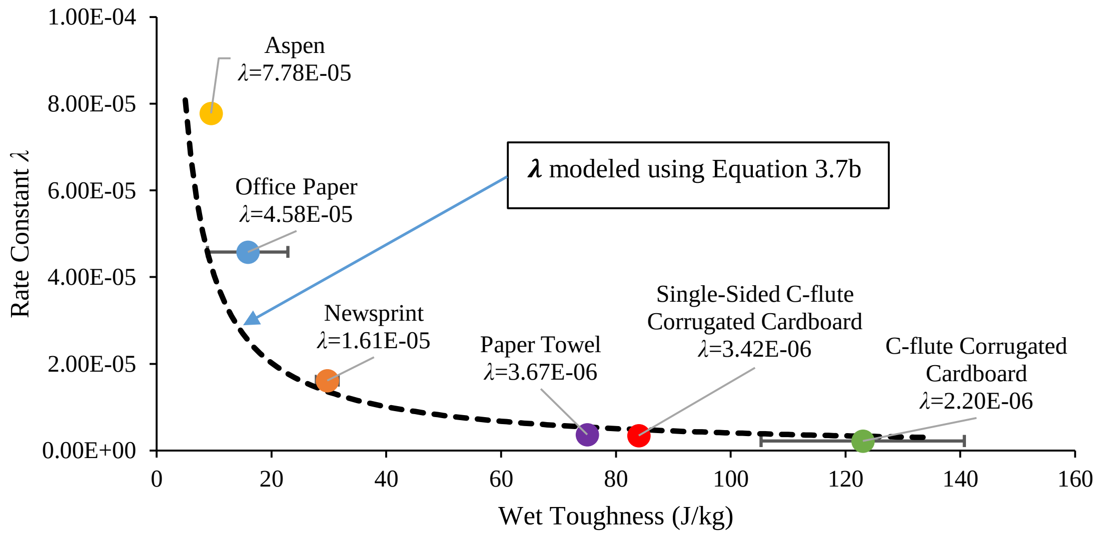

Figure 3.5: The predicted λ (using Equation 3.7b) vs. toughness is compared to the measured λ vs. toughness for different pulp types. All measurements of λ were measured using Rotor A operating at a 13m/s tip speed in a 5% consistency pulp suspension at 20°C with a vat fill level of 220L. The wet toughness for all materials was obtained following the TAPPI T456 om-10 standard for wet-tensile testing.

The inputs to Equation 3.7b are the pulp mass concentration (C), vat volume (V_{Vat}), material toughness (σ), and the rotor swept volume (V_{Swept}). Of these four inputs, only V_{Swept} is not a directly measured quantity. The rotor swept volume is an estimate of the region of sufficient turbulence intensity to break down waste paper. Pertaining to Figure 3.5, notice that the use of a constant rotor swept volume as the input to Equation 3.7b results in an over-prediction of repulping rate for the tough materials and an under-prediction of the repulping rate for the weak materials like kraft aspen. This indicates that a larger region of lower intensity turbulence is able to repulp the weak materials. As the material toughness increases, the region of sufficient intensity for repulping decreases. Nevertheless, the use of a constant rotor swept volume provides a good estimate of the repulping rate covering the very weakest (kraft aspen) to the very strongest (corrugated cardboard) materials likely to be repulped.

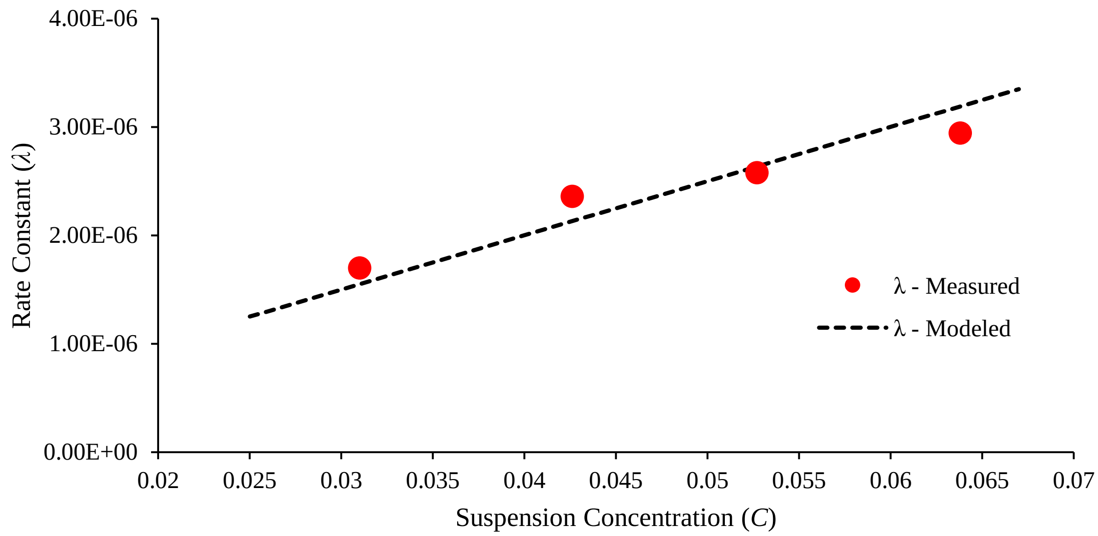

Figure 3.6: The predicted λ (using Equation 3.7b) vs. suspension concentration is compared to the measured λ vs. suspension concentration. All measurements of λ were measured using Rotor B operating at a 13m/s tip speed in a 5% consistency C-flute corrugated cardboard pulp suspension at 20°C with a vat fill level of 220L.

Figure 3.6 shows the predicted λ (using Equation 3.7b) versus the measured λ for different pulp suspension concentrations. The varied parameter here is concentration (C). Notice the linear dependence of the repulping rate on consistency. This confirms the validity of the assumption that rotor shaft power is split linearly between repulping and direct dissipation by turbulence based on the mass concentration of flakes in suspension.

Figure 3.7 shows the predicted λ (using Equation 3.7b) versus the measured λ for different vat fill volumes. The varied parameter here is rotor swept volume/vat volume (V_{Swept}/V_{Vat}) - specifically V_{Vat} as the rotor size is fixed. Note that the model fits the experimental data until the vat fill volume drops below 0.14m^3 at which point the efficiency of the machine sharply drops. The baffles in the laboratory repulper do not extend all the way to the vat bottom and once the vat level drops to 0.12m^3, the pulp suspension begins to show solid body motion, or swirl, around the vat.

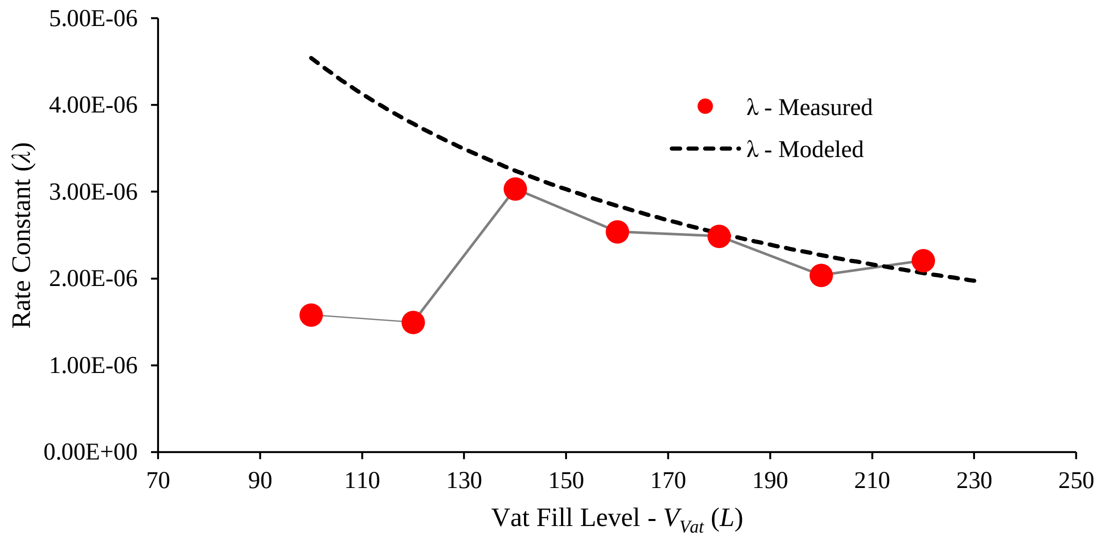

Figure 3.7: The predicted $\boldsymbol{\lambda}$ (using Equation 3.7b) vs. vat fill level ($\boldsymbol{V_{Vat}}$) is compared to the measured $\boldsymbol{\lambda}$ vs. vat fill level. Notice that at vat levels of 120L and less that the measured performance falls off of the model prediction. This performance drop correlates with the onset of solid-body swirl of the suspension in the repulper. At these low vat levels, the repulper baffles lose effectiveness. All measurements of $\boldsymbol{\lambda}$ were measured using Rotor C operating at a 14m/s tip speed in a 5% consistency C-flute corrugated cardboard pulp suspension at 20$^{\mathbf{o}}$C.

3.3.4 Mixing and $\boldsymbol{\lambda}$

Figure 3.8 shows the empty repulper, the suspension free surface at a fill volume of 200L, and the free surface at a vat volume of 120L. The solid body motion suggests that below a fill volume of 140L, the laboratory repulper is under-baffled.

Figure 3.8: The suspension free surface is shown at a vat fill volume of 200L (middle) and a vat fill volume of 120L (Right). Notice that the top of the rotor is revealed by the swirling suspension at the vat fill level of 120L. The rotor tip speed for both fill levels is 14m/s.

The under-baffled condition can be confirmed by plotting the rotor power number (N_P) versus the rotor Reynolds number (Re). The impeller power number in a sufficiently baffled mixing vessel will become independent of the impeller Reynolds number at high impeller speeds.

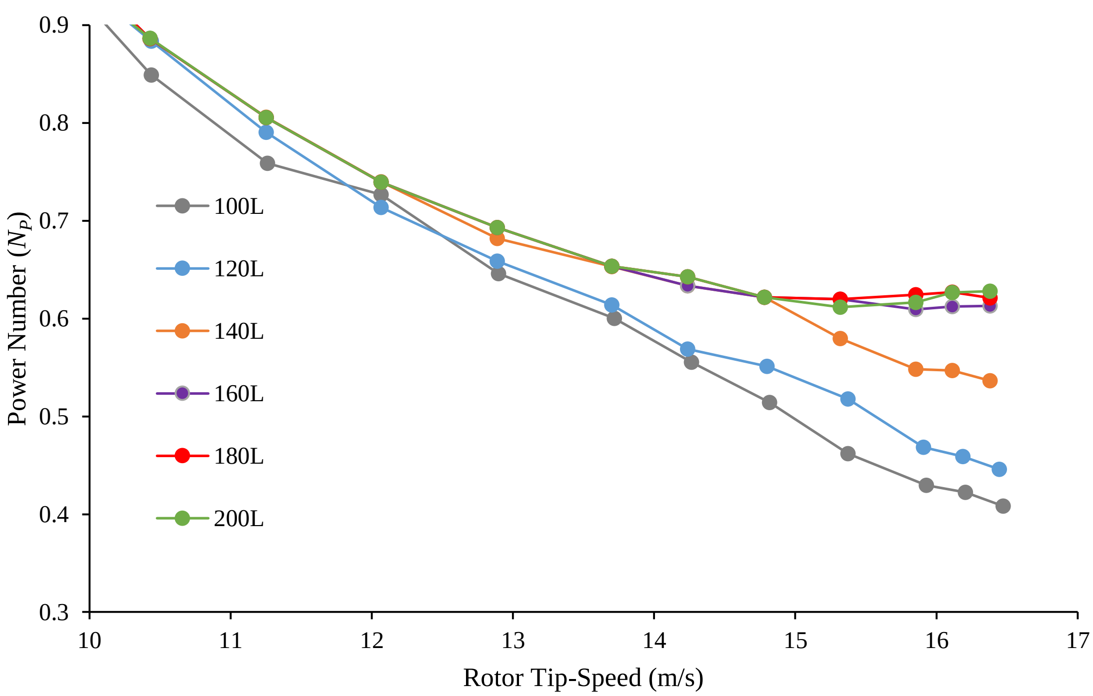

Figure 3.9: Rotor Power number versus tip-speed (as viscosity is unknown) for different vat fill levels. Notice that at low fill levels, the baffles in the repulper become ineffective and the condition of Reynolds independence is no longer achievable. The above plot defines the operating window in terms of rotor tip-speed and vat fill level for the laboratory repulper.

In an under-baffled vessel, the impeller power number will continue to decrease with increasing Reynolds number – the condition of Reynolds independence may not be achievable (see Figure 1.6) even for very high impeller speeds depending on the vat and impeller combination (Bates et al. 1966).

Figure 3.9 shows power number plotted against the rotor tip speed (v_{tip}) with Rotor C for varying vat volumes. The rotor tip-speed is used in place of the rotor Reynolds number, as the viscosity of the pulp suspension is not known. As the suspension is likely fluidized near the rotor, the pulp suspension near the rotor is likely behaving in a Newtonian fashion thus justifying the use of rotor tip-speed in place of the rotor Reynolds number.

The rotor tip-speed for all of the vat-volume tests shown in Figure 3.9 is 14m/s. Notice in Figure 3.9 that at a test speed of 14m/s, the rotor power number drops once the vat volume falls to 120L. This confirms that the laboratory repulper is under-baffled for a rotor tip speed of 14m/s and at vat volumes less than 140L. Notice also that at tip speeds greater than approximately 15m/s, Figure 3.9 shows that the laboratory repulper is under-baffled for a vat volume of 140L as well. As shown in Figure 3.7, the measured rate λ, agrees with the model prediction (Equation 3.7b) for a vat volume of 140L and a tip-speed of 14m/s. The data in Figure 3.9 implies that the efficiency of the laboratory repulper should drop off from the model prediction for rotor tip-speeds greater than 15m/s when the vat volume is 140L. In Section 2.2.4, it was found that the efficiency of the laboratory repulper was unchanging for tip-speeds between 12-15m/s for Rotors A, B, and C. The form of Equation 3.7b echoes this finding. The finding here suggests that this is only the case when the repulper is operating at a level where it is sufficiently baffled. It also indicates that efficient mixing is a key to efficient repulper operation as solid body motion goes hand-in-hand with poor mixing.

3.3.5 Temperature Dependency

The rate constant λ has been shown to vary inversely with material toughness by:

$$\lambda \propto \frac{1}{\sigma} \tag{3.8}$$

What about the past research that shows a linear dependence of the rate constants on material properties? The past research was accomplished using newsprint and stronger materials only (Bennington et al. 1998a; Brouillette et al. 2003; Holik 1988). The portion of the curve shown in Figure 3.5 extending from newsprint to the right could easily be fit with a straight line.

Kouko et al. (2014) and Back and Andersson (1992) showed that the toughness wet paper decreases linearly with increasing temperature. This means that:

$$\sigma(T) = -aT + b \tag{3.9}$$

where T is temperature and a and b are pulp type dependent constants. By extension of Equation 3.9:

$$\lambda \propto \frac{1}{-aT + b} \tag{3.10}$$

It is expected then that changes in temperature should move the repulping rate along the hyperbolic curve represented by Equation 3.10. Cho et al. (2009) reported a linear dependence for the repulping rate on temperature. A linear functional relationship for λ vs. temperature was found here as well and is shown in is Figure 3.10.

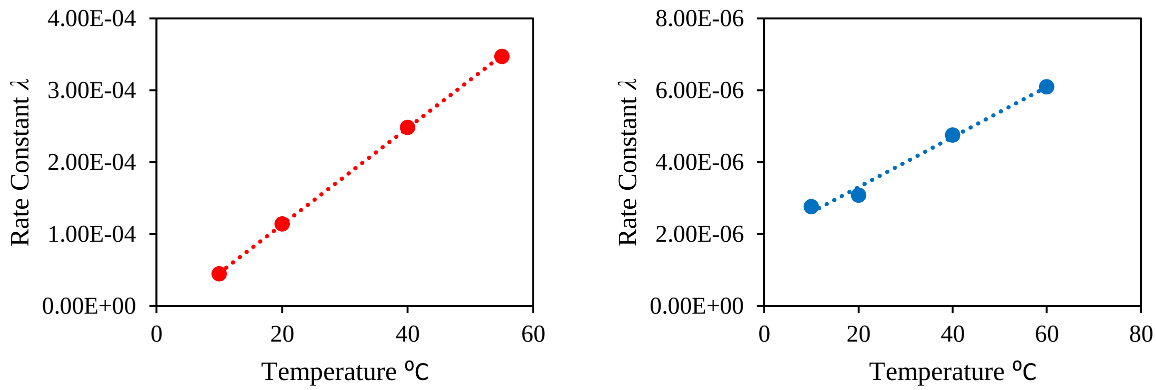

Figure 3.10: Although the rate constant λ varies in an inversely proportional manner to suspension temperature (see Equation 3.10), the dependency of λ on temperature for both kraft aspen (left) and C-flute corrugated cardboard (right) can be approximated as being linear.

The linear fits from testing with C-flute corrugated cardboard and kraft aspen are given by Equation 3.11:

$$\lambda_{Aspen}[T] = 6.194 \times 10^{-6}\, T \tag{3.11a}$$

$$\lambda_{corrugated}[T] = 6.990 \times 10^{-8} T + 1.90 \times 10^{-6} \tag{3.11b}$$

How does this reconcile with the expectation that the repulping rate should depend on temperature in the form of Equation 3.10? The materials tested here are kraft aspen and C-flute corrugated cardboard, the least tough and toughest materials tested respectively. Looking back to Figure 3.5, both of these materials lay out at the far left and far right of the hyperbolic curve shown in the figure. Over the range of test temperatures, the toughness of both materials remains on a portion of the hyperbola that could be approximated by a straight line. For this reason, the repulping rate of these two materials can be fit with a straight line.

Temperature dependence can be added to the model presented here where the material toughness is a function of temperature. This gives Equations 3.7a and 3.7b as:

$$k(T) = \frac{1}{\sigma(T)} \frac{V_{Swept}}{V_{Vat}} \frac{P}{m_P} C \tag{3.7a}$$

$$\lambda(T) = \frac{1}{\sigma(T)} \frac{V_{Swept}}{V_{Vat}} C \tag{3.7b}$$

The dependence of material toughness (σ) on temperature can be found from the measured rates k and λ. Equations 3.7a and 3.7b can be combined with the linear fits given by Equations 3.11a and 3.11b and the repulping conditions in terms of V_{Swept}/V_{Vat}, C etc. at which the fits in Figure 3.10 were made:

$$\sigma(T)_{Aspen} = 4.540 \times 10^{-4} \cdot \frac{1}{6.194 \times 10^{-6} T} \tag{3.12a}$$

$$\sigma(T)_{Corrugated} = 2.875 \times 10^{-4} \cdot \frac{1}{6.990 \times 10^{-8} T + 1.900 \times 10^{-6}} \tag{3.12b}$$

3.4 Chapter Conclusion

Now to address points 1-5 from the beginning of this section. Repulping efficiency improves with increasing consistency as more flakes are in the vicinity of the rotor at any given time. The rotor power is dissipated either directly by turbulence or by repulping with the split of rotor power going to each based on the concentration of flakes in suspension.

The time and energy required for repulping depend on how much energy the feed material can absorb before rupturing which is quantified by material toughness, or the area under the material stress-strain curve. A tougher material can absorb more energy than a weaker one and therefore requires more energy to be repulped. Increased temperature reduces material toughness and therefore the time and energy required for repulping.

Savolainen et al. (1991) and Bennington et al. (1998b) showed that increasing the diameter of the rotor relative to that of the vat reduces the time and energy required for repulping. This can be explained by the model presented here. With each increase in the rotor size relative to the vat size (or reduction in vat size relative to the rotor size), flakes spend relatively more time at the rotor being repulped rather than in the rest of the vat not being repulped. Although a larger rotor will result in higher rotor power requirements for a given rotor speed, it will make for faster and more energy efficient deflaking.

Finally, addressing point 5, the rotor/vat combination is extremely important for efficient repulping. A given rotor/vat combination should enable rotor operation in the fully turbulent flow regime. An under-baffled vat allows for solid body rotation of the pulp suspension. This means poor mixing and therefore uneven circulation of the waste paper to the rotor for disintegration.

The model derived here assumes perfect mixing and perfect circulation in the repulper and represents a best efficiency for a given set of operating conditions. The efficiency of the laboratory repulper could be improved for low fill volumes if the baffles were modified to stop solid body rotation at these low volumes.

All this points to an ideal repulper being one with a large rotor/vat volume ratio having a rotor/vat combination able to support highly turbulent flow at the rotor and efficiently mix pulp suspensions at consistencies of approximately 15% - the limiting consistency at which pulp suspensions can be fluidized (Gullichsen and Harkonen 1981). This description almost describes an HC repulper and brings about a caveat concerning the application of the presented model to estimate the performance of high-consistency repulpers. In a high-consistency repulper, the rotor occupies almost the entire vat making the $V_{Swept}/V_{Vat} \approx 1$. HC repulper rotors operate in lamina/transitional flow regimes with a good portion of the flow around the rotor being laminar (Bennington et al. 1998a; 1998b). Therefore, V_{Swept} does not define a fully turbulent region of fluidized pulp in the case of the HC repulper and the model in the presented form is only applicable to LC repulping. Furthermore, the suspension in an HC repulper often does not even completely cover the rotor. Avoiding solid body swirl of the suspension at such a low fill level is difficult. The model only applies to a situation where the suspension is not swirling.

For existing repulpers, mills can improve throughput and energy efficiency by lowering the repulper vat level and raising consistency. As most repulpers installed in mills are not driven by a variable frequency drive, a power number versus Reynolds number plot to find the best operating point is not possible. Therefore, operators should lower the vat level until the point is found where rotor power drops and solid body motion is observed. The level should then be raised back to the lowest level before the rotor power dropped. This is the best efficiency point for the repulper at the test consistency. Raising suspension consistency will provide a baffle-like effect through an increase in the apparent viscosity of the suspension and will allow lower vat fill levels without swirl.

Hypothesis 2 is confirmed:

- **Hypothesis 2: The time and energy required for repulping depend on feed pulp toughness, not tensile strength.**

The rate constant λ does not depend on wet-tensile strength but on wet-toughness. Figures 3.4 and 3.5 confirm this.

- **Hypothesis 5: Efficient mixing depends on both the rotor and vat as a system and is critical for efficient repulping.**

Hypothesis 5 is confirmed by the drastic drop-off in repulping efficiency after the onset of solid-body swirl of the suspension within the repulper.

The repulping model presented in this chapter relies on Hypotheses 3 and 4. The validity of hypotheses 3 and 4 are further tested in the next section.

Chapter 4: Scale-Up

The model presented in the previous chapter is used here to scale the repulping performance of the 0.25m^3 laboratory repulper to a 15m^3 industrial repulper. The model given by Equation 3.7, and in the form of Equation 4.1 in conjunction with data from the laboratory repulper, are used in this chapter to predict the repulping performance of a 15m^3 industrial repulper:

$$\frac{k_2}{k_1} = \frac{P_2 m_{p1} C_2 V_{2\,Swept} V_{1\,Vat} \sigma(T)_1}{P_1 m_{p2} C_1 V_{1\,Swept} V_{2\,Vat} \sigma(T)_2} \tag{4.1a}$$

$$\frac{\lambda_2}{\lambda_1} = \frac{C_2 V_{2\,Swept} V_{1\,Vat} \sigma(T)_1}{C_1 V_{1\,Swept} V_{2\,Vat} \sigma(T)_2} \tag{4.1b}$$

where the subscripts 1 and 2 refer to each repulper being compared.

4.1 Methods and Materials

In this chapter, the repulping performance of the laboratory repulper is compared with a 15m^3 industrial repulper in a running mill.

The specifications of the laboratory repulper are compared with the industrial repulper in Table 4.1.

Table 4.1: The specifications of the laboratory repulper are compared with an industrial repulper. A method for scaling repulping performance between these two machines is presented in this chapter. The method is based on the repulping model presented in the previous chapter.

	Laboratory Repulper	15m^3 Industrial Repulper
Installed Power	7.5hp	300hp
Vat Volume	0.25m^3	15m^3
Rotor Diameter	233.7mm	900mm
Rotor Diameter/Vat Diameter Ratio	0.31	0.30
Rotor Tip Speed	11-16.5m/s	18m/s
Rotor Power/Vat Volume	7-20kW/m^3	15kW/m^3

The performance of the industrial repulper was determined using the same methods as those used earlier to measure the performance of the laboratory repulper. Figure 4.1 shows an interior view of the industrial repulper being compared to the laboratory repulper in this chapter.

Figure 4.1: View looking inside the 15m^3 industrial scale repulper that the repulping performance of the 0.25m^3 laboratory repulper is being scaled to. Note that Rotor A is installed here - $V_{Swept} = 0.98m^3$. Photo taken by the author.

4.2 Results

4.2.1 Scaling for Rotor Power

Repulper rotors operate at high speed. Figure 3.9 shows that with sufficient baffling, the rotors within the laboratory repulper operate in, near-fully turbulent to fully turbulent flow over the range of rotor tip speeds used in this study. Therefore, the rotor power in one repulper can be estimated from the power number obtained in the other repulper using constant power number scaling as per Equation 4.2:

$$\frac{P_1}{\rho v_{Tip_1}^3 D_1^2} = \frac{P_2}{\rho v_{Tip_2}^3 D_2^2} \tag{4.2}$$

where v_{Tip} is rotor tip-speed and again the subscripts “1” and “2” refer to each repulper being compared. Constant power number scaling between the laboratory repulper and a 15m^3 industrial repulper with both repulpers using Rotor A is shown in Figure 4.2. The repulping time rate constant k can then be estimated using the model in the form of Equation 4.1a.

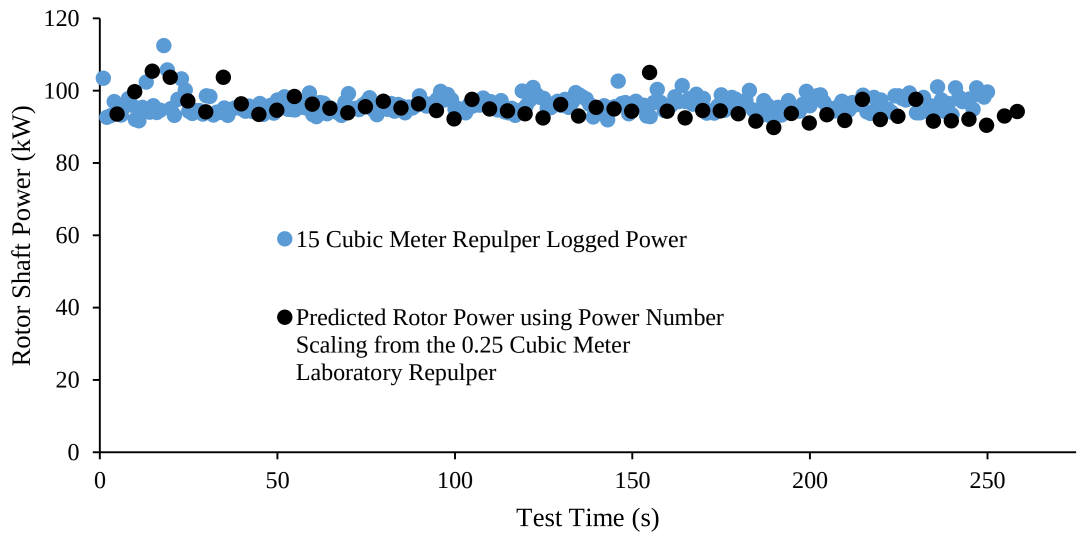

Figure 4.2: The measured rotor shaft power in a 15m^3 repulper and the predicted rotor shaft power using constant power number scaling from the measured rotor power in the 0.25m^3 laboratory repulper. Rotor A is installed in both repulpers and both repulpers are processing a 2.5% consistency kraft aspen suspension. The rotor-tip speed in the laboratory repulper is 11m/s and the rotor tip-speed in the 15m^3 repulper is 18m/s.

4.2.2 Scaling for k and λ

In this section, Equations 3.7, 4.1 and 4.2 are used to predict the repulping performance of a 15m^3 industrial repulper based on scaling from the laboratory repulper.

4.2.2.1 Direct Application of Equation 3.7

Repulping data collected from the 15m^3 industrial repulper was done so with this repulper operating in a running tissue mill. This limited the test conditions to those required by the mill processes following repulping. The operating conditions for the 15m^3 repulper are given in Table 4.2. The toughness of kraft aspen is unknown at the test temperature of 37^0 C but it can be estimated using Equation 3.12a found from testing in the 0.25m^3 laboratory repulper as shown below.

Table 4.2: 15m^3 Industrial Repulper Operating Conditions

Operating Conditions for 15m^3 Repulper	
Pulp Type	Kraft Aspen
σ - Toughness	Unknown for 37^0 test temperature
Suspension Temperature	37^0
V_{Swept}	0.098m^3
V_{Vat}	15m^3
C – Mass Concentration	0.027
m_p – Mass of Pulp	450kg
P – Rotor Power	94.5kW

Use Equation 3.12a to estimate toughness @ 37^{0}C

$$\sigma(37)_{Aspen} = 4.540 \times 10^{-4} \cdot \frac{1}{6.194 \times 10^{-6}(37)}$$

$$\sigma(37)_{Aspen} = 1.98 \text{ J/kg}$$

With an estimate for the toughness of kraft aspen at 37^{0}C, the rate constants k and λ can be estimated using Equation 3.7:

$$\lambda(T) = \frac{1}{\sigma(T)} \frac{V_{Swept}}{V_{Vat}} C = \frac{1}{1.98\frac{\text{J}}{\text{kg}}} \frac{0.098m^3}{15m^3} 0.027 = \boxed{8.91 \times 10^{-5} \frac{\text{kg}}{\text{J}}}$$

$$k(T) = \lambda(T) \frac{P}{m_p} = 8.91 \times 10^{-5} \frac{\text{kg}}{\text{J}} \frac{94{,}500\text{W}}{450\text{kg}} = \boxed{1.87 \times 10^{-2} \frac{1}{s}}$$

The accuracy of the prediction is shown in Table 4.3:

Table 4.3: Predicted k and λ using Equation 3.7 compared with measured k and λ values for the 15m³ industrial repulper.

	Measured for 15m³ Repulper	Predicted for 15m³ Repulper	% Difference
k	1.790 x10^{-2} 1/s	1.87 x10^{-2} 1/s	4.5%
λ	8.509x10^{-5} kg/J	8.91x10^{-5} kg/J	4.8%

The accuracy of the prediction using Equation 3.7 is better than 5%.

4.2.2.2 V_{Swept}/V_{Vat}

In the case that both material properties and the rotor power in one repulper is not known, Equations 4.1 and 4.2 can be used to scale performance between repulpers.

Table 4.4: Scaling comparison between the 0.25m³ laboratory repulper and a 15m³ industrial repulper for different V_{Swept}/V_{Vat}.

Operating Conditions	Laboratory Repulper	Industrial Repulper
Rotor Style	Rotor A	Rotor A
Pulp Type	Kraft Aspen	Kraft Aspen
Rotor Diameter	233.7mm	900mm
Rotor Height	40mm	154mm
V_{swept}	0.00171m³	0.098m³
V_{Vat}	0.2m³	15m³
C – mass concentration	0.027	0.027
Suspension Temperature	37°C	37°C
σ –Pulp Toughness	Not needed – constant temperature comparison.	Not needed – constant temperature comparison.
m_p – mass of pulp	5.3kg	450kg
P – Rotor Power/Rotor Tip-Speed	1.65kW/ 11m/s	94.5kW/ 18m/s
k – Measured	4.220 x10^{-2} 1/s	1.790 x10^{-2} 1/s
λ –Measured	1.356 x10^{-4} kg/J	8.509x10^{-5} kg/J

Prediction	Measured Industrial Repulper	Predicted for Industrial Repulper	% Difference
P	94.5kW	107kW (Eqn.4.2)	13.2%
k	1.790 x10^{-2} 1/s	2.164x10^{-2} 1/s (Eqns. 4.1a and 4.2)	21.0%
λ	8.509x10^{-5} kg/J	1.036x10^{-4} kg/J (Eqn.4.1b)	21.8%

Here, data from testing with the laboratory repulper and Equations 4.1 and 4.2 are used to predict the repulping performance of the $15m^3$ industrial repulper. This comparison is shown in Table 4.4. In this case, Rotor A is installed in both repulpers, the pulp concentration (C) in both repulpers is 0.027, and the suspension temperature in both repulpers is 37°C. The varied parameter is V_{Swept}/V_{Vat}. The full list of model input parameters are shown in the table.

4.2.2.3 V_{Swept}/V_{Vat}, Concentration (C)

A comparison between the laboratory repulper and the industrial scale repulper is presented again in Table 4.5. In this case, Rotor A is installed in both repulpers and the suspension temperature in both repulpers is 37°C. The varied parameters are V_{Swept}/V_{Vat} and suspension concentration. For this comparison, the suspension concentration in the laboratory repulper is 0.048 and again the suspension concentration in the industrial repulper is 0.027.

Table 4.5: Scaling comparison between the $0.25m^3$ laboratory repulper and a $15m^3$ industrial repulper for different V_{Swept}/V_{Vat} and suspension concentration (C).

Operating Conditions	**Laboratory Repulper**	**Industrial Repulper**
Rotor Style	Rotor A	Rotor A
Pulp Type	Kraft Aspen	Kraft Aspen
Rotor Diameter	233.7mm	900mm
Rotor Height	40mm	154mm
V_{swept}	$0.00171m^3$	$0.098m^3$
V_{Vat}	$0.2m^3$	$15m^3$
C – mass concentration	0.05	0.027
Suspension Temperature	37°C	37°C
σ –Pulp Toughness	Not needed – constant temperature comparison.	Not needed – constant temperature comparison.
m_p – mass of pulp	10kg	450kg
P – Rotor Power/Rotor Tip-Speed	1.75kW/ 11m/s	94.5kW/ 18m/s
k – Measured	3.756×10^{-2} 1/s	1.790×10^{-2} 1/s
λ –Measured	2.039×10^{-4} kg/J	8.509×10^{-5} kg/J

Prediction	**Measured Industrial Repulper**	**Predicted for Industrial Repulper**	**% Difference**
P	94.5kW	113kW (Eqn. 4.2)	19.6%
k	1.790×10^{-2} 1/s	2.237×10^{-2} 1/s (Eqn. 4.1a and 4.2)	25.0%
λ	8.509×10^{-5} kg/J	8.414×10^{-5} kg/J (Eqn. 4.1b)	1.01%

4.3 Discussion

The industrial repulper is 60 times larger in volume than the laboratory repulper yet the predictions made using Equation 3.7 are accurate to within 5%. Furthermore, for cases where the feed pulp material properties as well as the rotor power in one repulper are not known, comparisons can made between repulpers of different sizes and having different operating conditions using Equations 4.1, and 4.2. This is shown accurate for the comparisons presented in Tables 4.4 and 4.5 between the laboratory repulper and the industrial repulper.

4.4 Chapter Conclusion

The presented analytical model provides a link between pulp material properties, pulp suspension concentration, pulp suspension temperature, rotor and vat geometry, and repulping time and energy. The model accurately predicts the repulping time and energy requirements in both a $0.25m^3$ laboratory scale repulper and a $15m^3$ industrial scale repulper.

Hypotheses 3 and 4 are rewritten below:

- **Hypothesis 3: LC Repulping occurs due to turbulence produced by the blunt vane shapes used by repulper rotors – specifically in the form of vane trailing vortices.**
- **Hypothesis 4: The relative time spent by flakes circulating past the repulper rotor versus in the rest of the vat in part determines repulping efficiency.**

The model presented in the last two chapters is based directly on these two hypotheses. Given the accuracy of the model in both a $0.25m^3$ and a $15m^3$ industrial repulper, it stands to reason that both of these hypotheses are very plausible. In the opinion of the author, the accuracy of the model confirms Hypothesis 4 and at least partially confirms Hypothesis 3 in that high intensity turbulence in the vicinity of the rotor is responsible for repulping. However, the model does not consider trailing vortices. The identification of the existence of trailing vortices like those seen with mixing impellers is the subject of the next two chapters of this thesis.

Chapter 5: Repulper Rotor Flow Fields

Rotor manufacturers routinely introduce new rotor designs having novel vane shapes claimed to provide substantial reductions in repulping time and energy use. The three rotors tested in this thesis differ not only in vane shape but also in terms vane height, vane length and in the number of vanes used by each rotor. Despite these differences, each rotor repulps with similar, but statistically different, efficiency (see Section 2.2.5).

Based on the work presented in this thesis so far, it appears that high intensity turbulence produced by LC repulper rotors is responsible for repulping. Among the many LC repulper rotor designs since the first repulpers were put into use in 1939 (*Pulping of Secondary Fiber* 1990), and among all of the novel vane shapes and other design features seen on LC repulper rotors, one continuity pervades among all LC repulper rotors – they all use extremely blunt vanes arranged radially around a center hub. The rotors tested in this thesis follow this theme.

Mixing impeller designs used for turbulent stirred mixing also have blunt vanes. Mixing impellers produce powerful trailing vortices behind each of their impeller vanes. (Jaworski et al. 2001; Kresta and Wood 1993; Lee and Yianneskis 1998; Nienow and Wilson 1974; Shafer et al. 1998; Shafer et al. 2000; Sharp and Adrian 2001; Stoots and Calabrese 1995; Shekhar et al. 2012; Van't Riet and Smith 1975; Yianneskis et al. 1987; Yianneskis and Whitelaw 1993). The dissipation of rotor power in these vortices is extremely high and it is widely accepted that the majority of mixing takes place within these vortices (Kresta and Wood 1993).

It is reasonable to expect that the blunt shapes of repulper rotors produce similar vortices and that these vortices are responsible for the majority of repulping.

In this chapter, the flow field produced by each of the rotors studied in this thesis is simulated using computational fluid dynamics (CFD). There are two goals:

1. Gain an estimate of the spatial distribution of the dissipation rotor shaft power by turbulence for each rotor.
2. Identify the presence of the trailing vortices suspected to be produced by the blunt shapes of repulper rotors.

It is hoped that investigating the above two points will provide further test Hypotheses 3 and 4 from Section 1.5.2:

- **Hypothesis 3: LC Repulping occurs due to turbulence produced by the blunt vane shapes used by repulper rotors – specifically in the form of vane trailing vortices.**

- **Hypothesis 4: The relative time spent by flakes circulating past the repulper rotor versus in the rest of the vat in part determines repulping efficiency.**

The model presented by Equation 3.7 relies on the quantity V_{Swept}/V_{Vat} which arises from Hypotheses 3 and 4. The validity of this quantity is further tested here.

It is also hoped that the simulations performed may provide insight toward why Hypothesis 7 from section 1.5.2 is true:

- **Hypothesis 7: Repulper rotor design affects the time and energy required for repulping.**

The reason(s) why Hypothesis 7 is true is(are) unknown. This chapter begins attempts to uncover the reason(s) by simulating the flow field produced by each test rotor.

5.1 Methods and Materials

With stirred mixers, the spatial distribution of turbulence dissipation has been estimated both using forms of optical velocimetry and through the use of CFD simulations.

The laboratory repulper, is made of stainless steel and is on average more than 35 times larger in volume than the mixing vessels used in the mixing velocimetry studies cited in Section 1.3.1 of this thesis. The common technique used for conducting velocimetry studies in stirred mixers is to have a transparent cylindrical mixing vessel placed within a transparent square tank with water filling the space between the mixing vessel and tank. This not only allows for the unimpeded line of sight to the impeller required when using optical velocimetry techniques, but also solves any reflection/refraction problems caused by the cylindrical shape of the mixing vessel. The large size and steel construction of the laboratory repulper prevent the application of this technique to the laboratory repulper and for this reason, the flow field produced by Rotors A, B, and C is simulated using CFD.

Pulp suspensions have extremely complex rheology. It is so far not possible to completely simulate the behavior of pulp suspensions due to both the enormous computing power that is required to simulate individual fibers in suspension and due to our incomplete understanding of pulp suspensions. The strain-rate dependent behavior of pulp suspensions can be approximated by the Herschel-Bulkley non-Newtonian model up to moderate strain-rates (Derakhshandeh et al. 2011). As noted previously, in fully turbulent flow, the fibers in pulp suspensions fluidize in an analogous fashion to solids suspended in a fluidized bed reactor (Bennington and Kerekes 1996; Derakhshandeh et al. 2011). As the flow at, and very near the repulper rotor is of interest in this study, the fluidized flow at the repulper rotor is approximated with water. For all simulations presented here, water is simulation fluid. In this light, the results presented in this chapter should be considered to be only an estimate of the actual flow field produced by each repulper rotor near the rotor only.

RANS simulations of stirred mixing have proven to qualitatively predict the flow field within stirred mixers and have been shown to evolve the important trailing vortices produced by various mixing impeller types (Joshi et al. 2011). The standard k-epsilon model (Launder and Spalding 1974) is likely the most common turbulence model used for RANS simulations of turbulent mixing.

Authors report that the $k - \varepsilon$ model is able to resolve the important flow field features produced by mixing impellers, specifically the important trailing vortices (Fokema and Kresta 1994; Javed et al. 2006; Kresta and Wood 1991; Kumaresan and Joshi 2006; Lee et al. 1996; Ng et al. 1998; Nogueira et al. 2012; Ranade 1997; Ranade 2001; Venneker and van den Akker 1997). The $k - \varepsilon$ model is used for all simulations presented here.

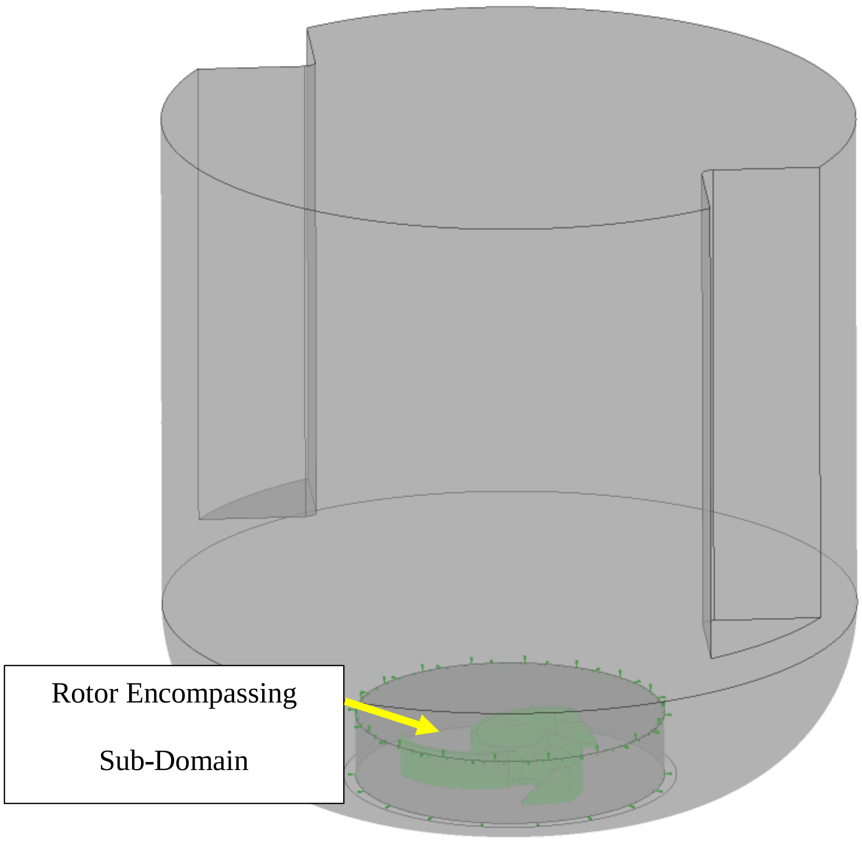

Figure 5.1: The simulation domain is split into two sub-domains – one encompassing the rotor and the other making up the rest of the repulper vat. The revolution of the rotor is simulated using both the frozen-rotor approach and the sliding mesh approach. The frozen-rotor approach is a quasi-steady-state approach in which a velocity transform is applied across the domain boundaries between the two domains although the rotor itself remains fixed in position with respect to the vat. The sliding mesh approach is a transient approach in which the sub-domain encompassing the rotor is rotated with respect to the vat domain at every time step. With this approach, the position of the rotor is not fixed with respect to the vat.

The simulation domain is shown in Figure 5.1. All walls are modeled as no-slip boundaries. The domain is made up of two subdomains, one encompassing the rotor and the other making up the rest of the vat. Both the Frozen-Rotor and Sliding Mesh techniques are used to account for the repulper rotor rotation.

With the frozen rotor approach, the rotor and vat remain fixed in position relative to one another and a relative rotational velocity is applied across the boundaries between the rotor and vat. This makes the Frozen Rotor approach a quasi-steady state approach and thus significant computing resources are saved compared to a fully transient sliding mesh approach. The frozen rotor approach has proven to be accurate for modelling rotor/vat combinations where the interaction between the rotor and vat baffles is weak – i.e. for rotors/impellers having many blades/vanes (Joshi et al. 2011). The Sliding Mesh approach, as just mentioned, is a fully transient approach whereby the mesh block encompassing a rotor is rotated at each time step with respect to the mesh block making up the vat. Therefore, the rotor moves with respect to a stationary vat. This approach can account for situations where a rotor has a strong interaction with a vat's baffles and is suitable for the simulation of rotors having few vanes like Rotor A in this study.

The repulper free surface is not modeled. Instead, a lid is added to the simulation domain. The lid is modeled as a no-slip boundary. A comparison between rotor power as calculated from the simulations and measured rotor power in the actual laboratory repulper is presented in the next section and is done so with measurements taken from the laboratory repulper also having a lid and completely bled of any air.

In this study, the flow is developed in the repulper vat using the frozen rotor approach. This avoids modeling the transient rotor start-up. After a converged solution is achieved using the frozen rotor approach, 10 full rotor revolutions are simulated for each rotor using the sliding mesh approach with a time step of 10^{-4}s. This time step gives a resolution of 0.78° of rotor rotation per time step for a 16m/s rotor tip-speed. All simulations were converged to RMS residuals of 10^{-5}. The Ansys CFX is used for all simulations and the CFX manual states that this convergence level is sufficient for engineering applications (*Ansys CFX Manual Release* 14.5 2013).

Paraskevas (1983) indicated that cavitation is produced by LC repulper rotors. For this reason, the simulations here are multiphase and include the Rayleigh-Plesset cavitation model. The velocity field of the evolved water vapor bubbles is set to follow the velocity field of the liquid water phase with no slip between the phases. Cavitation simulations were run at a temperature of 25°C. The vapor pressure of water at this temperature is 3170Pa. Table 5.1 shows the simulations run here.

Table 5.1: Table of all simulations performed.

Rotor	**Mesh Sizes (# of cells)**	**Frame Change Model**	**Turbulence Model**	**Cavitation Model**	**Rotor Test Tip Speeds**
Rotor A	1. 536,626 2. 916,523 3. 2,321,020 4. 4,345,668 (grid converged)	Frozen Rotor to develop flow as initial solution/Sliding Mesh for 10 rotor revolutions –10^{-4}s time step	k-epsilon	Rayleigh-Plesset (for grid converged mesh size only)	12m/s, 13m/s, 14m/s, 15m/s, 16m/s
Rotor B	1. 1,294,106 2. 2,452,215 3. 3,777,231 (grid converged)	Frozen Rotor to develop flow as initial solution/Sliding Mesh for 10 rotor revolutions –10^{-4}s time step	k-epsilon	Rayleigh-Plesset (for grid converged mesh size only)	12m/s, 13m/s, 14m/s, 15m/s, 16m/s
Rotor C	1. 483,017 2. 1,371,928 3. 2,088,635 4. 3,941,572 (grid converged)	Frozen Rotor to develop flow as initial solution/Sliding Mesh for 10 rotor revolutions –10^{-4}s time step	k-epsilon	Rayleigh-Plesset (for grid converged mesh size only)	12m/s, 13m/s, 14m/s, 15m/s, 16m/s

5.2 Results and Discussion

The mesh sensitivity results for each rotor geometry are shown in Figure 5.2.

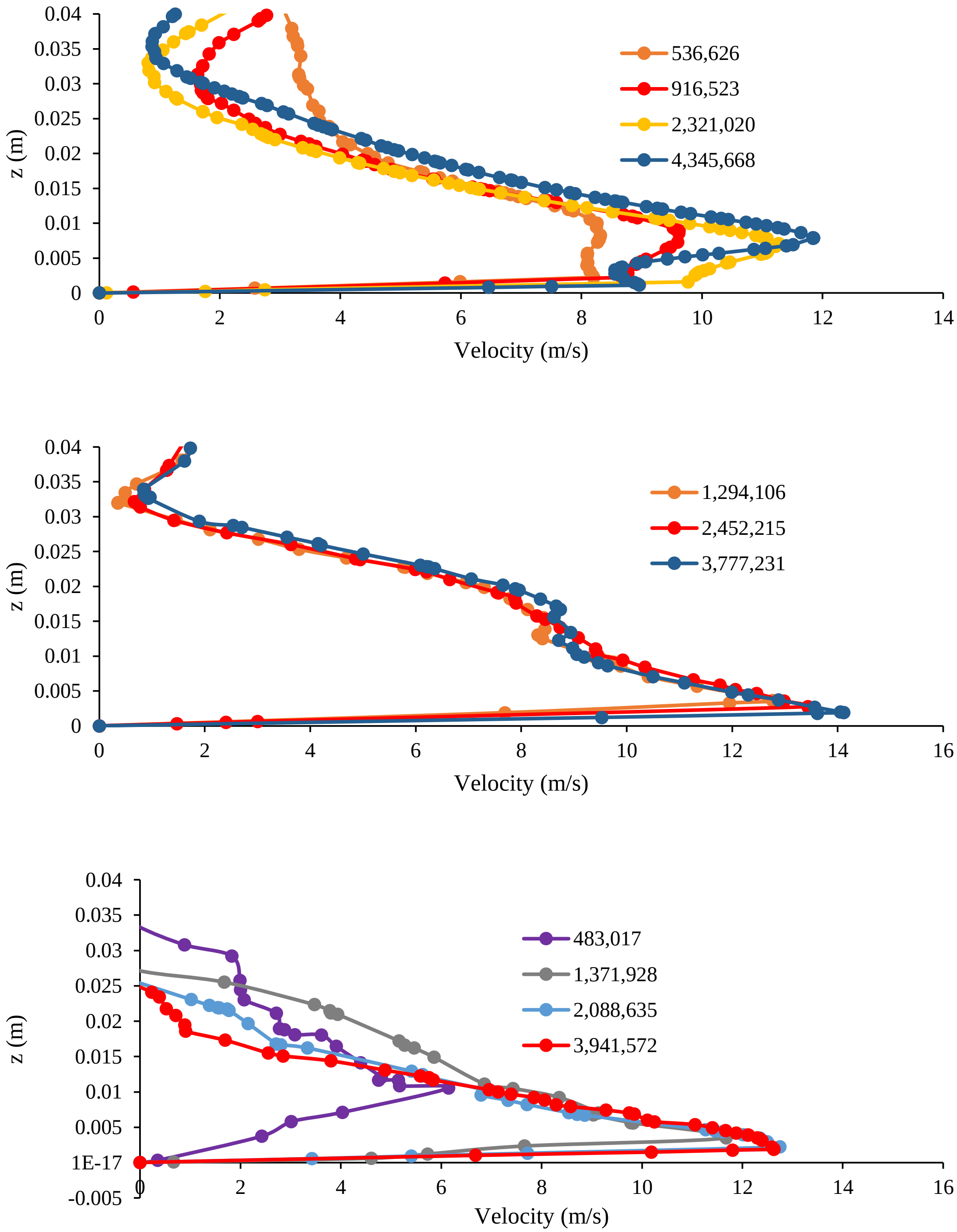

Figure 5.2: Mesh sensitivity results. The vane-tip radial velocity profile for a 16m/s rotor tip-speed is used to determine grid convergence. From top to bottom: results for Rotor A, Rotor B, and Rotor C.

Only Rotor A showed a significant interaction with the repulper vat baffles. The calculated torque vs. rotor rotation angle is shown in Figure 5.3. Rotors B and C did not show a regular variation in rotor torque with changing rotor rotation angle.

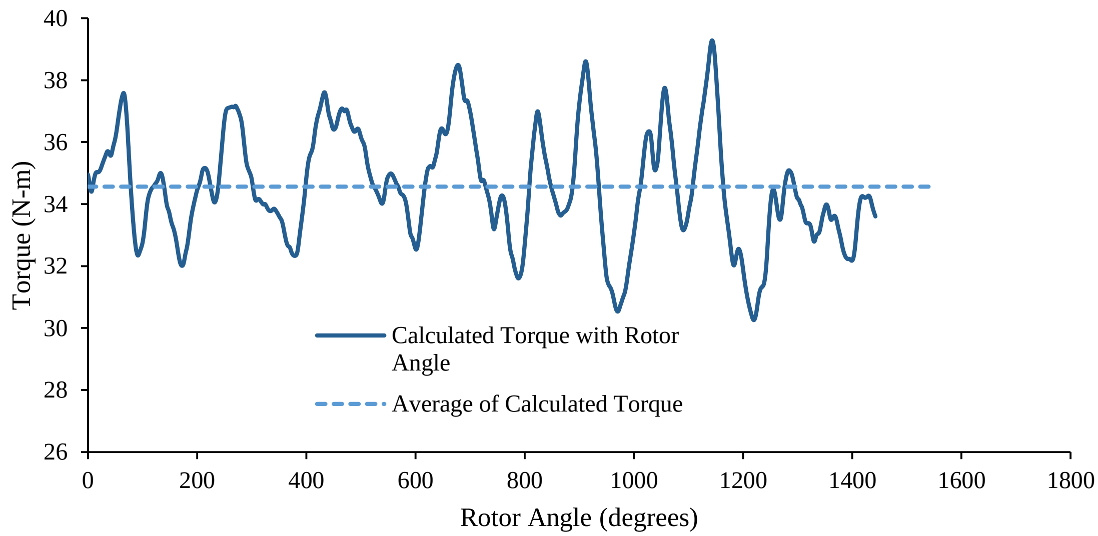

Figure 5.3: Rotor A showed a significant interaction with the repulper vat baffles. The calculated torque vs. rotor rotation angle for Rotor A is shown above for a simulated rotor tip-speed of 16m/s. Rotors B and C did not show a significant interaction with the baffles and the calculated torque stayed relatively constant with changing rotor angle with respect to the baffles for these two rotors.

The calculated rotor torque for varying tip speeds is compared with the experimentally measured torque in the laboratory repulper in Figure 5.3.

Recall that the goals of this chapter concern Hypotheses 3, 4 and 7:

- **Hypothesis 3: LC Repulping occurs due to turbulence produced by the blunt vane shapes used by repulper rotors – specifically in the form of vane trailing vortices.**
- **Hypothesis 4: The relative time spent by flakes circulating past the repulper rotor versus in the rest of the vat in part determines repulping efficiency.**
- **Hypothesis 7: Repulper rotor design affects the time and energy required for repulping.**

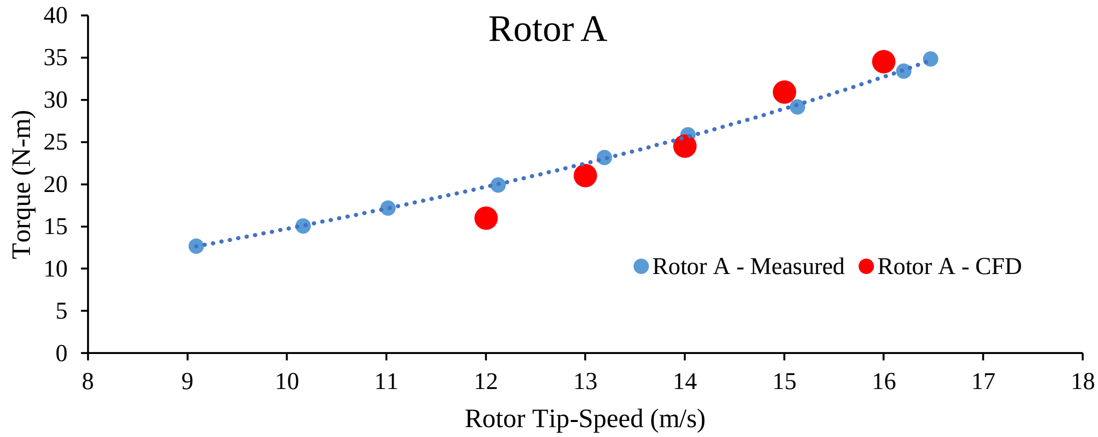

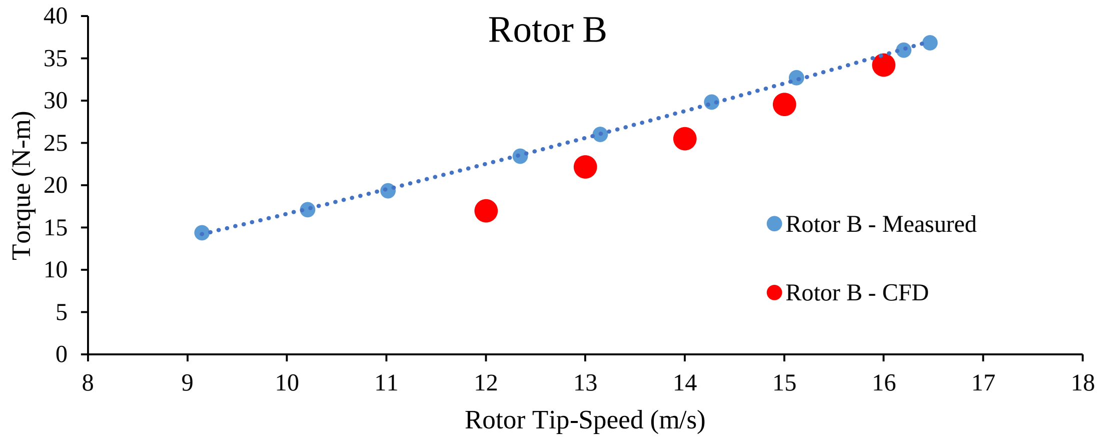

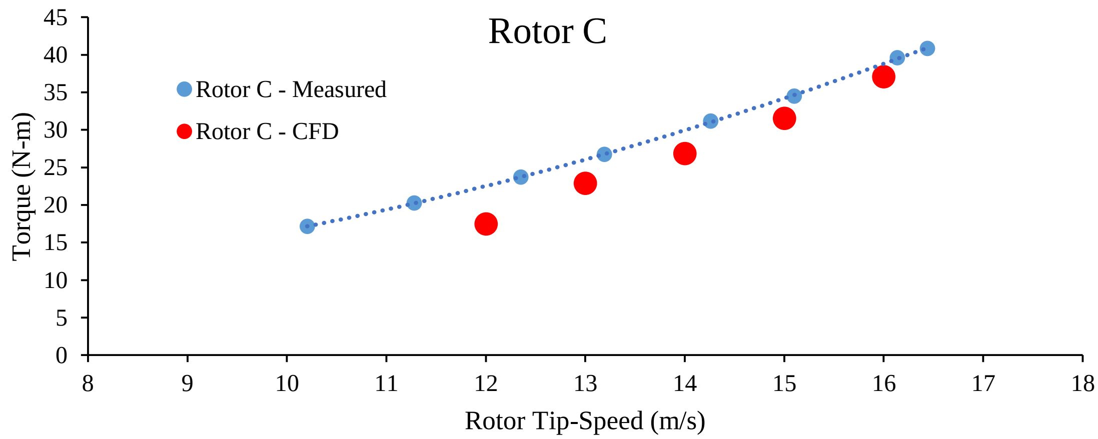

Figure 5.4: A comparison of rotor torque as measured from the laboratory repulper and as calculated with the CFD simulations. The comparison here is made using water and with a lid installed on, and the air bled from, the laboratory in order to match the simulation domain. The CFD calculated torque shown represents the average of torque calculated at each time step over a full rotor revolution. Only grid-converged CFD results are shown.

Do these rotors produce powerful trailing vortices as is the case for the similarly shaped mixing impellers? Is the rotor power dissipated by turbulence within the vicinity of the rotor as is the case for mixing impellers? The model presented by Equation 3.7 relies on the quantity V_{Swept}/V_{Vat} under the assumption that all of the rotor power is dissipated within a volume approximated by the rotor swept volume. Is this assumption valid? Finally, can the simulations performed here be used to explain the measured differences in rotor performance?

5.2.1 Trailing Vortices and Cavitation

Hypothesis 3 makes the statement that the blunt shapes of repulper rotors produce powerful trailing vortices in a manner analogous to mixing impellers. The dissipation of mixing impeller power is extremely high in these vortices and it is widely acknowledged that the majority of mixing in a stirred mixing operation is accomplished in these vortices (Kresta and Wood 1993). Hypothesis 3 makes an analogous claim for repulper rotors and thus one of the aims of these simulations is to identify if powerful trailing vortices are produced by LC repulper rotors.

Figure 5.5 displays velocity streamlines for each rotor at a simulated tip-speed of 16m/s. The streamlines show that the simulations predict the presence of trailing vortices behind the vanes of each rotor.

Paraskevas (1983) stated that LC repulper rotors produce significant cavitation. In this light, the velocity fields of all three rotors were simulated using the Rayleigh-Plesset cavitation model. Figure 5.6 shows that the simulations predict vortex induced cavitation within the trailing vortices behind the vanes of each rotor. The simulated tip-speed here is also 16m/s.

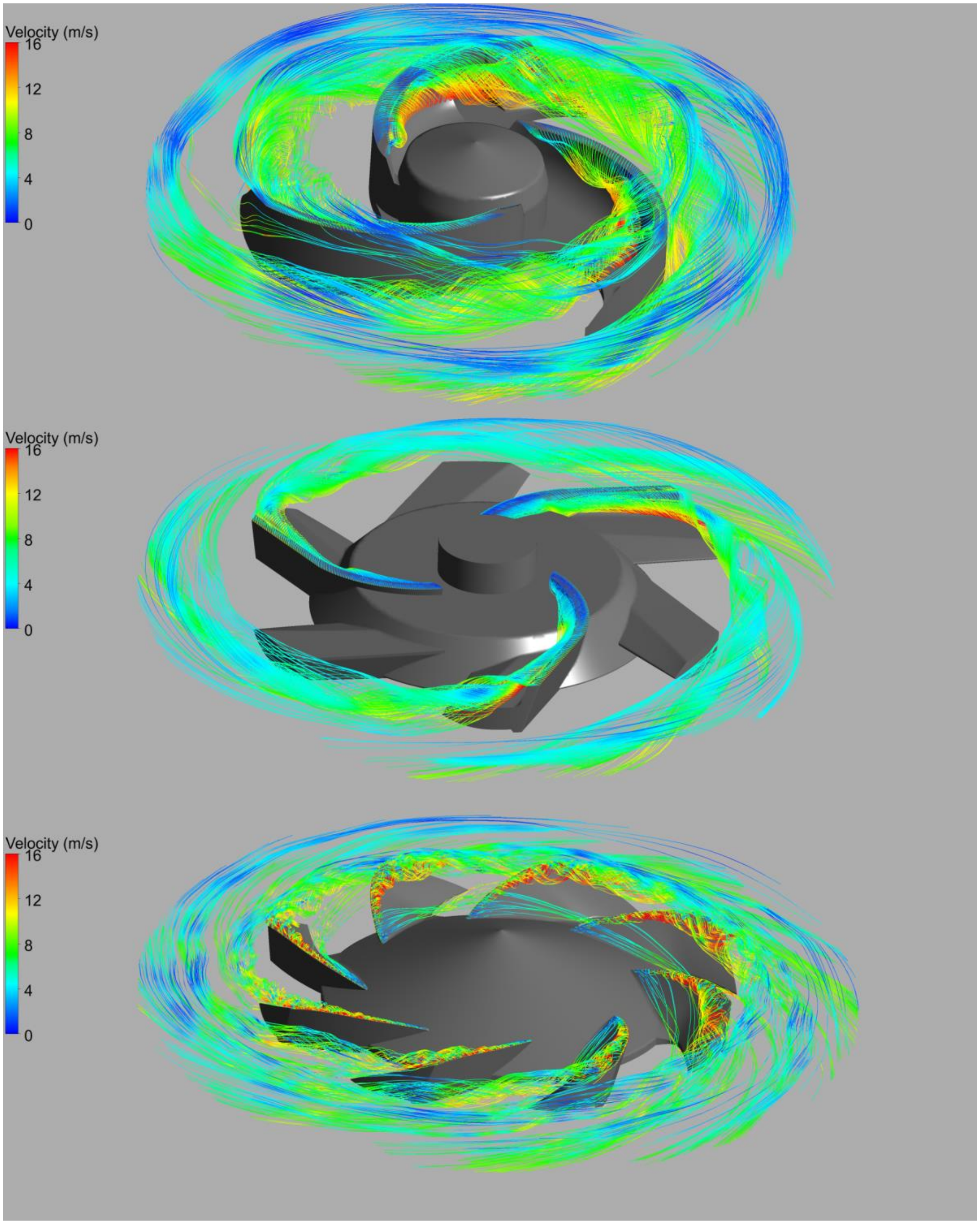

Figure 5.5: Streamlines showing the presence of trailing vortices behind the vanes of each rotor. The simulated tip-speed for all three rotors is 16m/s. All three rotors rotate counterclockwise. From top to bottom: Rotors A, B, and C.

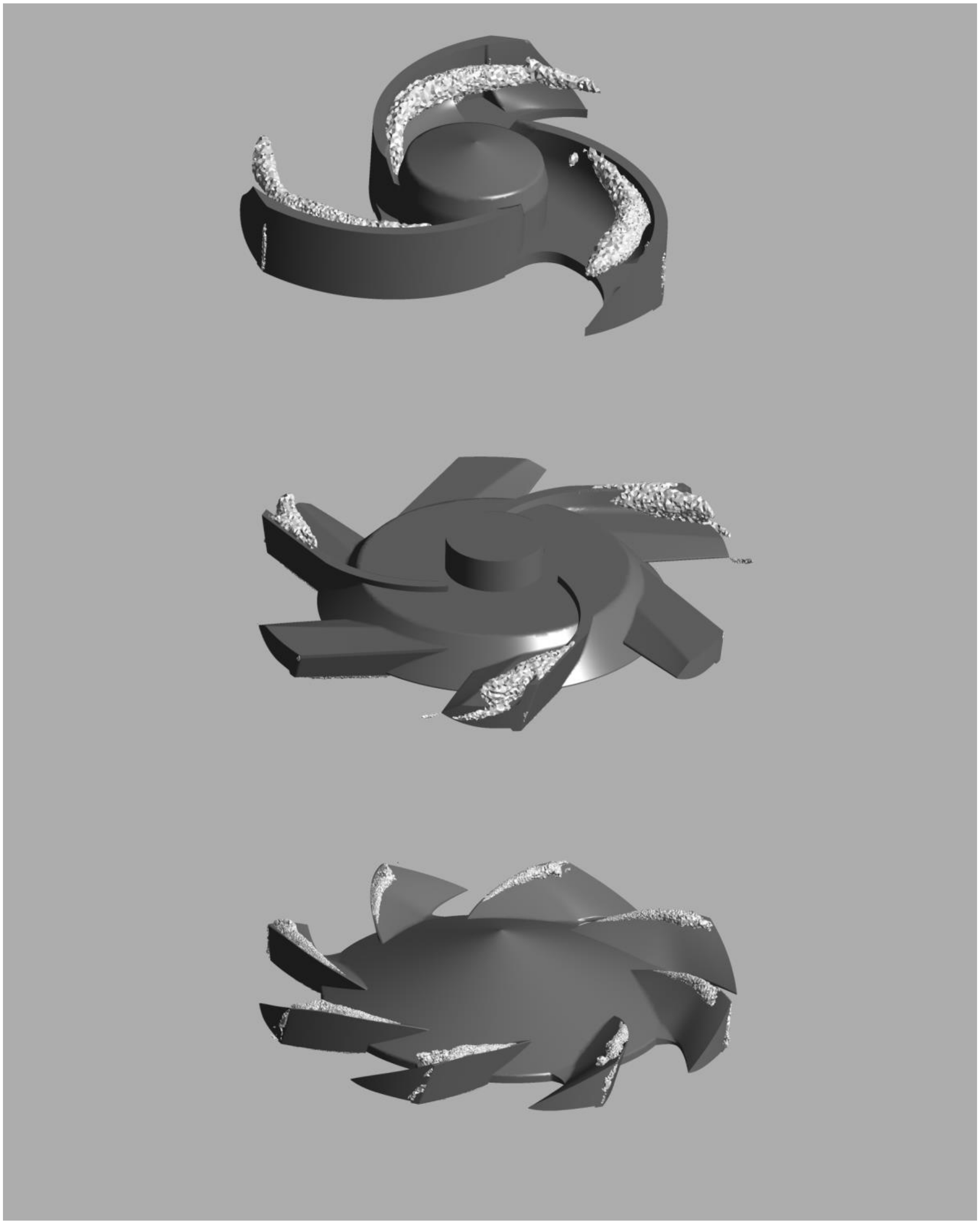

Figure 5.6: Cavitation within the cores of the trailing vortices behind the vanes of each rotor. The simulated tip-speed for all three rotors is 16m/s. The simulation temperature is 25°C. The vapor pressure of water at this temperature is 3170Pa. All three rotors rotate counterclockwise. From top to bottom: Rotor A, Rotor B, and Rotor C.

The presence of cavitation explains the presence of previously baffling pitting damage on the vane trailing edges of Rotor A where no impact with flakes is possible. This is shown in Figure 5.7. It appears now that this damage is a result of interactions with vane trailing vortex induced cavitation. It should be noted that this damage to Rotor A was accumulated from operation exclusively in 5% consistency C-flute corrugated cardboard suspensions indicating that the trailing vortices and cavitation produced by each rotor are also present when the rotors are operating in pulp suspensions.

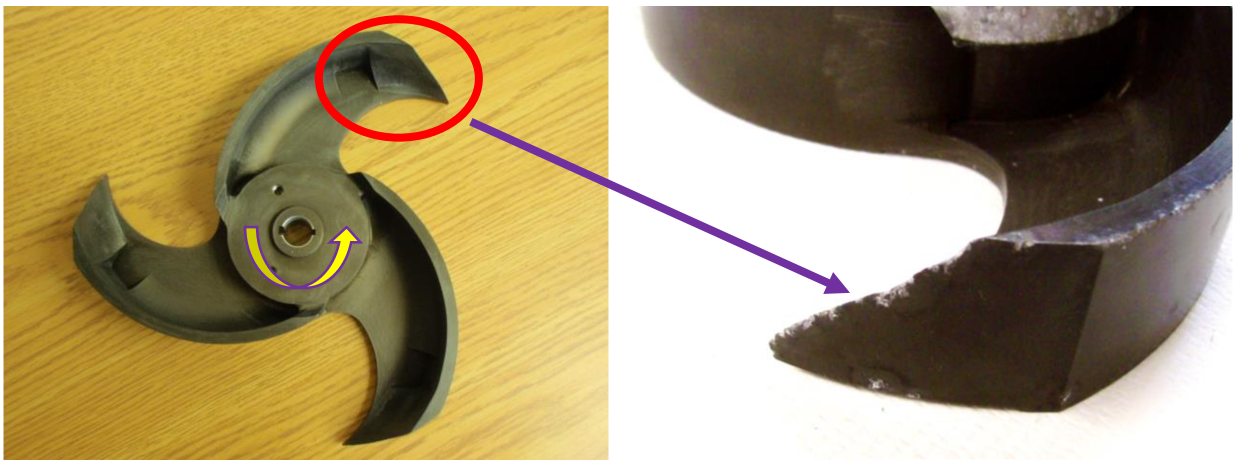

Figure 5.7: Cavitation damage on the trailing vane edges of Rotor A. The view above is looking down at the top of Rotor A. Rotor A rotates counterclockwise.

5.2.2 The Spatial Distribution of Rotor Power Dissipation

The model described by Equation 3.7 has been shown to accurately predict repulping performance in both the 0.25m^3 laboratory repulper built for this study and a 15m^3 industrial repulper. The model presented by Equation 3.7 relies on the quantity V_{Swept}/V_{Vat} under the assumption that all of the rotor power is dissipated within a volume approximated by the rotor swept volume. The simulated spatial distribution of rotor power dissipation by turbulence is shown in this section. The dissipation due to turbulence is calculated directly by the epsilon-equation of the k-epsilon model. Details on the k-epsilon model are given in Launder and Spalding (1974). Figures 5.8 and 5.9 show the simulated spatial distribution of rotor power dissipation by turbulence from the vantage looking down at the rotor and from the vantage looking

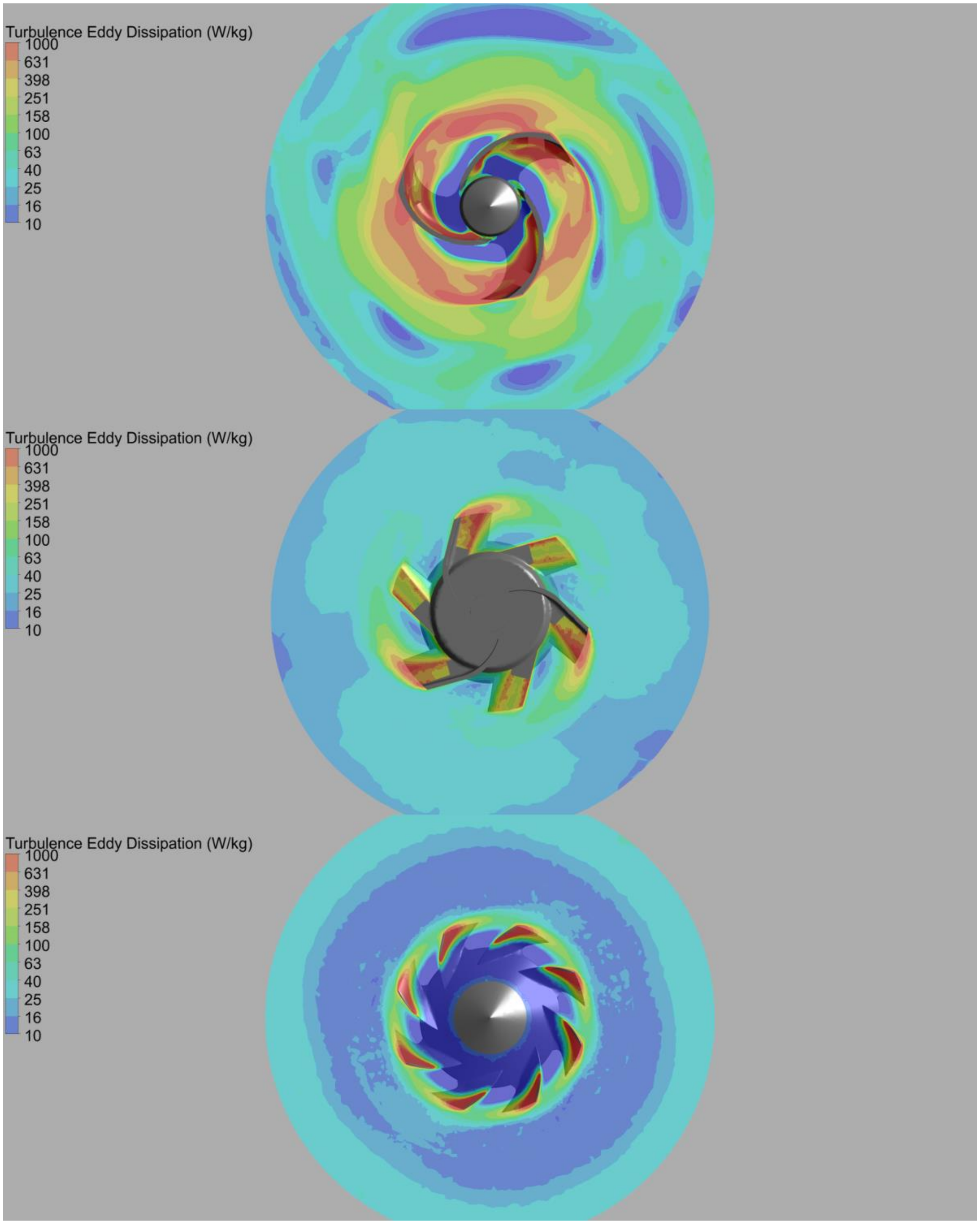

Figure 5.8: The turbulence eddy dissipation for each rotor at a simulated tip-speed of 16m/s is shown. The view here is looking down on the rotors from above. Each rotor rotates counterclockwise. Contours of turbulence eddy dissipation are plotted on a plane bisecting the trailing vortices for each rotor with the plane's normal vector parallel to each rotor's rotation axis. Note that the color legend uses a logarithmic scale. The majority of the dissipation is limited to the vicinity of the rotor.

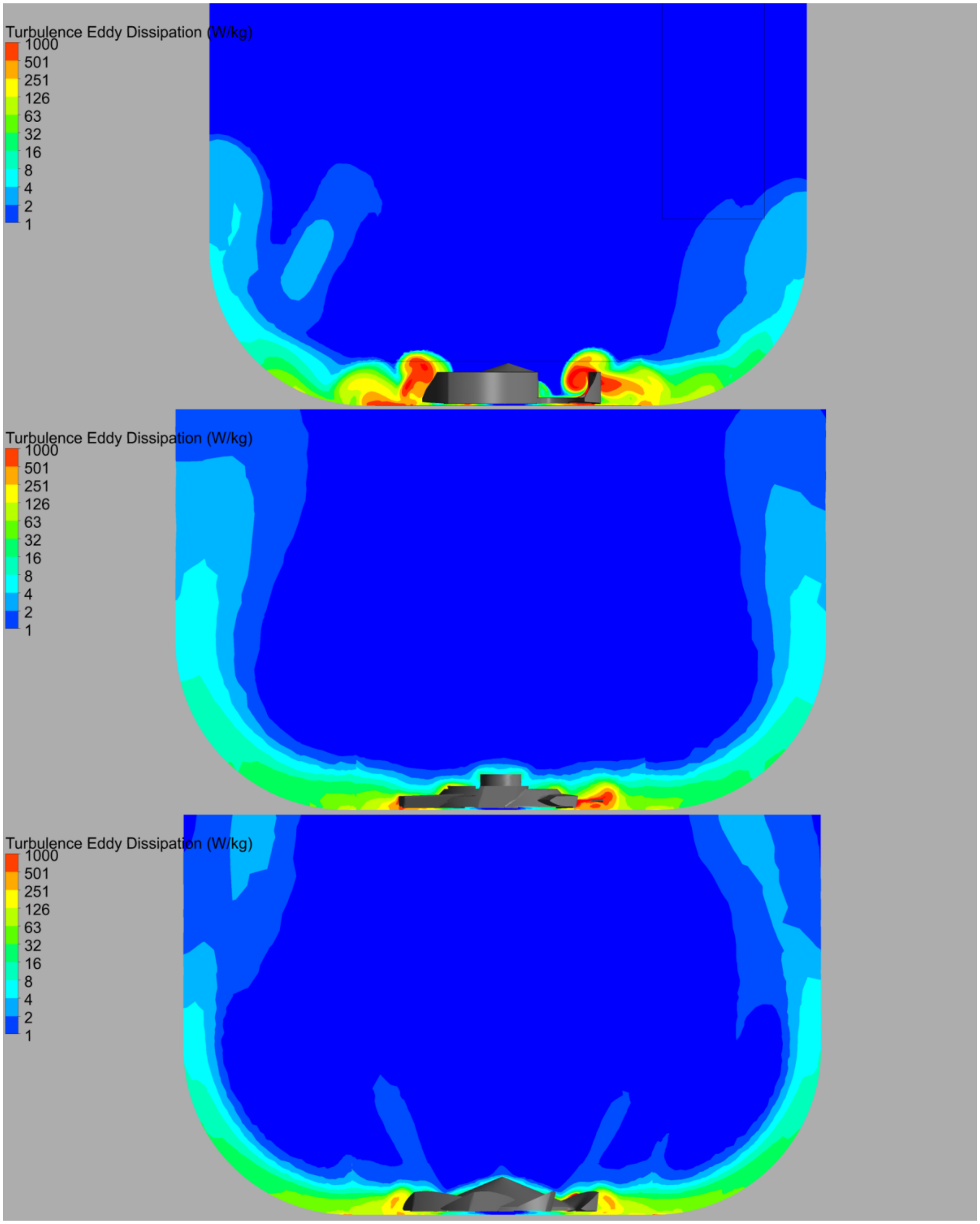

Figure 5.9: The turbulence eddy dissipation for each rotor at a simulated tip-speed of 16m/s is shown. The view here is looking sideways at the repulper vat and rotors. Each rotor rotates counterclockwise. Contours of turbulence eddy dissipation are plotted on a plane bisecting the repulper vat with the plane's normal vector perpendicular to each rotor's axis of rotation. Note that the color legend uses a logarithmic scale. The majority of the dissipation is limited to the vicinity of the rotor.

from the side of the repulper vat respectively. Notice that the legend used for each figure is logarithmic. Both figures show that high-intensity dissipation is limited to the vicinity of the rotor for all three rotors. The highest dissipation for each rotor is in the trailing vortices. The dissipation in the vortices produced by each rotor is calculated to be more than 200 times the average in the rest of the vat.

Table 5.2 compares the calculated dissipation of rotor power from the k-epsilon turbulence model to the power calculated from rotor form drag and the power measured in the laboratory repulper.

Table 5.2: The power dissipated by turbulence is compared with the power calculated from form-drag and the measured power in the laboratory repulper. The k-epsilon model over-predicts the dissipation by turbulence.

Rotor	Rotor Tip-Speed	Total Power Dissipated by Turbulence Eddy Dissipation (epsilon equation)	Rotor Power Calculated from Pressure Integration Over Rotor	Measured Rotor Power in The Laboratory Repulper
Rotor A	16m/s	5954 W	4730 W	4771 W
Rotor B	16m/s	6867 W	4688 W	5051 W
Rotor C	16m/s	8355 W	5081 W	5596 W

The k-epsilon turbulence model over-predicts the dissipation by turbulence. Recall from Section 1.3.1 that authors historically report that the $k - \varepsilon$ model under-predicts the turbulent kinetic energy and dissipation in stirred mixing simulations (Fokema and Kresta 1994; Javed et al. 2006; Kresta and Wood 1991; Kumaresan and Joshi 2006; Lee et al. 1996; Ng et al. 1998; Nogueira et al. 2012; Ranade 1997; Ranade 2001; Venneker and van den Akker 1997). The over-prediction of the dissipation of rotor power by turbulence here may be explained by the fact that the rotor simulations here were done at a Reynolds number an order of magnitude higher than the stirred mixing simulations cited above were. Also, 2-equation turbulence models like the k-epsilon model are susceptible to over-predicting turbulence when simulations involve regions of high stagnation pressure. The implementation of 2-equation models in modern CFD software includes rate-clipping to avoid the susceptibility of these models to the over-production of turbulence.

For 2-equation eddy-viscosity models, the production of turbulence is modeled using the Boussinesq-approximation (Boussinesq 1877) which is implemented for the 2-equation $k - \varepsilon$ model by:

$$P_k = \mu_t S^2 \tag{5.1}$$

$$S = \sqrt{2\, S_{ij} S_{ij}};\, S_{ij} = \tfrac{1}{2}\left(\frac{\partial U_i}{\partial x_j} + \frac{\partial U_j}{\partial x_i}\right) \tag{5.2}$$

where P_k is the turbulence energy, μ_t is eddy-viscosity, and S is the magnitude of the strain-rate (Launder and Sharma 1974). As the production of turbulence is calculated directly from the strain-rate, 2-equation models are liable to over-produce turbulence in regions of flows having very high strain-rates such as stagnation points. For example, 2-equation models are implemented in Ansys CFX and Fluent with turbulence production limiters by the method proposed by Menter (1994):

$$P_k = \min(P_k, C_{lim} \rho \varepsilon) \tag{5.3}$$

where C_{lim} is known as a “clip factor”. The value of C_{lim} varies for different models but is equal to 10 for $k - \omega$ based models for example (Menter 2009).

Contours of pressure are shown for each rotor in Figure 5.10. All three rotors do indeed show regions of high stagnation pressure. Notice also in the figure the very low pressure on the back-sides of each rotor vane for each rotor.

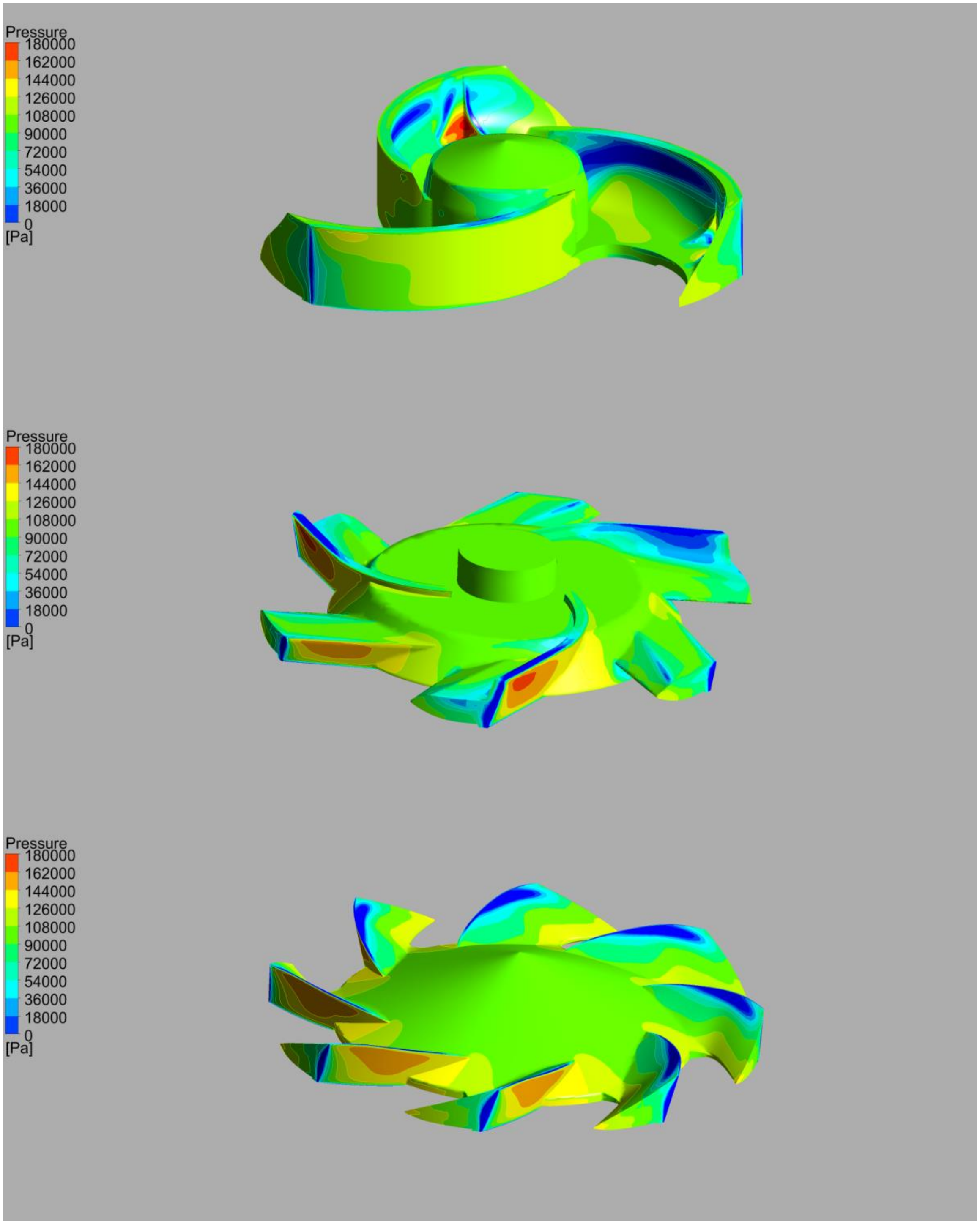

Figure 5.10: Contours of absolute pressure mapped on to the surface of each rotor. The simulated tip-speed for all three rotors is 16m/s. All three rotors rotate counterclockwise. From top to bottom: Rotor A, Rotor B, and Rotor C. High stagnation pressure on the vane faces of each rotor results in an overproduction of turbulence from the k-epsilon turbulence model.

5.2.3 Addressing Hypothesis 7

A statistically significant performance difference was measured between rotors A and B as shown in Section 2.2.5. Rotor A also proved to be the least efficient of the three rotors tested. According to the CFD simulations performed, the three test rotors differ in terms of the size (diameter) and number of trailing vortices produced as well as in the peak dissipation within the vortices they produce.

According to the simulations, the vortices produced by Rotor A contain lower peak dissipation values than the dissipation values within the vortices produced by the other two rotors. Section 2.2.4 shows that the energy required in repulping is independent of rotor tip speed. Figure 2.7b in Section 2.2.4 shows identical repulping performance over a tip-speed range of 12-15m/s. This tip speed range corresponds to a 2.5 fold increase in rotor power between 12m/s and 15m/s tip-speeds. It is for this reason that the author believes that looking at peak dissipation values to explain the measured difference in rotor performance might constitute a red-herring.

The author has performed many repulping tests with each of the test rotors to produce the results presented in this thesis. At least qualitatively, the ability of Rotor A to maintain suspension motion in the repulper vat appeared inferior to that of rotors B and C. Due to the asymptotic nature of Equation 1.3, repeated here for convenience, even a small difference in mixing performance between the rotors would result in substantial differences in energy use between each rotor:

$$\frac{dF}{dt} = -kF \tag{1.3a}$$

$$\frac{dF}{dE} = -\lambda F \tag{1.3b}$$

Recall from Section 3.3.4 that mixing greatly affects the time and energy required for repulping.

5.3 Chapter Conclusion

The simulations in this section provide strong evidence for the presence of trailing vortices produced behind the vanes of each rotor. Furthermore, the turbulence dissipation rate within these vortices is greater than 200 times the average dissipation in the rest of the vat. The simulations also provide further evidence that the majority of the dissipation of rotor power by turbulence in a repulper is done so very near the rotor and this provides further support for the validity of the V_{Swept}/V_{Vat} term from Equation 3.7.

The simulations provide further evidence of the plausibility Hypotheses 3 and 4:

- **Hypothesis 3: LC Repulping occurs due to turbulence produced by the blunt vane shapes used by repulper rotors – specifically in the form of vane trailing vortices.**
- **Hypothesis 4: The relative time spent by flakes circulating past the repulper rotor versus in the rest of the vat in part determines repulping efficiency.**

Chapter 6: High Speed Filming

The work in the previous chapters strongly suggests that high-intensity turbulence produced by repulper rotors in the vicinity of a repulper rotor is responsible for the breakup of waste paper in a repulper. The CFD simulations presented in the previous chapter predict that each rotor will produce strong trailing vortices and that cavitation will be present in the cores of these vortices. If cavitation is indeed present, it will be visible and high-speed film can be used to confirm the presence of trailing vortices for each rotor. The aim of the filming here is to further test Hypotheses 3 and to provide insight toward explaining why Hypothesis 7 is so:

- **Hypothesis 3: LC Repulping occurs due to turbulence produced by the blunt vane shapes used by repulper rotors – specifically in the form of vane trailing vortices.**
- **Hypothesis 7: Repulper rotor design affects the time and energy required for repulping.**

Recall the 4 mechanisms that are generally thought to be responsible for repulping:

- Flakes are broken down by being sheared between the rotor and extraction plate.
- Flakes are broken down by direct impact with the rotor.
- Flakes are worn down by fiber-to-flake/flake-to-flake rubbing.
- Flakes are broken down by turbulence.

High-speed film can also be used to film flakes interacting with repulper rotors, albeit in a very dilute pulp suspension as pulp suspensions become opaque even at very low consistencies. This rules out filming to observe flake-to-flake rubbing but does allow for the possibility to observe the other 3 above-listed repulping mechanisms.

6.1 Methods and Materials

To allow for close up filming of the test rotors, a small porthole was installed at rotor level in the laboratory repulper. The top opening of the repulper was sealed with an optical grade acrylic lid. The lid not only allows for filming from the vantage above the rotor, but also stops entrainment of air from the repulper free surface and allows for the bleeding of already entrained air from the repulper. The removal of entrained air is essential for clear filming. Even a small amount of entrained air results in enough bubbles to make filming impossible. The modified repulper and filming arrangement is shown in Figure 6.1.

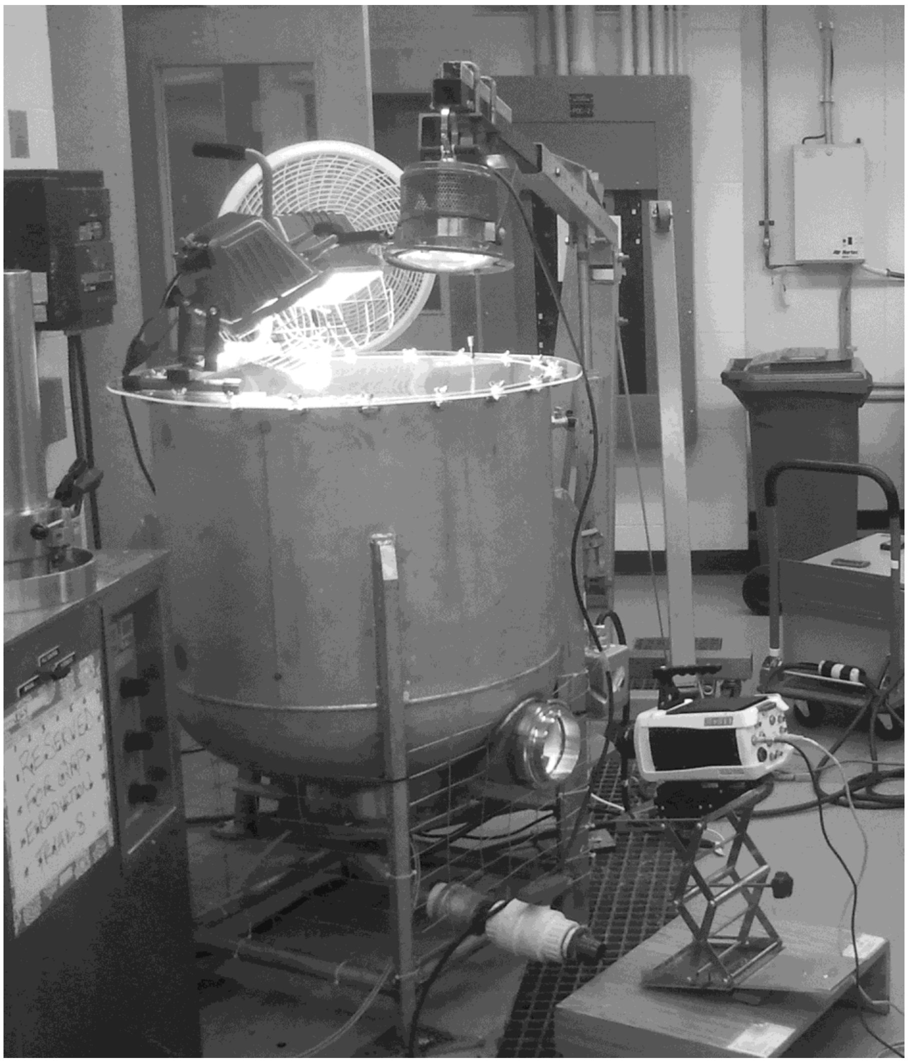

Figure 6.1: The laboratory repulper was modified with the addition of a porthole at rotor level to allow for close up filming of repulper rotors. A sealed lid was also added to allow for entrained air to be bled from the repulper before filming. Bubbles from entrained air reduce visibility within the repulper.

Filming was conducted in order to confirm/deny the presence of the vortex induced cavitation predicted by the CFD simulations of the previous chapter and filming was conducted to observe the interaction of flakes with each test rotor.

Table 6.1 recounts all films made to identify the presence of the vortex-induced cavitation predicted by the CFD simulations of the previous chapter. Each rotor was filmed at tip-speeds ranging from 9m/s (found to be the onset of cavitation for all three rotors) to 16m/s in water at 20°C.

Table 6.1: Filming schedule for the identification of rotor vane trailing vortices.

Rotor	**Filmed Rotor Tip-Speeds (m/s)**
Rotor A	9, 10, 11, 12, 13, 14, 15, 16
Rotor B	9, 10, 11, 12, 13, 14, 15, 16
Rotor C	9, 10, 11, 12, 13, 14, 15, 16

After the completion of the filming schedule described by Table 6.1, the three rotors were also filmed interacting with C-flute corrugated cardboard. Strips of corrugated cardboard having dimensions of 100x50mm were added to the repulper before filming. Only a handful of cardboard strips could be added at a time as even a small concertation of repulped cardboard was enough to turn the water in the repulper opaque. Table 6.2 gives the schedule of films conducted for each rotor interacting with C-flute corrugated cardboard. Interactions between C-flute corrugated cardboard flakes and each rotor were tabulated in terms of either:

1. Shearing between the rotor and extraction plate.
2. Flake impact with the rotor.

3. Flake interaction with trailing vortices.

Each of the above three interaction types was tabulated by flake size. In total, 580 rotor-to-flake interactions were tabulated.

Table 6.2: Filming schedule for rotor interaction with C-flute corrugated cardboard.

Rotor	**Waste Paper Type**	**Filmed Rotor Tip-Speeds (m/s)**
Rotor A	C-flute corrugated cardboard	12, 13, 14, 15, 16
Rotor B	C-flute corrugated cardboard	12, 13, 14, 15, 16
Rotor C	C-flute corrugated cardboard	12, 13, 14, 15, 16

The frame rate used for all filming was 11,000 frames per second. This corresponds to 0.714 degrees of rotor rotation per frame when the rotor is operating at a tip speed of 16m/s (1308 rpm). All films were filmed at a resolution of 1024 x 512 pixels.

6.2 Results and Discussion

6.2.1 Trailing Vortices and Cavitation

The CFD simulations presented in Chapter 5 predicted that each of the rotors tested here produced powerful trailing vortices. The CFD simulations also predicted that the pressure in the centers of these trailing vortices would be less than the vapor pressure of water at the simulation temperature of 25°C. Figure 6.2 shows that each rotor does produce trailing vortices behind each rotor vane as indicated by cavitation. The cavitation makes for a convenient flow tracer and shows that the trailing vortices are present as predicted by the CFD simulations in Chapter 5.

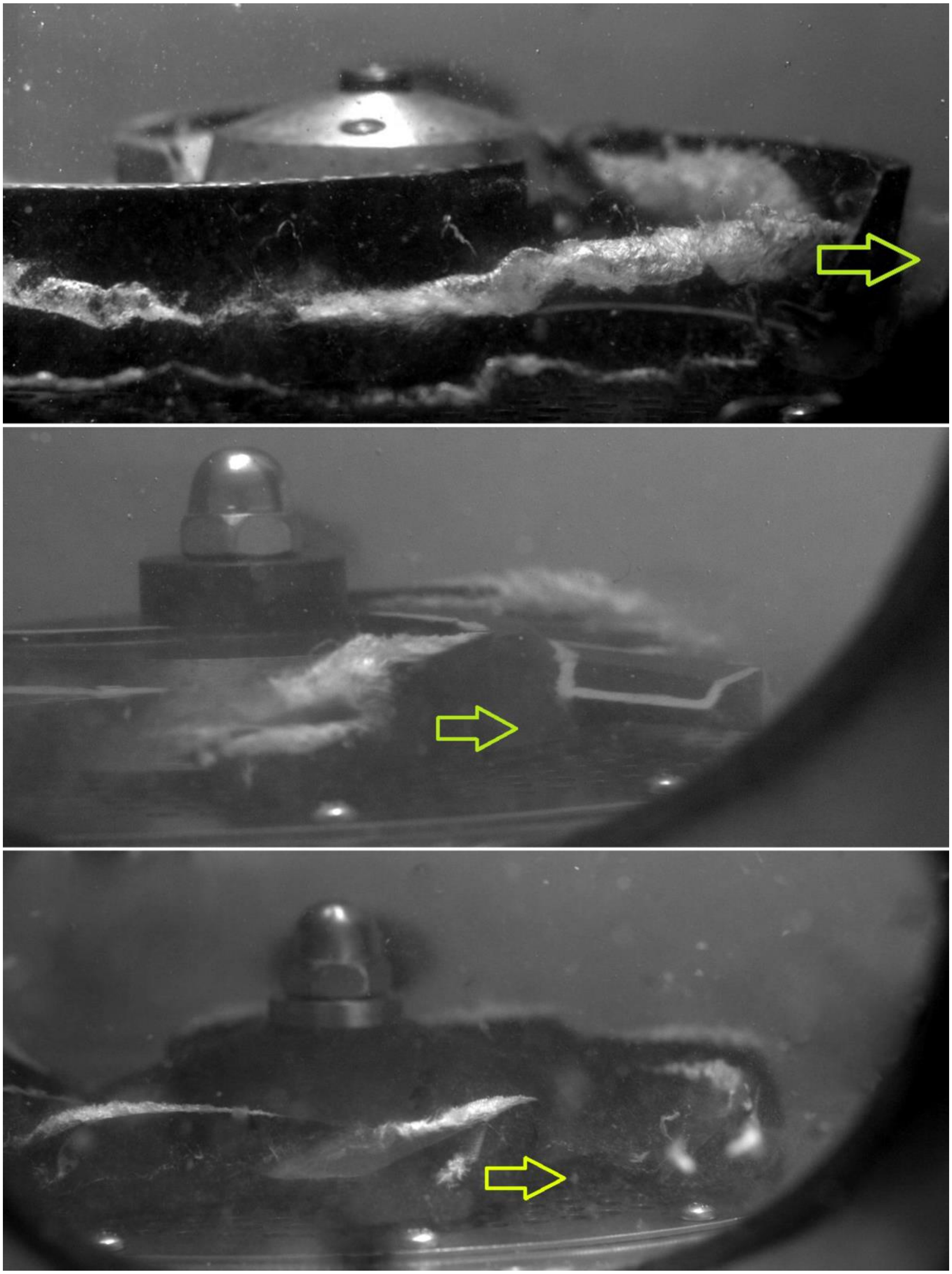

Figure 6.2: Cavitation reveals the trailing vortices behind the vanes of each rotor. From top to bottom: Rotor A, Rotor B, and Rotor C. All three rotors have a tip-speed of 13m/s. The vanes of each rotor are moving in the direction of the arrows in the figure.

The rotor tip-speed correlating with the onset of cavitation for each rotor is approximately 9.2m/s. The amount of cavitation increases greatly with increasing rotor speed as evidenced by Figure 6.3.

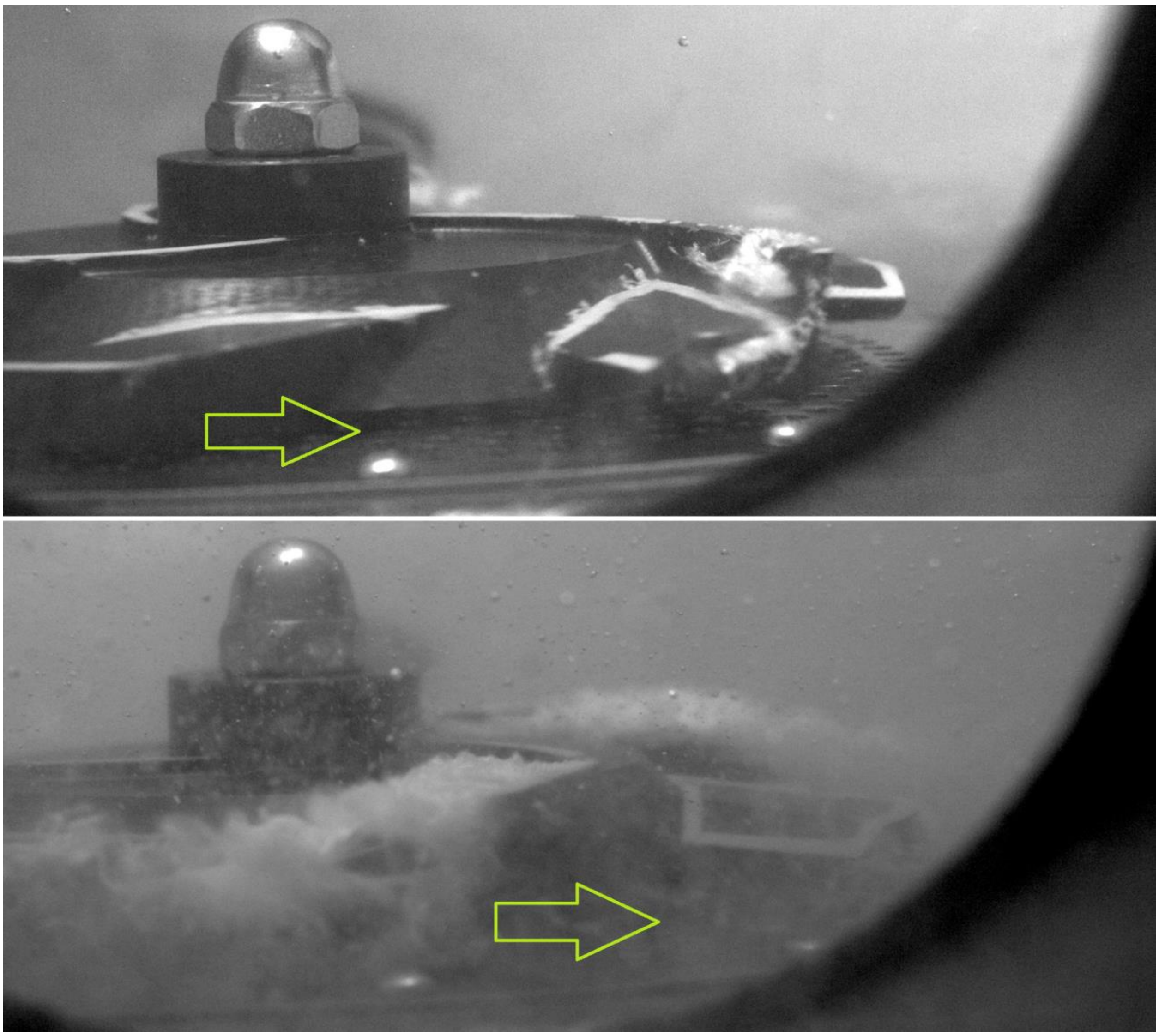

Figure 6.3: Rotor B shown at different tip-speeds. Top: Rotor B with a tip-speed of 11m/s. Bottom: Rotor B with a tip-speed of 16m/s. The amount of cavitation greatly increases with increasing rotor speed. The rotor vanes in the figure above are moving in the direction indicated by the arrows.

6.2.2 Rotor-to-Flake Interactions

Both rotor-to-flake impacts and the interaction of flakes with the trailing vortices of each rotor was captured with the high-speed filming. Not one incident of a flake being sheared between any of the test rotors and the extraction plate was recorded out of a total of 580 rotor-to-flake interactions.

The nature of rotor-to-flake impact was observed to depend on the rigidity of the C-flute corrugated cardboard flake impacting the rotor. Flakes of corrugated cardboard still in laminated form (flutes still sandwiched between both upper and lower sheets) were observed to partially deform and bounce off of the test rotors upon impact. These still laminated flakes maintained enough rigidity to allow for a partially elastic impact to take place. Once flakes of C-flute corrugated cardboard became delaminated, they were observed to drape and slide over the vanes of the test rotors seemingly unaffected by contact with the rotor. Both impact scenarios are shown in Figure 6.4.

Flakes were also observed to be twisted and stretched to partial, or complete failure in the trailing vortices produced by each rotor. This is shown for Rotor A in Figure 6.5.

A total of 580 impacts and flake-to-vortex interaction were observed with filming. These interactions are tabulated by rotor and interaction type in Table 6.3. These interactions are tabulated by rotor, interaction type, and approximate flake size in Figure 6.6.

Figure 6.6 shows that no flake-to-rotor impacts were observed for flakes smaller than approximately 20mm. It appeared from the films that the stagnation pressure on the faces of approaching rotor vanes would sweep these small flakes away from the rotor. With larger flakes, the effect of stagnation pressure in this capacity is less pronounced. Recall that the CFD simulations presented in Chapter 5 predicted significant stagnation pressure on the vane faces of each rotor (Figure 5.10).

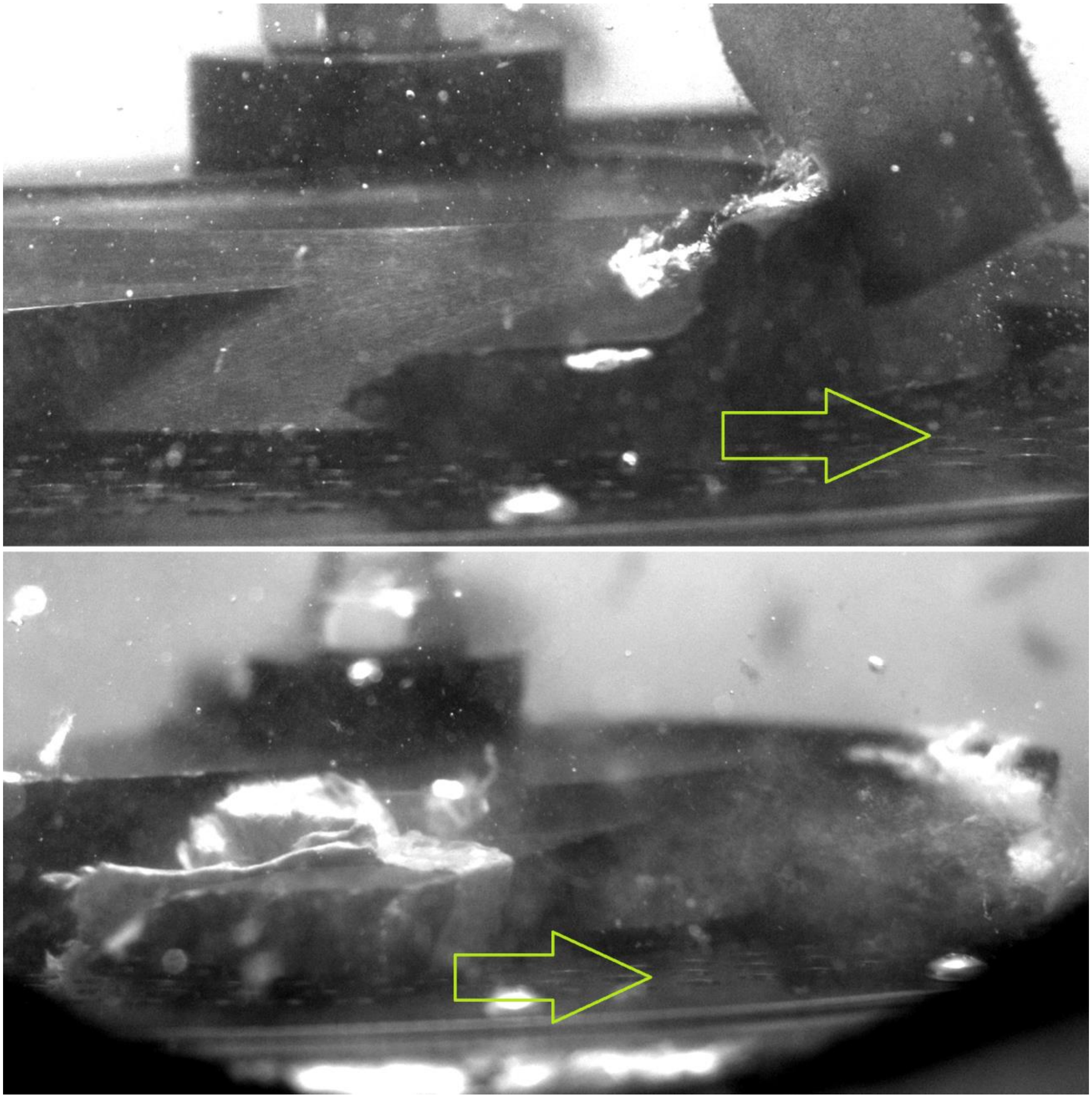

Figure 6.4: Two impact scenarios were observed. Flakes having some rigidity were observed to have partially elastic collisions with the test rotors (Top). Once flakes were partially broken down they were flexible enough to drape and slide over rotor vanes seemingly undamaged (Bottom). Rotor B is shown in both parts of the figure here at a tip speed of 11m/s. The rotor vanes are moving in the direction of the arrows.

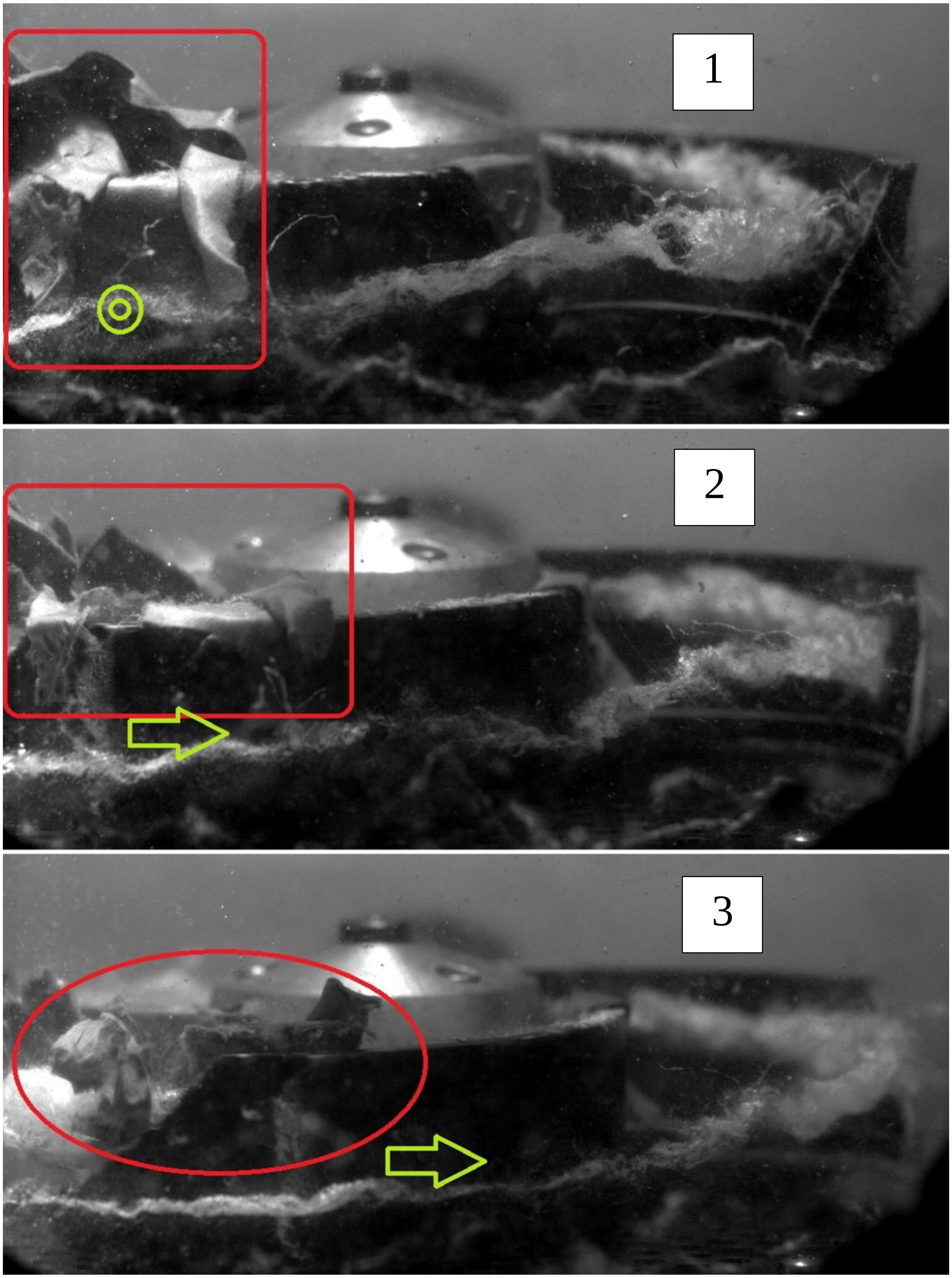
1
2
3

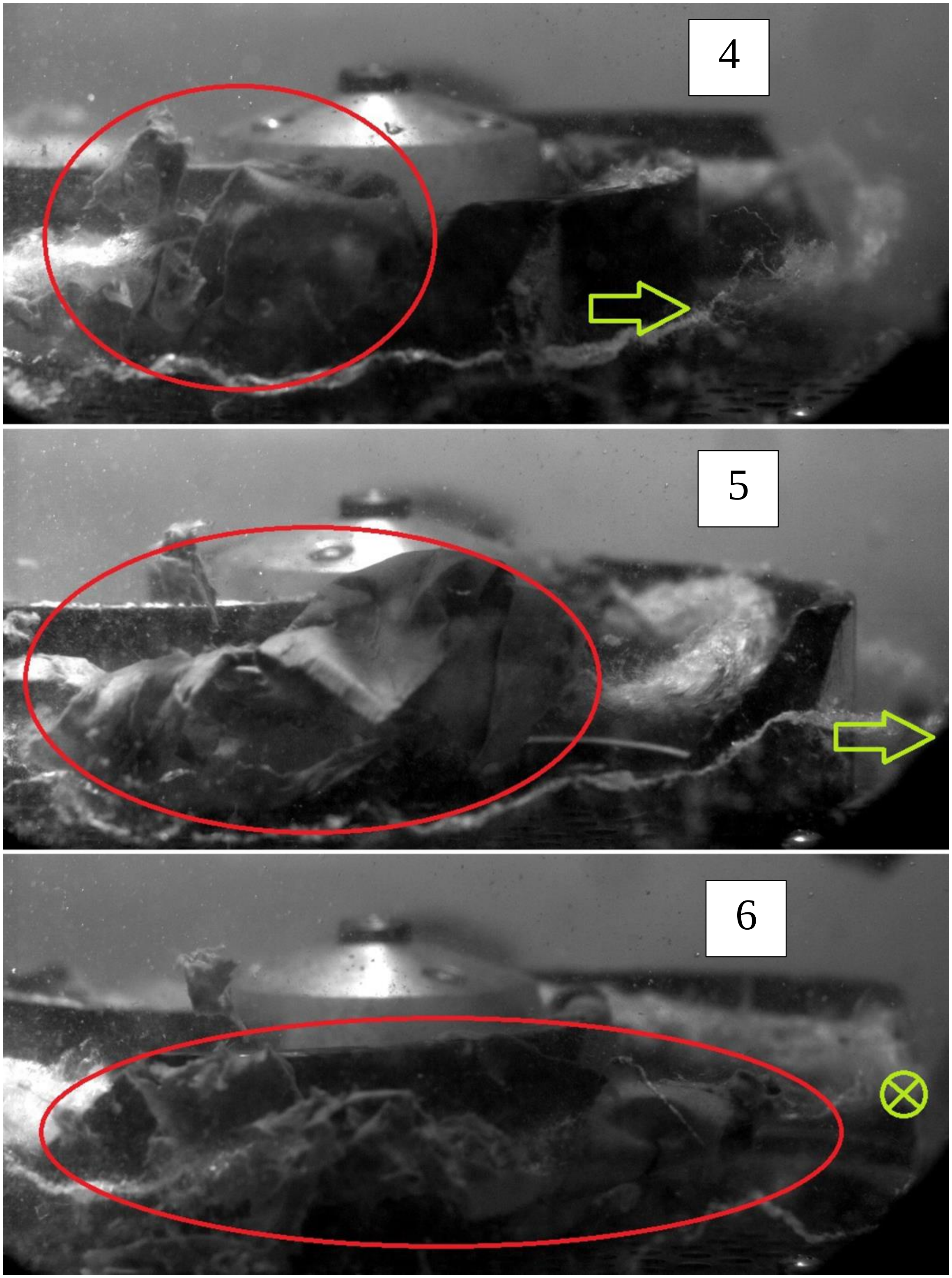

Figure 6.5: A large flake of C-flute corrugated cardboard being twisted and stretched in a trailing vortex of Rotor A. The rotor tip-speed here is 14m/s and the sequence runs 1-6. The rotor is rotating in the direction indicated by the arrows.

Table 6.3: Tabulation of filmed flake-to-rotor interactions. The total number of flake-to-rotor interactions observed for each rotor corresponds to the number of vanes each rotor has. Rotor A has 3 vanes, Rotor B has 6 vanes, and Rotor C has 8 vanes. Therefore, for equal film time, Rotor C has more vanes pass through the filming field of view.

Rotor	# of Flake-to-Rotor Impacts	# of Flake-to-Vortex Interactions	# of Events in which Flakes were Sheared Between a Rotor and Extraction Plate	Total # of Flake-to-Rotor Interactions
Rotor A	4	132	0	136
Rotor B	25	185	0	210
Rotor C	30	204	0	234
Total-all Rotors	59	521	0	580

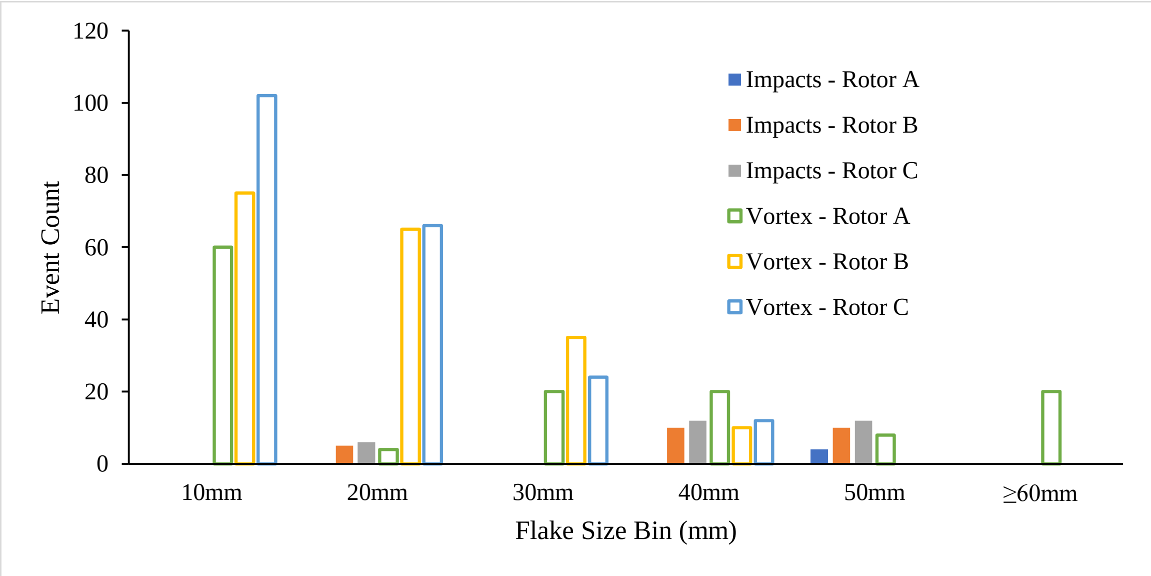

Figure 6.6: Flake-to-rotor impacts and flake-to-vortex interactions as observed for each rotor by flake size.

The difference in observed impacts vs. observed flake-to-vortex interactions is likely because the stagnation pressure on approaching vane fronts acts like a “source” to push flakes away from the approaching vane faces thus preventing impact while the low pressure vortex cores act like “sinks” to attract flakes.

6.3 Chapter Conclusions

The filming conducted here provides further evidence to support Hypotheses 3 and 6:

- **Hypothesis 3: LC Repulping occurs due to turbulence produced by the blunt vane shapes used by repulper rotors – specifically in the form of vane trailing vortices.**
- **Hypothesis 6: Flake attrition between the extraction plate and rotor is not an important repulping mechanism.**

The trailing vortices suspected to be present with each rotor based on the vortices produced by the similarly shaped mining impellers and by the CFD predictions in Chapter 5 are present. Flakes of C-flute corrugated cardboard were observed to be twisted and stretched to partial or complete failure in these vortices.

Although some flake-to-rotor impacts were observed, flake-to-vortex interactions were far more common. This is likely because the stagnation pressure on approaching vane fronts acts like a “source” to push flakes away from the approaching vane faces thus preventing impact while the low pressure vortex cores act like “sinks” to attract flakes.

The filming completed here provides further evidence in favor of Hypothesis 3.

Not a single flake was observed to be sheared between any of the test rotors and the laboratory repulper extraction plate providing further evidence to support Hypothesis 6.

Chapter 7: Conclusions and Recommendations

7.1 Conclusions

The work in this thesis focused on confirming/denying 7 hypotheses. Conclusions based on the tests each of these hypotheses as presented in the chapters of this thesis are now given.

- **Hypothesis 1: The final flake content in a repulping operation depends on the total energy input to the repulping operation and is independent of the rate of energy addition (rotor power).**

Repulping is a comminution process where waste paper is broken down to be reused. In other comminution processes, such as the ball-milling of minerals, the degree of breakdown depends on the total energy input to the process and the mechanical properties of the material being broken down. The power input to a comminution process determines the speed of the process but has no impact on the completeness of the process. Based on this, the breakage rate kinetics in repulping were proposed be in the form of:

$$\frac{dF}{dE} = -\lambda F \tag{1.3b}$$

where E is specific energy (energy/mass), F is flake content, and λ is a rate constant. In order for Hypothesis 1 to be true, the rate constant λ must be independent of rotor power. This was confirmed true by the finding illustrated by Figure 2.7 that λ is indeed independent of rotor power. Figure 2.7 showed that over a tip-speed range of 12-15m/s for C-flute corrugated cardboard and 11-14m/s for kraft aspen that λ was unchanging despite a 2.5 fold increase in rotor power between the slowest and fastest tip-speeds. The tests in Chapter 2 showed that λ depended on the pulp type being repulped, suspension consistency, suspension temperature, rotor design, and vat fill volume. Hypothesis 1 is confirmed to be true. The major implication of this is given by:

$$PR \propto \lambda P \tag{2.2}$$

where PR is the repulping production rate in time and P is rotor power. As λ and rotor power are independent of one another, the rotor speed can be increased to increase the throughput of the repulper with no impact on energy costs. The factors found to affect λ can be altered (i.e. increase consistency of temperature) to improve the production rate for a given rotor power.

- **Hypothesis 2: The time and energy required for repulping depend on feed pulp toughness, not tensile strength.**

Bennington et al. (1998), Brouillette et al. (2003), and Holik et al. (1988) all attempted to relate the time and energy required for repulping to the feed pulp wet-tensile strength. In other comminution processes, it is known that measures of material toughness correlate with the energy required to breakdown a material, not tensile strength. This forms the basis for Hypothesis 2. In Chapter 3, the rate constant λ as measured in the laboratory repulper was compared with both wet-tensile strength and wet-toughness (stress-strain area) as measured for kraft aspen, office paper, newsprint, unbleached paper towel, single-sided C-flute corrugated cardboard, and standard double sided C-flute corrugated cardboard. These materials were chosen as they ranged from a low-strength ingredient commonly used in tissue paper to provide softness (kraft aspen) to C-flute corrugated cardboard, a material used for heavy-duty packaging. Figure 3.4 shows that λ does not correlate with tensile strength. Unbleached paper towel, showed the second lowest tensile strength but proved as difficult to repulp (almost equal λ's) as single-sided C-flute corrugated cardboard, a material having four times the tensile strength of paper towel. Although paper towel showed low tensile strength, it showed much higher elongation than the other test materials (see Figures 3.1-3.3). This high elongation meant paper towel had toughness similar to that of single-sided C-flute corrugated cardboard thus explaining the almost equal λ's measured for these two materials. Figure 3.5 shows that λ correlates with material toughness. This confirms the validity of Hypothesis 2.

- **Hypothesis 3: LC Repulping occurs due to turbulence produced by the blunt vane shapes used by repulper rotors – specifically in the form of vane trailing vortices.**
- **Hypothesis 4: The relative time spent by flakes circulating past the repulper rotor versus in the rest of the vat in part determines repulping efficiency.**

Hypotheses 3 and 4 were tested in Chapters 3-6 in this thesis. A repulping model based on these two hypotheses and Hypothesis 2 is tested in Chapters 3 and 4 in both the 0.25m^3 laboratory repulper designed and built for this thesis study and a 15m^3 industrial repulper operating in a running mill. This model is described by Equations 3.7a and 3.7b:

$$\frac{dF}{dt} = -kF = -\frac{1}{\sigma(T)}\frac{V_{Swept}}{V_{Vat}}\frac{P}{m_P}CF \tag{3.5}$$

$$\frac{dF}{dE} = -\lambda F = -\frac{1}{\sigma(T)}\frac{V_{Swept}}{V_{Vat}}CF \tag{3.6}$$

where σ is material toughness having SI units of [J/kg], T is temperature, V_{Swept} is the repulper rotor swept volume as defined by Equation 3.1, V_{Vat} is the volume of the repulper vat, m_p is the mass of pulp in suspension, P is rotor power, and C is the mass concentration of pulp in suspension. The variation of k and λ with wet material toughness σ is based on Hypothesis 2. Wet material toughness is linearly dependent on temperature (Kouko et al. 2014). The parameter V_{Swept}/V_{Vat} arises from Hypotheses 3 and 4 and represents the time spent by flakes in the region of sufficient turbulence intensity near the rotor to be broken up (V_{Swept}) versus the time spent by flakes away from the rotor in the rest of the vat not being broken up (V_{Vat}). This is based on the assumption that the pulp suspension flow near the rotor is turbulent and that the rotor power is dissipated very near the rotor by turbulence as is the case with impeller power in turbulent stirred mixing applications. The quantity CF defines the split of rotor power going to flakes and the rest of the suspension. This is based off the work in Bennington et al. (1998a) that showed that cumulative contact from the rotor to the pulp suspension correlated with the completeness of a repulping operation. This amount of this contact was linearly dependent on the suspension concentration.

The rate constant λ as predicted by the model represented by Equation 3.7b was compared with λ as measured with the laboratory repulper for varying material toughness (σ), suspension concentration (C) and varying vat fill volume (V_{Swept}/V_{Vat}). This is shown in Figures 3.5, 3.6, and 3.7. The model predictions correlated with the experimental measurements with a $R^2 = 0.99$ so long as the laboratory repulper was operating at a vat level where its baffles were effective. The baffles in the laboratory repulper proved to be inadequate for low vat fill levels and solid-body swirl of the pulp suspension was observed along with a drop in rotor power. Solid-body swirl is indicative of poor mixing and the performance of the laboratory repulper fell off of the model prediction when solid-body swirl occurred.

The model represented by Equation 3.7 was also shown to predict k and λ values within 5% for a 15m^3 repulper operating in a running tissue mill. For cases where the feed pulp material properties are not known, Equation 3.7 can be used in the form of Equation 4.1 to predict the performance of a 15m^3 industrial repulper operating in a running mill from the performance of the 0.25m^3 laboratory repulper with the same feed pulp type and same suspension temperature (the feed pulp toughness varies with temperature):

$$\frac{k_2}{k_1} = \frac{P_2 m_{p1} C_2 V_{2\,Swept} V_{1\,Vat} \sigma(T)_1}{P_1 m_{p2} C_1 V_{1\,Swept} V_{2\,Vat} \sigma(T)_2} \tag{4.1a}$$

$$\frac{\lambda_2}{\lambda_1} = \frac{C_2 V_{2\,Swept} V_{1\,Vat} \sigma(T)_1}{C_1 V_{1\,Swept} V_{2\,Vat} \sigma(T)_2} \tag{4.1b}$$

The rotor power for the industrial repulper can be predicted using constant power number scaling as per Equation 4.2:

$$\frac{P_1}{\rho v_{Tip_1}^3 D_1^2} = \frac{P_2}{\rho v_{Tip_2}^3 D_2^2} \tag{4.2}$$

where the subscripts refer to “repulper 1” and “repulper 2”.

Equation 4.1b proved accurate to approximately 10% for the prediction of λ. Predictions for k and rotor power (P) using Equations 4.1a and 4.2 were accurate to within approximately 20%. The main source of error in the prediction of k using Equation 4.1a was a result of the prediction of rotor power (P) using Equation 4.2 as rotor power (P) is an input to Equation 4.1a. The 20% error in predicting the rotor power (P) in the 15m^3 industrial repulper is likely a result of the 11m/s rotor tip-speed used by the laboratory repulper for the prediction. At this tip-speed, the laboratory repulper is operating in near fully turbulent flow but still in the transitional regime (see Figure 3.9 in Section 3.3.4). The 15m^3 industrial repulper is operating with a tip-speed of 18m/s for the comparison – a tip-speed likely placing rotor operation in fully turbulent flow. As constant power number scaling relies on both impellers/rotors being in the fully turbulent flow regime, this is likely the source of the error in the prediction of rotor power in the 15m^3 industrial repulper.

The accuracy of the model predictions in both the 0.25m^{3}laboratory repulper and a 15m^3 industrial repulper at the very least confirm that the hypotheses on which the model is based are very plausible.

Hypotheses 3 and 4 are further tested in Chapters 5 and 6. The CFD simulations in Chapter 5 predict the presence of powerful trailing vortices produced by each rotor. These trailing vortices along with the prediction of vortex induced cavitation are shown in Figures 5.5 and 5.6 respectively. The CFD simulations also predict that the dissipation of rotor power via turbulence is accomplished right in the vicinity of the rotor (Figures 5.8 and 5.9) providing further evidence of the validity of the parameter V_{Swept}/V_{Vat} from the repulping model recapped above. High-speed filming in Chapter 6 revealed the presence of trailing vortices as the cavitation predicted to be present by the simulations was found to be present and proved to be a convenient flow visualization tool (Figures 6.2 and 6.3). Rotor-to-flake interactions were also filmed in Chapter 6. Flakes of C-flute corrugated cardboard were filmed both impacting the test rotors and interacting with the trailing vortices produced by each rotor. Impacts occurred only when a flake maintained some rigidity. After some break-down and wetting, flakes were seen to drape and slide over rotor vanes seemingly undamaged (Figure 6.4). Flakes were filmed being twisted and stretched to partial failure by the trailing vortices produced by each rotor (Figure 6.5). In total, 580 rotor-to-flake interactions were filmed. Of these interactions, 59 were rotor-to-flake impacts and 521 were flakes being twisted and stretched in trailing vortices. The fact that flake-to-vortex interactions were far more common is likely because the stagnation pressure on approaching vane fronts acts like a "source" to push flakes away from the approaching vane faces thus preventing impact while the low pressure vortex cores act like "sinks" to attract flakes. The CFD simulations in Chapter 5 show high stagnation pressure on the vane faces of each rotor.

In conclusion, based on the accuracy of the model predictions and the presence of trailing vortices, it can be said that waste paper is broken up in a repulper at the repulper rotor only by turbulence. How much of this break up is accomplished specifically by the trailing vortices produced by each rotor is unknown. Hypothesis 3; LC Repulping occurs due to turbulence produced by the blunt vane shapes used by repulper rotors – specifically in the form of vane trailing vortices, is very plausible. Hypothesis 4; the relative time spent by flakes circulating past the repulper rotor versus in the rest of the vat in part determines repulping efficiency, is likely true.

- **Hypothesis 5: Efficient mixing depends on both the rotor and vat as a system and is critical for efficient repulping.**

Holik (1988) and Paraskevas (1983) along with repulper manufacturers state that complete mixing is important for efficient repulping operation. However, there are no published tests on the effect of mixing on repulping efficiency. As evidence suggests that waste paper is broken up by turbulence only in the immediate vicinity of the repulper rotor, it is logical that poor mixing would lead to poor repulping.

Sections 2.2.7, 3.3.3 and 3.3.4 provide evidence that complete mixing is indeed critical to achieving efficient repulper operation. The baffles in the laboratory repulper proved to be ineffective for low vat fill volumes and this allowed the suspension in the repulper to swirl. This swirl was accompanied by a drop in rotor power and a loss in repulping efficiency. As swirl is indicative of poor mixing, it can be said that poor mixing is indicative of poor repulping efficiency.

Section 3.3.4 gives an operation map for the laboratory repulper in the form of rotor power number vs. rotor tip speed for varying vat fill volumes (Figure 3.9). The figure shows combinations of rotor speeds and vat fill volumes where efficient mixing is occurring (Reynolds independence) and where poor mixing is occurring (power number decreases indefinitely with increasing rotor speed).

The repulping model described by Equation 3.7 shows that repulping efficiency improves as vat volume decreases. Therefore, the best efficiency operating point for a repulper is at the lowest vat fill volume possible before the onset of solid-body swirl of the suspension in the repulper. This point will also depend on rotor speed and consistency as increasing consistency has a baffle-like effect. This points to the ideal repulper being one which can fluidize a high consistency pulp suspension with a large V_{Swept}/V_{Vat} but without solid-body swirl.

Hypothesis 5 is confirmed true. Proper mixing is critical for efficient repulping.

- **Hypothesis 6: Flake attrition between the extraction plate and rotor is not an important repulping mechanism.**

Section 2.2.6 included repulping trails with varied rotor-to-extraction plate clearances. If flakes were being sheared between the rotor and extraction plate, and if this was a significant repulping mechanism, varying the rotor-to-extraction plate clearance should have had a profound effect on repulping efficiency. The experiments in Section 2.2.6 showed that varying clearance had no effect on the energy required for repulping.

Section 6.2.2 tabulated rotor-to-flake interactions observed using high-speed film. Of 580 tabulated interactions, not one instance of a flake being sheared between a rotor and extraction plate was observed.

Hypothesis 6 is confirmed. The shearing of flakes between a repulper rotor and extraction plate is not an important repulping mechanism.

- **Hypothesis 7: Repulper rotor design affects the time and energy required for repulping.**

This hypothesis is confirmed true by the tests presented in Figure 2.8 in Section 2.2.5. A statistically significant difference in performance between rotors A and B is shown in Figure 2.8. The error for each flake content determination shown in the figure is ±2.5% found as a 95% confidence interval based on a T-distribution consisting of 10 flake content samples at each of the six test intervals shown in the figure.

The author has performed many repulping tests with each of the test rotors to produce the results presented in this thesis. At least qualitatively, the ability of Rotor A to maintain suspension motion in the repulper vat appeared inferior to that of rotors B and C. Due to the asymptotic nature of Equation 1.3 even a small difference in mixing performance between the rotors would result in substantial differences in energy use between each rotor. Recall from section 3.3.4 that mixing greatly affects the time and energy required for repulping.

7.2 Limitations of this Work

A performance difference was measured between the rotors in this test, the difference was small but statistically significant. There major limitation of the work presented in this thesis is that no concrete explanation explaining why each of the test rotors perform with different efficiencies is given. At this point, all that is known is that all three rotors tested here produce powerful trailing vortices that may be responsible for repulping and that despite very different vane shapes etc., they all perform in a similar manner. This is not surprising given that these represent the current state of the art in repulping. To really determine what makes one repulper rotor better than another, rotors having extreme geometries should be tested based on the methodology presented in this thesis. These extreme geometries should include everything from very streamlined rotors to concave paddles with the concave side of the paddle facing the flow (like the Scaba 6SRGT mixing impeller in Figure 1.3). Extreme differences in such rotors may show more definitive performance differentiation than the rotors tested in this study. Also, as shown in Section 3.3.4 which focused on mixing and repulping, a repulper rotor and vat operate as a system. For this reason, the three rotors tested in this thesis may perform differently with different vat/baffle arrangements. Qualitatively, Rotor C best maintained suspension motion in the vat while Rotor A was the worst in this regard. Recall from Section 3.3.4 that mixing efficiency greatly affects repulping efficiency. That, albeit qualitatively, Rotor A does not maintain suspension motion as well as the other rotors suggests that Rotor A does not mix the suspension as thoroughly as other rotors and this may explain the inferior performance of Rotor A compared to the other rotors.

Another limitation of this thesis work is that the repulping model described by Equation 3.7 does not apply well to HC repulpers. For predicting the results reported by Bennington et al. (1998a) and Vilaseca et al. (2011), the model vastly under-predicts the energy required for repulping in the laboratory scale HC repulpers used in these studies. This may be because V_{Swept}, when applied to LC repulping defines a region of fully turbulent and fluidized flow. The flow may not be turbulent at the lower rotor speeds run by HC repulpers. It is very likely that HC repulpers operate in a transitional flow regime. This assumption is made based on the fact that underneath the HC rotor helix, HC rotors and LC rotors are very similar. Some HC rotors are literally a LC rotor with a helix stuck on top. At the tip speeds run by the HC repulper used by Bennington et al. (1998a; 1998b), the rotors within laboratory LC repulper built for this study are operating in an almost laminar flow regime (see Figure 3.9).

The repulping model presented in this thesis assumes that the all of the rotor shaft power input to the pulp suspension is dissipated by turbulence very close to the rotor. The pulp suspension in the rest of the vat is circulating though and this takes some power. In the case of a high speed rotor operating in Reynolds independent flow, the power consumed to circulate the suspension throughout the repulper is likely negligible compared to the power dissipated by turbulence. However, if the rotor were to be slowed down far enough into the transitional flow regime, the power consumed to circulate the suspension in the repulper may no longer be negligible compared to the power dissipated by the turbulence responsible for deflaking. In this case, the performance of the repulper will fall off of that predicted by the model. This may in fact be the case with HC repulpers.

The model may also over-predict the performance of HC repulpers as HC repulpers operate at very low vat levels, often with the top of the rotor helix protruding from the suspension. The height of HC rotors is about equal to their diameter (Bahr 1990). Although by the model this should produce more efficient repulping, practical experience with the LC repulper built for this study shows that solid body motion of the suspension is hard to avoid when vat levels are low. Solid body motion means poor mixing and therefore inefficient repulping. Bennington et al. (1998a) set the suspension level to be equal to the tops of the rotor vanes underneath the rotor helix. Bennington et al. (1998a) noted swirling around the periphery of the vat with this low suspension level. For repulping newspaper, the LC laboratory repulper operating at 5% consistency and a vat fill level of $0.2m^3$ (no swirl for these operating conditions) is about twice as efficient as the HC repulper used in the Bennington et al. (1998a) study for the same task based on the performance of the HC repulper as reported in Bennington et al. (1998a).

Something not examined in this thesis is the affect repulping has on fiber properties. To repulp a tough material like C-flute corrugated cardboard takes a significant amount of energy, approximately 400 kW-h/Ton.

7.3 Recommendations for Future Work

Equations 3.2 and 3.3c are rewritten below for convenience. The repulping model presented in this thesis work is in part derived from these two equations.

$$\frac{dE_F}{dt} = \gamma P \tag{3.2}$$

$$\gamma = \frac{V_{Swept}}{V_{Vat}} CF \tag{3.3c}$$

The parameter γ represents the portion of rotor power imparted to the flakes from the rotor via turbulent fluid motion produced by the rotor. The definition of γ by Equation 3.3c is based on the postulates that flakes are broken up near the repulper rotor where turbulence is intense (V_{Swept}/V_{Vat}) and that the portion of rotor power impingent upon the flakes within the region defined by V_{Swept} depends on the concentration of flakes present within that region (CF). The parameter γ then represents the efficiency of rotor power transmission to deflaking and thus the efficiency of a repulper can be defined by γ.

The efficiency of the laboratory repulper can then be estimated by Equation 3.3c. All three rotors used for this thesis work have a $V_{Swept} \approx 10^{-3}$m^3 and the typical vat volume during a repulping test in the laboratory repulper is about 0.20m^3. With a suspension consistency of 5%, this gives the efficiency of the laboratory repulper as:

$$\gamma_{Lab} = \frac{10^{-3}}{0.20} 0.05\, F = 2.5 \times 10^{-4} F$$

As F varies from 0-1, the maximum efficiency of the laboratory repulper is then 0.025%. This is extremely poor! In fact, this means that at best, 99.975% of the rotor power input to the laboratory repulper is directly dissipated by turbulence without contributing at all to deflaking. This suggests that perhaps new repulping technologies/arrangements should be pursued. For instance, if the rotor were positioned halfway up the vat height as is common with stirred mixers, an axial flow repulper rotor would produce a "double flow loop" as is the case with stirred mixers. This would effectively cut the vat volume (V_{Vat}) in half and provide for much more efficient repulping. Taking this idea further, a number of rotors could be staggered axially along a single long shaft in a repulper. This would effectively split the parameter V_{Vat} into a number of smaller volumes as defined by the number of rotors on the long shaft. Furthermore, most repulpers use a rotor/vat diameter ratio of 0.3. These multiple rotors could be sized for a rotor/vat diameter larger than this. Using multiple rotors having a larger diameter would increase the V_{Swept}/V_{Vat} parameter greatly. Of course, mechanical strength and mixing concerns must be considered with the implementation of multiple rotors.

An interesting alternate arrangement is outlined in an old patent (Danforth 1963). This patent shows actual energy improvements in the form of TAPPI-Flake-content versus specific-energy plots for a novel rotor design. The novel design uses a concentric counter-rotating twin-rotor setup. The inner rotor has 8 backswept curved vanes and is ringed by a counter-rotating concentric ring carrying vortex generators. In essence, the rotor here is an original hydrapulper style rotor (see Figure 1.2) but with the outer ring of vortex generators moving in the opposite direction to the inner pumping vanes. The patent includes data showing considerable energy savings when both inner and outer rotors are operated compared to just the inner rotor being operated. The patent author explains this energy savings as being a result of no energy wasted against the repulper vat baffles as the counter rotating design requires no baffles. The patent author also states that up to 1000hp/ton could be input to the repulper vat by the counter-rotating rotor setup without swirl and without sloshing the pulp suspension out of the vat. For a single rotor in the same vat, only 200hp/ton could be input without swirl and/or sloshing of the suspension outside the vat.

If the performance data presented in this patent is correct, a different explanation than energy lost to dissipation by baffles may better explain the improved performance of the twin-rotor design. First, the power from the twin-rotors is likely dissipated by turbulence near the rotors - well away from the baffles. Second, any material being repulped has some resilience, i.e. some minimum energy input is required to rupture it. Repulping happens in the vicinity of the rotor. The high power input from the twin rotor setup likely expanded the volume around the rotor that exceeds the minimum intensity required to repulp the test material. This means more relative time spent being repulped versus not being repulped flowing around the vat. This arrangement also would allow for very high rotor power inputs without solid body swirling. It seems feasible that this dual rotor arrangement would be more efficient for repulping. However, as both inner and outer rotors were variable speed, the mechanical design for this setup would be extremely complicated, especially if only a single motor is used. If the substantial energy savings claimed for this setup in the patent are true, it is likely the complex mechanical arrangement that has kept this idea from being used in industry.

The model for repulping presented in this thesis does not apply well to HC repulping. This may be because HC repulping is done in the transitional flow regime as described above. The recommendation then is that repulping tests should be conducted at rotor speeds in the transitional, and even laminar flow regimes to determine the effect these flow regimes have on repulping efficiency.

Extreme rotor geometries ranging from streamlined to even blunter than the test rotors in this thesis should be tested. The rotors used in this study are all modern offerings by their respective manufacturers and thus it is not surprising that they perform similarly. Rotors having extreme geometries would likely be easier to differentiate performance-wise and this will help to identify important geometries for efficient repulping. The three rotors tested in this thesis should be re-tested with different vat/baffle arrangements as repulper rotors and repulper vats work as a system as per Section 3.3.4.

For mills operating existing repulpers, the best approach towards saving energy and increasing throughput would be to lower the vat level as low as possible before solid body motion of the suspension in the repulper is encountered. The onset of solid body motion will be marked by a drop in rotor power. Consistency should be raised as high as the processes further down the line will allow. Increasing consistency will also combat swirl in the repulper. Finally, if it is possible to increase the repulping temperature, this should be done as this will yield large energy savings and increased throughput.

At this point, based on the findings in this thesis, an ideal repulper using the current arrangement of a single bottom-mounted rotor in a vat is one which has a very large rotor that is able to produce fully turbulent flow in a high-consistency pulp suspension in a small vat while maintaining efficient mixing – i.e. no solid body motion.

It is hoped that the findings and analysis presented can be used in industry to improve the repulping process and reduce the energy consumption in repulping. It is also hoped that the findings and analysis presented here will pave the way toward improved repulper design.

References

Amanullah, A., Hjorth, S.A., Nienow, A.W. (1998). A new mathematical model to predict cavern diameters in highly shear thinning, power law liquids using axial flow impellers. *Chem. Eng. Sci.*, 53(3), 455–459.

Amaral, M.E., Renaud, M.E., Roux, J.C. (2000). Cinétique de disintegration des pâtes à papier: Modelisation du phénomène. *Revue ATIP*, 54(3-4), 76-87.

Andersson, O., Berkyto, E. (1951). Some factors affecting the stress–strain characteristics of paper. *Sven. Papp.tidn.*, 54(13), 437–444.

Ansys CFX Manual Release 14.5. (2013). Ansys Inc. Canonsburg PA.

Ashby, M.F. & Jones, D.R.H., (2003). *Engineering Materials 1, 2nd Edition.* Oxford, Great Britain: Butterworth Heinmann.

Assirelli, M., Bujalski, W., Eaglesham, A., Nienow, A.W. (2002). Study of micromixing in a stirred tank using a Rushton turbine: comparison of feed position and other mixing devices. *Transactions of the Institution of Chemical Engineers, Part A.*, 80(8), 855–863.

Assirelli, M., Bujalski, W., Eaglesham, A., Nienow, A.W. (2005). Intensifying micromixing in a semi-batch reactor using a rushton turbine. *Chem Eng Sci.*, 60 (8), 2333-2339.

Assirelli, M., Bujalski,W., Eaglesham, A., Nienow, A.W. (2008). Macro- and micromixing studies in an unbaffled vessel agitated by a Rushton turbine. *Chemical Engineering Science*, 63(1), 35–46.

Aue, J. & Fineran, B., (2006). Energy Efficient HM Rotor. *twogether Magazine*, 21(6), 14-16.

Austin L.G. (1984). Concepts in process design of mills. *Mining Engineering, SME-AIME,* 36 (6), 628–635.

Back, E.L. & Andersson, L.I. (1992). The effect of temperature on wet web strength properties. In: *Pan-Pacific Pulp and Paper Technology Conference*, *vol.B* (pp. 141–150).

Bahr, T. (1990). Recent developments in helical rotor pulpers. In M.J. Coleman (Ed.), *Recycling Paper from Fiber to Finished Product*, (pp. 597-600.). Atlanta GA: TAPPI Press.

Bakker, A. & van den Akker, H. E. A. (1994). Single-phase flow in stirred reactors. *Chem. Eng. Sci*. 72(7), 583–593.

Baldi, S. & Yianneskis, M. (2004). On the quantification of energy dissipation in the impeller stream of a stirred vessel from fluctuating velocity gradient measurements. *Chem Eng Sci*., 59(13), 2659-2671.

Batchelor, G. K. (1970). *The Theory of Homogeneous Turbulence*. London: Cambridge University Press.

Bates, R. L., Fondy, P.L., Fenic, J.G. (1966). Impeller characteristics and power. Chapter 3 In V.W. Uhl & J.B. Gray (Ed.), *Mixing: Theory and Practice*, New York: Academic Press.

Bearman, R.A., Barley, R.W., Hitchcock, A. (1991). Prediction of power consumption and product size in cone crushing. *Minerals Engineering*, 4(12), 1243–1256.

Bennington, C.P.J., Kerekes, R.J., Grace, J.R. (1990). The yield-stress of fibre suspensions. *Canadian Journal of Chemical Engineering*, 68(10), 748–757.

Bennington, C.P.J. & Kerekes, R.J. (1996). Power requirements for pulp suspension fluidization. *TAPPI Journal*, 79(2), 253-258.

Bennington, C.P.J., Sui, O.S., Smith, J.D. (1998a) The effect of mechanical action on waste paper defibering and ink removal in repulping operations. *JPPS*, 24(11), 341-348.

Bennington C.P.J., Smith J.D., Sui O.S., Wang M-H. (1998b). Characterization of repulper operation for newsprint deinking. In *TAPPI Pulping Conference Proceedings Book 3*(pp.1083-1095). Atlanta GA: TAPPI Press. 1083.

Bhardwaj N.K. & Rajan V. (2004). Wet strength paper repulping: effect of process variables. *Appita J.*, 57(4), 305-310.

Bhattacharya, S. & S. Kresta. (2002). CFD simulations of three-dimensional wall jets in a stirred tank. *Canadian Journal of Chemical Engineering*, 80(4), 695–709.

Bhole M., Ford C., Bennington C.P.J. (2009). Characterization of axial flow impellers in pulp fibre suspensions. *Chemical Engineering Research and Design*. 8(7), 648–653.

Bhole M., Hui L.K., Gomez C., Bennington C.P.J., Dumont G.A. (2011). The effect of off-wall clearance of a side-entering impeller on the mixing of pulp suspensions in a cylindrical stock chest. *Canadian Journal of Chemical Engineering*, 89(5), 985-995.

Bond, F.C. (1952). The third theory of comminution. *Trans. Am. Inst. Min. Metall. Pet. Eng.,* 193, 484-494.

Bond, F.C. (1960). Confirmation of the third theory. *Trans. Am. Inst. Min. Metall. Pet. Eng*., 217, 139-153.

Bond, F.C. (1961). *Crushing and grinding calculations*. Milwaukee, Wisconsin: Allis-Chalmers Publications.

Borodulina, S., Kulachenko, A., Galland, S., Nygårds, M. (2012). Stress–strain curve of paper revisited. *Nordic Pulp Paper Research Journal*, 27(2), 318–328.

Boussinesq, J. (1877). Essai sur la theorie des eaux courantes. *Memoirs presents par divers savants a l'Academie des Sciences,* 23(1), 1-680.

Brodkey, R. S. (1975). *Turbulence in Mixing Operations*. New York: Academic Press.

Brouillette F, Daneault C, Dorris G.M. (2003). Effect of initial repulping pH on the deflaking rate of recovered papers. *Pulp & Paper Canada*. 104(7), 35-41.

Calabrese, R. V. & Stoots, C. M. (1989) Flow in the impeller region of a stirred tank. *Chem. Engng Prog*., 85(5), 43-50.

Cho B.Y., Ryu J.Y., Song B.K. (2009). Factors influencing deflaking kinetics in repulping to produce molded pulp. *Journal of Industrial Engineering and Chemistry*. 15(1), 119-123.

Cooke, M., Middleton, J. C. and Bush, J. R. (1988) Mixing and mass transfer in filamentous fermentations. In R, King (Ed.), *Proc. 2nd Int. Conf. on Bioreactor Fluid Dynamics* (pp. 37-64). Cranfield, U.K.: BHR Group.

Cutter, L.A. (1966). Flow and turbulence in a stirred tank. *A.I.Ch.E. Journa*l, 12(1), 35–45.

Da-Wen Sun. (2012). *Handbook of frozen food processing and packaging 2nd edition*. Boca Raton Fl.: CRC Press.

Danforth, D.W. (1963). Apparatus and Method for Pulping. *U.S. patent*. 3,085,756.

Dalpke, B. & Kerekes, R.J. (2005). The influence of fibre properties on the apparent yield-stress of flocculated pulp suspensions. *Journal of Pulp and Paper Science,* 31(1), 39–43.

Damani, R., Powell, R.L., Hagen, N. (1993). Viscoelastic characterization of medium consistency pulp suspensions. *Canadian Journal of Chemical Engineering*, 71(5), 676–685.

Derakhshandeh, B., Hatzikiriakos, S.G., Bennington, C.P.J. (2010). Rheology of pulp fibre suspensions using ultrasonic Doppler velocimetry. *Rheol Acta*, 49(11–12), 1127–1140.

Derakhshandeh B., Kerekes R.J., Hatzikiriakos S.G., Bennington C.P.J. (2011). Rheology of pulp fibre suspensions: A critical review. *Chemical Engineering Science*, 66, 3460–3470.

Derksen, J. J. & van den Akker, H. E. A. (1999). Large eddy simulations on the flow driven by a Rushton turbine. *AIChE J.* 45(2), 209–2221.

Dong,L., S.T.Johansen, and T.A.Engh (1994). Flow induced by an impeller in an unbaffled tank 1: Experimental. *Chem. Eng. Sci*., 49 (4), 549–560.

Duffy, G.G. & Titchener, A.L. (1975). The disruptive shear-stress of pulp networks. *Svensk Papperstidning*, 78(13), 474–479.

Egan, J., Demler, J. Christopher, L. (2004). Redesigned pulper rotor offers energy savings at equal recycled stock quality. *Pulp & Paper*, 78(4), 34-38.

Ein-Mozaffari, F., Bennington, C.P.J., Dumont, G.A. (2005). Suspension yield-stress and the dynamic response of agitated pulp chests. *Chemical Engineering Science*, 60(8–9), 2399–2408.

Espy H.H. (1992). The chemistry of wet strength repulping. *Progress in Paper Recyling*., 1(4), 17-23.

Espy H.H. & Geist G.W. (1993). Persulfates as repulping agents for neutral alkaline wet-strength broke. *TAPPI J*., 16(2), 139-142.

Fabry, B., Roux, J.C., Carre, B., (2001). Characterization of friction during pulping: an interesting tool to achieve good deinking. *Journal of Pulp and Paper Science*, 27(8), 284-288.

Fan, J., Wang, Y., Fei, W. (2007). Large eddy simulations of flow instabilities in a stirred tank generated by a Rushton turbine. *Chin. J. Chem. Eng*., 15(2), 200–208.

Fischer S.A. (1997). Repulping wet strength paper. *TAPPI J*., 80(11), 141-147.

Fokema, M. D. & S. M. Kresta. (1994). Importance of using the correct impeller boundary conditions for CFD simulations of stirred tanks. *Canadian Journal of Chemical Engineering*, 72(2), 177–183.

Ford, C., Ein-Mozaffari, F., Bennington, C.P.J., Taghipour, F. (2006). Simulation of mixing dynamics in agitated pulp stock chests using CFD. *AIChE J*. 52(10), 3562–3569.

Fricker, A., Thompson, R., Manning, A. (2007). Novel solutions to new problems in paper deinking. *Pigment & Resin Technology*, 36(3), 141–152.

Fuerstenau, D.W. & Abouzeid, A.-Z.M. (2002). The energy efficiency of ball milling in comminution. *International Journal of Mineral Processing*, 67(1), 161–185.

Germano, M., Piomelli, U., Moin, P., Cabot, W.H. (1991). A dynamic subgrid-scale eddy viscosity model. *Phys. Fluids A*, 3(7), 1760-1765.

Goodman, J. (1899). *Mechanics Applied to Engineering*. London: Longman, Green & Company.

Gullichsen, J., Harkonen, E. (1981). Medium consistency technology. II. Storage dischargers and centrifugal pumps. *TAPPI Journal*, 64(6), 69-72.

Hartmann, H., Derksen, J. J. , Montavo, C., Pearson, J., Hamill, I. S., van den Akkar, H. E. A. (2004). Assessment of large eddy and RANS stirred tank simulations by means of *LDA. Chem.Eng. Sci*., 59(12), 2419–2432.

Head, V.P. (1952). A shear criterion for the hydraulic behavior of paper stocks in pumps, pipes, valves and flow meters. *TAPPI Journal*, 35(6), 260–266.

Hemrajani, R.R. & Tatterson, G.B. (2004). Mechanically stirred vessels. In P.L. Edward, V.A. Atiemo-Obeng, S.M. Kresta (Ed.), *Handbook of Industrial Mixing: Science and Practice* (pp. 345-390). New Jersey: John Wiley & Sons.

Herbst, J.A. & Fuerstenau, D.W. (1973). Mathematical simulation of dry ball milling using specific power information. *Trans. Am. Inst. Min. Metall. Pet. Eng.*, 254, 343-348.

Herbst, J.A. & Fuerstenau, D.W. (1980). Scale-up procedure for continuous grinding mill design using population balance models. *Int. J. Miner. Process*., 7(1), 1-31.

Herschel, W.H. & Bulkley, R. (1926). Konsistenzmessungen von Gummi-Benzollösungen. *Kolloid Zeitschrift*, 39(4), 291–300.

Hinze, J. O. (1987). *Turbulence, an Introduction to Its Mechanism and Theory, 2nd Edn*. Toronto: McGraw-Hill Classic Textbook Reissue, McGraw-Hill.

Hobbs, D. M., Alvarez, M. M., Muzzio, F. J. (1997). Mixing in globally chaotic flows: a self-similar process, *Fractals*, 5 (3), 395-425.

Hobbs, D. M., & F. J. Muzzio. (1998). Optimization of a static mixer using dynamical systems techniques. *Chem. Eng. Sci*., 53(18), 3199–3213.

Holik, H. (1988). Toward a better understanding of the defibering process. Proc., In *TAPPI Engineering Conference Proceedings* (pp. 223-232). Atlanta: TAPPI Press.

Holik, H. (2006). *Handbook of paper and board 6th edition*. Weinheim: WILEY-VCH Verlag GmbH & Co. KGaA.

Hoogendoorn, C. J., denHartog, A. P. (1967). Model studies on mixers in the viscous flow region. *Chem. Eng. Sci*., 22(12), 1689–1699.

Hui, L. K., Bennington, C. P. J., Dumont, G. A. (2009). Cavern formation in pulp suspensions using side-entering axial-flow impellers. *Chem. Eng. Sci*. 64(3), 509–519.

Hukki, R.T. (1962). Proposal for a solomonic settlement between the theories of von Rittinger, Kick, and Bond. *Trans. AIME*, 223, 403–408.

Hunt, J. C. R., Wray, A. & Moin, P. (1988). Eddies, stream, and convergence zones in turbulent flows. *Center for Turbulence Research*, Report CTR-S88.

Ibrahim, S. & Nienow, A. W. (1996). Power curves and flow patterns for a range of impellers in Newtonian fluids. *Chem. Eng. Res. Des*., 74(5), 679–688.

Jahoda, M., Mostek, M., Kukukova, A., Machon, V. (2007). CFD modelling of liquid homogenization in stirred tanks with one and two impellers using large eddy simulation. *Chem.Eng.Res.Des*. 85(5), 616–6625.

Javed, K. H., Mahmud, T., Zhu, J. M. (2006). Numerical simulation of turbulent batch mixing in a vessel agitated by a Rushton turbine. *Chem. Eng. Process*., 45(2), 99–112.

Jaworski Z., Dyster K.N., Nienow A.W. (2001). The effect of size, location and pumping direction of pitched blade turbine impellers on flow patterns: LDA measurements and CFD predictions, part A. *Trans IChemE.*, 79(8), 887-894.

Joshi J.B., Nere N.N., Rane V.C., Murthy B.N., Mathpati C.S., Patwardhan A.W., Ranade V.V. (2011). CFD simulation of stirred tanks: Comparison of turbulence models. Part I: Radianl flow impellers. *Canadian Journal of Chemical Engineering*, 89(2), 23-82.

Karcz, J., Cudak, M., Szoplik, J. (2005). Stirring of a liquid in a stirred tank with an eccentrically located impeller. *Chemical Engineering Science* 60(8-9), 2369–2380.

Kerekes, R.J. & Soszynski, R.M., Doo, P.A.T. (1985). The flocculation of pulp fibres. In: *Proceedings of the 8th Fundamental Research Symposium* (pp.265–310). Oxford England: Mechanical Engineering Publications.

Kerekes, R.J. & Schell, C.J. (1992). Characterization of fibre flocculation by a crowding factor. *Journal of Pulp and Paper Science*, 18(1), 32–38.

Khang, S. J., & Levenspiel, O. (1976). New scale-up and design method for stirrer agitated batch mixing vessels. *Chem. Eng. Sci*., 31(7), 569–577.

Kick, F. (1885*). Das Gesetz der proportionalen Widerstande und seine anwendung felix*. Leipzig, Germany.

Kolmogorov, A.N. (1941). Decay of isotropic turbulence in an incompressible viscous liquid. *C.R. Acad. Sci. USSR*. 31, 538-541.

Kouko J., Retulainen E., Kekko P. (2014). Straining and relaxation properties of wet paper during heating. *Mech Time-Depend Mater*, 18(4), 697–719.

Kramers, H., Baars, G.M., Knoll, W.H. (1953). A comparative study on the rate of mixing in stirred tanks. *Chemical Engineering Science* 2(1), 35–42.

Kresta, S. M. & P. E. Wood. (1991). Prediction of the three-dimensional turbulent flow in stirred tanks. *AIChE J*. 37(3), 448–460.

Kresta S.M. & Wood P.E. (1993). The flow field produced by a pitched blade turbine: Characterization of the turbulence and estimation of the dissipation rate. *Chemical Engineering Science*, 48(10), 1761-1774.

Kresta S.M. & Brodkey, R. (2004). Turbulence in mixing applications. In P.L. Edward, V.A. Atiemo-Obeng, and S.M. Kresta (Ed.), Handbook of industrial mixing: Science and practice (pp. 19-83). New Jersey: John Wiley & Sons.

Kresta S.M., Mao D., Roussinova V., (2006). Batch blend time in square stirred tanks. *Chemical Engineering Science*, 61(9), 2823 – 2825.

Kumaresan, T. & Joshi, J. B. (2006). Effects of the impeller design on the flow pattern and mixing in stirred tanks. *Chem. Eng. J*. 115(3), 173–193.

Lamberto, D. J., Muzzio, F. J., Swanson, P. D. (1996). Using time-dependent rpm to enhance mixing in stirred vessels. *Chem. Eng. Sci*., 51 (5), 733–741.

Langheinrich, C., Eddleston, T., Stevenson, N. C., Emery, A. N., Clayton, T. M., Slater, N. K. H., Nienow, A. W. (1998). Liquid homogenization studies in animal cell bioreactors of up to 8 m^3 in volume. *Food Bioprod. Process*. 76(2), 107–116.

Laufhutte, H. D. and Mersmann. A. (1985). Dissipation of power in stirred vessels. In *Proceedings of 5th European Conference on Mixing*. BHRA Fluid Engineering: Wurtzberg Germany.

Launder B.E. & Spalding, D.B. (1974). The numerical computation of turbulent flow. *Computer Methods in Applied Mechanics and Engineering*, 3(2), 269–289.

Launder, B. E., & Sharma, B. I. (1974). Application of the energy dissipation model of turbulence to the calculation of flow near a spinning disc. *Letters in Heat and Mass Transfer*, 1(2), 131-138.

Lee, K. C., Ng, K., Yianneskis, M. (1996). Sliding mesh predictions of the flows around Rushton impellers. *IChemE. Symp. Ser*., 140, 1–12.

Lee, K.C., Yianneskis, M. (1998). Turbulence properties of the impeller stream of a Rushton turbine. *AIChE. Journal*, 44(1), 13–24.

Martinez, D.M., Buckley, K., Lindstrom, A., Thiruvengadaswamy, R., Olson, J.A., Ruth, T.J., Kerekes, R.J. (2001). Characterizing the mobility of papermaking fibres during sedimentation. The Science of Papermaking 12th Fundamental Research Symposium. In *The Pulp and Paper Fundamental Research Society* (25-254), Oxford.

Martinez, D.M., Kiiskinen, H., Ahlman, A.K., Kerekes, R.J. (2003). On the mobility of flowing papermaking suspensions and its relationship to formation. *J Pulp Pap Sci*, 29(10), 341–347.

Mason, S.G. (1950). The motion of fibres in flowing fluids. *Pulp and Paper Canada Magazine* 51(5), 93–100.

Menter, F.R. (1994). Two-equation eddy-viscosity turbulence models for engineering applications. *AIAA-Journal*., 32(8), 1598 – 1605.

Menter F.R. (2009). Review of the shear-stress transport turbulence model from an industrial perspective. *International Journal of Computational Fluid Dynamics*, 23(4), 305-316.

Micale, G., Brucato, A., Grisafi, F., Ciofalo, M. (1999). Prediction of flow fields in a dual impeller stirred vessel. *AIChE J*., 45(3), 445–464.

Montante, G., Lee, K. C., Brucato, A., Yianneskis, M. (1999). An experimental study on double- to single- loop flow pattern transition in stirred vessels. *Canadian Journal of Chemical Engineering*, 77(4), 649–659.

Mozaryn, W., Janssen, L. P. B. M., Van Dierendonck, L. L., (1994). Design rule for pumping devices in a loop polymerization reactor. *Chem. Eng. Res. Des*. 72 (A3), 461-464.

Muller W., (2010). 20% energy savings due to IntensaPulper IP-R. *twogether Magazine*. 30, 36-37.

Murthy, B. N. & Joshi, J. B. (2008). Assessment of standard k−ε, RSM and LES turbulence models in a baffled stirred vessel agitated by various impeller designs. *Chem. Eng. Sci*. 63(22), 5468–5495.

Myers J.M., Reeder M.F., Fasano J.B. (2002). Optimize mixing by using proper baffles. *Chemical Engineering Progress*, 98(2), 42-47.

Napier-Munn, T.J., Morrell, S., Morrison, R.D., Kojovic, T. (1999). Mineral comminution circuits: Their operation and optimization. In *JKMRC Monograph Series in Mining and Mineral Processing 2 (pp.53-53).* Queensland Australia: Julius Kruttschnitt Mineral Research Centre.

Neimo, L. (1999), Wet strengthening of paper. In *Papermaking science and technology Book 4* (Chapter 13). Finland: Fapet Oy.

Ng, K., Fentiman, N. J., Lee, K. C., Yianneskis, M. (1998). Assessment of sliding mesh CFD predictions and LDA measurements of the flow in a tank stirred by a Rushton impeller. *Chem. Eng. Res. Des*., 76(6), 737–747.

Nicoud, F., Ducros, F. (1999). Subgrid-scale stress modelling based on the square of the velocity gradient tensor. *Flow, Turbulence and Combustion*, 62(3), 183-200.

Nienow, A.W. & Wisdom, D.J. (1974). Flow over disc turbine blades. *Chemical Engineering Science*, 29(9), 1994–1997.

Nienow, A.W. (1997). On impeller circulation and mixing effectiveness in the turbulent flow regime. *Chemical Engineering Science*, 52(15), 2557-2565.

Nogueira E.S., Pinto J.C., Vianna Jr. A.S. (2012). Analysis of energy dissipation in stirred suspension polymerization reactors using computational fluid dynamics. *Canadian Journal of Chemical Engineering*, 90(4), 983-995.

Olson, J. A. & Kerekes, R. J. (1998). The motion of fibres in turbulent flow. *J. Fluid Mech*. 377, 47-64.

Olson, J. A. (2001). The motion of fibres in turbulent flow, stochastic simulation of isotropic homogeneous turbulence. *Intl J. Multiphase Flow*, 27(12), 2083-2103.

Olson, J. A., Frigaard, I., Candice, C., Hamalainen, J. P. (2004). Modelling a turbulent fibre suspension flowing in a planar contraction: The one-dimensional headbox. *Intl J. Multiphase Flow*, 30(1), 51-56.

Oshinowo, L., Jaworski, Z., Dyster, K. N., Marshall, E., Nienow, A. W. (2000). Predicting the tangential velocity field in stirred tanks using multiple reference frames (MRF) model with validation by LDA measurements. In H.E.A. van den Akker & J.J. Derksen (Ed.) *Proceedings of the 10th European. Conference on Mixing* (pp.281–289). Delft, Amsterdam; Elsevier Science B.V.

Ostwald W. (1929). Ueber die rechnerische Darstellung des Strukturgebietes der Viskosität. *Kolloid-Zeitschrift*, 47(2), 176-187.

Paraskevas, S. (1983). High consistency repulping benefits & drawbacks. In *Proceedings of the TAPPI Pulping Conference* (pp. 129-132). Atlanta: TAPPI Press.

Parsheh M., Brown L.B., Aidun C.K. (2005). On the orientation of stiff fibres suspended in turbulent flow in a planar contraction. *J. Fluid Mech*., 545, 245–269.

Prochazka, J. & Landau, J. (1961). Studies on mixing: XII. Homogenization of liquids in the turbulent regime. *Coll. Czech. Chem. Commun*. 26, 2961–2973.

Pulping of Secondary Fiber. (1990). In M.J. Coleman (Ed.), *Recycling Paper from Fiber to Finished Product*, (pp. 597-600.). Atlanta GA: TAPPI Press.

Ranade, V. V. (1997). An efficient computational model for simulating flow in stirred vessels: A case of Rushton turbine. *Chem.Eng. Sci*., 52(24), 4473–4484.

Ranade V.V. (2001). Trailing vortices of a Rushton turbine: PIV measurements and CFD simulations with snapshot approach. *Chemical Engineering Research and Design*, 79(1), 3-12.

Reid, K.J. (1965). A solution to the batch grinding equation. *Chem. Eng. Sci*., 20(11), 953-963.

Richardson, L. F. (1922). *Weather prediction by numerical process*. London: Cambridge University Press.

Rittinger, R.P. (1867). Lehrbuch der aufbereitungskunde. Berlin, Germany: Verlag Ernst and Korn.

Roux, J.C., Franc, N., Duffy, F.F., Fabry, B., (2001). Shear factor: A new way to characterize fiber suspension shear. *TAPPI Journal*, 84(8), 1-18.

Rushton J.H. & Costich E.W. (1950). Power characteristics of mixing impellers Part II. *Chem. Eng. Prog.*, 46(9), 467-476.

Ruszkowski, S. (1994). A rational method for measuring blending performance and comparison of different impeller types. In *Proceeding of the 8th European Mixing Conference* (pp. 283-291). Rugby, U.K.: Institute of Chemical Engineers.

Sano, Y., & Usui, H. (1987). Effects of paddle dimensions and baffle conditions on the interrelations among discharge flow rate, mixing power and mixing time in mixing vessels. Journal of Chemical Engineering Japan, 20(4), 399–404.

Savolainen A., Jussila T., Nikula S. (1991). Defibering and specific energy consumption in bale pulpers. *TAPPI Journal*. 74(11), 147-153.

Schafer, M., Yianneskis, M., Wachter, P., Durst, F. (1998). Trailing vortices around a 45 pitched-blade impeller. *AIChEJ*, 44(6), 1233–1246.

Schafer, M., Yu, J., Genenger, B., Durst, F. (2000). Turbulence generation by different types of impeller. In H.E.A. van den Akker & J.J. Derksen (Ed.) *Proceedings of the 10th European. Conference on Mixing*. Delft, Amsterdam; Elsevier Science B.V.

Schoenert, K. (1972). Role of fracture physics in understanding comminution phenomena. *Transactions of Society of Mining Engineers-AIME*, 252, 21–26.

Seth, R.J., Page, D.H. (1983). The stress–strain curve of paper. In J. Brander (Ed.) *The Role of Fundamental Research in Paper Making, vol. 1*(pp. 421–452). New York: Mechanical Engineering Publications Ltd.

Sharp, K.V. & Adrian, R.J. (2001). PIV study of small-scale flow structure around a Rushton turbine. *A.I.Ch.E. J.*, 47(4), 766–778.

Shekhar, C., Nishino, K., Yamane, Y., Huang, J. (2012). Stereo-PIV measurement of turbulence characteristics in a flow mixer. *Journal of Visualization*, 15(4), 293-308.

Smagorinsky, J. (1963). General circulation experiments with the primitive equations. *Month. Weath. Rev*., 93, 99-165.

Smith R.W. & Lee K.H. (1968). A comparison of data from bond type simulated closed circuit and batch grindability tests. *Transactions of SME/AIME*, 241, 91-99.

Soos M., Kaufmann R., Winteler R., Kroupa M., Luthi B. (2013). Determination of maximum turbulent energy dissipation rate generated by a Rushton impeller through large eddy simulation. *AIChE Journal*, 59(10), 3642-3658.

Soszynski, R.M. & Kerekes, R.J. (1988). Elastic interlocking of nylon fibres suspended in liquid, Part 1, nature of cohesion among fibres. *Nordic Pulp Paper Research Journal*, 3(4), 172–179.

Stoots, C.M. & Calabrese, R.V. (1995). Mean velocity field relative to a Rushton turbine blade. *AIChE Journal* 41(1), 1–11.

Swerin, A., Powell, R.L., Odberg, L. (1992). Linear and non-linear dynamic viscoelasticity of pulp fibre suspensions. *Nordic Pulp Paper Research Journal*, 7(3), 126–143.

TAPPI 456 om-10 standard for wet tensile testing of paper. (1983). *The Technical Association of the Pulp and Paper Industry (TAPPI).* Retrieved December 2015 from http://www.tappi.org/content/pdf/standards/subject_index_tms.pdf

TAPPI T-270 pm-88 standard for flake content measurement. (1988). *The Technical Association of the Pulp and Paper Industry (TAPPI).* Retrieved December 2015 from http://www.tappi.org/content/pdf/standards/subject_index_tms.pdf

Thalen, N. & Wahren, D. (1964). Shear modulus and ultimate shear strength of some paper pulp fiber networks. *Svensk Papperstidn*. 67(7), 259–264.

United States Environmental Protection Agency. (2015). *Advancing Sustainable Materials Management: 2013 Fact Sheet*. Washington DC: United States Environmental Protection Agency Solid Waste and Emergency Response (5306P).

U.S. Energy Information Administration. (2015). *Electric Power Monthly, October 2015*. Washington DC: United States Department of Energy.

Van't Riet, K. & Smith, J.M. (1975). The trailing vortex system produced by Rushton turbine agitators. *Chemical Engineering Science*, 30(9), 1093–1105.

Venneker, B. C. H. & van den Akker, H. E. A. (1997). CFD calculations of the turbulent flow of shear-thinning fluids in agitated tanks. In J. Bertrand, J. Villermaux (Eds.*) Proceedings of the 9th European Conference on Mixing* (pp. 179-186). Paris, France: Groupe Français de Génie des Procédés.

Vilaseca, F., Puig, J., Angels Pelach, M., El Mansouri N.E., Alcala, M, Roux, J.C., Mutje, P. (2011). Study and modeling of the disintegration kinetics of coated paper. *Bioresources*, 6(2), 1659-1669.

Vokes, R.F. (1963). Paper machinery. *U.S. Pat.* 3,073,535.

Voncken, R. M., Holmes, D. B., Den Hartog, H.W. (1964). Fluid flow in turbine stirred baffled tanks, Part 1, circulation time. *Chem. Engng Sci*. 19(3), 209-213.

Walker, W.H., Lewis, W.K., McAdams, W.H., Gilliland, E.R. (1937). *Principles of Chemical Engineering*. New York: McGraw-Hill.

Wang L.J., Yang R., Zhang H., Wang L. (2004). Study on repulping wet strength paper. *China Pulp and Paper*. 23(4), 64 – 65.

Weetman R.J. & Oldshue J.Y. (1988). Comparison of axial Flow impellers. In Proceedings of the 6th European Conference on Mixing. Pavia Italy.

Weetman, R.J. & Coyle C.K. (1989). The use of fluidfoil impellers in mixing applications. *AIChE Annual Meeting*. Nov. 5-10, San Francisco USA.

White, F.M. (2003). *Fluid Mechanics 5th Edition*. New York: McGraw-Hill.

Wikstrom, T. & Rasmuson, A. (1998). Yield-stress of pulp suspensions: The influence of fibre properties and processing conditions. *Nordic Pulp and Paper Resource Journal*, 13(3), 243–250.

Wu H. & Patterson G. (1989). Laser-Doppler measurements of turbulent flow parameters in a stirred mixer. *Chem Eng Sci*., 44(10), 2207-2221.

Yang L., Cheng P., Fan P., Mao Z. (2013). Micromixing of solid-liquid systems in a stirred tank with double impellers. *Chem Eng Technol*. 36(3), 443-449.

Yeoh, S. L., Papadakis, G., Yianneskis, M. (2005). Determination of mixing time and degree of homogeneity in stirred vessels with large eddy simulation. *Chem. Eng. Sci*., 60(8-9), 2293–2302.

Yianneskis, M., Popiolek, Z., Whitelaw, J.H. (1987). An experimental study of the steady and unsteady flow characteristics of stirred reactors. *Journal of Fluid Mechanics*, 175, 537–555.

Yianneskis, M. & Whitelaw, J.H. (1993). On the structure of the trailing vortices around Rushton turbine-blades. *Transactions of the Institution of Chemical Engineers*, *Part A*, 71, 543–550.

Zadghaffari, Moghaddas, R., J. S., Revstedt, J. (2010). Large-eddy simulation of turbulent flow in a stirred tank driven by a Rushton turbine. *Comp. Fluids*, 39(7), 1183–1190.

Zhou, G. & Kresta, S.M. (1996). Impact of tank geometry on the maximum turbulence energy dissipation rate of impellers. *AIChE Journal*, 42(9), 2476–2490.

Zhou, G. & Kresta, S. M. (1998). Evolution of drop size distribution in liquid-liquid dispersions for various impellers. *Chem. Eng. Sci.*, 53 (11), 2063–2079.

Zwietering T. N. (1958). Suspending solid particles in liquid by agitators. *Chemical Engineering Science*, 8(3-4), 244-253.

Appendix

Appendix A.

Appendix A describes the laboratory repulper designed and built for this thesis work in more detail.

A.1 The Laboratory Repulper and Test Rotors in More Detail

To study repulping, a repulper is required. All of the studies presented in this thesis center around the use of a laboratory scale low consistency repulper designed and built specifically for this study. This machine has a capacity of $0.25m^3$ and is a faithful replica in scale of full sized repulpers. The laboratory repulper is constructed of a combination of 304 and 316 stainless steel. Three test rotors were constructed in scale from billet aluminum for the studies in this thesis. Each rotor represents a state of the art offering from a different manufacturer with each being used in mills all over the world. The laboratory repulper is shown in Figure A.1.

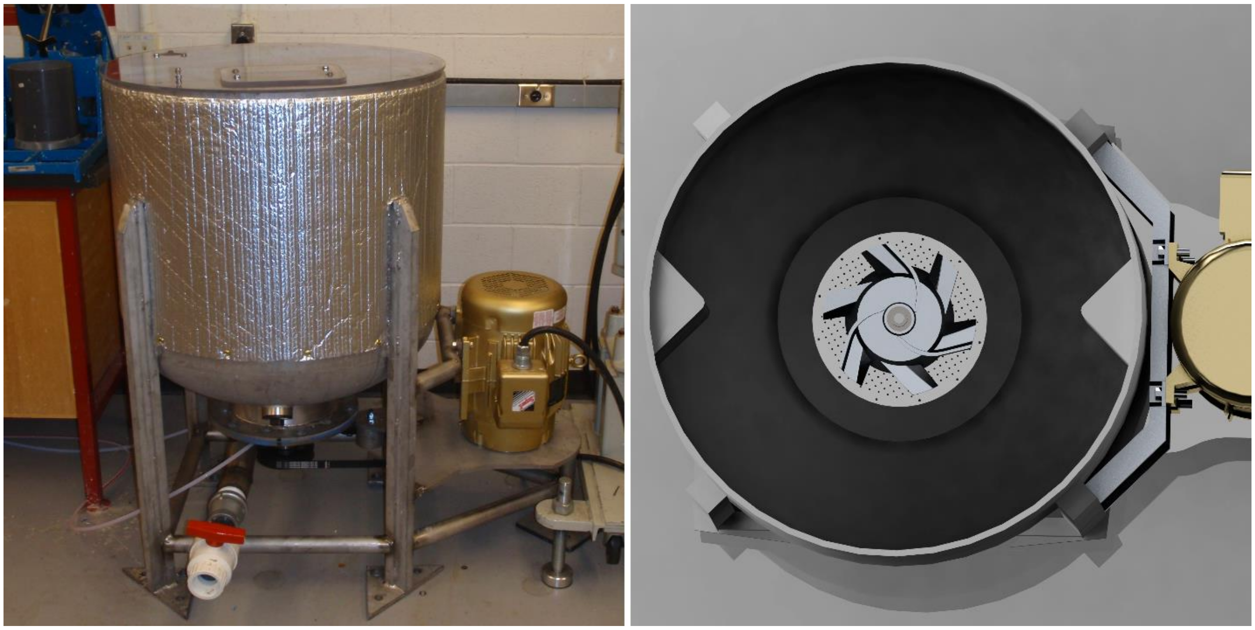

Figure A.1: The laboratory repulper. This machine was designed and built specifically for this study.

The three test rotor are shown in Figure A.2. All three rotors have a diameter of 233.7mm. The height of each rotor is different leading to different swept volumes for each rotor. The swept volumes for rotors A, B, and C are $0.00171m^3$, $0.00112m^3$ and $0.00109m^3$ respectively (rotor swept volume is important in this thesis).

Figure A.2: The test rotors used for this study. Each rotor represents a state of the art offering from a different rotor manufacturer. All three rotors are shown from above and all three spin counterclockwise. From left to right: Rotor A, Rotor B, and Rotor C.

The main design goal concerning the laboratory repulper was to ensure that any experimental findings obtained using the laboratory repulper would also be relevant in full sized industrial repulpers. The ability to scale results from the laboratory repulper to industrial repulpers is of the utmost importance. This requirement for relevant scaling would dictate the general arrangement/concept of the machine. Designing in durability, usability, and features to make the laboratory repulper a good piece of lab equipment were added after the general arrangement dictated by scaling requirements was determined.

Recall form the “Introduction” section that the rotor-to-vat diameter ratio impacts both the time and energy required for repulping (Bennington 1998b; Savolainen et al. 1991). Industrial LC repulpers use rotor-to-vat diameter ratios of about 0.3. So, in order to have scalability between the laboratory repulper and industrial repulpers, this rotor-to-vat diameter ratio is also used by the laboratory repulper.

Further on, this thesis presents an accurate method for modeling repulping performance and for scaling repulping performance between repulpers of different sizes having different operating conditions. However, this knowledge was not known a priori so the design for scaling made allowance for two common scaling methods used when scaling - the very similar to repulpers - stirred mixers.

During the design phase for this machine, it was thought that in order for results from the laboratory repulper to scale to full size industrial repulpers, the laboratory repulper should match the industrial repulpers in terms of both rotor tip-speed and intensity – i.e. power/vat volume. An installed power of 7.5hp and a variable frequency drive allow this to be possible. The installed power was chosen using constant power number scaling from an industrial repulper as, in water at least, a LC repulper rotor would operate at Reynolds numbers of $Re > 10^6$. The laboratory repulper is compared with industrial repulpers in Table A.1.

Table A. 1: The specifications of the laboratory repulper are compared with industrial repulpers.

	Laboratory Repulper	$15m^3$ Industrial Repulper	$85m^3$ Industrial Repulper
Installed Power	7.5hp	150hp	500hp
Vat Volume	$0.25m^3$	$15m^3$	$85m^3$
Rotor Diameter	233.7mm	900mm	1575mm
Rotor Diameter/Vat Diameter Ratio	0.31	0.30	0.30
Rotor Tip Speed	Up to 16.5m/s	15-20m/s	15-20m/s
Rotor Power/Vat Volume	7-20 kW/m^3	7.5 kW/m^3	4.4 kW/m^3

The laboratory repulper can operate in both batch and continuous modes. An extraction plate having a 3.175mm diameter hole-pattern works in conjunction with a plenum underneath the extraction plate to allow for the continuous operation mode.

Notice from Figure A.1 that the laboratory repulper does not use standard baffling. Instead, two large, triangular baffles are used in order to maintain vat turnover with pulp suspensions.

In order for the laboratory repulper to be a good piece of lab equipment, the problem posed by shaft sealing needed to be addressed. Most pieces of industrial equipment in which a rotating shaft is inserted into a process fluid must use a shaft seal of some sort. Two common seal types are rope seals and mechanical seals. The laboratory repulper uses mechanical seals as rope seals consume much more shaft power from friction against the shaft which they are sealing than do mechanical seals. However, both types of seals still require cooling water for reliable operation. In a full size industrial repulper, this seal cooling water is often leaked directly into the process fluid.

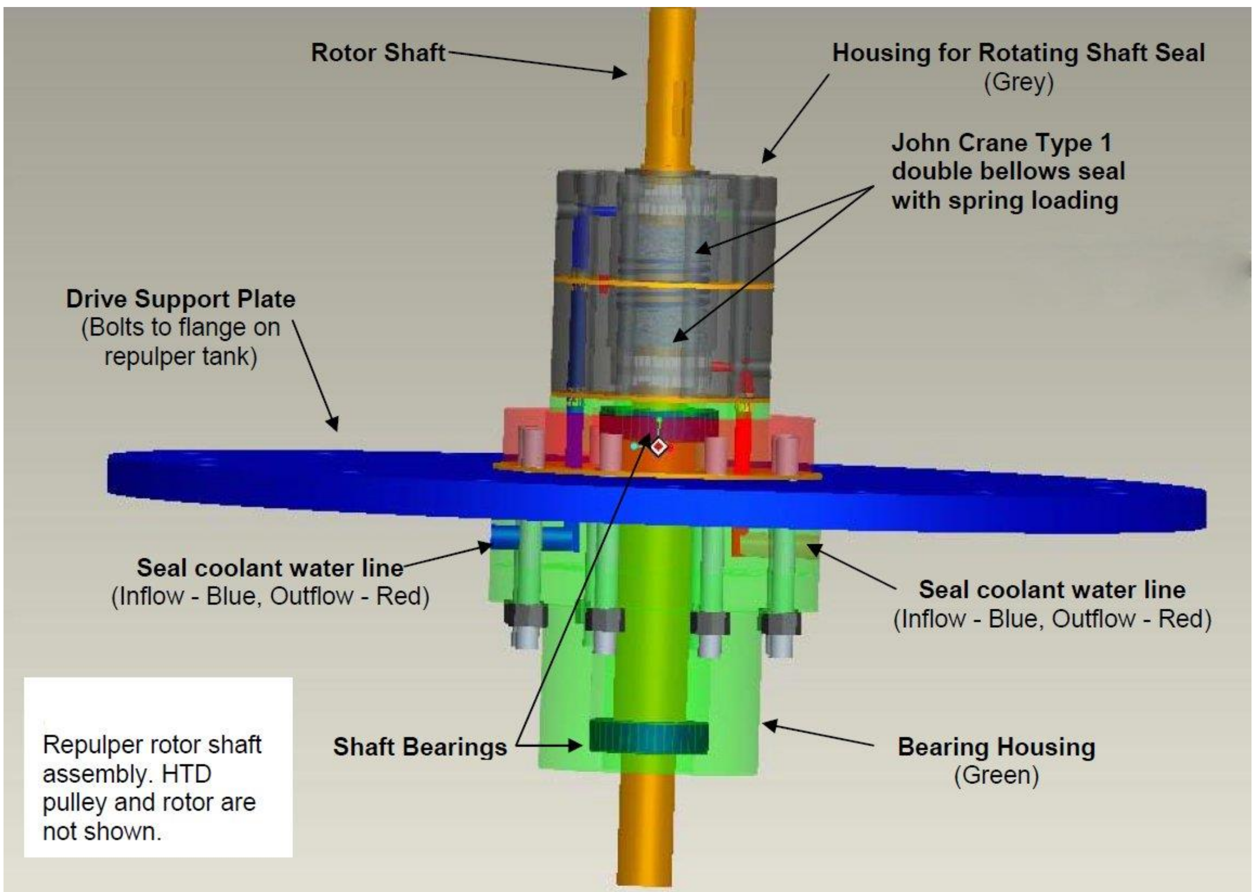

Figure A.3: Back-to-back leak-less double-seal arrangement used by the laboratory repulper.

This would be problematic for testing in the laboratory repulper as this seal water would dramatically alter the pulp suspension consistency during the course of a batch repulping run. For this reason, the laboratory repulper uses a back-to-back double mechanical seal arrangement which is commonly used in petrochemical applications where seal cooling water cannot mix with the process fluids. This double seal arrangement effectively places a pair of seals in a closed cooling loop so that no cooling water can enter the laboratory repulper. The double seal arrangement and rotor driveshaft arrangement are shown in Figure A.3.

Another important criteria in terms of the laboratory repulper being a good piece of lab equipment is accurate rotor power measurement. This is needed in order to measure the energy use in repulping. A 7.5hp variable frequency drive is combined with a 575V, 1800 rpm, TEFC 3-phase AC motor having a C-face mounting arrangement. The dynamometer measured efficiency for this motor is between 90% and 91.7% from half load to full load which, given the chosen gearing for the repulper HTD synchronous drive, correlates to a repulper rotor design tip speed envelope of 11 – 16.5m/s. This is important for reliable power measurement and stable operation as the efficiency of AC motors drops drastically below 50% loading. The variable frequency drive is housed in a NEMA approved enclosure and has a CSA approved panel. Power monitoring is handled through a PC connectable integral power monitoring system within the VFD drive. Rotor power and rotor speed are recorded directly from the variable frequency drive to a PC. The recorded power is corrected for motor dynamometer efficiency and driveline losses. The major contributor to driveline loss is the double mechanical seal arrangement. Through measurement of the temperature and flow rate of the seal cooling water, the total power loss from the mechanical seals equates to about 3% of the rotor shaft power.

The laboratory repulper was also designed to be reliable and to require very little maintenance. This is not only important from the standpoint of being a reliable piece of laboratory equipment, but when not performing repulping experiments, the laboratory repulper performs pilot plant repulping. To this end, the rotor shaft has been designed for infinite fatigue life with a factor of safety of 5 based on the Goodman criterion (Goodman 1899). The rotor shaft/seal/bearing housing incorporates internally drilled cooling water passages to give additional reliability over external piping. Stainless grommets bridge cooling passages between adjoining housing sections take pressure off of the gaskets to reduce the likelihood of leaking. The use of grommets in this way is commonly used to join high pressure oil passages between cylinder blocks and cylinder heads to protect head gaskets in automotive racing engines. The laboratory repulper is designed for 10,000 hours of operation between bearing, seal and drive belt replacements.

A.2 Laboratory Repulper Dimensions and Drawings

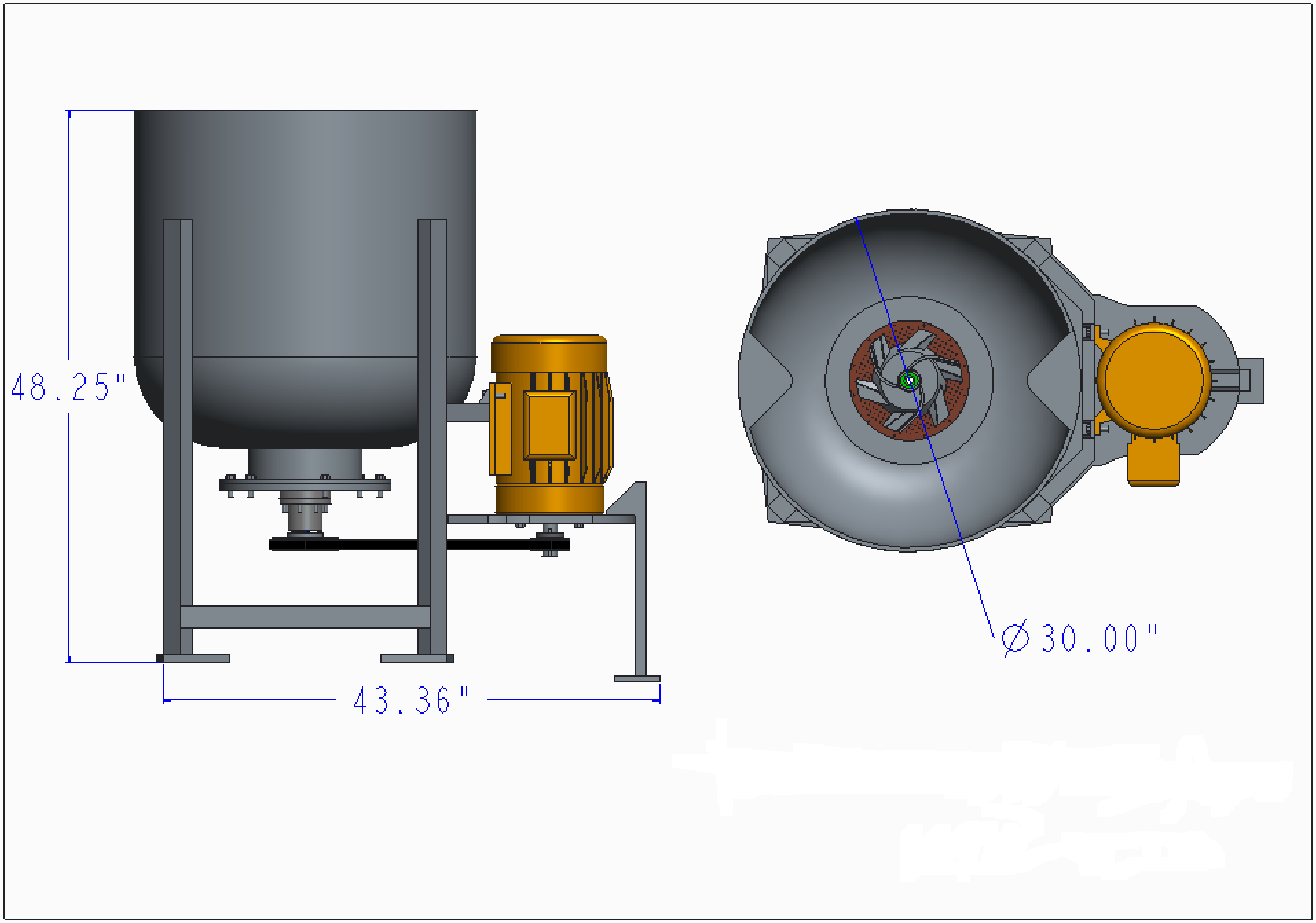

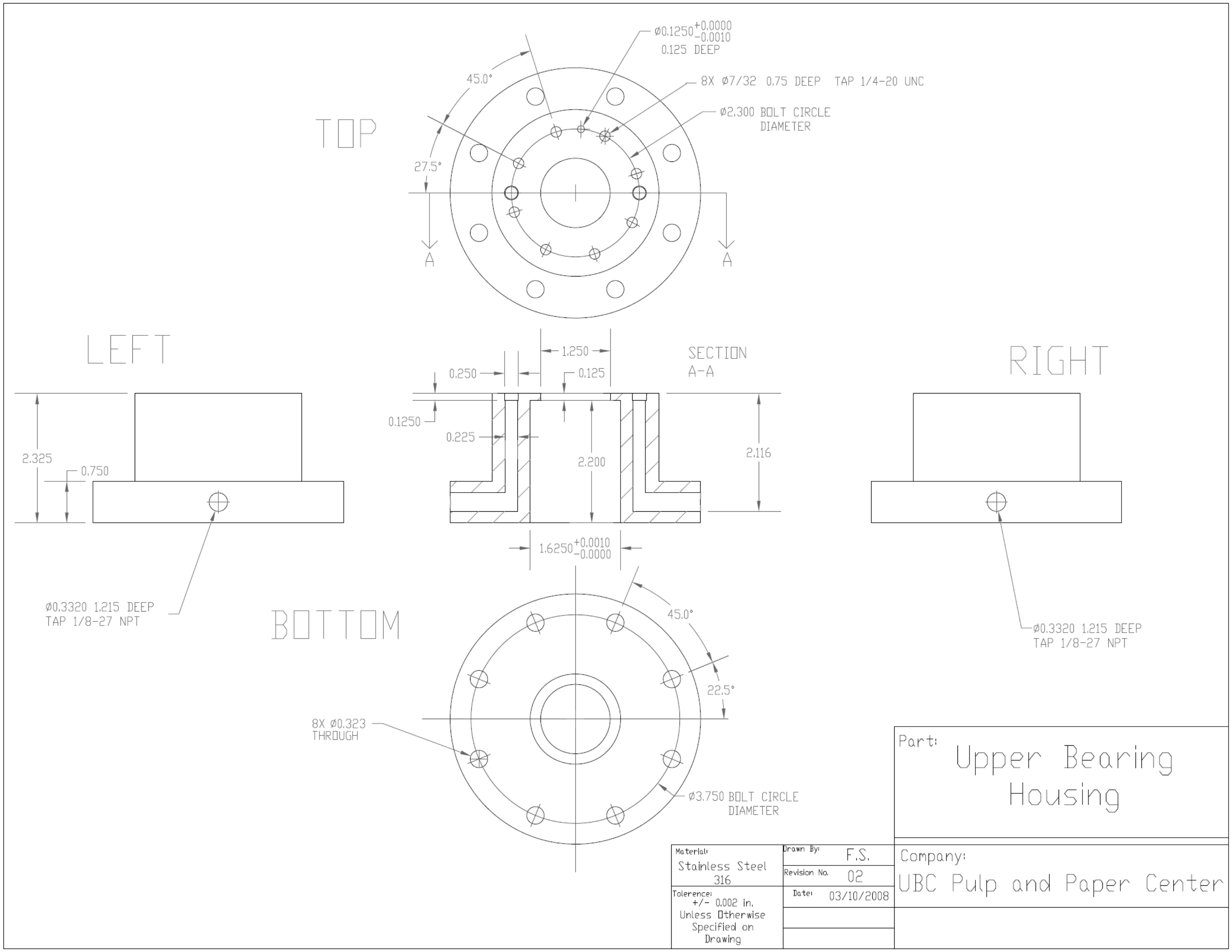
ø0.1250 +0.0000 −0.0010
0.125 DEEP
8X ø7/32 0.75 DEEP TAP 1/4-20 UNC
ø2.300 BOLT CIRCLE DIAMETER
45.0°
27.5°
TOP
A
A
LEFT
SECTION A-A
RIGHT
1.250
0.250
0.125
0.1250
0.225
2.200
2.116
2.325
0.750
1.6250 +0.0010 −0.0000
ø0.3320 1.215 DEEP TAP 1/8-27 NPT
ø0.3320 1.215 DEEP TAP 1/8-27 NPT
BOTTOM
45.0°
22.5°
8X ø0.323 THROUGH
ø3.750 BOLT CIRCLE DIAMETER
Part: Upper Bearing Housing
Material: Stainless Steel 316
Drawn By: F.S.
Revision No. 02
Date: 03/10/2008
Tolerence: +/- 0.002 in. Unless Otherwise Specified on Drawing
Company: UBC Pulp and Paper Center

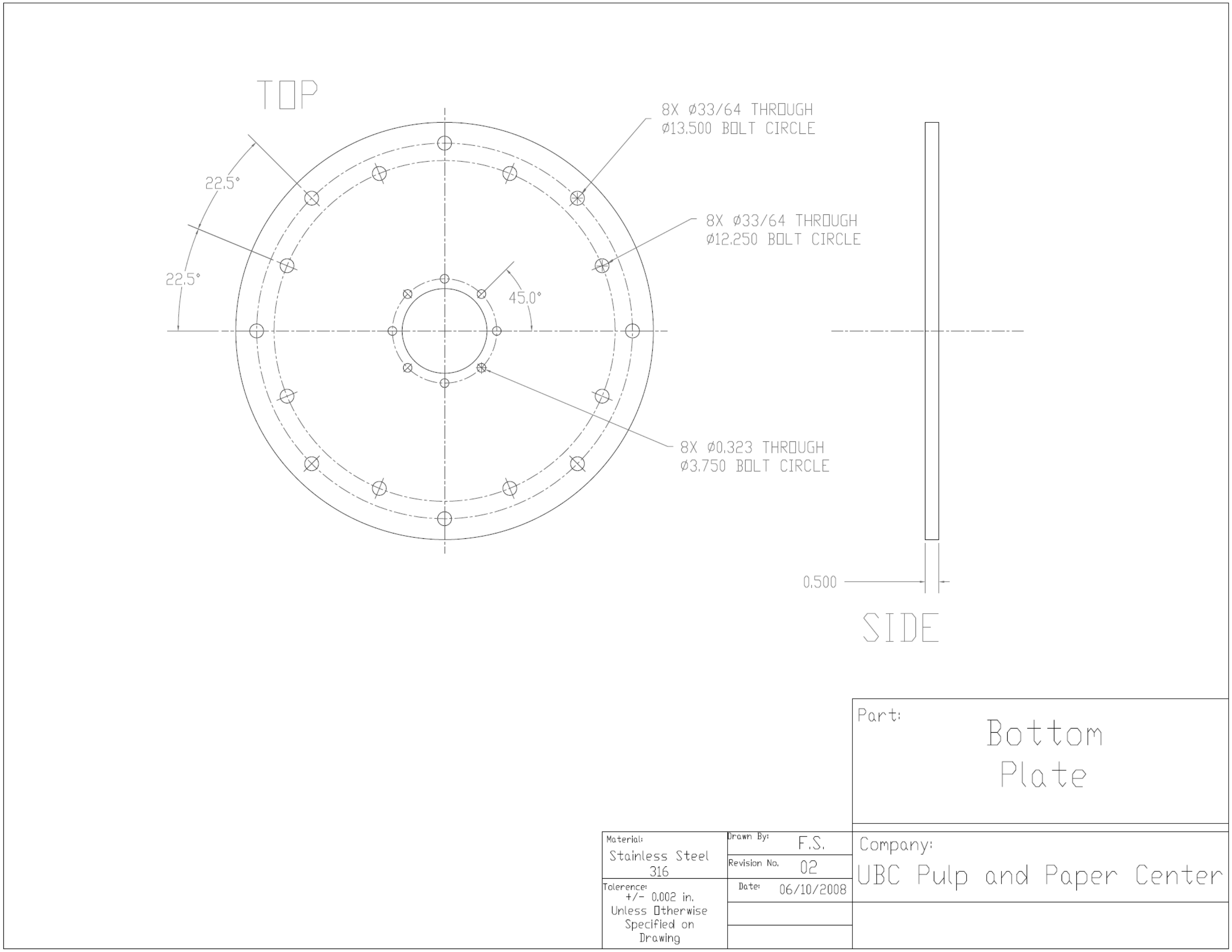
TOP
8X ø33/64 THROUGH
ø13.500 BOLT CIRCLE
8X ø33/64 THROUGH
ø12.250 BOLT CIRCLE
8X ø0.323 THROUGH
ø3.750 BOLT CIRCLE
22.5°
22.5°
45.0°
0.500
SIDE
Part:
Bottom
Plate
Material:
Stainless Steel
316
Drawn By:
F.S.
Revision No.
02
Tolerence:
+/- 0.002 in.
Unless Otherwise
Specified on
Drawing
Date:
06/10/2008
Company:
UBC Pulp and Paper Center

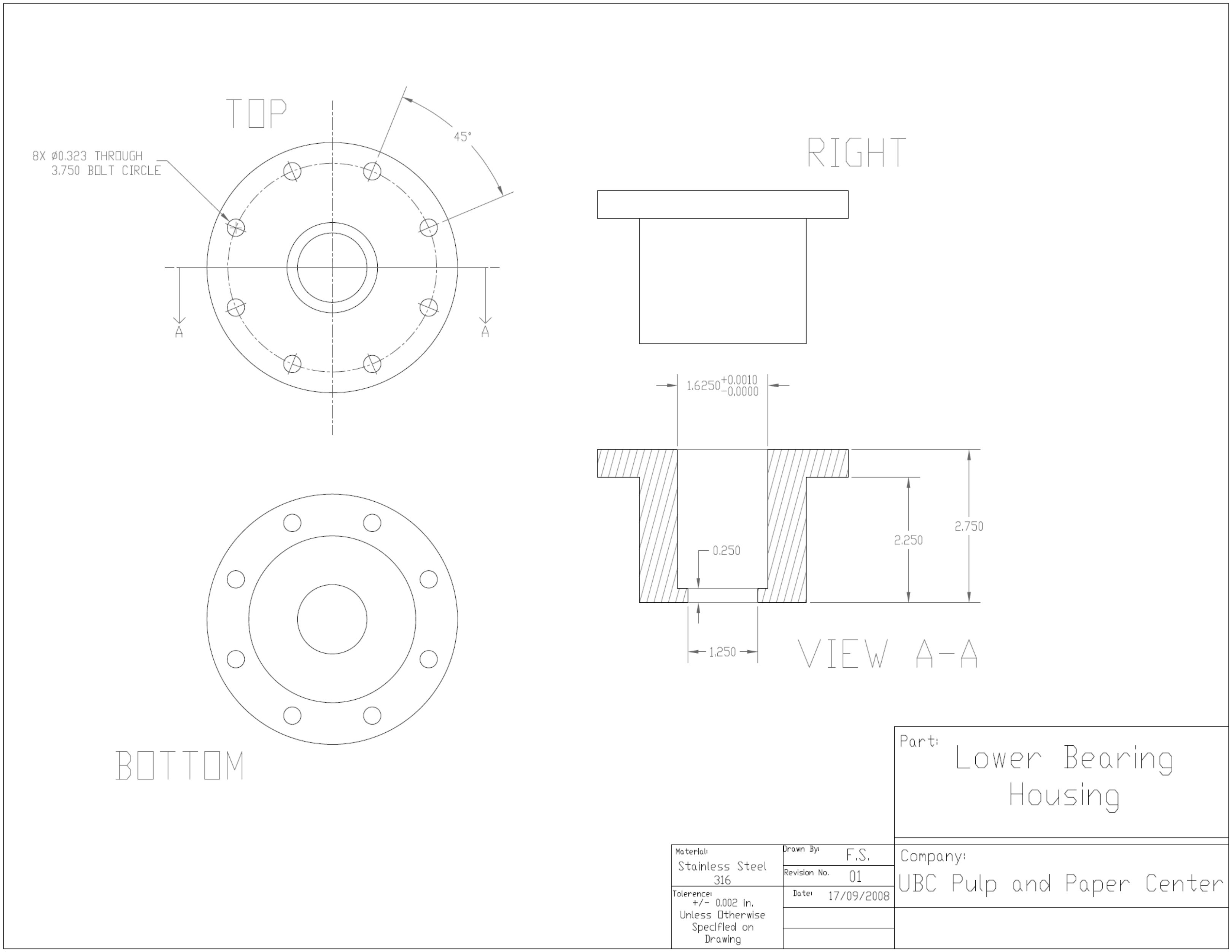
TOP
8X ⌀0.323 THROUGH
3.750 BOLT CIRCLE
45°
A
A
RIGHT
1.6250 +0.0010 −0.0000
0.250
2.250
2.750
1.250
VIEW A-A
BOTTOM
Part:
Lower Bearing Housing
Material:
Stainless Steel 316
Tolerence:
+/- 0.002 in.
Unless Otherwise Specified on Drawing
Drawn By:
F.S.
Revision No.
01
Date:
17/09/2008
Company:
UBC Pulp and Paper Center

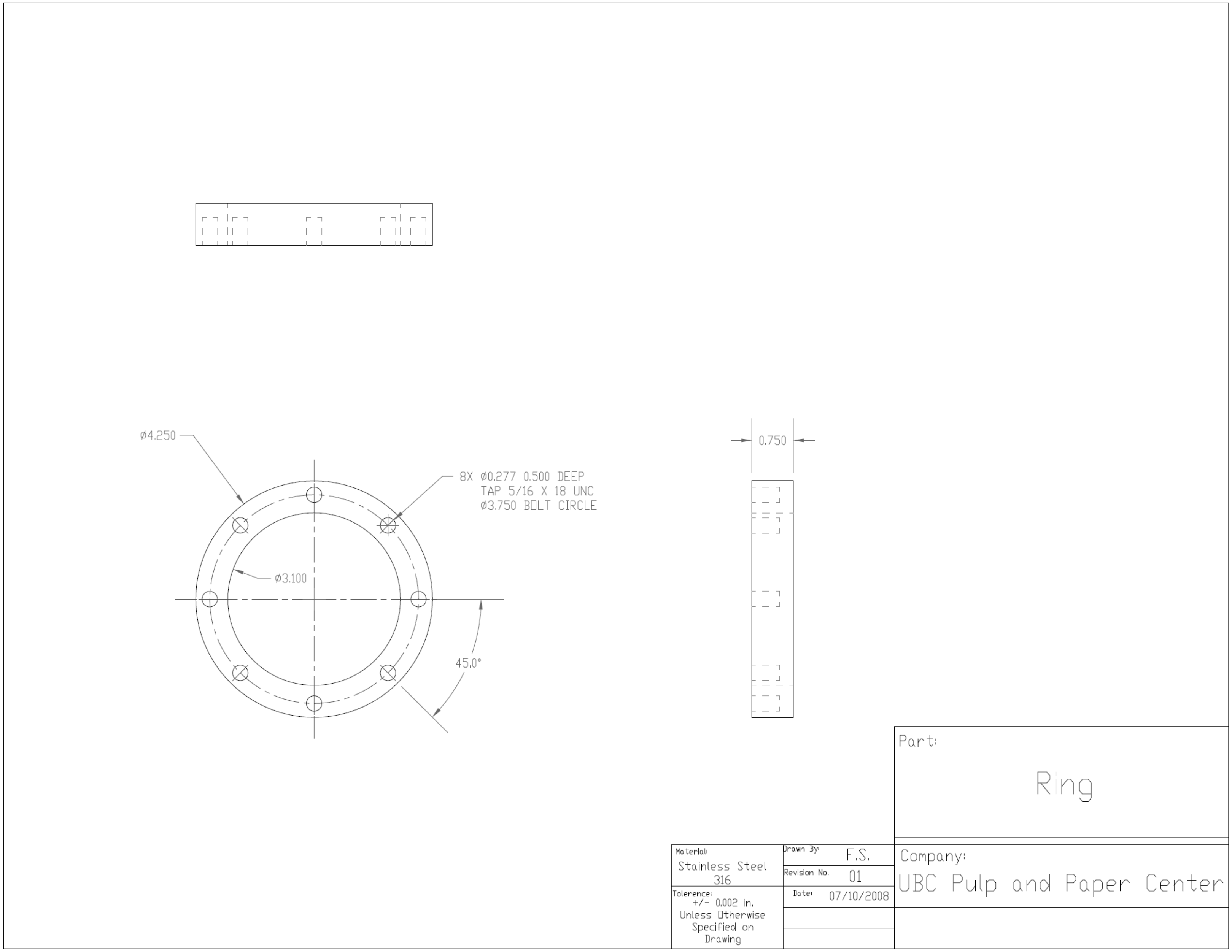

Ø4.250
8X Ø0.277 0.500 DEEP
TAP 5/16 X 18 UNC
Ø3.750 BOLT CIRCLE
Ø3.100
45.0°
0.750
Part:
Ring
Material:
Stainless Steel
316
Drawn By:
F.S.
Revision No.
01
Date:
07/10/2008
Tolerence:
+/- 0.002 in.
Unless Otherwise
Specified on
Drawing
Company:
UBC Pulp and Paper Center

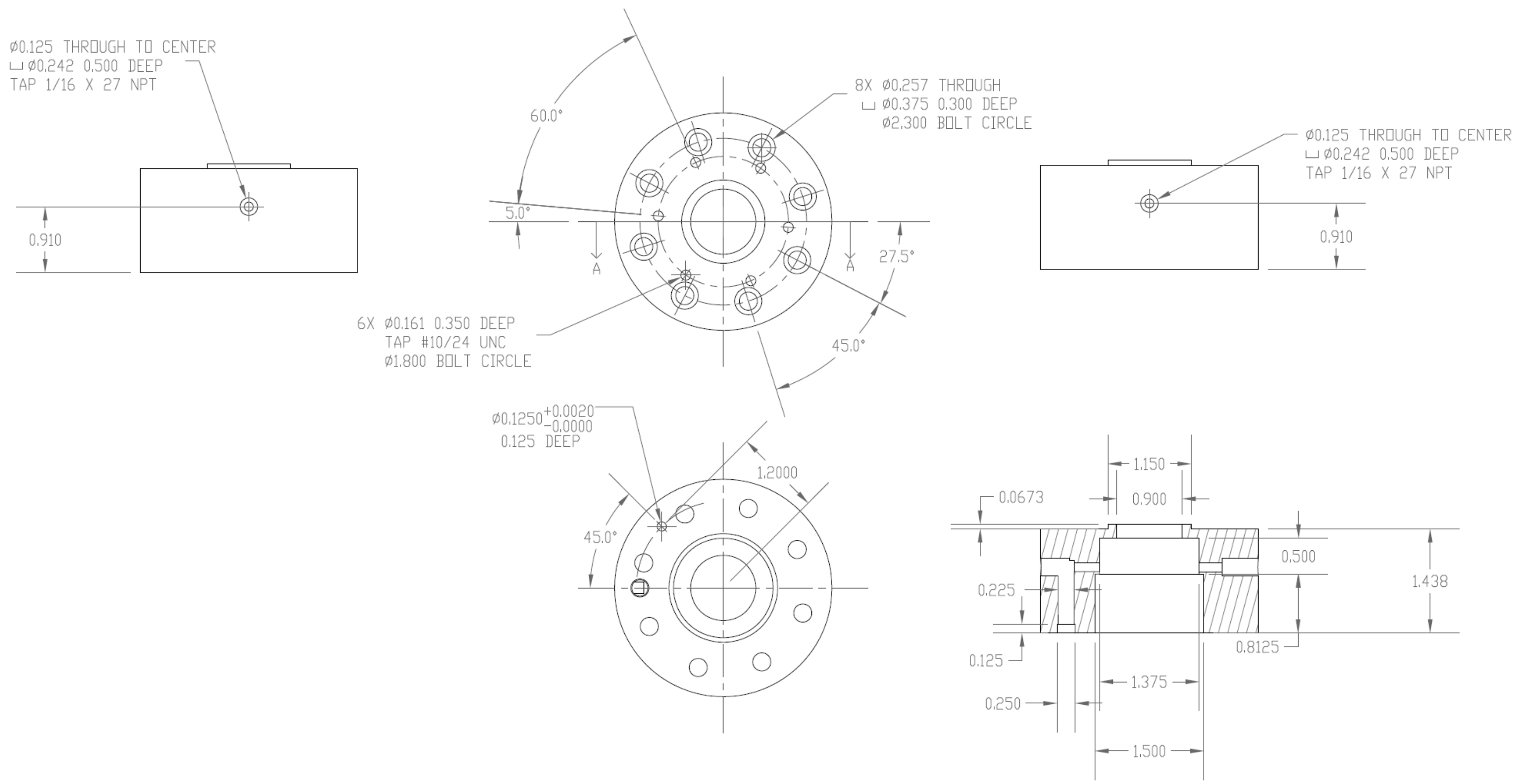

Part: Upper Seal Housing

Material: Stainless Steel 316	Drawn By: F.S.	Company: UBC Pulp and Paper Center
	Revision No. 01	
Tolerence: +/- 0.002 in. Unless Otherwise Specified on Drawing	Date: 17/09/2008	

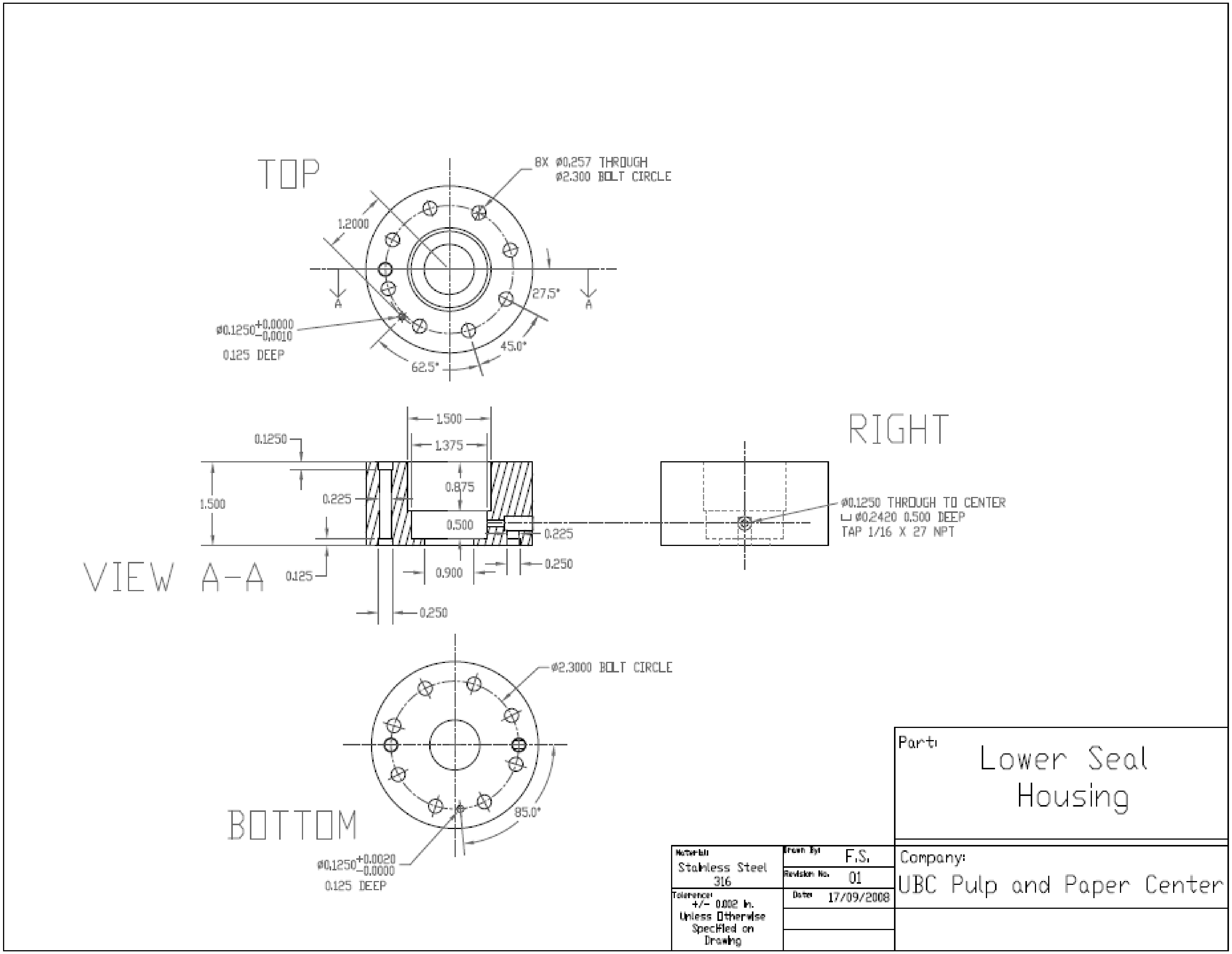
TOP
8X ø0.257 THROUGH
ø2.300 BOLT CIRCLE
1.2000
27.5°
A
A
ø0.1250 +0.0000 −0.0010
0.125 DEEP
45.0°
62.5°
1.500
1.375
0.1250
1.500
0.225
0.875
0.500
0.225
VIEW A-A
0.125
0.900
0.250
0.250
RIGHT
ø0.1250 THROUGH TO CENTER
⌴ ø0.2420 0.500 DEEP
TAP 1/16 X 27 NPT
ø2.3000 BOLT CIRCLE
BOTTOM
85.0°
ø0.1250 +0.0020 −0.0000
0.125 DEEP
Part:
Lower Seal Housing
Material:
Stainless Steel 316
Drawn By:
F.S.
Revision No.
01
Tolerance:
+/- 0.002 in.
Unless Otherwise Specified on Drawing
Date:
17/09/2008
Company:
UBC Pulp and Paper Center

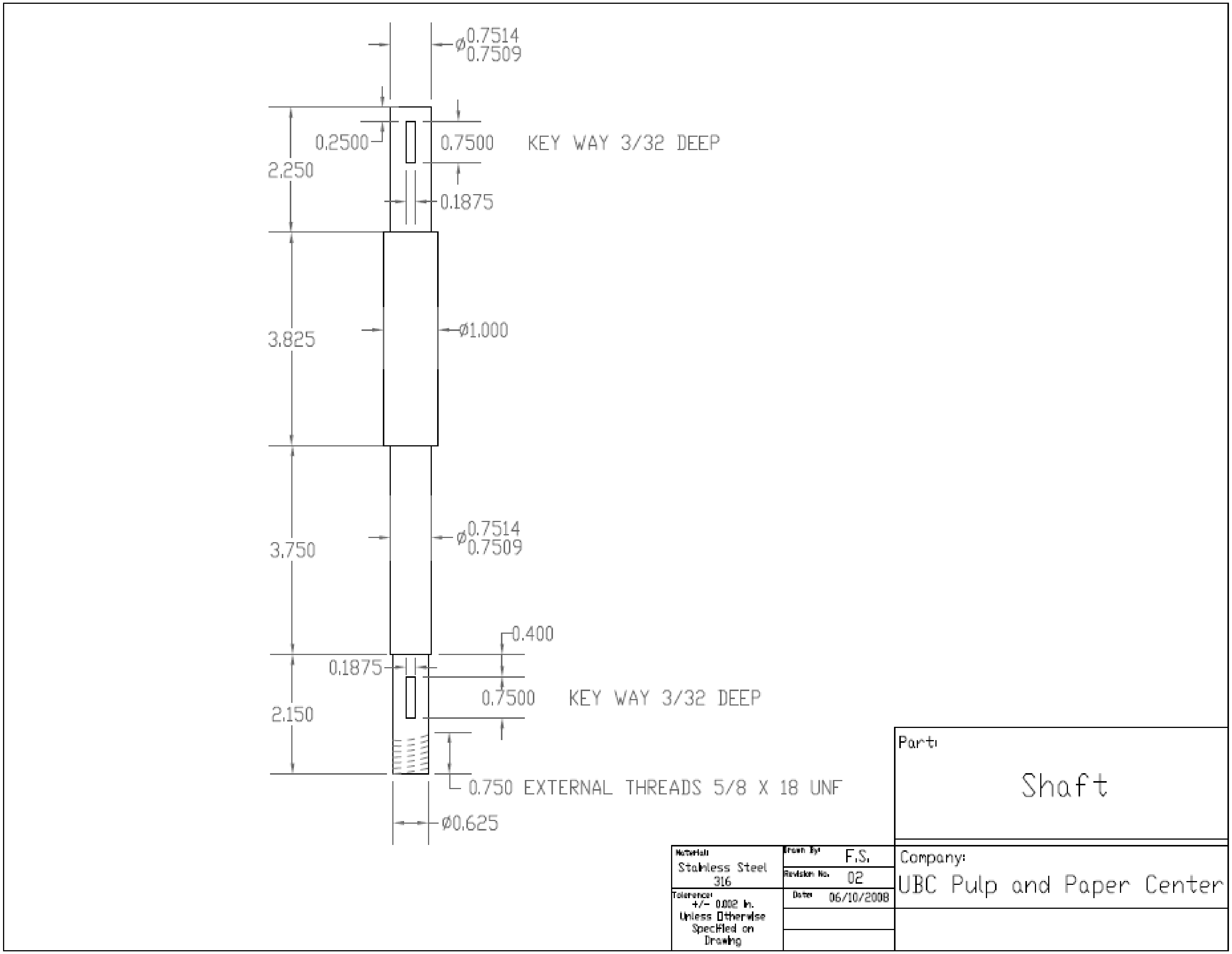

ø0.7514 0.7509
0.2500
0.7500
KEY WAY 3/32 DEEP
2.250
0.1875
3.825
ø1.000
3.750
ø0.7514 0.7509
0.400
0.1875
0.7500
KEY WAY 3/32 DEEP
2.150
0.750 EXTERNAL THREADS 5/8 X 18 UNF
ø0.625
Part:
Shaft
Material:
Stainless Steel 316
Drawn By:
F.S.
Revision No.
02
Tolerance:
+/- 0.002 in.
Unless Otherwise Specified on Drawing
Date:
06/10/2008
Company:
UBC Pulp and Paper Center

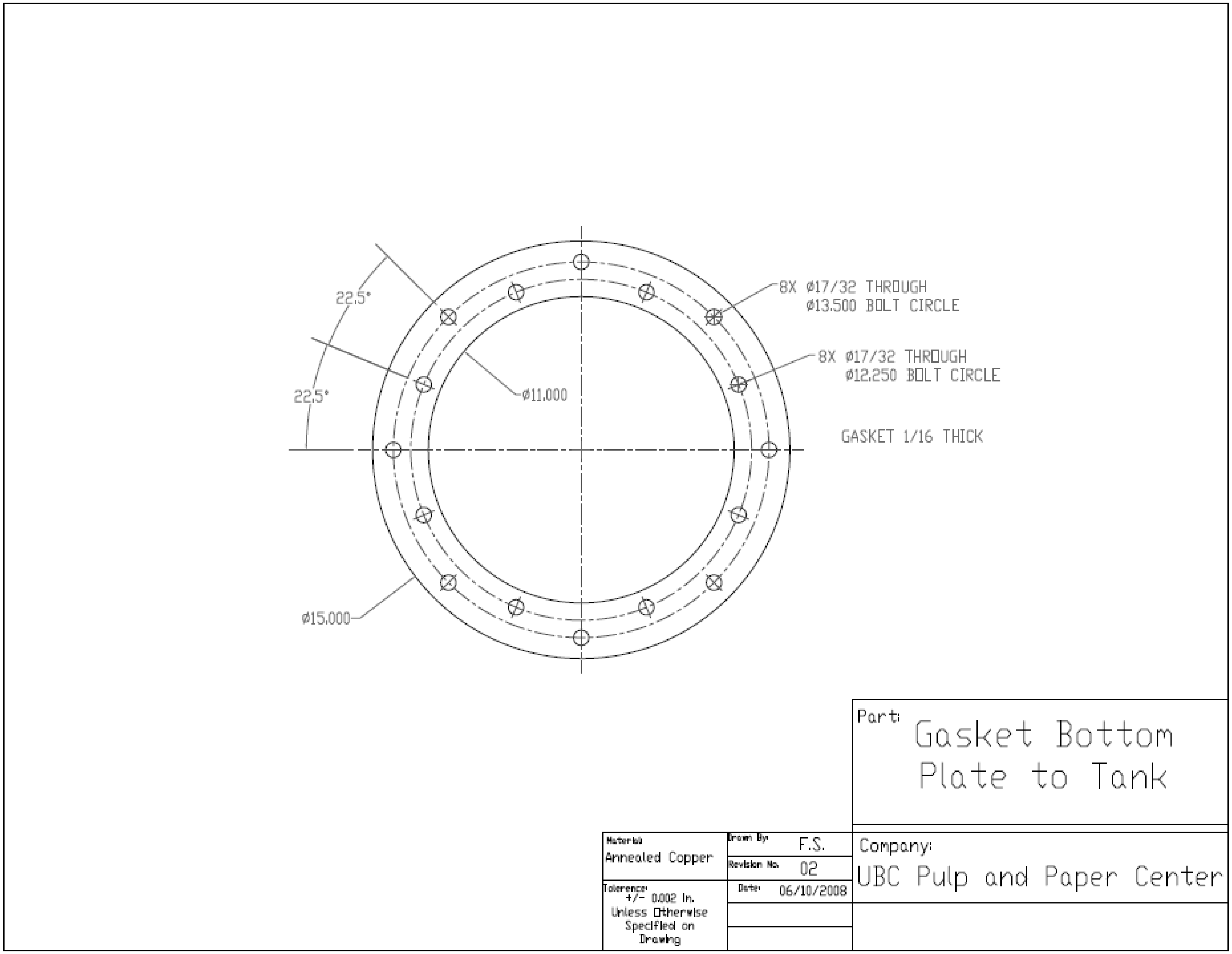
22.5°
22.5°
8X ø17/32 THROUGH
ø13.500 BOLT CIRCLE
8X ø17/32 THROUGH
ø12.250 BOLT CIRCLE
ø11.000
GASKET 1/16 THICK
ø15.000
Part:
Gasket Bottom
Plate to Tank
Material:
Annealed Copper
Drawn By:
F.S.
Revision No.
02
Tolerance:
+/- 0.002 In.
Unless Otherwise
Specified on
Drawing
Date:
06/10/2008
Company:
UBC Pulp and Paper Center

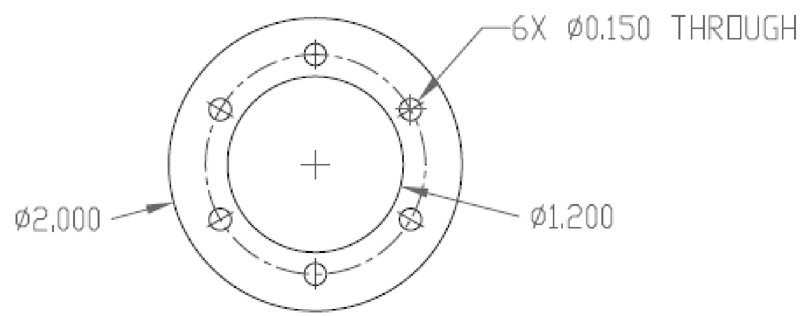

GASKET 1/16
THICK

Material: Annealed Copper	Drawn By: F.S.	Part: Gasket Upper Seal to Pulper Plate
	Revision No. 01	Company: UBC Pulp and Paper Center
Tolerence: +/- 0.002 In. Unless Otherwise Specified on Drawing	Date: 06/10/2008	

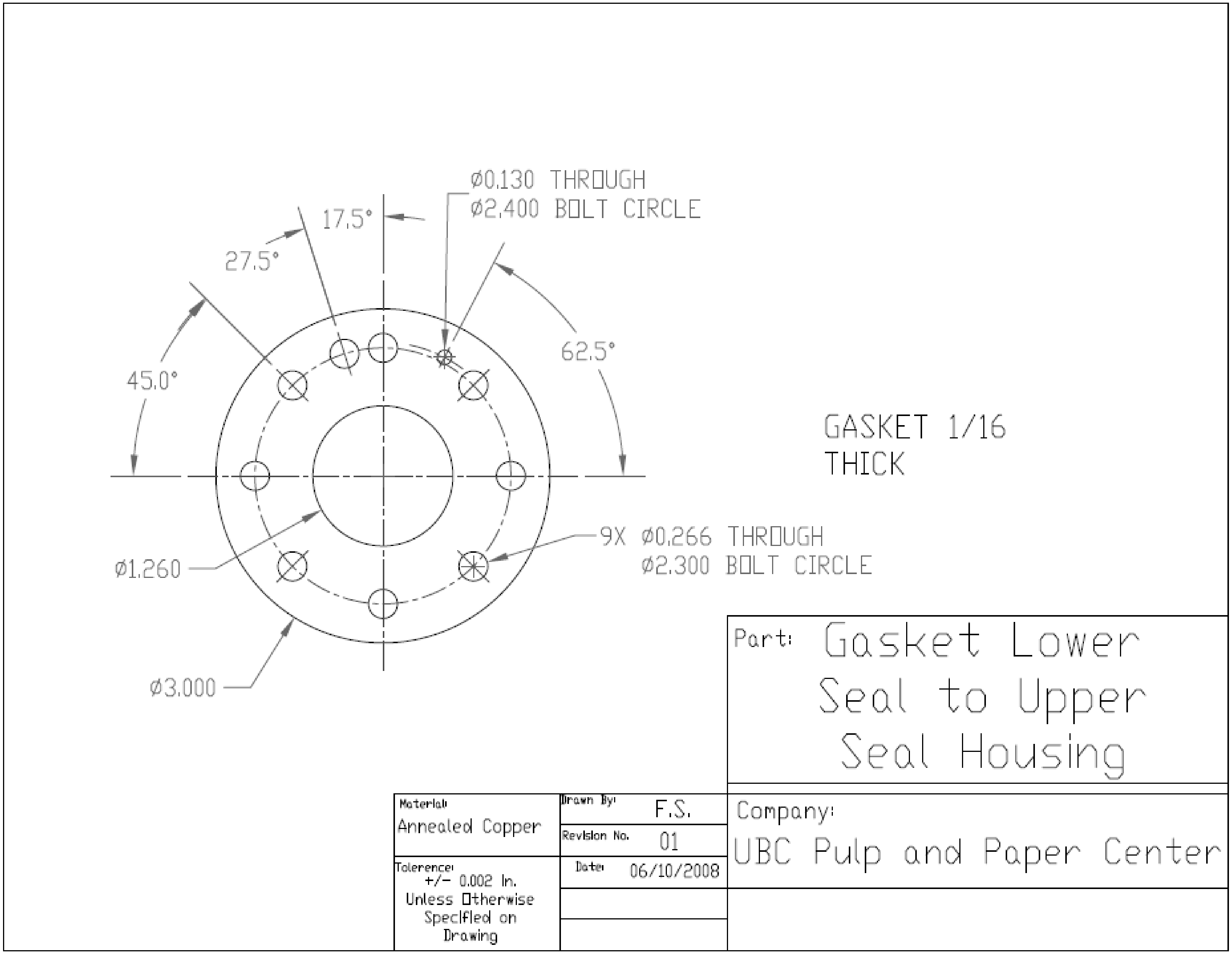
Ø0.130 THROUGH
Ø2.400 BOLT CIRCLE
17.5°
27.5°
45.0°
62.5°
GASKET 1/16
THICK
9X Ø0.266 THROUGH
Ø2.300 BOLT CIRCLE
Ø1.260
Ø3.000
Part: Gasket Lower Seal to Upper Seal Housing
Material: Annealed Copper
Drawn By: F.S.
Revision No. 01
Date: 06/10/2008
Tolerence: +/- 0.002 In. Unless Otherwise Specified on Drawing
Company: UBC Pulp and Paper Center

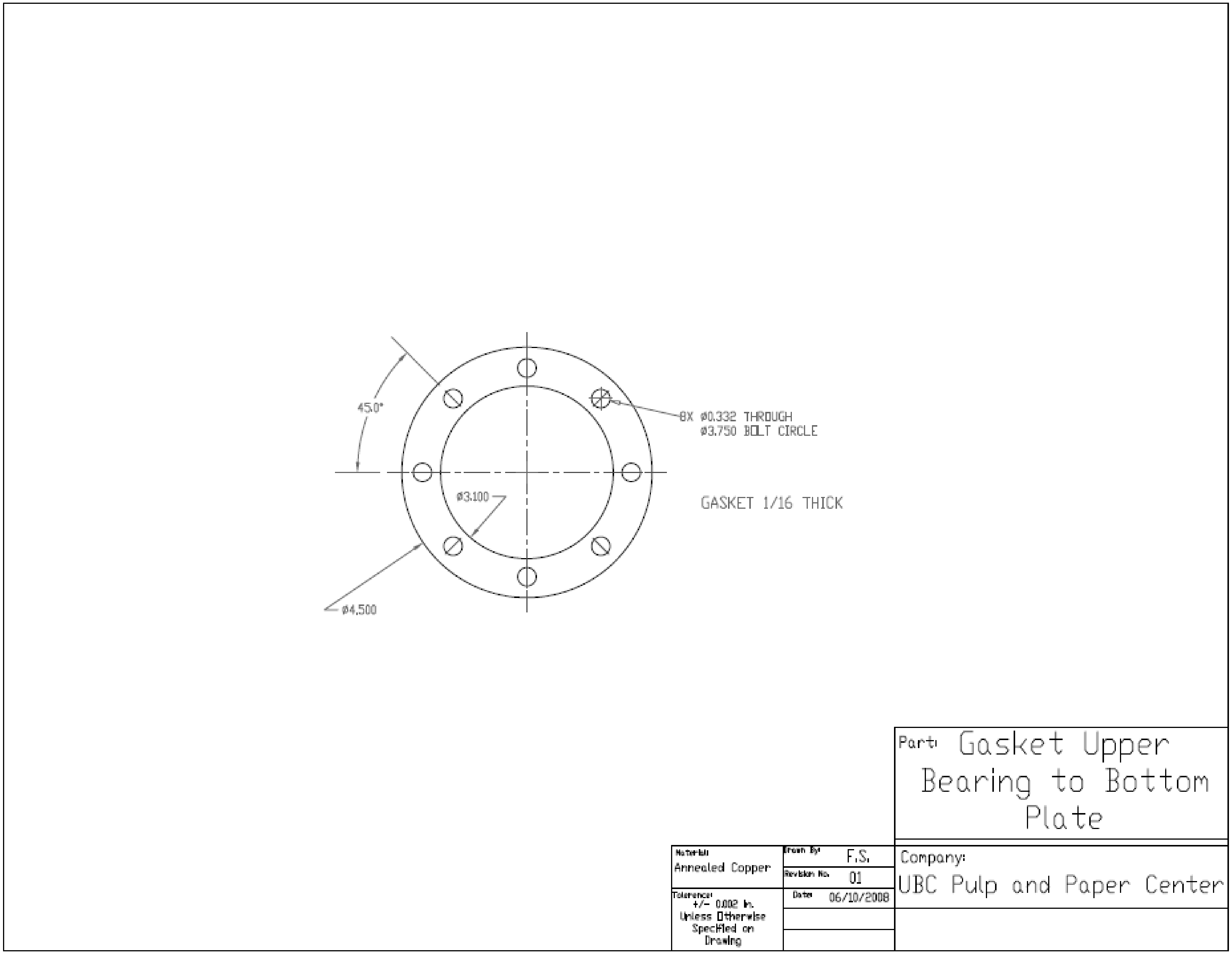
45.0°
8X ø0.332 THROUGH
ø3.750 BOLT CIRCLE
ø3.100
GASKET 1/16 THICK
ø4.500
Part: Gasket Upper Bearing to Bottom Plate
Material: Annealed Copper
Drawn By: F.S.
Revision No. 01
Date: 06/10/2008
Tolerance: +/- 0.002 in. Unless Otherwise Specified on Drawing
Company: UBC Pulp and Paper Center

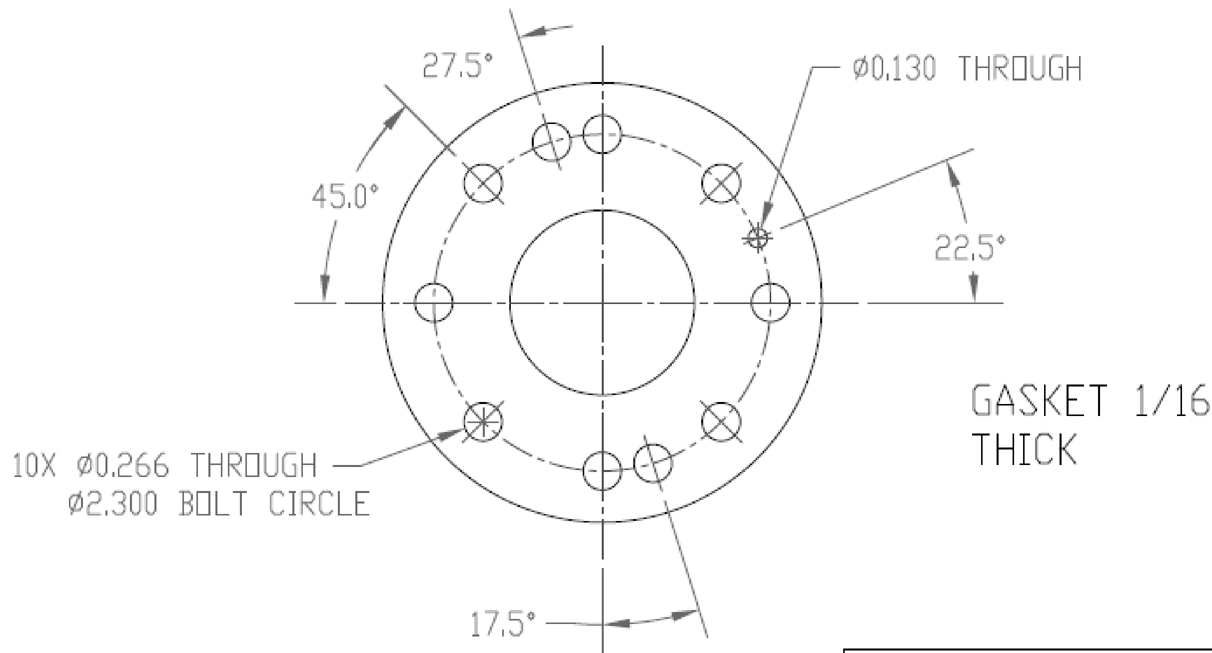

Part: Gasket Upper Bearing to Lower Seal Housing

Material: Annealed Copper	Drawn By: F.S.	Company: UBC Pulp and Paper Center
	Revision No. 01	
Tolerence: +/- 0.002 In. Unless Otherwise Specified on Drawing	Date: 06/10/2008	

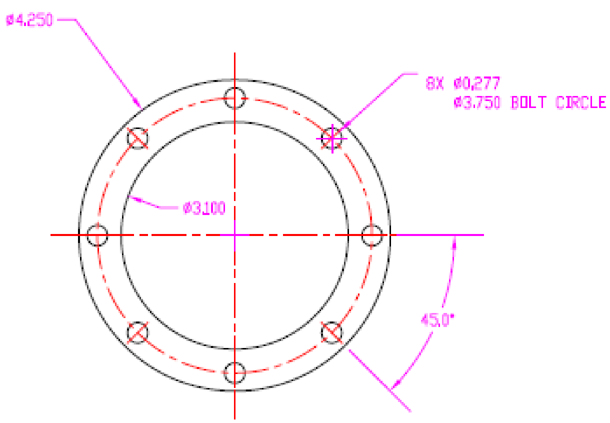

		Part: Ring Gaket
Material: Annealed Copper	Drawn By: F.S. Revision No. 01	Company: UBC Pulp and Paper Center
Tolerance: +/- 0.002 in. Unless Otherwise Specified on Drawing	Date: 07/10/2008	

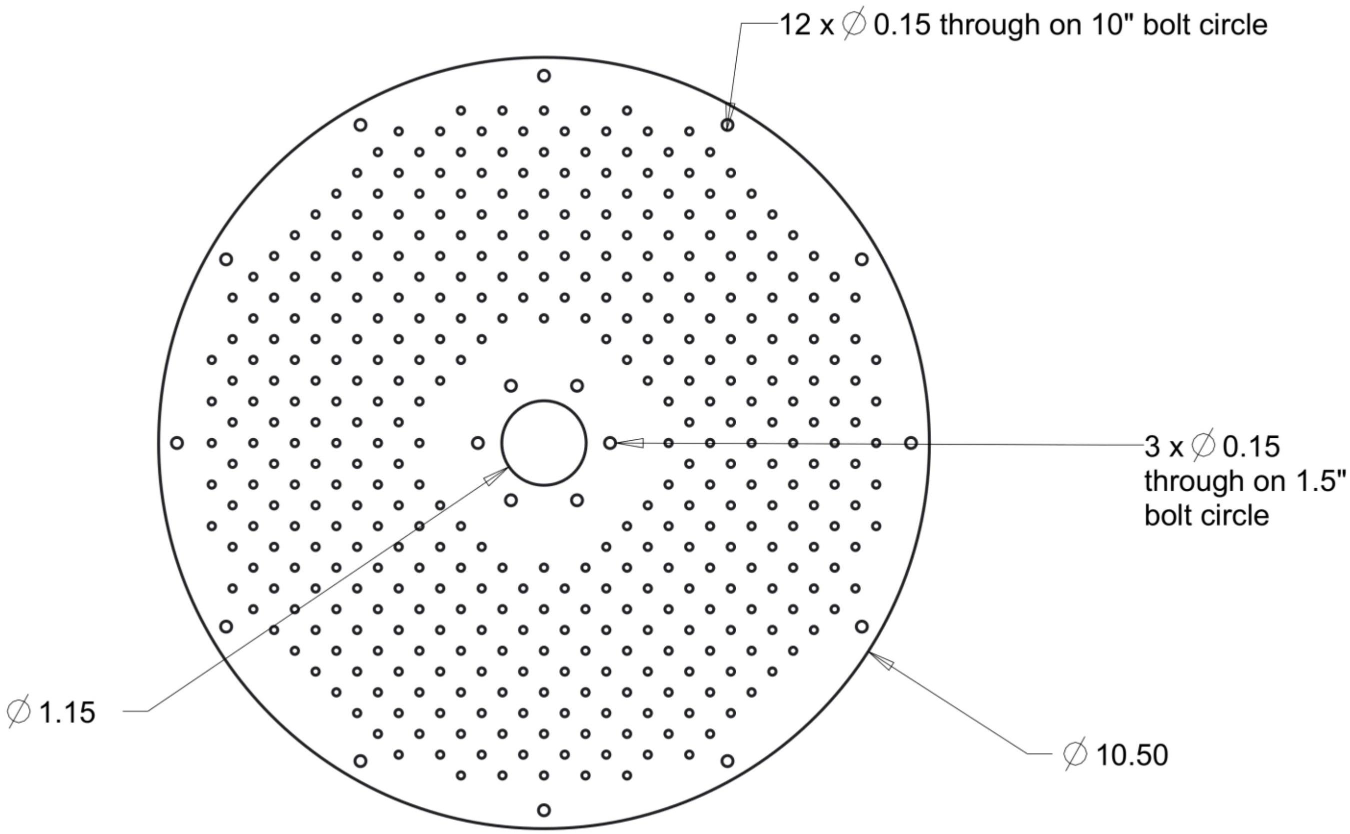

The extraction plate hole-pattern shown here is for example only. Any pattern which fits within the dimensions of the plate can be used.

Extraction Plate

SCALE 0.500

A.3 Test Samples and Flake Content

Samples taken during repulping tests were tested for the level of disintegration, or "flake content", using the TAPPI T-270 pm-88 standard for flake content measurement. The flake content is the dimensionless ratio of the dry mass of flakes (unbroken pulp/paper) to the total dry mass of pulp in suspension (flakes and fibers). The mass of flakes can be found using a Somerville Screen like the one in Figure A.4. A sample having a mix of flakes and fibers is gently agitated and bathed in the Somerville Screen. Fibers pass through the slots while the flakes are retained. These flakes are then collected and dried. The weight of these flakes is then compared with the total dry mass of pulp in suspension which is known from the consistency of the sample. The experimental error for flake content measurements was determined as a 95% confidence interval based on a T-distribution consisting of 10 flake content tests and was found to be ±2.5%.

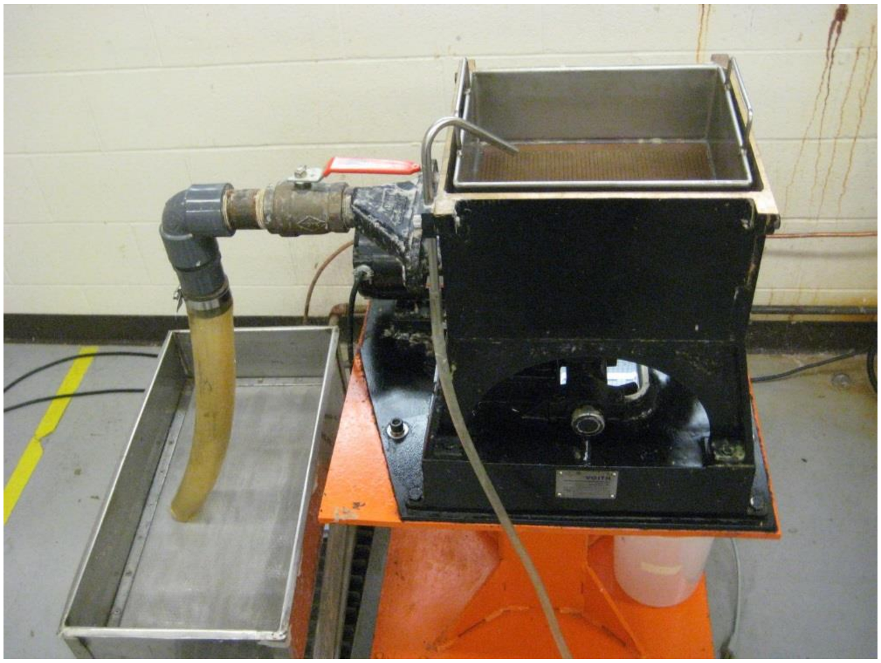

Figure A.4 : A Somerville Screen used for flake content measurement. Fibers pass through the screen and are collected in the basket below. Flakes are retained in the screen. The flakes can then be dried and weighed to determine flake content. The screen slot-width used here is 300 microns.

The measured flake content is then be correlated with both the repulping time and energy obtained from rotor power logging during testing. The rate constants from Equation 1.3 can then be found from curve fitting as shown by Figure A.5. All repulping tests results presented in this thesis are from batch repulping runs.

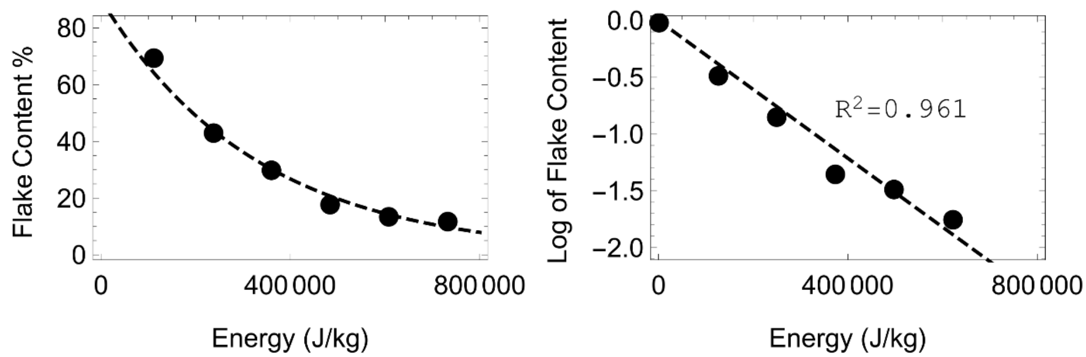

Figure A.5: Repulping rate data can be found from curve-fitting as shown above.

Flake content is correlated with the time and energy logged during repulping to get the curves like those above. A sample of logged data from a repulping test is given below:

Time (seconds)	Time (Minutes)	Power Factor	Electrical Power	Mechanical Power	Energy kJ	Power Number	Reynolds #	Motor RPM	Rotor RPM	Rotor Angualr Velocity	Rotor Tip Speed (m/s)
4.797	0.07995	0.47	1.54	1.386	6.648642	0.097285789	1209.3908	1100.799	864.897	90.57180204	10.211
9.797	0.163283333	0.466	1.573	1.416	13.72864	0.099827198	1207.6142	1099.195	863.637	90.43985515	10.196
14.797	0.246616667	0.482	1.607	1.446	20.95864	0.10172577	1208.5618	1099.974	864.249	90.50394364	10.204
19.797	0.32995	0.477	1.563	1.406	27.98864	0.098599308	1209.7462	1101.135	865.161	90.59944806	10.214
24.797	0.413283333	0.482	1.58	1.422	35.09864	0.100024875	1208.5618	1100.019	864.285	90.50771355	10.204
29.797	0.496616667	0.483	1.618	1.456	42.37864	0.102493294	1208.3249	1099.744	864.069	90.48509409	10.202
34.797	0.57995	0.522	1.763	1.587	50.31364	0.111789378	1207.9696	1099.5	863.877	90.46498789	10.199
39.797	0.663283333	0.501	1.694	1.525	57.93864	0.107243192	1208.6802	1100.111	864.357	90.51525338	10.205
44.797	0.746616667	0.515	1.744	1.57	65.78864	0.110721029	1207.4958	1099.072	863.541	90.42980206	10.195
49.797	0.82995	0.522	1.844	1.66	74.08864	0.117019304	1207.7327	1099.225	863.661	90.44236843	10.197
54.797	0.913283333	0.499	1.677	1.509	81.63364	0.105998773	1209.154	1100.524	864.681	90.54918258	10.209
59.797	0.996616667	0.556	1.905	1.714	90.20364	0.121184246	1206.5483	1098.14	862.809	90.3531472	10.187
64.797	1.07995	0.546	1.89	1.701	98.70864	0.12174149	1201.5738	1093.684	859.307	89.98641861	10.145
69.797	1.163283333	0.542	1.898	1.708	107.2486	0.120583851	1207.1405	1098.675	863.229	90.39712949	10.192
74.797	1.246616667	0.534	1.904	1.714	115.8186	0.120967085	1207.2589	1098.797	863.325	90.40718259	10.193
79.797	1.32995	0.534	1.912	1.721	124.4236	0.121466181	1207.2589	1098.782	863.313	90.40592595	10.193
84.797	1.413283333	0.538	1.94	1.746	133.1536	0.123513713	1206.3114	1097.942	862.653	90.33681091	10.185
89.797	1.496616667	0.534	1.901	1.711	141.7086	0.120906545	1206.7852	1098.339	862.965	90.36948348	10.189
94.797	1.57995	0.541	1.947	1.752	150.4686	0.12428534	1205.127	1096.918	861.849	90.25261623	10.175
99.797	1.663283333	0.565	2.005	1.804	159.4886	0.127723261	1205.9561	1097.636	862.413	90.31167817	10.182
104.797	1.746616667	0.562	1.983	1.784	168.4086	0.129263414	1196.7178	1089.204	855.788	89.61790979	10.104
109.797	1.82995	0.558	2	1.8	177.4086	0.12774377	1205.0086	1096.766	861.729	90.24004986	10.174
114.797	1.913283333	0.538	2.056	1.85	186.6586	0.131215449	1205.2454	1096.979	861.897	90.25764278	10.176
119.797	1.996616667	0.569	2.015	1.814	195.7286	0.128882653	1204.5348	1096.353	861.405	90.20612066	10.17
124.797	2.07995	0.552	2.015	1.813	204.7936	0.128585769	1205.2454	1096.995	861.909	90.25889942	10.176
129.797	2.163283333	0.579	2.166	1.949	214.5386	0.138225701	1205.2454	1097.01	861.921	90.26015605	10.176
134.797	2.246616667	0.555	2.028	1.825	223.6636	0.129296399	1205.7192	1097.392	862.221	90.29157198	10.18
139.797	2.32995	0.568	2.047	1.842	232.8736	0.130538952	1205.6008	1097.285	862.137	90.28277552	10.179
144.797	2.413283333	0.544	2.06	1.854	242.1436	0.131422293	1205.4823	1097.193	862.065	90.2752357	10.178
149.797	2.496616667	0.556	2.067	1.86	251.4436	0.13162212	1206.193	1097.82	862.557	90.32675782	10.184

Figure A.6: A sample of the data recorded for each repulping test. This is taken from a test using Rotor B and C-flute corrugated cardboard. Data is automatically collected every 5 seconds.